IOWA STATE UNIVERSITY
Digital Repository

Graduate Theses and Dissertations

Iowa State University Capstones, Theses and Dissertations

2019

Non-perturbative applications of quantum chromodynamics

Meijian Li
Iowa State University

Follow this and additional works at: https://lib.dr.iastate.edu/etd

 Part of the Physics Commons

Recommended Citation

Li, Meijian, "Non-perturbative applications of quantum chromodynamics" (2019). *Graduate Theses and Dissertations*. 17733.
https://lib.dr.iastate.edu/etd/17733

This Dissertation is brought to you for free and open access by the Iowa State University Capstones, Theses and Dissertations at Iowa State University Digital Repository. It has been accepted for inclusion in Graduate Theses and Dissertations by an authorized administrator of Iowa State University Digital Repository. For more information, please contact digirep@iastate.edu.

www.manaraa.com

Non-perturbative applications of quantum chromodynamics

by

Meijian Li

A dissertation submitted to the graduate faculty

in partial fulfillment of the requirements for the degree of

DOCTOR OF PHILOSOPHY

Major: Nuclear Physics

Program of Study Committee:
James P. Vary, Major Professor
James P. Vary
Kirill Tuchin
Pieter Maris
Marzia Rosati
James Cochran
Glenn Luecke

The student author, whose presentation of the scholarship herein was approved by the program of study committee, is solely responsible for the content of this dissertation. The Graduate College will ensure this dissertation is globally accessible and will not permit alterations after a degree is conferred.

Iowa State University

Ames, Iowa

2019

Copyright © Meijian Li, 2019. All rights reserved.

www.manaraa.com

DEDICATION

谨以此文献给：

我最亲爱的妈妈，秦伟，我最可爱的爸爸，李洪余，和我最好的朋友与丈夫，钱文扬。

I would like to dedicate this dissertation to my parents, Wei Qin and Hongyu Li, and my husband, Wenyang Qian. To my mom, who keeps bringing beautiful little things (wooden blocks, baby silkworm, strawberry sprout,...) to me after she brought me to this world. To my dad, who always inspires me with all his originative ideas ever since I was a little kid on the back seat of his bike. To my husband, for the wonderful and countless conversations we had and will have, on physics and everything else.

www.manaraa.com

TABLE OF CONTENTS

Page

www.manaraa.com

www.manaraa.com

LIST OF TABLES

www.manaraa.com

www.manaraa.com

LIST OF FIGURES

www.manaraa.com

www.manaraa.com

www.manaraa.com

www.manaraa.com

www.manaraa.com

www.manaraa.com

www.manaraa.com

www.manaraa.com

ACKNOWLEDGMENTS

I would like to take this opportunity to express my thanks to those who helped me with various aspects of conducting research and the writing of this thesis.

First and foremost, I would like to express my sincere gratitude to my advisor Professor James P. Vary for his guidance, patience and support throughout my Ph.D. study and research. His insights and words of encouragement have often inspired me and brought joys to my research. I am very lucky to have him as my advisor and his mentorship will benefit me for the rest of my life. I should also thank Professor Pieter Maris for being an inspiring unofficial co-advisor to me. He is always thoughtful and willing to sit down with me to help. Discussions with him is always fruitful and I have learned so many things from him. I also wish to thank Professor Kirill Tuchin for his help in my research and for insightful discussions. I would also like to thank other committee members for their efforts and contributions to this work: Professor Marzia Rosati, Professor James Cochran, and Professor Glenn Luecke.

I would like to thank my current and previous collaborators and colleagues, from whom I have learned a lot over the years. Dr. Xingbo Zhao, who is also a professor now, has often inspired me with his enthusiasm in research. Dr. Yang Li has spent much time explaining many fundamental questions to me with his brilliant mini lectures. Dr. Shaoyang Jia is always nice and insightful to discuss various questions with. I should also thank Wenyang Qian, Shuo Tang, Anji Yu, Dr. Guangyao Chen, Dr. Lekha Adihkari and many other colleagues for their constant help and discussions.

I also appreciate the inspiring discussions with, including but not limited to, Professor Vladimir A. Karmanov, Professor Tobias Frederico, Professor Wayne N. Polyzou, Dr. Sofia Leitao, Professor Stanley J. Brodsky, Professor Chueng-Ryong Ji, Professor Ho-Meoyng Choi, Dr. Matthew Sievert and Professor Tuomas Lappi.

www.manaraa.com

Finally, I would like to thank all my families and friends, without whom I would not be able to complete this study. Especially thanks to my parents for supporting my interest in physics over the years and to my husband for encouraging me during my hardest days.

www.manaraa.com

ABSTRACT

We investigate quantum chromodynamics (QCD) in the non-perturbative regime with the light-front Hamiltonian formalism. Our explorations are from two aspects, the hadron bound states and the high energy scatterings.

We first study the heavy quarkonia system within the basis light-front quantization approach. We review solving the heavy quarkonium system in the valence Fock sector with effective Hamiltonian, and discuss how one could extend the framework to higher Fock space. We then study the properties of heavy quarkonia through electromagnetic processes, via elastic form factors, radiative transitions and decay constants. We investigate the effect of different current components, different magnetic projections of the states and different reference frames in the valence Fock sector calculation on the light front. We suggest preferred choices based on our analysis, and carry out numerical calculations of those quantities with the valence light-front wavefunctions. Comparisons are made with experimental data and other theoretical calculations.

We also apply the light-front Hamiltonian approach to a time-dependent problem, the quark nucleus scattering. We carry out an explicit evolution of the quark by decomposing the time-evolution operator into many time increments. We calculate the scattering cross sections and study the evolution of the quark in the color space and the coordinate space. We reveal interesting sub-eikonal effects on the quark's transverse location.

Those studies also show exciting possibilities for future applications of QCD bound states and time-dependent problems in the non-perturbative quantum field theory.

www.manaraa.com

CHAPTER 1. INTRODUCTION: QUANTUM FIELD THEORY ON THE LIGHT FRONT

Solving quantum field theories from first principles is the key to addressing fundamental questions such as 'what is matter made of?'. This thesis addresses the non-perturbative approach to quantum field theories within the light-front Hamiltonian formalism, with two different but related investigations, the hadron bound states and the high energy scatterings. This chapter provides the necessary background information of quantum field theory in the light-front Hamiltonian formulation.

1.1 Quantum field theory

Quantum field theory arose out of the confluence of special relativity and quantum mechanics. To quote from A. Zee in his book of the quantum field theory [16], "quantum field theory was born of the necessity of dealing with the marriage of special relativity and quantum mechanics, just as the new science of string theory is being born of the necessity of dealing with the marriage of general relativity and quantum mechanics." In the quantum field theory, particles are treated as excited states (also called quanta) of their underlying fields. Interactions between particles are described by interaction terms in the Lagrangian involving their corresponding fields. A physical field can be thought of as the assignment of a physical quantity at each point of space and time. Quantum field theory is therefore a tool that one can use to apply to any particular theory of particles.

There are four fundamental interactions of nature, namely, the electromagnetic, the weak, the strong and the gravitational interaction. The Standard Model of particle physics is the theory describing the first three of them in a unified framework. An interaction is described as an exchange of bosons between the objects affected, such as a photon for the electromagnetic interaction and a gluon for the strong interaction. In the Standard Model, the electromagnetic and the weak interactions are described uniformly as a Yang–Mills field with an SU(2)× U(1) gauge group. The strong interaction is described by a Yang-Mills theory of the

www.manaraa.com

SU(3) gauge group, known as quantum chromodynamics (QCD). The fundamental particles of the strong interaction are quarks and gluons, which make up composite hadrons such as the proton, neutron and pion. The basic fermions are quarks in three different color states, forming the fundamental representation of the SU(3) group. The gauge bosons are gluons in eight different color states, forming the adjoint representation of the SU(3) group. QCD exhibits two main properties, color confinement and asymptotic freedom. Color confinement is the phenomenon that color charged particles (such as quarks and gluons) cannot be isolated, and therefore cannot be directly observed. Quarks and gluons must clump together to form colorless (color singlet) bound states, hadrons or glueballs. This is a dynamical property and cannot be obtained from perturbation theory. Asymptotic freedom is a property that causes interactions between particles to become asymptotically weaker as the energy scale increases and the corresponding length scale decreases. This property allows the perturbative calculations at high energies. The main tool of the perturbative calculations are the Feynman diagrams, where one expands the path integral in an increasing power of the coupling. However, such method breaks down for strong coupling regime. Non-perturbative treatments of QCD are required to address those most challenging and exciting problems of nuclear physics, including the confinement, the dynamical chiral symmetry breaking and the properties of QCD bound states.

Our investigation of the non-perturbative QCD uses the light-front quantum field theory. The quantum states are defined on the light-front time $x^+ = x^0 + x^3$ (see conventions of the light-front coordinates in Appendix A.1). Diagonalizing the QCD Hamiltonian directly provides the hadron spectrum and wavefunctions. The wavefunctions encode the information of the internal structures of the bound states, and observables can be obtained by evaluating the associated operators on the states. This formalism could also generate real-time evolution of quantum fields, which could be applied to study high energy scattering processes. There are also many other non-perturbative approaches to solve the quantum field theory, including effective field theories [17], QCD sum rules [18], lattice QCD [19, 20], and Dyson-Schwinger equations (DSEs) [21, 22, 23, 24, 25].

www.manaraa.com

1.2 Forms of relativistic dynamics

Since quantum field theory is formulated to reconcile quantum mechanics with special relativity, let us first study how symmetries like Lorentz invariance appear in quantum setting. In particular, we would like to combine the principle of relativity with the Hamiltonian formulation of dynamics.

Einstein's principle of relativity requires that physical laws shall be invariant under transformations from one space-time coordinate system to another, or in other words, invariant in all inertial frames of reference. The whole group of the transformations is the inhomogeneous Lorentz group, also known as the Poincaré group. Quantum theory postulates that physical states are represented by rays[1] in Hilbert space. Therefore we need to implement a representation of the Poincaré group. The Poincaré algebra is the Lie algebra of the Poincaré group, and it is given by the commutation relations:

$$\begin{aligned} [P^\mu, P^\nu] &= 0\,, \\ [P^\mu, M^{\alpha\beta}] &= i(g^{\mu\alpha}P^\beta - g^{\mu\beta}P^\alpha)\,, \\ [M^{\mu\nu}, M^{\rho\sigma}] &= i(g^{\mu\sigma}M^{\nu\rho} - g^{\nu\sigma}M^{\mu\rho} + g^{\nu\rho}M^{\mu\sigma} - g^{\mu\rho}M^{\nu\sigma})\,. \end{aligned} \tag{1.1}$$

It has ten generators, four generators of translations $P^\mu = (P^0, P^1, P^2, P^3)$ and six generators of Lorentz transformations $M^{\mu\nu}$. The latter can be further split into the three generators of rotations $J^i = 1/2\epsilon^{ijk}M^{jk}$ and 3 generators of boosts $K^i = M^{0i}$. The cyclic symbol ϵ^{ijk} is 1 if the indices ijk are in cyclic order, and 0 otherwise.

In quantum mechanics, and also in the quantum field theory, the dynamical evolution of a quantum state satisfies the Schrödinger equation,

$$i\frac{\partial}{\partial t}\,|\psi(t)\rangle = H\,|\psi(t)\rangle\ . \tag{1.2}$$

For stationary states,

$$|\psi(t)\rangle = e^{-iEt}\,|\psi(0)\rangle\ , \tag{1.3}$$

and it leads to the bound-state equation

$$H\,|\psi(0)\rangle = E\,|\psi(0)\rangle\ , \tag{1.4}$$

[1] A ray is a set of normalized vectors differed by multiplying an arbitrary scalar of unit magnitude [26].

www.manaraa.com

where E is the bound state energy. Though in its original form the time t is the regular time, there are actually multiple choices of the time variable as a foliation of spacetime[2]. P. A. M. Dirac brought up three forms of relativistic dynamics, namely the instant form, the point form, and the front form [28].

In the instant form, one works with dynamical variables referring to physical conditions at some instant of time, x^0. The Hamiltonian is P^0. The transformations of coordinates associated with the momenta P^1, P^2, P^3 and the rotations J^1, J^2, J^3, leave the instant invariant, and are thus kinematic. The energy P^0, and the boosts K^1, K^2, K^3 are dynamical. The instant form seems most intuitive since its time variable is the regular time. Although it is the conventional choice for quantizing field theories, it has many disadvantages. The experiment determining the wavefunction $\psi(t, \vec{x})$ solved from the evolution equation of Eq. (1.2) requires the simultaneous measurement of all positions of the state. A more practical experimental measurement scatters one plane-wave laser beam, and the signal reaches each part of the object at the same light-front time $x^+ = t + z/c$ (this is the same with the definition $x^+ = x^0 + x^3$ with the unit $c = 1$).

The point form of dynamics describes physical conditions on the three-dimensional surface, $\tau = \sqrt{x^\mu x_\mu - a^2} = \sqrt{(x^0)^2 - (x^1)^2 - (x^2)^2 - (x^3)^2 - a^2}$ with $x^0 > 0$. The energy P^0, and the momenta P^1, P^2, P^3 are all dynamical. The kinematic group consists of the boosts K^1, K^2, K^3 and the rotations J^1, J^2, J^3, which leave the origin point invariant. The point form of relativistic quantum mechanics has been advocated as an appropriate framework for calculating the electroweak structure of mesons and baryons within the scope of constituent-quark models [29, 30, 31].

The front form considers the three-dimensional surface in space-time formed by a plane wave front advancing with the velocity of light. The theory describes physical conditions at some constant light-front time $x^+ = x^0 + x^3$. The front form has the largest number(seven) of kinematic generators that leaves the light front invariant. They are, the transverse momentum P^1, P^2, the longitudinal momentum $P^+ = P^0 + P^3$, the transverse boosts $E^1 = K^1 + J^2$, $E^2 = K^2 - J^1$, the rotation in the x-y plane J^3, and the boost in the longitudinal direction K^3. The remaining generators $\{P^- = P^0 - P^3, F^1 = J^1 + K^2, F^2 = J^2 - K^1\}$ are dynamical. P^- is the light-front Hamiltonian. It is usually convenient to use the light-front coordinates

[2]By foliation it means that the manifold of spacetime is decomposed into hypersurfaces and there exists a smooth scalar field (the "time") which is regular in the sense that its gradient never vanishes, such that each hypersurface is a level surface of this scalar field. See more discussions on foliation in Ref. [27] for more discussions.

www.manaraa.com

when implementing the light-front dynamics. We include the conventions of the light-front coordinates in this thesis in Appendix A.1.

A visualization of the "time" in these three forms is presented in Fig. 1.1. Be aware that there also exists two other forms of dynamics, with the time defined as $\tau_z = \sqrt{(x^0)^2 - (x^3)^2 - a^2}$ with $x^0 > 0$ and $\tau_\perp = \sqrt{(x^0)^2 - (x^1)^2 - (x^2)^2 - a^2}$ with $x^0 > 0$ respectively, though they have a rather small kinematical group and are not commonly used [32].

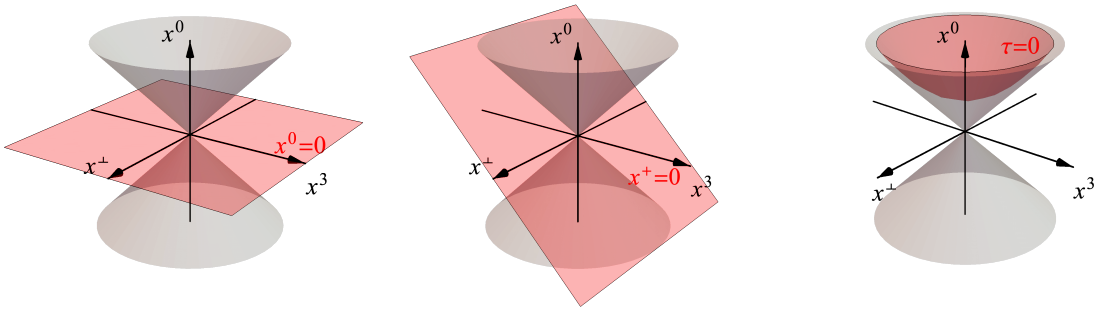

(a) instant form (b) front form (c) point form

Figure 1.1 "Time" in the three forms of dynamics. The gray cones are the reference surfaces of the light cones, $t = \sqrt{(x^0)^2 + (x^3)^2}$. The equal-"time" surfaces are in red. In (a), the instant form, time is defined as x^0 and the shown equal-time surface is $x^0 = 0$. In (b), the front form, time is defined as $x^+ = x^0 + x^3$ and the shown equal-light-front-time surface is $x^+ = 0$. In (c), the point form, time is defined as $\tau = \sqrt{x^\mu x_\mu - a^2}$ with $x^0 > 0$ and the shown equal-point-time surface is $\tau = 0$.

The investigations carried out in this work employ the front form. The quantum field theory quantized on the light-front surface $x^+ = 0$ is the light front quantum field theory. In the following section, we will carry out the canonical quantization of the QCD on the light front.

1.3 Light front quantum field theory of QCD

The strong interaction between quarks and gluons is described by QCD, and its Lagrangian reads

$$\mathcal{L}_{QCD} = -\frac{1}{4} F^{\mu\nu}{}_a F^a_{\mu\nu} + \overline{\Psi}(i\gamma^\mu \boldsymbol{D}_\mu - \boldsymbol{m})\Psi \,. \tag{1.5}$$

www.manaraa.com

A_a^ν is color vector potential, with the gluon index $a = 1, 2, \ldots, 8$. The quark field $\Psi_{\alpha,c}$, carries the Dirac index $\alpha = 1, 2, \ldots, 4$ and the color index $c = 1, 2, 3$, which are usually suppressed in expressions like $\overline{\Psi}\gamma^\mu \boldsymbol{D}_\mu \Psi = \overline{\Psi}_c \gamma^\mu (\boldsymbol{D}_\mu)_{cc'} \Psi_{c'}$. $\boldsymbol{m} = m\boldsymbol{I}_3 = m\delta_{cc'}$ is diagonal in color space. The vector potential can be parameterized as $(\boldsymbol{A}_\mu)_{cc'} = T^a_{cc'} A^\mu_a$ by the color matrices $T^a_{cc'}$, and its matrix form can be found in Appendix A.7. $F^{\mu\nu}_a \equiv \partial^\mu A^\nu_a - \partial^\nu A^\mu_a - g f^{abc} A^\mu_b A^\nu_c$ is the field tensor, and $\boldsymbol{D}^\mu \equiv \partial_\mu \boldsymbol{I}_3 + ig\boldsymbol{A}^\mu$ is the covariant derivative. We follow the convention of the covariant derivative from Ref. [33], such that g is the chromo-electric charge of the anti-fermion. Note that there exists another widely used convention that assigns g to the chromo-electric charge of the fermion instead [34]. The structure constants f^{abc} are complete anti-symmetric, $f^{abc} = f^{cab} = -f^{acb}$. In the following derivations, we will drop the identity operator in the color space, $\boldsymbol{I}_3$, for simplicity. We present the canonical Hamiltonian obtained from the QCD Lagrangian, and we leave the details of the derivation in Appendix B.

The QCD Lagrangian is a functional of the twelve components $\boldsymbol{A}^\mu$, Ψ_α, $\overline{\Psi}_\alpha$ and their space-time derivatives. The equations of motion are the color-Maxwell equation,

$$\partial_\lambda F^{\lambda\kappa}_s = g J^\kappa_s, \quad \text{with the current density} J^\kappa_s \equiv f^{sac} F^{\kappa\mu}_a A^c_\mu + \overline{\Psi}\gamma^\kappa T^s \Psi \,, \tag{1.6}$$

and the color-Dirac equation,

$$\left[i\gamma^\mu (\partial_\mu + ig\boldsymbol{A}_\mu) - m \right] \Psi = 0 \,. \tag{1.7}$$

We take the most convenient gauge choice in light-front quantization, the light-cone gauge $A^+ = 0$ [35, 36]. The + component of Eq. (1.6) does not contain time derivatives, making A^- a constrained variable. From the fermion equation of motion of Eq. (1.7), we could also identify the projected component $\Psi_- = \Lambda^- \Psi$ (see definitions of the projection operators $\Lambda^\pm$ in Appendix A.1) as a constrained variable. The dynamical degrees of freedom are $\Psi_+ = \Lambda^+ \Psi$ and A_i ($i = 1, 2$).

The Hamiltonian density is obtained through a Legendre transformation,

$$\mathcal{P}_+ = (\partial_+ A^s_\kappa)\Pi^+_{A^s_\kappa} + (\partial_+ \Psi)\Pi^+_\Psi + (\partial_+ \overline{\Psi})\Pi^+_{\overline{\Psi}} - \mathcal{L} \,, \tag{1.8}$$

www.manaraa.com

where the generalized momentum fields are $\Pi_r^\kappa \equiv \delta\mathcal{L}/\delta(\partial_\kappa\phi_r)$. The light-front QCD Hamiltonian $P^- = 2P_+ = 2\int \mathrm{d}x_+\,\mathrm{d}^2x_\perp\,\mathcal{P}_+$ is then derived as,

$$\begin{aligned} P^-_{QCD} = \int \mathrm{d}x^-\,\mathrm{d}^2x_\perp \Big\{ & -\frac{1}{2}A^j_a(i\nabla_\perp)^2A^a_j + \frac{1}{2}\bar\Psi\gamma^+\frac{m^2-\nabla^2_\perp}{i\partial^+}\Psi \\ & - gf^{abc}\partial^i A^j_a A^b_i A^c_j + gJ^+_a A^a_+ + g\bar\Psi\gamma^j \boldsymbol{A}_i\Psi \\ & - \frac{1}{2}g^2J^+_a\frac{1}{(\partial^+)^2}J^+_a + \frac{g^2}{4}f^{abc}A^i_bA^j_cf^{aef}A^e_iA^f_j \\ & + \frac{g^2}{2}\bar\Psi\gamma^j\boldsymbol{A}_i\frac{\gamma^+}{i\partial^+}\gamma^j\boldsymbol{A}_j\Psi\Big\}\,. \end{aligned} \tag{1.9}$$

The two terms in the first line are the kinetic energy for the gauge field and the fermion respectively. The three terms in the second line can be written collectively as $gJ^\mu_aA^a_\mu$, which include the three-gluon-interaction, the gluon emission and quark-antiquark-pair-production processes. The two terms in the third line are the instantaneous-gluon-interaction and the four-gluon-interaction respectively. The last line contains the instantaneous-fermion-interaction. The vertex diagrams for these interactions are shown in Fig. 1.2

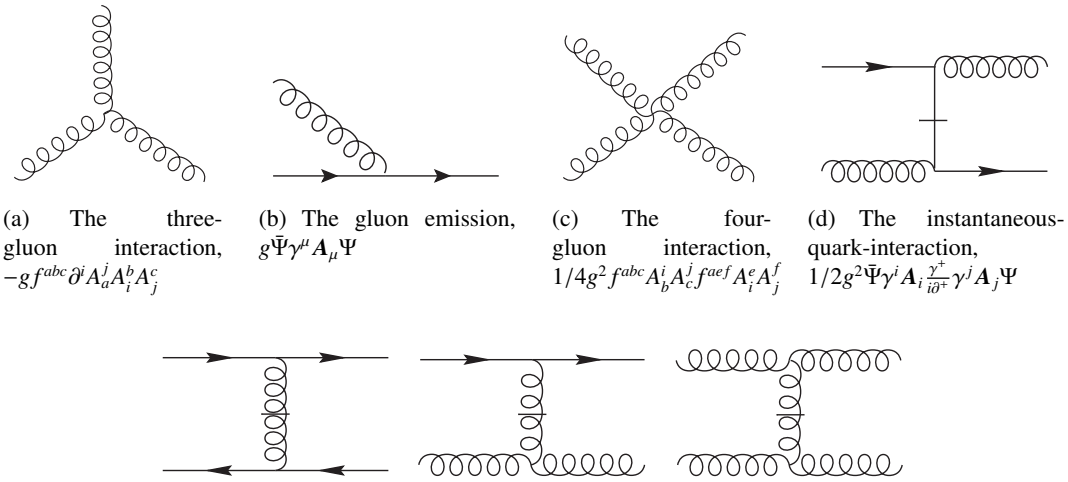

(a) The three-gluon interaction, $-gf^{abc}\partial^iA^j_aA^b_iA^c_j$

(b) The gluon emission, $g\bar\Psi\gamma^\mu\boldsymbol{A}_\mu\Psi$

(c) The four-gluon interaction, $1/4g^2f^{abc}A^i_bA^j_cf^{aef}A^e_iA^f_j$

(d) The instantaneous-quark-interaction, $1/2g^2\bar\Psi\gamma^i\boldsymbol{A}_i\frac{\gamma^+}{i\partial^+}\gamma^j\boldsymbol{A}_j\Psi$

(e) The instantaneous-gluon-interaction, $-1/2g^2J^+_a\frac{1}{(\partial^+)^2}J^+_a$

Figure 1.2 Vertex diagram representation of the light-front QCD Hamiltonian in Eq. (1.9). The solid lines represent the quark operators, and the curly lines represent the gluon operators. The instantaneous quark (gluon) propagator $1/(i\partial^+)$ $[1/(\partial^+)^2]$ is represented by a quark (gluon) line with a bar across it.

www.manaraa.com

The fields for QCD admit free-field expansions at $x^+ = 0$ [33],

$$\Psi_{\alpha cf}(x) = \sum_{\lambda=\pm\frac{1}{2}} \int \frac{\mathrm{d}^2 p_\perp \, \mathrm{d}p^+}{(2\pi)^3 2p^+} \theta(p^+) \left[b_q(p) u_\alpha(p,\lambda) e^{-ip\cdot x} + d_q^\dagger(p) v_\alpha(p,\lambda) e^{ip\cdot x} \right] , \tag{1.10}$$

$$A_{\mu a}(x) = \sum_{\lambda=\pm 1} \int \frac{\mathrm{d}^2 p_\perp \, \mathrm{d}p^+}{(2\pi)^3 2p^+} \theta(p^+) \left[a_q(p) \epsilon_\mu(p,\lambda) e^{-ip\cdot x} + a_q^\dagger(p) \epsilon_\mu^*(p,\lambda) e^{ip\cdot x} \right] , \tag{1.11}$$

where $\theta(p^+)$ is the Heaviside unit step function. α denotes the spinor components of Ψ, and μ denotes the vector components of A. λ is the light-front helicity of the corresponding field ($\lambda = \pm 1/2$ for quarks and $\lambda = \pm 1$ for gluons). $c = 1, 2, 3$ and $a = 1, 2, \ldots, 8$ are the color indices of quarks (antiquarks) and gluons respectively. q contains the quantum numbers of single particle state, for fermion $q = \{\lambda, c, f(\text{flavor})\}$ and for gluons $q = \{\lambda, a\}$. The creation and annihilation operators obey the commutation and anti-commutation relations. For gluons,

$$[a_{\lambda a}(p), a^\dagger_{\lambda' a'}(p')] = 2p^+ \theta(p^+) (2\pi)^3 \delta^3(p - p') \delta_{\lambda\lambda'} \delta_{aa'} , \tag{1.12}$$

where $\delta^3(p - p') = \delta(p^+ - p'^+) \delta^2(\vec{p}_\perp - \vec{p}'_\perp)$. For quarks and antiquarks,

$$\begin{aligned} \{b_{\lambda cf}(p), b^\dagger_{\lambda' c' f'}(p')\} &= 2p^+ \theta(p^+) (2\pi)^3 \delta^3(p - p') \delta_{\lambda\lambda'} \delta_{cc'} \delta_{ff'} \\ \{d_{\lambda cf}(p), d^\dagger_{\lambda' c' f'}(p')\} &= 2p^+ \theta(p^+) (2\pi)^3 \delta^3(p - p') \delta_{\lambda\lambda'} \delta_{cc'} \delta_{ff'} . \end{aligned} \tag{1.13}$$

All the other commutation and anti-commutation relations vanish,

$$[a_{\lambda a}(p), a_{\lambda' a'}(p')] = \{b_{\lambda cf}(p), b_{\lambda' c' f'}(p')\} = \{d_{\lambda cf}(p), d_{\lambda' c' f'}(p')\} = \{b_{\lambda cf}(p), d^\dagger_{\lambda' c' f'}(p')\} = \cdots = 0 . \tag{1.14}$$

The anti-commutation relation for the fermion fields follows as

$$\begin{aligned} \{\Psi_{\alpha cf}(x), \Psi^\dagger_{\beta c' f'}(y)\} &= \sum_{\lambda,\lambda'} \int \frac{\mathrm{d}^2 p_\perp \, \mathrm{d}p^+}{(2\pi)^3 2p^+} \int \frac{\mathrm{d}^2 k_\perp \, \mathrm{d}k^+}{(2\pi)^3 2k^+} \Big[\{b_q(p), b^\dagger_{q'}(k)\} u_\alpha(p,\lambda) [\bar{u}(k,\lambda') \gamma^0]_\beta \\ &\quad e^{-ip\cdot x + ik\cdot y} + \{d_q^\dagger(p), d_{q'}(k)\} v_\alpha(p,\lambda) [\bar{v}(q,\lambda') \gamma^0]_\beta e^{ip\cdot x - ik\cdot y} \Big] \\ &= \sum_\lambda \int \frac{\mathrm{d}^2 p_\perp \, \mathrm{d}p^+}{(2\pi)^3 2p^+} \left[u(p,\lambda) \bar{u}(p,\lambda) \gamma^0 e^{-ip\cdot(x-y)} + v(p,\lambda) \bar{v}(p,\lambda) \gamma^0 e^{ip\cdot(x-y)} \right]_{\alpha\beta} \delta_{\lambda\lambda'} \delta_{c,c'} \delta_{f,f'} \\ &= \int \frac{\mathrm{d}^2 p_\perp \, \mathrm{d}p^+}{(2\pi)^3 2p^+} \left[(\not{p} + m) \gamma^0 e^{-ip\cdot(x-y)} + (\not{p} - m) \gamma^0 e^{ip\cdot(x-y)} \right]_{\alpha\beta} \delta_{c,c'} \delta_{f,f'} . \end{aligned} \tag{1.15}$$

www.manaraa.com

The commutation relation for the dynamical components ($i = 1, 2$) of the gluon fields reads

$$
\begin{aligned}
[A_{ia}(x), A^{\dagger}_{ja'}(y)] &= \sum_{\lambda,\lambda'} \int \frac{\mathrm{d}^2 p_\perp \, \mathrm{d}p^+}{(2\pi)^3 2p^+} \int \frac{\mathrm{d}^2 k_\perp \, \mathrm{d}k^+}{(2\pi)^3 2k^+} \Big[[a_q(p), a^{\dagger}_{q'}(k)] \epsilon_i(p,\lambda) \epsilon^*_j(k,\lambda') e^{-ip\cdot x + ik\cdot y} \\
&\quad + [a^{\dagger}_q(p), a_{q'}(k)] \epsilon^*_i(p,\lambda) \epsilon_j(k,\lambda') e^{ip\cdot x - ik\cdot y} \Big] \\
&= \sum_{\lambda} \int \frac{\mathrm{d}^2 p_\perp \, \mathrm{d}p^+}{(2\pi)^3 2p^+} \left[\epsilon_i(p,\lambda) \epsilon^*_j(p,\lambda) e^{-ip\cdot(x-y)} + \epsilon^*_i(p,\lambda) \epsilon_j(p,\lambda) e^{ip\cdot(x-y)} \right] \delta_{\lambda\lambda'} \delta_{aa'} \\
&= \sum_{\lambda} \int \frac{\mathrm{d}^2 p_\perp \, \mathrm{d}p^+}{(2\pi)^3 2p^+} \left[e^{-ip\cdot(x-y)} + e^{ip\cdot(x-y)} \right] \delta_{ij} \delta_{\lambda\lambda'} \delta_{aa'} \ .
\end{aligned}
\tag{1.16}
$$

1.3.1 Fock space representation

The Hilbert space for the single-particle creation and destruction operators is the Fock space. The Fock space can be decomposed into sectors with n Fock particles, in which the number of quarks, antiquarks and gluons, N, $\bar{N}$ and $\tilde{N}$, respectively and $n = N + \bar{N} + \tilde{N}$. Fock states can be defined in terms of the eigenstates of the free-field Hamiltonian, i.e., the light-front kinetic operator, and can be obtained by applying the creation operators on the Fock vacuum $|0\rangle$. The hadron state vector $|\psi_h(P, j, m_j)\rangle$ can be expanded in the Fock space. We use j as the total spin of meson and m_j as its magnetic projection. In the single particle coordinates, it reads

$$
\begin{aligned}
|\psi_h(P, j, m_j)\rangle &= \sum_{n=0}^{\infty} \int \prod_{i=1}^{n} \frac{\mathrm{d}\kappa_i^+ \, \mathrm{d}^2 \kappa_{i\perp}}{(2\pi)^3 2\kappa_i^+} \theta(\kappa_i^+) 2P^+ \theta(P^+) (2\pi)^3 \delta^3(\kappa_1 + \kappa_2 + \cdots + \kappa_n - P) \\
&\quad \times \sum_{\{l_i, s_i\}} \psi^{(m_j)}_{n/h}(\{\kappa_i, s_i, l_i\}) c^{\dagger}_{s_1 l_1}(\kappa_1) \ldots c^{\dagger}_{s_n l_n}(\kappa_n) |0\rangle \ ,
\end{aligned}
\tag{1.17}
$$

where i is the index of the Fock particle, and it takes values of $i = 1, \ldots, n$ for the n-particle sector. $c^{\dagger}_{s_i l_i}(\kappa_i)$ is the creation operator for the corresponding constituent (quark, antiquark or gluon). κ_i is the momentum, and each particle is on its mass-shell $\kappa_i^2 = m_i^2$. l is the color index, and s is the spin projection of the particle. $\sum_{\{l_i, s_i\}}$ means the sum of all color and spin arrangements in the string of the creation operators resulting in a sum over a unique set of creation operators with the restriction of producing color-singlet projected states. The construction of the global color singlets for multi-particle states can be found in Ref. [1]. We suppress flavor indices but they can be included in a straightforward manner. $\psi^{(m_j)}_{n/h}(\{\kappa_i, s_i, l_i\})$ are the projection of the physical states to the Fock states, called the light-front wavefunctions (LFWFs).

www.manaraa.com

In the relative particle coordinates, we define

$$x_i \equiv \frac{\kappa_i^+}{P^+}, \qquad \vec{k}_{i\perp} \equiv \vec{\kappa}_{i\perp} - x\vec{P}_\perp \ . \tag{1.18}$$

x_i are known as the longitudinal momentum fractions; $\vec{k}_{i\perp}$ are the relative transverse momenta. They are independent of the total momentum of the bound state, and satisfy $0 < x_i < 1$, $\sum^n x_i = 1$ and $\sum \vec{k}_{i\perp} = \vec{0}$. The hadron state vector now reads,

$$\begin{aligned} |\psi_h(P, j, m_j)\rangle = &\sum_{n=0}^{\infty} \int \prod_{i=1}^{n} \frac{\mathrm{d}x_i \, \mathrm{d}^2 k_{i\perp}}{(2\pi)^3 2x_i} 2(2\pi)^3 \delta(x_1 + x_2 + \cdots + x_n - 1) \delta^2(\vec{k}_{1\perp} + \vec{k}_{2\perp} + \cdots + \vec{k}_{n\perp}) \\ &\times \sum_{\{l_i, s_i\}} \psi_{n/h}^{(m_j)}(\{x_i, \vec{k}_{i\perp}, s_i, l_i\}) c^\dagger_{s_1 l_1}(x_1 P^+, \vec{k}_{1\perp} + x_1 \vec{P}_\perp) \cdots c^\dagger_{s_n l_n}(x_n P^+, \vec{k}_{n\perp} + x_n \vec{P}_\perp) \, |0\rangle \ , \end{aligned} \tag{1.19}$$

with the LFWFs $\psi_{n/h}^{(m_j)}(\{x_i, \vec{k}_{i\perp}, s_i, l_i\})$ in the relative coordinates.

The hadron state vector is normalized as,

$$\langle \psi_h(P, j, m_j) | \psi_{h'}(P', j', m'_j) \rangle = 2P^+ \theta(P^+) (2\pi)^3 \delta^3(P - P') \delta_{m_j, m'_j} \delta_{j, j'} \delta_{h, h'} \ . \tag{1.20}$$

Then the normalization of the LFWFs reads,

$$\sum_{n=0}^{\infty} \int \prod_{i=1}^{n} \frac{\mathrm{d}x_i \, \mathrm{d}^2 k_{i\perp}}{(2\pi)^3 2x_i} 2(2\pi)^3 \delta(x_1 + \cdots + x_n - 1) \delta^2(\vec{k}_{1\perp} + \cdots + \vec{k}_{n\perp}) \sum_{\{l_i, s_i\}} \left| \psi_{n/h}^{(m_j)}(\{x_i, \vec{k}_{i\perp}, s_i, l_i\}) \right|^2 = 1 \ . \tag{1.21}$$

For practical calculations, the infinite Fock space needs to be truncated. For heavy quarkonium, the valence quark (q) + antiquark ($\bar{q}$) Fock sector $|q\bar{q}\rangle$ makes the leading contribution, and is followed by higher Fock sectors which could include a gluon (g) such as $|q\bar{q}g\rangle$ as well as $|q\bar{q}q\bar{q}\rangle$. The order of the higher Fock sectors to include in calculations is related to the description of the model and the specific problem. In solving the meson bound states from the light-front QCD Hamiltonian, it is natural to include the $|q\bar{q}g\rangle$ sector besides the valence sector, such that the quark-gluon interaction from QCD could be directly implemented. However, in the cases of the radiative transition such as $J/\psi \to \eta_c + \gamma^{(*)}$ and the strong decay such as $\omega \to \pi^+ + \pi^-$, it is essential to take into account the $|q\bar{q}q\bar{q}\rangle$ sector since the $|q\bar{q}q\bar{q}\rangle \to |q\bar{q}\rangle$ term would make nontrivial contributions. We will write out the light-front wavefunction representation in both the $|q\bar{q}\rangle$ space and the $|q\bar{q}\rangle + |q\bar{q}q\bar{q}\rangle$ space where we anticipate adopting effective interactions to account for the exchange of gluons.

www.manaraa.com

- $|q\bar{q}\rangle$

The projection of the quarkonium state on the $|q\bar{q}\rangle$ sector reads,

$$\begin{aligned}|h_{q\bar{q}}(P,j,m_j)\rangle =& \sum_{s,\bar{s}}\int\frac{\mathrm{d}k_q^+\,\mathrm{d}^2k_{q\perp}}{(2\pi)^3 2k_q^+}\theta(k_q^+)\int\frac{\mathrm{d}k_{\bar{q}}^+\,\mathrm{d}^2k_{\bar{q}\perp}}{(2\pi)^3 2k_{\bar{q}}^+}\theta(k_{\bar{q}}^+)2P^+\theta(P^+)(2\pi)^3\delta^3(k_q+k_{\bar{q}}-P)\\ &\times\frac{1}{\sqrt{N_c}}\sum_{i=1}^{N_c}\psi^{(m_j)}_{s\bar{s}/h}(k_q,k_{\bar{q}})b^\dagger_{si}(k_1)d^\dagger_{\bar{s}i}(k_2)\,|0\rangle \\ =&\sum_{s,\bar{s}}\int\frac{\mathrm{d}k_q^+\,\mathrm{d}^2k_{q\perp}P^+}{(2\pi)^3 2k_q^+(P^+-k_q^+)}\frac{1}{\sqrt{N_c}}\sum_{i=1}^{N_c}\psi^{(m_j)}_{s\bar{s}/h}(k_q,P-k_q)b^\dagger_{si}(k_q)d^\dagger_{\bar{s}i}(P-k_q)\,|0\rangle\ .\end{aligned} \tag{1.22}$$

k_q ($k_{\bar{q}}$) is the momentum of the quark (antiquark) and s ($\bar{s}$) is the spin projection. In the $|q\bar{q}\rangle$ sector, it is convenient to decouple the color configuration from the spatial and spin parts of the LFWFs. Here we write the color singlet configuration of the $q\bar{q}$ state, $1/\sqrt{3}(r\bar{r}+g\bar{g}+b\bar{b})$, explicitly with color index i and $N_c=3$ in the above equation. $\psi^{(m_j)}_{s\bar{s}/h}(k_q,k_{\bar{q}})$ contains the spacial and spin parts of the wavefunction. In terms of the relative momenta,

$$x\equiv\frac{k_q^+}{P^+},\qquad \vec{k}_\perp\equiv\vec{k}_{q\perp}-x\vec{P}_\perp\ . \tag{1.23}$$

The quarkonium state reads,

$$\begin{aligned}|h_{q\bar{q}}(P,j,m_j)\rangle =& \sum_{s,\bar{s}}\int_0^1\frac{\mathrm{d}x}{2x(1-x)}\int\frac{\mathrm{d}^2k_\perp}{(2\pi)^3}\psi^{(m_j)}_{s\bar{s}/h}(\vec{k}_\perp,x)\\ &\times\frac{1}{\sqrt{N_c}}\sum_{i=1}^{N_c}b^\dagger_{si}(xP^+,\vec{k}_\perp+x\vec{P}_\perp)d^\dagger_{\bar{s}i}((1-x)P^+,-\vec{k}_\perp+(1-x)\vec{P}_\perp)\,|0\rangle\ .\end{aligned} \tag{1.24}$$

The normalization relation of the valence LFWF $\psi^{(m_j)}_{s\bar{s}/h}(\vec{k}_\perp,x)$ is

$$\sum_{s,\bar{s}}\int_0^1\frac{\mathrm{d}x}{2x(1-x)}\int\frac{\mathrm{d}^2k_\perp}{(2\pi)^3}\psi^{(m_j')*}_{s\bar{s}/h'}(\vec{k}_\perp,x)\psi^{(m_j)}_{s\bar{s}/h}(\vec{k}_\perp,x)=\delta_{hh'}\delta_{m_j,m_j'}\delta_{h,h'}\ . \tag{1.25}$$

The normalization relation of the hadron state vector follows as

$$\langle h_{q\bar{q}}(P,j,m_j)|h'_{q\bar{q}}(P',j',m_j')\rangle=2P^+(2\pi)^3\delta^3(P-P')\delta_{hh'}\delta_{m_j,m_j'}\delta_{j,j'}\ . \tag{1.26}$$

www.manaraa.com

- $|q\bar{q}\rangle + |q\bar{q}q\bar{q}\rangle$

The projection of the quarkonium state on the $|q\bar{q}\rangle + |q\bar{q}q\bar{q}\rangle$ space reads,

$$
\begin{aligned}
|h_{q\bar{q}q\bar{q}}(P,j,m_j)\rangle = & \sum_{s,\bar{s}} \int \frac{\mathrm{d}k_q^+ \,\mathrm{d}^2 k_{q\perp}}{(2\pi)^3 2k_q^+}\theta(k_q^+) \int \frac{\mathrm{d}k_{\bar{q}}^+ \,\mathrm{d}^2 k_{\bar{q}\perp}}{(2\pi)^3 2k_{\bar{q}}^+}\theta(k_{\bar{q}}^+) 2P^+\theta(P^+)(2\pi)^3\delta^3(k_q + k_{\bar{q}} - P) \\
& \times \frac{1}{\sqrt{N_c}} \sum_{i=1}^{N_c} \psi^{(m_j)}_{s\bar{s}/h}(k_q, k_{\bar{q}}) b^\dagger_{si}(k_q) d^\dagger_{\bar{s}i}(k_{\bar{q}})\,|0\rangle \\
& + \int \prod_{i=1}^{4} \frac{\mathrm{d}k_i^+ \,\mathrm{d}^2 k_{i\perp}}{(2\pi)^3 2k_i^+}\theta(k_i^+) 2P^+\theta(P^+)(2\pi)^3\delta^3(k_1 + k_2 + k_3 + k_4 - P) \\
& \times \sum_{\{l_i,s_i\}} \psi^{(m_j)}_{s_1 s_2 s_3 s_4/h}(\{k_i, l_i\}) b^\dagger_{s_1 l_1}(k_1) d^\dagger_{s_2 l_2}(k_2) b^\dagger_{s_3 l_3}(k_3) d^\dagger_{s_4 l_4}(k_4)\,|0\rangle \\
= & \sum_{s,\bar{s}} \int_0^1 \frac{\mathrm{d}x}{2x(1-x)} \int \frac{\mathrm{d}^2 k_\perp}{(2\pi)^3} \psi^{(m_j)}_{s\bar{s}/h}(\vec{k}_\perp, x) \\
& \times \frac{1}{\sqrt{N_c}} \sum_{i=1}^{N_c} b^\dagger_{si}(xP^+, \vec{k}_\perp + x\vec{P}_\perp) d^\dagger_{\bar{s}i}((1-x)P^+, -\vec{k}_\perp + (1-x)\vec{P}_\perp)\,|0\rangle \\
& + \int \prod_{i=1}^{4} \frac{\mathrm{d}x_i \,\mathrm{d}^2 k_{i\perp}}{(2\pi)^3 2x_i} 2(2\pi)^3 \delta\Big(\sum x_i - 1\Big) \delta^2\Big(\sum \vec{k}_{i\perp}\Big) \\
& \times \sum_{\{l_i,s_i\}} \psi^{(m_j)}_{s_1 s_2 s_3 s_4/h}(\{\vec{k}_{i\perp}, x_i, l_i\}) b^\dagger_{s_1 l_1}(x_1 P^+, \vec{k}_{1\perp} + x_1\vec{P}_\perp) d^\dagger_{s_2 l_2}(x_2 P^+, \vec{k}_{2\perp} + x_2\vec{P}_\perp) \\
& \times b^\dagger_{s_3 l_3}(x_3 P^+, \vec{k}_{3\perp} + x_3\vec{P}_\perp) d^\dagger_{s_4 l_4}(x_4 P^+, \vec{k}_{4\perp} + x_4\vec{P}_\perp)\,|0\rangle \ .
\end{aligned}
\tag{1.27}
$$

The LFWFs in the $|q\bar{q}\rangle$ and the $|q\bar{q}q\bar{q}\rangle$ sectors are written as $\psi^{(m_j)}_{s\bar{s}/h}(\vec{k}_\perp, x)$ and $\psi^{(m_j)}_{s_1 s_2 s_3 s_4/h}(\{\vec{k}_{i\perp}, x_i\})$, respectively. Note that the valence part of the LFWF in this case, $\psi^{(m_j)}_{s\bar{s}/h}(\vec{k}_\perp, x)$, is different from the LFWF solved in the sole valence sector as in Eq. (1.22). The normalization relation of the physical state as in Eq. (1.20) now contains two contributions, one from the $|q\bar{q}\rangle$ sector and the other from the $|q\bar{q}q\bar{q}\rangle$ sector. The entire LFWF on the $|q\bar{q}\rangle + |q\bar{q}q\bar{q}\rangle$ space is normalized as

$$
\begin{aligned}
1 = & \sum_{s,\bar{s}} \int_0^1 \frac{\mathrm{d}x}{2x(1-x)} \int \frac{\mathrm{d}^2 k_\perp}{(2\pi)^3} |\psi^{(m_j)}_{s\bar{s}/h}(\vec{k}_\perp, x)|^2 \\
& + \int \prod_{i=1}^{4} \frac{\mathrm{d}x_i \,\mathrm{d}^2 k_{i\perp}}{(2\pi)^3 2x_i} 2(2\pi)^3 \delta\Big(\sum x_i - 1\Big) \delta^2\Big(\sum \vec{k}_{i\perp}\Big) \sum_{\{l_i,s_i\}} \Big|\psi^{(m_j)}_{s_1 s_2 s_3 s_4/h}(\{\vec{k}_{i\perp}, x_i, l_i\})\Big|^2 \ .
\end{aligned}
\tag{1.28}
$$

www.manaraa.com

1.3.2 The light-front Schrödinger equation

In light-front dynamics, the quantum state of the system is defined at fixed light-front time, x^+, and its dynamical evolution satisfies the Schrödinger equation,

$$i\frac{\partial}{\partial x^+}\left|\psi; x^+\right\rangle = \frac{1}{2}\hat{P}^-(x^+)\left|\psi; x^+\right\rangle \ . \tag{1.29}$$

P^- is the Hamiltonian that is conjugate to the light-front time x^+. $|\psi\rangle$ is an expansion in multi-particle occupation number Fock states, as we have discussed in Section 1.3.1. It could admit explicit time-dependence in general, as is typical for a system interacting with a background field. The problem could then be solved with given initial conditions.

$$\left|\psi; x^+\right\rangle = \mathcal{T}_+ \exp[-\frac{i}{2}\int_0^{x^+} \mathrm{d}z^+ \hat{P}^-(z^+)]\left|\psi; 0\right\rangle \ . \tag{1.30}$$

This is, however, a nontrivial task, since one would need to deal with the time-ordered integral. In the perturbation theory, one would expand the time-ordered exponential into series and only keep the first few terms. Such treatment would become less amenable for interactions with strong fields. It is of our interest to solve these problems in the non-perturbative regime. We decompose the time evolution operator into many small steps in light-front time x^+, and calculate the evolution of the state step by step. In doing so, we are able to access the intermediate states during the evolution, and reveal non-perturbative effects. This approach is known as the time-dependent Basis Light-Front Quantization (tBLFQ), and it is first brought up in 2013 where it was applied to solve a strong background field QED problem, the non-linear Compton scattering [37]. It is then followed by another investigation, the interaction of an electron with intense electromagnetic fields [38]. We will discuss the general procedure of the tBLFQ approach, and make its first application to a QCD problem, the quark-nucleus scattering, in Chapter 3.

For the investigation to the relativistic bound states, the Lagrangian does not have an explicit time dependence, Hamiltonian eigenvalue equation reduces to,

$$\hat{P}^-\left|\psi\right\rangle = P^-\left|\psi\right\rangle, \text{with } \ P^- = \frac{M^2 + \vec{P}_\perp^2}{P^+} \ . \tag{1.31}$$

The eigenstate can be labeled with six quantum numbers, the invariant mass M, the longitudinal momentum P^+, the transverse momentum $\vec{P}_\perp$, the generalized total spin j and its longitudinal projection m_j (cf.

www.manaraa.com

Eq. (1.17)), as

$$|\psi\rangle = |\psi; M, P^+, \vec{P}_\perp, j, m_j\rangle \ . \tag{1.32}$$

Solving Eq. (1.31) directly produces the mass eigenvalues M and the wavefunctions of the eigenstates. This is much easier than solving the instant form eigenvalue equation. First, the square-root operator in the instant form, $H = \sqrt{M^2 + \vec{P}^2}$, is replaced by a simpler dispersion relation. Second, we have $P^+ > 0$ by its definition $P^+ = P^0 + P^3 = \sqrt{M^2 + \vec{P}_\perp^2 + (P^3)^2} + P^3$ for massive quanta. This is crucial since it makes the light-front vacuum trivial, for which $P^+_{vac} = 0$. To form a zero-momentum state, each of the Fock particles must have vanishing k_a^+ so that $P^+ = \sum_a k_a^+ \to 0$, the Fock space vacuum $|0\rangle$ is then an exact eigenstate of the full light-front Hamiltonian. In contrast, in the instant form, the zero-momentum state ($\vec{P} = \sum_a \vec{k}_a = \vec{0}$) consists of an arbitrary number of Fock particles with either positive or negative components of $\vec{k}_a$, so the physical vacuum is very complicated. This makes it difficult to interpret the eigensolutions of the instant form Schrödinger equation. One might already notice that for QCD, with massless gluon quanta, it is possible to have a zero-momentum state ($P^+ = 0$) which is not zero-particle. This is known as the zero-mode. The curious readers of the light-front vacuum and zero modes are encouraged to read Chapter 7 of Ref. [33].

In the Fock space representation, the Hamiltonian eigenvalue equation, Eq. (1.31), becomes a matrix equation. A variety of methods have been developed to solve the eigenvalue equations, such as the transverse lattice [39], the similarity transformations [40], the coupled integral equation approach [41, 42]. The Discretized Light-Cone Quantization (DLCQ) uses the discretized momentum basis [43]. The discretization is achieved by imposing periodic (usually for bosons) or anti-periodic (usually for fermions) boundary condition in the coordinate space of a finite volume. Explicitly, $-L \le x^- \le L$, $-L_\perp \le x^1, x^2 \le L_\perp$, and the normalization volume is $\Omega = 2L(2L_\perp)^2$. There is a corresponding discrete grid in the momentum space: $p^+ \to n\pi/L$, $\vec{p}_\perp \to (n_x\pi/L, n_y\pi/L)$. One expands the quantum fields into plane wave states e^{-ipx}, Eqs. (1.10) and (1.11) become

$$\Psi_{\alpha cf}(x) = \sum_q \frac{1}{2L(2L_\perp)^2 2p^+} \left[b_q u_\alpha(p,\lambda) e^{-ip\cdot x} + d_q^\dagger v_\alpha(p,\lambda) e^{ip\cdot x} \right] , \tag{1.33}$$

$$A_{\mu a}(x) = \sum_q \frac{1}{2L(2L_\perp)^2 2p^+} \left[a_q \epsilon_\mu(p,\lambda) e^{-ip\cdot x} + a_q^\dagger \epsilon_\mu(p,\lambda)^* e^{ip\cdot x} \right] , \tag{1.34}$$

www.manaraa.com

where q contains the quantum numbers of single particle state, $\{n, n^1, n^2, \lambda, c(\text{color}), f(\text{flavor})\}$. In practical calculations, both the Fock space and the discretized momentum basis are truncated, and the eigenvalue equation is solved by diagonalizing the Hamiltonian matrix numerically. There have been a number of successful applications to field theories in two or more dimensions of the DLCQ approach [44].

Basis Light-Front Quantization (BLFQ) generalizes the discretized momentum basis of the DLCQ approach to any complete and orthogonal basis [1]. To put it explicitly, if $f_i(p^+)$ and $g_j(\vec{p}_\perp)$ are the basis functions, we can expand the field operators of Eqs. (1.10) and (1.11) on the basis as

$$b_q(p^+, \vec{p}_\perp) = \sum_{i,j} b_{\bar{q}} f_i(p^+) g_j(\vec{p}_\perp) \,. \tag{1.35}$$

where $\bar{q}$ is the shorthand for the set of quantum numbers with i and j. Optimal choices of the basis functions usually preserve the symmetries of the Hamiltonian and approximate the eigenstates, so as to achieve efficiency for numerical computations.

The BLFQ approach has been applied to solve a range of QED and QCD problems with success. The QED applications include the positronium [45], the electron anomalous magnetic moment [46] and electron generalized parton distribution [47]. The applications to QCD include the heavy quarkonium [48, 3], the unequal mass heavy mesons [49] and the charged light mesons [50]. There are also other works in process, including the heavy-light system, the light mesons, the baryons and the glueballs [51, 52]. We will discuss the BLFQ approach in more details, with its application to the heavy quarkonium in Chapter 2.

www.manaraa.com

CHAPTER 2. BASIS LIGHT-FRONT QUANTIZATION APPROACH TO BOUND STATES

In this chapter, we study the QCD bound-state systems in the Basis Light-Front Quantization (BLFQ) approach. In particular, we investigate the heavy quarkonium system. We review the formalism for solving the quarkonium system with the effective Hamiltonian approach and the application in the $|q\bar{q}\rangle$ sector. Then we extend the framework to the $|q\bar{q}\rangle + |q\bar{q}q\bar{q}\rangle$ sectors. We further study the properties of the quarkonium through electromagnetic processes, via calculating the elastic form factors, the radiative transition form factors and the decay widths.

2.1 The heavy quarkonium

Heavy quarkonium is the bound-state system of quark-antiquark pair, and it is often dubbed as the "hydrogen atom" of Quantum Chromodynamics(QCD) though it has a closer kinship with positronium. It provides an ideal testing ground for various investigations to understand QCD [53].

The quarkonium state $|\psi_h\rangle$ is an eigenstate of the light-front Hamiltonian, and satisfies

$$H_{LF}\,|\psi_h\rangle = M_h^2\,|\psi_h\rangle \ , \tag{2.1}$$

where $H_{LF} = P^+P^- + \vec{P}_\perp^2$ is the light-front Hamiltonian and M_h is the mass of the bound state. Each eigenstate $|\psi_h\rangle$ can be labeled with six eigenvalues, M_h, P^+, $\vec{P}_\perp$, the total spin j and its longitudinal projection m_j.

Projecting the Hamiltonian eigenvalue equation of Eq. (2.1) onto the Fock space results in an infinite number of coupled integral eigenvalue equations. The solutions of these equations consist of the spectrum and the corresponding wavefunctions, which could fully describe the bound state system. Fock states can be defined in terms of the eigenstates of the free-field Hamiltonian, i.e., the light-front kinetic operator, and

www.manaraa.com

can be obtained by applying the creation operators on the Fock vacuum $|0\rangle$:

$$\begin{aligned} Q_0 &\equiv |q\bar{q}:\ k_i^+, \vec{k}_{i\perp}, \lambda_i\rangle = b^\dagger_{\lambda_1}(k_1) d^\dagger_{\lambda_2}(k_2)\,|0\rangle \\ Q_1 &\equiv |q\bar{q}g:\ k_i^+, \vec{k}_{i\perp}, \lambda_i\rangle = b^\dagger_{\lambda_1}(k_1) d^\dagger_{\lambda_2}(k_2) a^\dagger_{\lambda_3}(k_3)\,|0\rangle \\ Q_2 &\equiv |q\bar{q}q\bar{q}:\ k_i^+, \vec{k}_{i\perp}, \lambda_i\rangle = b^\dagger_{\lambda_1}(k_1) d^\dagger_{\lambda_2}(k_2) b^\dagger_{\lambda_3}(k_3) d^\dagger_{\lambda_4}(k_4)\,|0\rangle \\ &\dots \end{aligned} \tag{2.2}$$

For convenience, we have labeled the various Fock states with index $n = 1, 2, \ldots$. Each Fock state Q_n is an eigenstate of P^+ and $\vec{P}_\perp$, satisfying $P^+ = \sum_i k_i^+$ and $\vec{P}_\perp = \sum_i \vec{k}_\perp$.

In practical calculations, only a finite number of the leading Fock sectors are considered. The eigenvalue equation, Eq. (2.1), can be written explicitly on the finite Fock basis truncated as,

$$\sum_{j=1}^{N} H_{ij}\,|\psi_j\rangle = M_h^2\,|\psi_i\rangle \qquad \text{for all } i = 1, 2, \ldots, N\,. \tag{2.3}$$

We define the block matrices $H_{ij} \equiv Q_i H_{LF} Q_j$, and the projected eigenstates $|\psi_i\rangle \equiv Q_i\,|\psi_h\rangle$. One could then proceed to solve the coupled matrix equations in Eq. (2.3). The resulting eigenstate can be written as $|\psi_h\rangle = \sum_{n=1}^{N} \int \mathrm{d}[k_i] Q_n\,|\psi_n\rangle$.

Even with a finite truncation scheme, solving the Hamiltonian matrix becomes a major challenge in numerical calculations with increasing number of Fock sectors. Could we include the physics from higher Fock sectors while carrying out the calculation at a smaller feasible Fock space? A well known and widely used method is the effective interactions. In field theories, it was first introduced by I.Tamm [41] and rediscovered by S.M.Dancoff [42] to describe the two nucleon forces. It reduces and solves the field equations according to the number of Fock particles.

Although the Tamm-Dancoff approach was applied originally in the instant form, we can derive it analogously in the front form. The Fock space could be arbitrarily divided into two parts, namely the P-space and the Q-space. By choosing a specific partition, we wish to formulate an effective potential acting only in the P-space but including the effects generated by the Q-space. The Hamiltonian matrix equation, Eq. (2.3), can then be rewritten as a coupled matrix equation involving the block matrices $H_{\alpha\beta} \equiv \langle\alpha|H_{LF}|\beta\rangle$ and the

www.manaraa.com

projected eigenfunctions $|\psi_h\rangle_\alpha = \langle\alpha|\psi_h\rangle$ with $(\alpha, \beta = P, Q)$:

$$H_{PP}\,|\psi\rangle_P + H_{PQ}\,|\psi\rangle_Q = \omega\,|\psi\rangle_P \ , \tag{2.4a}$$

$$H_{QP}\,|\psi\rangle_P + H_{QQ}\,|\psi\rangle_Q = \omega\,|\psi\rangle_Q \ . \tag{2.4b}$$

The mass eigenvalue is unknown at this point, and it is written as $\omega = M_h^2$ in the above equations. One can express the Q-space wavefunction $|\psi_h\rangle_Q$ in terms of the P-space wavefunction $|\psi_h\rangle_P$ from Eq. (2.4b) as,

$$|\psi\rangle_Q = \frac{1}{\omega - H_{QQ}} H_{QP}\,|\psi\rangle_P \ . \tag{2.5}$$

Plugging it into Eq. (2.4a), we arrive at an eigenvalue equation with an "effective Hamiltonian" acting only in the P-space:

$$H_{\rm eff}\,|\psi\rangle_P = \omega\,|\psi\rangle_P \ , \tag{2.6}$$

with

$$H_{\rm eff} = H_{PP} + H_{PQ}\frac{1}{\omega - H_{QQ}} H_{QP} \ . \tag{2.7}$$

We can see that the effective interaction contains two parts: the original block matrix H_{PP}, and a contribution where the system is scattered virtually into the Q-space and then scattered back to the P-space.

One key problem now is to compute the energy denominator $(\omega - H_{QQ})^{-1}$, since the value of ω is unknown before solving the equations. One could start with some fixed value of ω as the "starting point energy" and calculate $M_h^2(\omega)$ from the eigenvalue equation. The true eigenvalues are determined by varying ω until $\omega = M_h^2(\omega)$ [54, 55]. This procedure, involving inverting a Q-space matrix, however, does not seem to reduce the numerical work of diagonalizing the (P+Q)-space matrix directly. An alternative way is to substitute the eigenvalue ω by T^*, the average kinetic energy of the initial and final P-space states [56]. The idea is to reduce the matrix $\omega - H_{QQ}$ to its dominant term as a c-number. The Q-space matrix H_{QQ} splits into a diagonal kinetic term T_{QQ} and an off-diagonal interaction term U_{QQ}. The inverse matrix could then be written as

$$\frac{1}{\omega - H_{QQ}} = \frac{1}{T^* - T_{QQ} - \delta U(\omega)}, \qquad \delta U(\omega) = \omega - T^* - U_{QQ} \ . \tag{2.8}$$

In the case of a sufficiently small $\delta U(\omega)$, the energy denominator can be approximated by the kinetic energy $T^* - T_{QQ}$, which no longer depends on the energy eigenvalue.

www.manaraa.com

2.1.1 Heavy quarkonium in the valence Fock sector

In solving bound state systems with effective Hamiltonian approaches, the simplest P-space one can choose is the valence Fock sector. For heavy quarkonium, constituent quark models have shown reasonable first approximations in non-relativistic potential models [57, 58]. In the following, we illustrate the formulation of the effective Hamiltonian in the valence Fock sector by choosing $Q_0 = |q\bar{q}\rangle$ as the P-space and $Q_1 = |q\bar{q}g\rangle$ as the Q-space. The eigenvalue equation now reads (signifying the Q_i by its index "i" in the following),

$$\left(H_{00} + H_{01}\frac{1}{\omega - H_{11}}H_{10}\right)\psi_0 = \omega\psi_0 \ . \tag{2.9}$$

We can write the Hamiltonian as a summation of the kinetic energy and the interaction operator, $H = T + U$. The diagonal block H_{ii} contains T_{ii} and U_{ii}, and the off-diagonal block is $H_{ij} = U_{ij}$, $(i \neq j)$. The interaction matrix U is illustrated in Table 2.1.

Table 2.1 The interaction matrix U for a meson in the Fock space $|q\bar{q}\rangle + |q\bar{q}g\rangle$. The matrix elements are represented by diagrams. For each diagram where the gluon couples to the quark, there also exists a corresponding diagram with the gluon coupling to the antiquark. Diagrams in the red frames are excluded by gauge cutoff, see details in the text.

Q_n sector	$Q_0 = \|q\bar{q}\rangle$	$Q_1 = \|q\bar{q}g\rangle$
$Q_0 = \langle q\bar{q}\|$	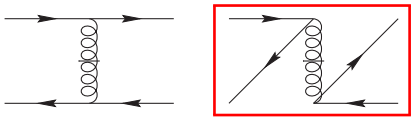	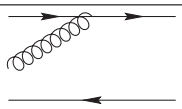
$Q_1 = \langle q\bar{q}g\|$	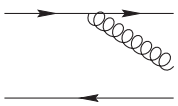	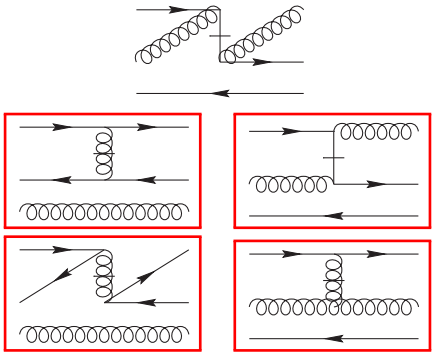

www.manaraa.com

We first focus on the denominator of the second term in Eq. (2.9). To maintain the gauge invariance in the truncated Fock space, we implement the "gauge cutoff" formulated by Tang, Brodsky, and Pauli [59], that is, the instantaneous parton graph is only retained if the corresponding propagating parton graph contributes in the truncated theory. As a consequence, some instantaneous interactions in U_{00} and U_{11} are excluded. For example, the left diagram in the second row of U_{11} should not be considered since the corresponding $|q\bar{q}gg\rangle$ sector is absent in the model. Those excluded terms are marked with red frames in Table 2.1. The second diagram in U_{00} also vanishes for another reason: zero for the color factor. We further adopt the approximation $\delta U(\omega) \approx 0$ in Eq. (2.8), i.e. $U_{11} \to 0$. In principle, this approximation can be improved systematically by performing an expansion in $\delta U(\omega)$ and retaining terms order-by-order in that expansion. The energy denominator now reduces to $T^* - T_{11}$.

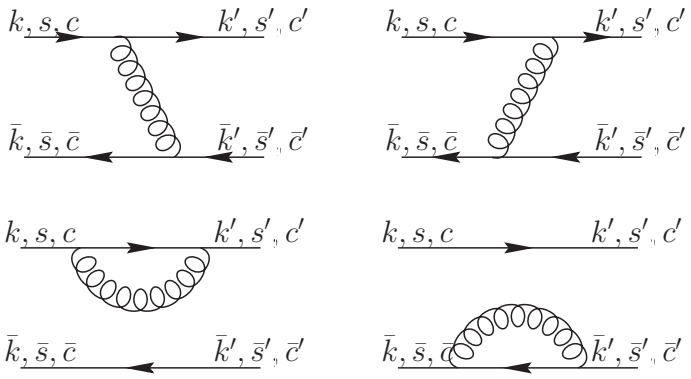

Figure 2.1 Iterated interactions generated in the two-body effective interaction. The top two panels are the gluon-exchange diagrams. The bottom two panels are the fermion-self-energy contributions. Each fermion lines are labled by its momentum (k), spin (s) and color (c).

The first term in Eq. (2.9), H_{00}, contains an instantaneous gluon-exchange interaction, U_{00}. The second term, by stitching U_{01} and U_{10}, generates both fermion-self-energy loops and exchanges of gluons between the quark and the antiquark as shown in Fig. 2.1. We simplify the interaction by neglecting the self-energy terms in these investigations and we will adopt the strategy of using quark masses as adjustable parameters (called "constituent quarks"). The remaining one-gluon exchange can be combined together with the instantaneous contributions from U_{00} into one term, namely V_{OGE}. In the BLFQ formalism of ref. [3], the

www.manaraa.com

one-gluon exchange term reads,

$$V_{\rm OGE} = -\frac{C_F 4\pi\alpha_s(q^2)}{q^2}\bar{u}_{s'}(k')\gamma_\mu u_s(k)\bar{v}_{\bar{s}}(\bar{k})\gamma^\mu v_{\bar{s}'}(\bar{k}') \ . \tag{2.10}$$

The energy denominator can now be interpreted as the average 4-momentum squared carried by the exchanged gluon, $q^2 = -(1/2)(k'-k)^2-(1/2)(\bar{k}'-\bar{k})^2$. C_F is the color factor of the one-gluon exchange diagram, and its calculation follows the corresponding QCD vertices [60]. Here the initial and final quark-antiquark pairs are both in the color singlet configuration, thereby $C_F = 1/4(1/\sqrt{3}c'^\dagger T^\alpha c)(1/\sqrt{3}c^\dagger T^\alpha c') = 4/3$, where T^α ($\alpha = 1,\ldots,8$) are the Gell-Mann matrices and c, c' = red, blue, green are the color vectors, their expressions can be found in Appendix A.7. The overall"-" sign in Eq. (2.10) results from the anti-communitation relation of the fermion fields in calculating the vertices, in analogy to the Coulomb potential between two opposite charges in electrodynamics. This term implements the short-distance physics between the quark and the antiquark, and determines the spin structure of the mesons. The eigenvalue equation of Eq. (2.9) then reduces to

$$(T_{00} + V_{\rm OGE})\psi_0 = \omega_0\psi_0 \ . \tag{2.11}$$

The one-gluon exchange interaction $V_{\rm OGE}$ is identical to the one-photon exchange in quantum electrodynamics (QED), except for the color factor. The eigenvalue equation of Eq. (2.11) with the one-photon exchange has been applied to the positronium system in the basis function approach by Ref. [45]. In the relative coordinate presentation, the kinetic term can be written as $T_{00} = (\vec{k}_\perp^2 + m_q^2)/x + (\vec{k}_\perp^2 + m_{\bar{q}}^2)/(1-x)$. $x = p_q^+/P^+$ is the longitudinal momentum fraction of the quark and $\vec{k}_\perp = \vec{k}_{q\perp} - x\vec{P}_\perp$ is the relative transverse momentum.

One can imagine that expanding the Q-space directly would introduce more interaction terms. Apart from the standard way of including interactions from a finite Q-space, phenomenological approaches also bring valuable insights. Light-front holography constructs an effective Hamiltonian based on inspirations from string theory. It addresses confinement, an essential feature of QCD, by holographic mapping gravity in a higher-dimensional anti-de Sitter(AdS) space to light-front dynamics [61]. In the soft-wall model, a 2-dimensional soft-wall confinement originates from the gravitational background field [62]. Y. Li et al. further improved the confinement by including the longitudinal degree of freedom [48, 3],

$$V_{\rm confinement} = \kappa^4 x(1-x)r_\perp^2 - \frac{\kappa^4}{(m_q + m_{\bar{q}})^2}\partial_x(x(1-x)\partial_x) \ . \tag{2.12}$$

www.manaraa.com

κ is the strength of the confinement, $r_\perp = |\vec{r}_{q\perp} - \vec{r}_{\bar{q}\perp}|$ is the transverse separation of the partons. This phenomenological confinement takes into account the long-distance physics, and provides another approximation to QCD. The eigenvalue equation provides a more extensive model of QCD by absorbing the confining potential,

$$(T_{00} + V_{\rm OGE} + V_{\rm confinement})\psi_0 = \omega\psi_0 \ . \tag{2.13}$$

Conventionally, all the contributions in the Hamiltonian excluding the kinetic energy are combined and the resulting interaction is referred to as the effective interaction, $V_{\rm eff} = V_{\rm OGE} + V_{\rm confinement}$. The mass spectrum and LFWFs are the direct solutions of the eigenvalue equation, and could be obtained as in BLFQ by diagonalizing the Hamiltonian in a basis representation.

2.1.1.1 Basis Representation of $|q\bar{q}\rangle$ sector

Solving the eigenvalue equation of Eq. (2.13) following BLFQ in a basis function approach is advantageous. In solving the heavy quarkonium system, the work in Ref. [3] chooses the eigenfunctions of part of the Hamiltonian, $T_{00} + V_{\rm confinement}$, as the basis functions, which largely reduces the numerical efforts. The basis consists of the 2D harmonic oscillator (HO) function ϕ_{nm} in the transverse direction, and the modified Jacobi polynomial χ_l in the longitudinal direction. The transverse basis function is

$$\phi_{nm}(\vec{k}_\perp) = \kappa^{-1}\sqrt{\frac{4\pi n!}{(n+|m|)!}}\left(\frac{k_\perp}{\kappa}\right)^{|m|}\exp(-(k_\perp)^2/(2\kappa^2))L_n^{|m|}((k_\perp)^2/\kappa^2)\exp(im\theta)\ , \tag{2.14}$$

where $k_\perp = |\vec{k}_\perp|$ and $\theta = \arg k_\perp$. $n = 0, 1, 2, \ldots$ is the principal number and $m = 0, \pm1, \pm2, \ldots$ is the orbital number. Its orthonormality relation is

$$\int \frac{\mathrm{d}^2\vec{k}_\perp}{(2\pi)^2}\phi^*_{n'm'}(\vec{k}_\perp)\phi_{nm}(\vec{k}_\perp) = \delta_{nn'}\delta_{mm'} \ . \tag{2.15}$$

The longitudinal basis function is

$$\chi_l(x) = \sqrt{4\pi(2l+\alpha+\beta+1)}\sqrt{\frac{\Gamma(l+1)\Gamma(l+\alpha+\beta+1)}{\Gamma(l+\alpha+1)\Gamma(l+\beta+1)}}x^{\beta/2}(1-x)^{\alpha/2}P_l^{(\alpha,\beta)}(2x-1)\ , \tag{2.16}$$

where $P_l^{(\alpha,\beta)}$ is the Jacobi polynomial. Its orthonormality relation is

$$\frac{1}{4\pi}\int_0^1 \mathrm{d}x\chi_l(x)\chi_{l'}(x) = \delta_{ll'} \ . \tag{2.17}$$

www.manaraa.com

Each basis state is thus characterized by five quantum numbers $\{n, m, l, s, \bar{s}\}$, where $s(\bar{s})$ is the spin of the quark(antiquark). The basis is constructed to conserve the magnetic projection of the total angular momentum: $m_j = m + s + \bar{s}$. m is interpreted as the orbital angular momentum projection. The basis space is truncated by their reference energies in dimensionless units:

$$2n + |m| + 1 \leq N_{\max}, \qquad 0 \leq l \leq L_{\max}. \tag{2.18}$$

Consequently, the $N_{\max}$-truncation provides a natural pair of UV and IR cutoffs: $\Lambda_{\perp,\mathrm{UV}} \simeq \kappa \sqrt{N_{\max}}$, $\lambda_{\perp,\mathrm{IR}} \simeq \kappa/\sqrt{N_{\max}}$. $L_{\max}$ represents the resolution of the basis in the longitudinal direction $\Delta x \approx L_{\max}^{-1}$, which also provides a pair of UV and IR cutoffs $\Lambda_{z,\mathrm{UV}} \simeq m_h \sqrt{L_{\max}}$, $\lambda_{z,\mathrm{IR}} \simeq m_h/\sqrt{L_{\max}}$, and m_h is the mass eigenvalue of the hadron.

The light-front wavefunction is an expansion on this basis function representation:

$$\psi^{(m_j)}_{s\bar{s}/h}(\vec{k}_\perp, x) = \sum_{n,m,l} \psi_h(n, m, l, s, \bar{s})\, \phi_{nm}(\vec{k}_\perp/\sqrt{x(1-x)})\chi_l(x). \tag{2.19}$$

$\psi_h(n, m, l, s, \bar{s})$ is the coefficient of the corresponding basis $\{n, m, l, s, \bar{s}\}$, and is obtained from diagonalizing the Hamiltonian.

The spectrum obtained from Eq. (2.13) in Ref. [3] agrees with the PDG data with an r.m.s mass deviation of 30 to 40 MeV for states below the open flavor thresholds. The light-front wavefunctions have been used to calculate several observables and are in reasonable agreement with experiments and other theoretical approaches [63, 64, 65, 66, 67, 9, 10]. We will discuss its applications in determining the elastic form factors and the transition form factors in the later sections.

2.1.2 Extension to higher Fock sectors

Solving the heavy quarkonium system in a larger Fock space could bring new aspects and richer interpretations of non-perturbative dynamics. In the last section, we see that the one-gluon exchange effective potential V_{OGE} provides an appealing first approximation to the role of quark-gluon coupling in QCD. In this section, we extend the P-space to $|q\bar{q}\rangle + |q\bar{q}q\bar{q}\rangle$ and keep the Q-space as $|q\bar{q}g\rangle$. This extension on the Fock space is consistent with the holographic QCD, where the Fock states of hadrons can have any number of extra $q\bar{q}$ pairs created by the confining potential but no constituent dynamical gluons [68]. The eigenvalue

www.manaraa.com

equation in the extended P-space now reads (where the subscript "2" represents the space of the two-quark-two-antiquark states),

$$\left(H_{00}+H_{01}\frac{1}{\omega-H_{11}}H_{10}\right)\psi_0+\left(H_{01}\frac{1}{\omega-H_{11}}H_{12}+H_{02}\right)\psi_2=\omega\psi_0\ , \tag{2.20a}$$

$$\left(H_{20}+H_{21}\frac{1}{\omega-H_{11}}H_{10}\right)\psi_0+\left(H_{21}\frac{1}{\omega-H_{11}}H_{12}+H_{22}\right)\psi_2=\omega\psi_2\ . \tag{2.20b}$$

The interaction matrix U is illustrated in Table 2.2. We adopt the same gauge cutoff as in last section, and drop U_{11} in the energy denominator as a simplification and an approximation.

Table 2.2 The interaction matrix U for the quarkonium in the Fock space $|q\bar{q}\rangle+|q\bar{q}q\bar{q}\rangle+|q\bar{q}g\rangle$. The matrix elements are represented by diagrams. For each diagram where the gluon couples to the quark, there is a corresponding diagram with the gluon coupling to the antiquark. The diagram in the red frame is excluded by gauge cutoff. Diagrams in U_{00} and U_{11} that are excluded by gauge cutoff are not shown here, see Table 2.1 for reference.

Q_n sector	$Q_0=\|q\bar{q}\rangle$	$Q_2=\|q\bar{q}q\bar{q}\rangle$	$Q_1=\|q\bar{q}g\rangle$
$Q_0=\langle q\bar{q}\|$	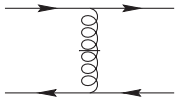	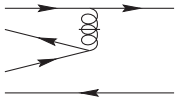	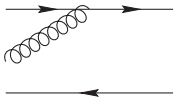
$Q_2=\langle q\bar{q}q\bar{q}\|$	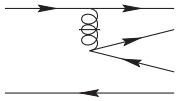	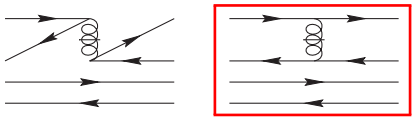	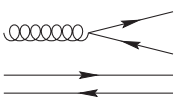
$Q_1=\langle q\bar{q}g\|$	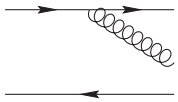	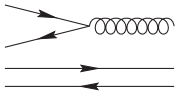	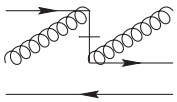

Let us first analyze the block matrices within Q_0 and Q_2 respectively. The first term in Eq. (2.20a) is exactly the same as that in the valence eigenvalue equation, Eq. (2.9). There we isolate the kinetic energy and the one-gluon exchange contribution, and introduce a confining potential. We now generalize this procedure to Q_2 sector through the second term in Eq. (2.20b). The Hamiltonian in this term contains the kinetic energy T_{22} and an internal-annihilation-creation term, $V_{\rm IAC}\equiv U_{22}+H_{21}H_{12}/(T^*-T_{11})$. U_{22} is the instantaneous gluon contribution and is illustrated in Table. 2.2. The iterated interaction generates the non-instantaneous contribution, shown in Fig. 2.2.

www.manaraa.com

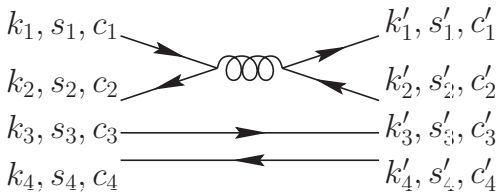

Figure 2.2 The internal-annihilation-creation interaction generated by stitching U_{21} and U_{12}. This term and U_{22} together form the full internal-annihilation-creation term $V_{\rm IAC}$. Each fermion lines are labeled by its momentum (k), spin (s) and color (c).

We can write out $V_{\rm IAC}$ explicitly in analogy to $V_{\rm OGE}$,

$$V_{\rm IAC} = \frac{C_{F22}4\pi\alpha_s(q^2)}{q^2}\bar{u}_{s'_1}(k'_1)\gamma_\mu v_{s'_2}(k'_2)\bar{v}_{s_2}(k_2)\gamma^\mu u_{s_1}(k)\ . \tag{2.21}$$

The energy denominator, $q^2 = -(1/2)(k_1+k_2)^2 - (1/2)(k'_1+k'_2)^2$, is the average 4-momentum squared carried by the intermediate gluon. $C_{F22} = 1/4(c'^\dagger_1 T^\alpha c'_2)(c^\dagger_2 T^\alpha c_1)(c'^\dagger_3 c_3)(c^\dagger_4 c'_4)$ is the color factor. In this term, both the initial and the final $q\bar{q}q\bar{q}$-states are in the color singlet configurations. If c_1 and c_2 form a color singlet, $C_{F22} = 1/4(1/3T^\alpha_{ii})(1/3T^\alpha_{jj}) = 0$; if c_1 and c_2 are in the color octet state, $C_{F22} = 1/4(1/(2\sqrt{2})T^\alpha_{ij})(1/(2\sqrt{2})T^\alpha_{ji}) = 1/2$. $i, j = 1, 2, 3$ are dummy indices, see Appendix A.7 for the matrix format of T^α.

Now let us study the off-diagonal blocks in Eq. (2.20), which connects the two Fock sectors in the P-space, Q_0 and Q_2. Each of the two blocks also consists of an instantaneous contribution U_{02}, and a non-instantaneous contribution. The later is illustrated in Fig. 2.3. We combine the two contributions into one term, and name it as the one-gluon-binding interaction, $V_{\rm OGB}$.

$$\begin{aligned} V_{\rm OGB} = &-\frac{C_{F12}4\pi\alpha_s(q^2)}{q^2}\bar{u}_{s_1}(k_1)\gamma_\mu u_s(k)\bar{u}_{s_2}(k_2)\gamma^\mu v_{s_3}(k_3) \\ &+\frac{C_{F12}4\pi\alpha_s(q^2)}{q^2}\bar{v}_{\bar{s}}(\bar{k})\gamma_\mu v_{s_4}(k_4)\bar{u}_{s_2}(k_2)\gamma^\mu v_{s_3}(k_3)\ . \end{aligned} \tag{2.22}$$

The color factor is $C_{F12} = 1/4(c^\dagger_1 T^\alpha c)(c^\dagger_2 T^\alpha c_3)(c^\dagger_4 \bar{c})$ according to the notations in the first diagram of Fig. 2.3. The second diagram of Fig. 2.3 has the same color factor. From earlier discussion, we know that if c_2 and c_3 form a color singlet, the color factor would be 0. Therefore, in order to get a non-vanishing contribution, we must have $c_2 = c$, and let c_1 and c_3 form a color singlet. The resulting color factor is $C_{F12} = 1/4(1/3T^\alpha_{ji})(1/\sqrt{3}T^\alpha_{ij}) = 4\sqrt{3}/9$.

www.manaraa.com

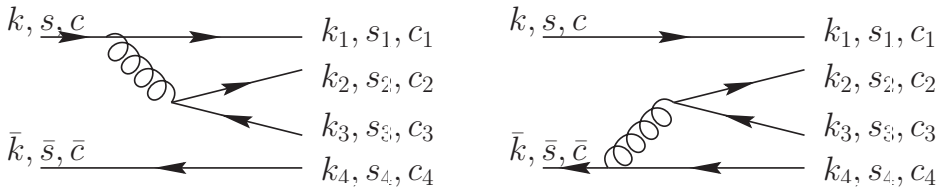

Figure 2.3 Iterated interactions generated by stitching U_{01} and U_{12}. Each fermion lines are labeled by its momentum (k), spin (s) and color (c).

We include the confining potential and extend it to the Q_2 sector and write the eigenvalue equation, Eq. (2.20) as,

$$(T_{00} + V_{\rm OGE} + V_{\rm confinement})\psi_0 + V^*_{\rm OGB}\psi_2 = \omega\psi_0 \ , \tag{2.23a}$$

$$V_{\rm OGB}\psi_0 + (T_{22} + V_{\rm IAC} + V_{\rm confinement,2})\psi_2 = \omega\psi_2 \ . \tag{2.23b}$$

In the single particle representation (as opposed to the relative motion representation discussed above for the $|q\bar{q}\rangle$ sector), the kinetic term can be written as $T_{22} = \sum_{i=1}^{4}(\vec{k}^2_{i\perp} + m_q^2)/x_i$. $V_{\rm confinement,2}$ is the confining potential in the Q_2 sector,

$$V_{\rm confinement,2} = \kappa^4 \sum_{i,j(i<j)} x_i x_j r^2_{ij,\perp} - \frac{\kappa^4}{(2m_f)^2} \sum_{i,j(i<j)} \partial_{x_i}(x_i x_j \partial_{x_j}) \ . \tag{2.24}$$

$r_{ij,\perp} = |\vec{r}_{i,\perp} - \vec{r}_{j,\perp}|$ is the transverse separation between the i-th and j-th partons. $x_i = p_i^+/P^+$ is the longitudinal momentum fraction of the i-th parton. In Eq. (2.24), we did not impose any dependence on the color structure of the Fock state as in the Q_0 sector of Eq. (2.12). One other possible treatment to take the same color factor as in the $V_{\rm IAC}$ term, C_{F22}. Solving the coupled equations(Eq. (2.23)) directly would lead to the mass spectrum and light-front wavefunctions in the $Q_0 + Q_2$ Fock space.

For heavy quarkonium system, the Q_0 sector is expected to provide the dominant contribution to the eigenstates so we consider using perturbation theory to find an approximation to the exact solutions. The unperturbed Hamiltonian is that in the $P = Q_0$ and $Q = Q_1$ space, and the unperturbed wavefunction is ψ_0 obtained from Eq. (2.13). The perturbation Hamiltonian is the $V_{\rm OGB}$ term, and it can be recognized by comparing the unperturbed eigenvalue equation, Eq. (2.13) and the perturbed one, Eq. (2.23a). We can now solve ψ_2 by plugging the unperturbed wavefunction ψ_0 into Eq. (2.23b). We could thereby obtain the full

www.manaraa.com

$P(= Q_0 + Q_2)$-space wavefunction according to the normalization relation, $|\psi_0|^2 + |\psi_2|^2 = 1$. The perturbed mass eigenvalue is obtained as $M_h'^2 = \omega_0|\psi_0|^2 + \omega_2|\psi_2|^2$.

An even simpler treatment is to omit the interaction within the Q_2 sector and neglect the perturbation on the mass eigenvalue. Then the Q_2 wavefunction could be solved from Eq. (2.23b) directly as $\psi_2 = V_{\rm OGB}\psi_0/(\omega_0 - T_{22})$. One could then renormalize the total light-front wavefunction to unity.

2.1.2.1 Basis representation of $|q\bar{q}q\bar{q}\rangle$ sector

We consider two identical quarks and two identical antiquarks in the $|q\bar{q}q\bar{q}\rangle$ sector. We know that the total wavefunction in the $|q\bar{q}q\bar{q}\rangle$ sector, consisting of the space, spin and color parts as $\psi = \psi_{\rm spatial}\psi_{\rm spin}\psi_{\rm color}$, should be antisymmetric under the exchange of identical fermions. For convenience, we label the two quarks as q_1, q_3 and the two antiquarks as $\bar{q}_2, \bar{q}_4$.

In the color space, there are two possible color singlet states. Following the notation in Ref. [69], these two states read,

$$\begin{aligned}\psi^A_{\rm color} &= (q_1q_3)^{\bar{3}} \otimes (\bar{q}_2\bar{q}_4)^3 = \frac{1}{\sqrt{12}}\epsilon^{\alpha\beta\gamma}\epsilon_{\alpha\lambda\sigma}q_{1,\beta}q_{3,\gamma}\bar{q}_2^{\lambda}\bar{q}_4^{\sigma}\ ,\\ \psi^S_{\rm color} &= (q_1q_3)^{6} \otimes (\bar{q}_2\bar{q}_4)^{\bar{6}} = \frac{1}{\sqrt{6}}d^{\alpha\beta\gamma}d_{\alpha\lambda\sigma}q_{1,\beta}q_{3,\gamma}\bar{q}_2^{\lambda}\bar{q}_4^{\sigma}\ ,\end{aligned} \tag{2.25}$$

where $d^{\alpha\beta\gamma}$ and $d_{\alpha\lambda\sigma}$ are

$$\begin{aligned}&d^{111} = d_{111} = d^{222} = d_{222} = d^{333} = d_{333} = 1,\\ &d^{412} = d_{412} = d^{421} = d_{421} = d^{523} = d_{523} = d^{532} = d_{532} = d^{613} = d_{613} = d^{631} = d_{631} = \frac{1}{\sqrt{2}}\ .\end{aligned} \tag{2.26}$$

$\psi^A_{\rm color}(\psi^S_{\rm color})$ is antisymmetric(symmetric) under transposition of q_1 and q_3 or $\bar{q}_2$ and $\bar{q}_4$. These two color singlet states are orthonormal by means of the irreducible representation of color SU(3).

We formulate the space-spin basis states using the single particle basis representation. Here we follow the basis constructed in Ref. [1] where the basis space consists of the 2D harmonic oscillator for the transverse modes and a discretized momentum space basis for the longitudinal modes. The 2D harmonic oscillator states are characterized by their principal quantum number $n = 0, 1, 2, \ldots$ and orbital quantum number $m = 0, \pm1, \pm2, \ldots$. The longitudinal modes are defined on $-L \le x^- \le L$ with periodic boundary

www.manaraa.com

conditions. The longitudinal momentum faction reads $x = k/K$ with $k = 1, 2, \ldots, K$, where K is the total longitudinal momentum and we neglect zero modes. As such, we can build the space-spin basis with quantum numbers, $\{\alpha_1, \alpha_2, \alpha_3, \alpha_4\}$, $\alpha_i = \{n_i, m_i, k_i, s_i\}$, where $i = 1, 2, 3, 4$ stands for the four partons. The chosen symmetries and cutoffs are expressed in terms of the sums over those quantum numbers, $M_t = \sum_i m_i$, $S = \sum_i S_i$, $\sum_i k_i = K$ and $\sum_i (2n_i + |m_i| + 1) \leq N_{\max}$. The magnetic projection of the total angular momentum is $m_j = M_t + S$. We only consider distinct states. For example, at $N_{\max} = K = 4$, there is only one distinct space-spin state at $m_j = 0$, and that is $\{\alpha_1 = \{0, 0, 1, -1/2\}, \alpha_2 = \{0, 0, 1, 1/2\}, \alpha_3 = \{0, 0, 1, -1/2\}, \alpha_4 = \{0, 0, 1, 1/2\}\}$. The number of distinct basis states for different $K = N_{\max}$ cases are shown in Table. 2.3.

Table 2.3 Number of distinct space-spin basis states in the $|q\bar{q}q\bar{q}\rangle$ sector at different $K = N_{\max}$ values. In the first case, M_t and S are conserved separately, as quoted from Ref. [1]. In the second case, the magnetic projection for the total angular momentum $m_j = M_t + S$ is conserved, which we will use in constructing the basis.

$K = N_{\max}$	4	6	8	10	12
$M_t = 0, S = 0$ [1]	1	236	5961	64240	427730
$m_j = 0$	1	336	10295	121808	860470

We then construct (anti)symmetric basis states using those distinct states as,

$$
\begin{aligned}
[\psi_{\text{spatial}}\psi_{\text{spin}}]^S &= \frac{1}{2}(\{\alpha_1, \alpha_2, \alpha_3, \alpha_4\} + \{\alpha_3, \alpha_2, \alpha_1, \alpha_4\} + \{\alpha_1, \alpha_4, \alpha_3, \alpha_2\} + \{\alpha_3, \alpha_4, \alpha_1, \alpha_2\}) \,, \\
[\psi_{\text{spatial}}\psi_{\text{spin}}]^A &= \frac{1}{2}(\{\alpha_1, \alpha_2, \alpha_3, \alpha_4\} - \{\alpha_3, \alpha_2, \alpha_1, \alpha_4\} - \{\alpha_1, \alpha_4, \alpha_3, \alpha_2\} + \{\alpha_3, \alpha_4, \alpha_1, \alpha_2\}) \,,
\end{aligned}
\tag{2.27}
$$

where $\alpha_1 \neq \alpha_3$ and $\alpha_2 \neq \alpha_4$. It is then straightforward to construct the basis states in the full space-spin-color space as $[\psi_{\text{spatial}}\psi_{\text{spin}}]^S \psi^A_{\text{color}}$ and $[\psi_{\text{spatial}}\psi_{\text{spin}}]^A \psi^S_{\text{color}}$.

An alternative way of constructing the color states is to treat the $q\bar{q}q\bar{q}$ state as two diquarks. This is particularly useful in considering the quarkonium decaying into two color singlets, such as the radiative decay $J/\psi \to \eta_c \gamma$. In this bases, there are two color singlet states,

$$
\begin{aligned}
\psi^1_{\text{color}} &= (q_1\bar{q}_2)^1 \otimes (q_3\bar{q}_4)^1 = \frac{1}{3} q_1^i \bar{q}_2^i q_3^j \bar{q}_4^j \,, \\
\psi^8_{\text{color}} &= (q_1\bar{q}_2)^8 \otimes (q_3\bar{q}_4)^8 = \frac{1}{2\sqrt{2}} (q_1^i \bar{q}_2^j - \frac{1}{3}\delta_{i,j} q_1^k \bar{q}_2^k)(q_3^j \bar{q}_4^i - \frac{1}{3}\delta_{i,j} q_3^k \bar{q}_4^k) \,,
\end{aligned}
\tag{2.28}
$$

www.manaraa.com

where $i, j, k = 1, 2, 3$ are the color indices of the quark and the antiquark. There is a one-to-one correspondence between the two bases in Eqs. (2.25) and (2.28),

$$\begin{aligned}\psi^1_{\text{color}} &= \frac{1}{\sqrt{3}}\psi^A_{\text{color}} + \sqrt{\frac{2}{3}}\psi^S_{\text{color}}\,,\\ \psi^8_{\text{color}} &= -\sqrt{\frac{2}{3}}\psi^A_{\text{color}} + \frac{1}{\sqrt{3}}\psi^S_{\text{color}}\,.\end{aligned} \tag{2.29}$$

Having defined the BLFQ framework for expanding the Fock space of the mesons, we note that the path is prepared for detailed calculations to follow which is outside the scope of the present work. We return to treat observables calculated with the light-front wavefunctions evaluated in the quark-antiquark Fock space.

2.2 The elastic form factor

In quantum field theory, the elastic electromagnetic form factors characterize the structure of a bound state system, which generalize the multipole expansion of the charge and current densities in the nonrelativistic quantum mechanics. The physical process that determines the elastic form factors is $\psi_h(P) + \gamma^{(*)}(q = P' - P) \to \psi_h(P')$. The form factors are defined as the Lorentz invariants arising in the Lorentz structure decomposition of the hadron matrix element $\langle\psi_h(P')|J^\mu(0)|\psi_h(P)\rangle$. For spin-j particles, assuming charge conjugation, parity and time reversal symmetries, there are $2j + 1$ independent Lorentz invariant form factors. The derivation of Lorentz covariant decomposition of hadron matrix elements can be found in Appendix D.

In calculating the form factors from the hadron matrix elements, one has the freedom of choosing current components and reference frames. Though in principle, those different choices should lead to the same result, different results could arise in practical calculations in a finite Fock space due to the violation of Lorentz symmetry. Here we derive the elastic form factors in light-front coordinates with different current components, and without specifying a reference frame at the outset. For this purpose, we first define a parameter space of the reference frame. Our discussions of the elastic form factor and the transition form factor in the next section will also follow this definition of frames.

www.manaraa.com

2.2.1 Frames and kinematics

Considering the process $\psi_A(P') \to \psi_B(P) + X(q = P' - P)$ or $\psi_B(P) + X(q = P' - P) \to \psi_A(P')$, the Lorentz invariant momentum transfer q^2 can be written as a function of two boost invariants [65, 10] according to the four-momentum conservation $q^2 = (P' - P)^2$,

$$q^2 = z m_A^2 - \frac{z}{1-z} m_B^2 - \frac{1}{1-z} \vec{\Delta}_\perp^2 \ . \tag{2.30}$$

where,

$$z \equiv (P'^+ - P^+)/P'^+, \qquad \vec{\Delta}_\perp \equiv \vec{q}_\perp - z\vec{P}'_\perp \ .$$

Both z and $\vec{\Delta}_\perp$ are invariant under the transverse Lorentz boost specified by the velocity vector $\vec{\beta}_\perp$,

$$v^+ \to v^+, \quad \vec{v}_\perp \to \vec{v}_\perp + v^+ \vec{\beta}_\perp \ . \tag{2.31}$$

z can be interpreted as the relative momentum transfer in the longitudinal direction, and $\vec{\Delta}_\perp$ describes the momentum transfer in the transverse direction. Note that z is restricted to $0 \le z < 1$ by definition. For each possible value of q^2, the values of the pair $(z, \vec{\Delta}_\perp)$ are not unique, and those different choices correspond to different reference frames (up to longitudinal and transverse light-front boost transformations). Fig. 2.4 should help visualize the functional form of $q^2(z, \vec{\Delta}_\perp)$. Since q^2 is relevant to the magnitude of $\vec{\Delta}_\perp$ but not its angle, we plot it in the $\arg \vec{\Delta}_\perp = 0, \pi$ plane. Form factors evaluated at different $(z, \vec{\Delta}_\perp)$ but at the same q^2 could reveal the frame dependence. In particular, we introduce two special frames for detailed consideration.

- Drell-Yan frame $(z = 0)$: $q^+ = 0$, $\vec{\Delta}_\perp = \vec{q}_\perp$ and $q^2 = -\vec{\Delta}_\perp^2$. This frame is shown as a single thick solid line in each panel of Fig. 2.4. The Drell-Yan frame is conventionally used together with the plus current J^+ to calculate the electromagnetic form factors. This choice, on the one hand, avoids spurious effects related to the orientation of the null hyperplane where the light-front wavefunction is defined and, on the other hand, it suppresses the contributions from the often-neglected pair creation process, at least for pseudoscalar mesons [70, 71, 72, 73, 74, 75]. For the transition form factor, this is only true if zero-mode contributions are neglected. The transition form factor obtained in the Drell-Yan frame is significantly restricted in the space-like region, i.e. $q^2 \le 0$. Although one could analytically continuate the form factor to the time-like region by changing $\vec{q}_\perp$ to $i\vec{q}_\perp$ [76, 77, 78], we elect to calculate transition form factors directly from wavefunctions.

www.manaraa.com

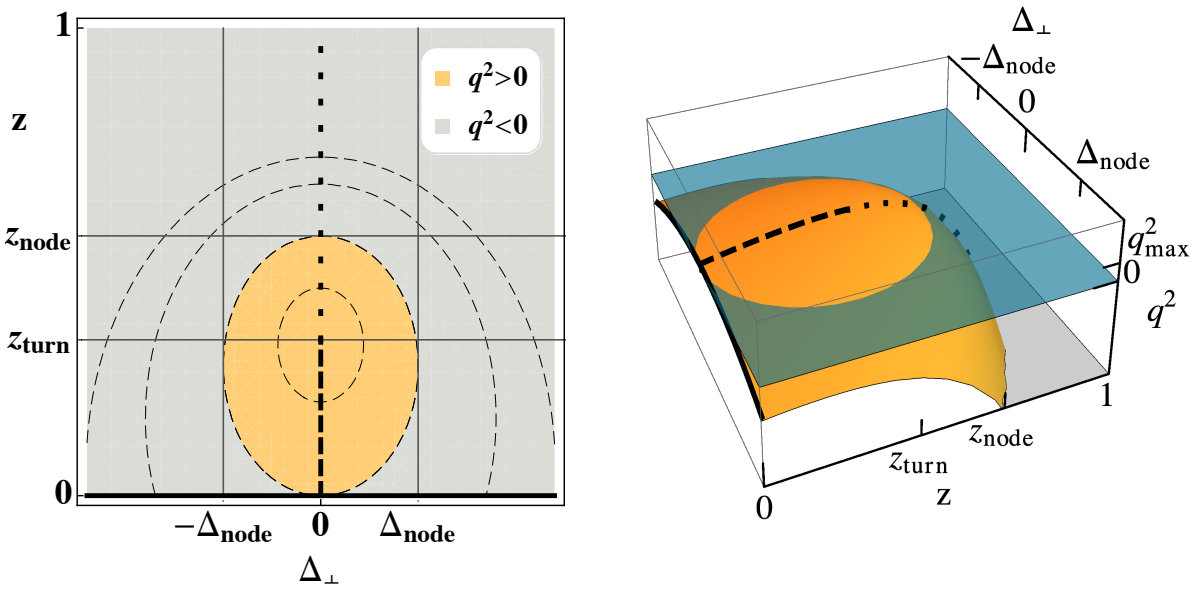

(a) Regional plot of $q^2(\Delta_\perp, z)$

(b) 3D plot of $q^2(\Delta_\perp, z)$

Figure 2.4 Visualization of the Lorentz invariant momentum transfer squared q^2 as a function of z and $\vec{\Delta}_\perp$ at $\arg \vec{\Delta}_\perp = 0, \pi$. (a): regional plot of q^2. The time-like region ($q^2 > 0$) is the orange oval shape, bounded by $\Delta_{\rm node} = (m_A^2 - m_B^2)/2m_A$ and $z_{\rm node} = 1 - m_B^2/m_A^2$. The space–like region ($q^2 < 0$) is in light gray. Contour lines of q^2 are indicated with thin dashed curves. The maximal value $q^2_{\rm max} = (m_A - m_B)^2$ occurs at ($z_{\rm turn} = 1 - m_B/m_A, \Delta_\perp = 0$). (b): 3D plot of q^2 showing a convex shape in the $(z, \Delta_\perp)$ representation. The blue flat plane is the reference plane of $q^2 = 0$. In each figure, the Drell-Yan frame is shown as a thick solid line, and the longitudinal I and II frames are shown as thick dotted and thick dashed lines respectively. (Figure adapted from Ref. [10].)

www.manaraa.com

- longitudinal frame ($\vec{\Delta}_\perp = 0$): $q^2 = zm_A^2 - zm_B^2/(1-z)$. Note that we use the same definition for the longitudinal frame as in Ref. [65, 10], which is different from those in the literature where $\vec{q}_\perp = 0$ is called the longitudinal frame [79, 80, 72, 78]. In this frame, we have access to the kinematic region up to $q^2_{\rm max} = (m_A - m_B)^2$, the point where the final meson does not recoil. This maximal value occurs at $z = 1 - m_B/m_A \equiv z_{\rm turn}$. For a given q^2, there are two solutions for z, corresponding to either the positive or the negative recoil direction of the final meson relative to the initial meson, namely,
  - longitudinal-I: $z = \left[m_A^2 - m_B^2 + q^2 + \sqrt{(m_A^2 - m_B^2 + q^2)^2 - 4m_A^2 q^2}\,\right]/(2m_A^2)$. $z_{\rm turn} \le z < 1$. This branch joins the second branch at $q^2 = q^2_{\rm max}$ with $z = z_{\rm turn}, \vec{\Delta}_\perp = 0$. The time-like region is accessed at $z_{\rm turn} \le z < z_{\rm node}$, and the space-like region is at $z_{\rm node} \le z < 1$, where $z_{\rm node} \equiv 1 - m_B^2/m_A^2$. The longitudinal-I frame is shown as thick dotted lines in Fig. 2.4.
  - longitudinal-II: $z = \left[m_A^2 - m_B^2 + q^2 - \sqrt{(m_A^2 - m_B^2 + q^2)^2 - 4m_A^2 q^2}\,\right]/(2m_A^2)$. $0 \le z \le z_{\rm turn}$. This second branch only exists in the time-like region, and it joins the Drell-Yan frame at $q^2 = 0$ with $z = 0, \vec{\Delta}_\perp = 0$. The longitudinal-II frame is shown as thick dashed lines in Fig. 2.4.

2.2.2 The hadron matrix element

The electromagnetic transition between two hadron states ψ_A and ψ_B is governed by the matrix element $\langle \psi_B(P, j, m_j)| J^\mu(x) |\psi_A(P', j', m'_j)\rangle$. The elastic process is a special case where $\psi_A = \psi_B$. In this section, we derive the light-front wavefunction representation of the hadron matrix element, which we will use later in calculating the elastic form factor and the transition form factor.

The electromagnetic (EM) current operator is defined as $J^\mu = \bar{\Psi}\gamma^\mu\Psi$. In the light-front representation,

$$J^\mu(x) = \sum_{\lambda_1,\lambda_2} \int \frac{\mathrm{d}^2 p_{1\perp}\,\mathrm{d}p_1^+}{(2\pi)^3 2p_1^+} \int \frac{\mathrm{d}^2 p_{2\perp}\,\mathrm{d}p_2^+}{(2\pi)^3 2p_2^+} \left[b^\dagger_{\lambda_2 c_2}(p_2)\bar{u}_{\lambda_2}(p_2)e^{ip_2\cdot x} + d_{\lambda_2 c_2}(p_2)\bar{v}_{\lambda_2}(p_2)e^{-ip_2\cdot x}\right] \gamma^\mu \left[b_{\lambda_1 c_1}(p_1)u_{\lambda_1}(p_1)e^{-ip_1\cdot x} + d^\dagger_{\lambda_1 c_1}(p_1)v_{\lambda_1}(p_1)e^{ip_1\cdot x}\right] . \tag{2.32}$$

www.manaraa.com

By spacetime translation invariance,

$$\begin{aligned}
&\langle\psi_B(P,j,m_j)|J^\mu(x)\,|\psi_A(P',j',m'_j)\rangle \\
&\quad=\langle\psi_B(P',j',m'_j)|\,\bar\Psi(x)\gamma^\mu\Psi(x)\,|\psi_A(P,j,m_j)\rangle \\
&\quad=\langle\psi_B(P,j,m_j)|\,e^{-i\hat px}\bar\Psi(0)e^{i\hat px}\gamma^\mu e^{-i\hat px}\Psi(0)e^{i\hat px}\,|\psi_A(P',j',m'_j)\rangle \\
&\quad=\langle\psi_B(P,j,m_j)|\,e^{-iPx}\bar\Psi(0)\gamma^\mu\Psi(0)e^{iP'x}\,|\psi_A(P',j',m'_j)\rangle \\
&\quad=\langle\psi_B(P,j,m_j)|\,J^\mu(0)\,|\psi_A(P',j',m'_j)\rangle\,e^{i(P'-P)x}\ .
\end{aligned}\tag{2.33}$$

The argument x only results in an overall phase factor, so in the literature one usually take $J^\mu(0)$ in calculating the matrix element.

We have shown in Section 1.3.1 that the meson state vector $|\psi_h(P,j,m_j)\rangle$ can be expanded in the light-front Fock space. The coefficients of the Fock expansion are the complete set of n-particle light-front wavefunctions, $\{\psi^{(m_j)}_{n/h}(x_i,\vec k_{i\perp},s_i)\}$. $x_i\equiv\kappa_i^+/P^+$ is the longitudinal momentum fraction of the i-th parton, and $\vec k_{i\perp}\equiv\vec\kappa_{i\perp}-x\vec P_\perp$ is the relative transverse momenta, with κ_i being the momenta of the corresponding parton. s is the spin of the parton. The electromagnetic current matrix element is in general given by the sum of the diagonal $n\to n$ and off-diagonal $n+2\to n$ transitions, as shown in Fig. 2.5.

$$\langle\psi_B|\,J^\mu\,|\psi_A\rangle=\langle\psi_B|\,J^\mu\,|\psi_A\rangle_{n\to n}+\langle\psi_B|\,J^\mu\,|\psi_A\rangle_{n+2\to n}\ .\tag{2.34}$$

In the former case, the external photon is coupled to a quark or an antiquark. In the latter case, a quark-antiquark pair is annihilated into the external photon.

2.2.2.1 $n\to n$ transition

For the $n\to n$ term, as in Fig. 2.5(a), the external photon is coupled to a quark or an antiquark, thus the electromagnetic current matrix element takes the form

$$\begin{aligned}
\langle\psi_B(P,j,m_j)|\,J^\mu(0)\,|\psi_A(P',j',m'_j)\rangle_{n\to n}&=\sum_n\prod_{i=1}^n\sum_{s'_i,s_1,l_i}\int_z^1\frac{\mathrm{d}x'_1}{2x'_1}\int_0^1\frac{\mathrm{d}x'_{i(i\neq1)}}{2x'_i}\int\frac{\mathrm{d}^2k'_{i\perp}}{(2\pi)^3}2(2\pi)^3\\
&\times\delta\left(\sum_{i=1}^n x'_i-1\right)\delta^{(2)}\left(\sum_{i=1}^n\vec k'_{i\perp}\right)\psi^{(m_j)*}_{n/B}(\{x_i,\vec k_{i\perp},s_i,l_i\})\,j^\mu_{s_1,s'_1}\,\psi^{(m'_j)}_{n/A}(\{x'_i,\vec k'_{i\perp},s'_i,l_i\})\ ,
\end{aligned}\tag{2.35}$$

www.manaraa.com

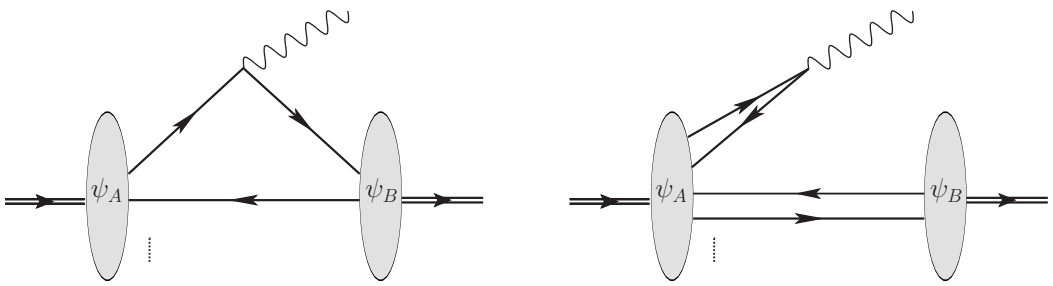

(a) $n \to n$ transition (b) $n+2 \to n$ transition

Figure 2.5 Light-front wavefunction representation of the hadron matrix element. The double-lines represents the hadrons. The solid lines represent the partons. The wavy lines represent the external photon. The shaded areas represent the light-front wavefunctions. These diagrams are ordered by light-front time x^+, which flows from left to right. In (a), the $n \to n$ transition, parton number is conserved, whereas in (b), the $n+2 \to n$ transition, parton number is reduced by 2 due to pair annihilation. (Figure adapted from Ref. [10].)

where the EM current $j^\mu_{s_1,s_1'} = \bar{u}_{s_1'}(\kappa_1')\gamma^\mu u_{s_1}(\kappa_1)$ if the struck parton is a quark, and $j^\mu_{s_1,s_1'} = \bar{v}_{s_1}(\kappa_1)\gamma^\mu v_{s_1'}(\kappa_1')$ if the struck parton is an antiquark. We will restore the quark charge in the current when calculating observables. l_i is the color index of the i-th parton. The relative coordinates and constraint conditions of partons are

$$\begin{cases} x_1' = x_1 + z(1-x_1), \vec{k}_{1\perp}' = \vec{k}_{1\perp} + (1-x_1)\vec{\Delta}_\perp, l_1 = l_1', & \text{for the struck parton } (i=1) \\ x_i' = x_i(1-z), \vec{k}_{i\perp}' = \vec{k}_{i\perp} - x_i\vec{\Delta}_\perp, l_i = l_i', s_i = s_i', & \text{for the spectators } (i=2,\ldots,n)\,. \end{cases} \tag{2.36}$$

Note that the condition of $x_1 \in [0,1]$ sets the valid range of x_1' to $[z,1]$, see the bounds of the integral over x_1' in Eq. (2.35).

www.manaraa.com

A detailed derivation of the $2 \to 2$ transition

In the case where the hadrons are solved in the $|q\bar{q}\rangle$ Fock sector, only the $n \to n$ ($n = 2$) term would contribute to the transition,

$$
\begin{aligned}
&\langle \psi_{q\bar{q}/B}(P, j, m_j)|J^{\mu}(0)\,|\psi_{q\bar{q}/A}(P', j', m'_j)\rangle \\
&\quad = \frac{1}{N_c}\sum_{i,j=1}^{N_c}\langle 0|\sum_{s,\bar{s}}\int_0^1 \frac{\mathrm{d}x}{2x(1-x)}\int\frac{\mathrm{d}^2k_{\perp}}{(2\pi)^3}\psi^{(m_j)*}_{s\bar{s}/B}(\vec{k}_{\perp}, x) \\
&\quad d_{j\bar{s}}((1-x)P^+, -\vec{k}_{\perp}+(1-x)\vec{P}_{\perp})b_{js}(xP^+, \vec{k}_{\perp}+x\vec{P}_{\perp}) \\
&\quad \times\sum_{\lambda_1,\lambda_2}\int\frac{\mathrm{d}^2\vec{p}^1_{\perp}\,\mathrm{d}p_1^+}{(2\pi)^3 2p_1^+}\int\frac{\mathrm{d}^2\vec{p}^2_{\perp}\,\mathrm{d}p_2^+}{(2\pi)^3 2p_2^+}\left[b^{\dagger}_{\lambda_2 c_2}(p_2)\bar{u}_{\lambda_2}(p_2)+d_{\lambda_2 c_2}(p_2)\bar{v}_{\lambda_2}(p_2)\right] \\
&\quad \gamma^{\mu}\left[b_{\lambda_1 c_1}(p_1)u_{\lambda_1}(p_1)+d^{\dagger}_{\lambda_1 c_1}(p_1)v_{\lambda_1}(p_1)\right] \\
&\quad \times\sum_{s',\bar{s}'}\int_0^1\frac{\mathrm{d}x'}{2x'(1-x')}\int\frac{\mathrm{d}^2\vec{k}'_{\perp}}{(2\pi)^3}\psi^{(m'_j)}_{s'\bar{s}'/A}(\vec{k}'_{\perp}, x') \\
&\quad b^{\dagger}_{is'}(x'P'^+, \vec{k}'_{\perp}+x'\vec{P}'_{\perp})d^{\dagger}_{i\bar{s}'}((1-x')P', -\vec{k}'_{\perp}+(1-x')\vec{P}'_{\perp})\,|0\rangle\ .
\end{aligned}
\tag{2.37}
$$

There are two non-vanishing terms as we pair up the creation and annihilation operators. One is the contribution from the quark radiation and the other from the antiquark. We will use J^{μ}_q ($J^{\mu}_{\bar{q}}$) as the operator acting on the quark (antiquark).

$$
\begin{aligned}
&\langle \psi_{q\bar{q}/B}(P, j, m_j)|\,J^{\mu}_q(0)\,|\psi_{q\bar{q}/A}(P', j', m'_j)\rangle \\
&= \frac{1}{N_c}\sum_{i,j=1}^{N_c}\langle 0|\sum_{s,\bar{s}}\int_0^1 \frac{\mathrm{d}x}{2x(1-x)}\int\frac{\mathrm{d}^2k_{\perp}}{(2\pi)^3}\psi^{(m_j)*}_{s\bar{s}/B}(\vec{k}_{\perp}, x) \\
&\quad d_{j\bar{s}}((1-x)P^+, -\vec{k}_{\perp}+(1-x)\vec{P}_{\perp})b_{js}(xP^+, \vec{k}_{\perp}+x\vec{P}_{\perp}) \\
&\quad \times\sum_{\lambda_1,\lambda_2}\int\frac{\mathrm{d}^2\vec{p}^1_{\perp}\,\mathrm{d}p_1^+}{(2\pi)^3 2p_1^+}\int\frac{\mathrm{d}^2\vec{p}^2_{\perp}\,\mathrm{d}p_2^+}{(2\pi)^3 2p_2^+}b^{\dagger}_{\lambda_2 c_2}(p_2)\bar{u}_{\lambda_2}(p_2)\gamma^{\mu}b_{\lambda_1 c_1}(p_1)u_{\lambda_1}(p_1) \\
&\quad \times\sum_{s',\bar{s}'}\int_0^1\frac{\mathrm{d}x'}{2x'(1-x')}\int\frac{\mathrm{d}^2\vec{k}'_{\perp}}{(2\pi)^3}\psi^{(m'_j)}_{s\bar{s}/A}(\vec{k}'_{\perp}, x') \\
&\quad b^{\dagger}_{is'}(x'P'^+, \vec{k}'_{\perp}+x'\vec{P}'_{\perp})d^{\dagger}_{i\bar{s}'}((1-x')P', -\vec{k}'_{\perp}+(1-x')\vec{P}'_{\perp})\,|0\rangle
\end{aligned}
\tag{2.38}
$$

www.manaraa.com

Contracting the creation and annihilation operators,

$$
\begin{aligned}
&\langle\psi_{q\bar{q}/B}(P,j,m_j)|\, J_q^\mu(0)\,|\psi_{q\bar{q}/A}(P',j',m_j')\rangle \\
=&\frac{1}{N_c}\sum_{i,j=1}^{N_c}\sum_{\lambda_1,\lambda_2}\sum_{s',\bar{s}'}\sum_{s,\bar{s}}\int\frac{\mathrm{d}^2\vec{p}_\perp^{\,1}\,\mathrm{d}p_1^+}{(2\pi)^3 2p_1^+}\int\frac{\mathrm{d}^2\vec{p}_\perp^{\,2}\,\mathrm{d}p_2^+}{(2\pi)^3 2p_2^+}\int_0^1\frac{\mathrm{d}x'}{2x'(1-x')} \\
&\int\frac{\mathrm{d}^2\vec{k}'_\perp}{(2\pi)^3}\int_0^1\frac{\mathrm{d}x}{2x(1-x)}\int\frac{\mathrm{d}^2k_\perp}{(2\pi)^3}\psi^{(m_j')}_{s'\bar{s}'/A}(\vec{k}'_\perp,x')\psi^{(m_j)*}_{s\bar{s}/B}(\vec{k}_\perp,x) \\
&2p_2^+\theta(p_2^+)(2\pi)^3\delta(p_2^+-xP^+)\delta^2(\vec{p}_\perp^{\,2}-\vec{k}_\perp-x\vec{P}_\perp)\delta_{j,c_2}\delta_{s,\lambda_2} \\
&2p_1^+\theta(p_1^+)(2\pi)^3\delta(p_1^+-x'P'^+)\delta^2(\vec{p}_\perp^{\,1}-\vec{k}'_\perp-x'\vec{P}'_\perp)\delta_{i,c_1}\delta_{s',\lambda_1} \\
&2(1-x)P^+\theta(P^+)(2\pi)^3\delta((1-x')P'^+-(1-x)P^+) \\
&\delta^2(-\vec{k}'_\perp+(1-x')\vec{P}'_\perp+\vec{k}_\perp-(1-x)\vec{P}_\perp)\delta_{j,i}\delta_{\bar{s}',\bar{s}} \\
&\bar{u}_{\lambda_2}(p_2)\gamma^\mu u_{\lambda_1}(p_1)\,.
\end{aligned}
\tag{2.39}
$$

We could first integrate over x and $\vec{k}_\perp$ by the last two delta functions and get,

$$
x=1-(1-x')P'^+/P^+,\qquad \vec{k}_\perp=\vec{k}'_\perp-(1-x')\vec{P}'_\perp+(1-x)\vec{P}_\perp\,. \tag{2.40}
$$

Integrate over p_1, p_2, we get

$$
\begin{aligned}
&\langle\psi_{q\bar{q}/B}(P,j,m_j)|\, J_q^\mu(0)\,|\psi_{q\bar{q}/A}(P',j',m_j')\rangle \\
=&\sum_{s,\bar{s}}\int_{\max(0,1-P^+/P'^+)}^1\frac{\mathrm{d}x'}{2x'(1-x')}\int\frac{\mathrm{d}^2k'_\perp}{(2\pi)^3}\frac{1}{x}\sum_{s'}\psi^{(m_j')}_{s'\bar{s}/A}(\vec{k}'_\perp,x')\psi^{(m_j)*}_{s\bar{s}/B}(\vec{k}_\perp,x) \\
&\times\bar{u}_s(xP^+,\vec{k}_\perp+x\vec{P}_\perp)\gamma^\mu u_{s'}(x'P'^+,\vec{k}'_\perp+x'\vec{P}'_\perp)\,.
\end{aligned}
\tag{2.41}
$$

Note that the lower bound of the integral over x is not 0 when $P^+<P'^+$, which results from the condition $x\in[0,1]$. However, when evaluating the x'-integral numerically, it would be more convenient to have the integral range as $[0,1]$. This is actually possible by integrating over x' and $\vec{k}'_\perp$ instead in Eq. (2.39),

$$
\begin{aligned}
&\langle\psi_{q\bar{q}/B}(P,j,m_j)|\, J_q^\mu(0)\,|\psi_{q\bar{q}/A}(P',j',m_j')\rangle \\
=&\sum_{s,\bar{s}}\int_{\max(0,1-P'^+/P^+)}^1\frac{\mathrm{d}x}{2x(1-x)}\int\frac{\mathrm{d}^2\vec{k}_\perp}{(2\pi)^3}\frac{1}{x'}\sum_{s'}\psi^{(m_j')}_{s'\bar{s}/A}(\vec{k}'_\perp,x')\psi^{(m_j)*}_{s\bar{s}/B}(\vec{k}_\perp,x) \\
&\times\bar{u}_s(xP^+,\vec{k}_\perp+x\vec{P}_\perp)\gamma^\mu u_{s'}(x'P'^+,\vec{k}'_\perp+x'\vec{P}'_\perp)\,,
\end{aligned}
\tag{2.42}
$$

www.manaraa.com

where

$$x' = 1 - (1-x)P^+/P'^+, \qquad \vec{k}'_\perp = \vec{k}_\perp - (1-x)\vec{P}_\perp + (1-x')\vec{P}'_\perp \ . \tag{2.43}$$

As expected, the lower bound of the integral over x is 0 when $P^+ < P'^+$. Eqs. (2.41) and (2.42) are equivalent, and one could choose the one that facilitates the numerical calculations. If one considers the process $\psi_A(P') \to \psi_B(P) + \gamma^{(*)}(q = P' - P)$ where $P^+ < P'^+$, it is more convenient to use the expression in Eq. (2.42). However, if one considers the process $\psi_A(P') + \gamma^{(*)}(q = P - P') \to \psi_B(P)$, which is usually the case in calculating the elastic form factor, where $P^+ > P'^+$, it would be more convenient to use the expression in Eq. (2.41). In analogy, we get the hadron matrix element of the antiquark current,

$$\begin{aligned}
&\langle \psi_{q\bar{q}/B}(P, j, m_j)|\, J^\mu_{\bar{q}}(0)\, |\psi_{q\bar{q}/A}(P', j', m'_j)\rangle \\
&= -\sum_{s,\bar{s}} \int_0^{\min(1, P^+/P'^+)} \frac{\mathrm{d}x'}{2x'(1-x')} \int \frac{\mathrm{d}^2 k'_\perp}{(2\pi)^3} \frac{1}{1-x} \sum_{\bar{s}'} \psi^{(m_j)*}_{s\bar{s}/B}(\vec{k}_\perp, x) \psi^{(m'_j)}_{s\bar{s}'/A}(\vec{k}'_\perp, x') \\
&\times \bar{v}_{\bar{s}'}((1-x')P'^+, -\vec{k}'_\perp + (1-x')\vec{P}'_\perp)\gamma^\mu v_{\bar{s}}((1-x)P^+, -\vec{k}_\perp + (1-x)\vec{P}_\perp) \ ,
\end{aligned} \tag{2.44}$$

where

$$x = x'P'^+/P^+ \ , \qquad \vec{k}_\perp = \vec{k}'_\perp + x'(P^+\vec{P}'_\perp - P'^+\vec{P}_\perp)/P^+ \ . \tag{2.45}$$

The "-" sign in Eq. (2.44) implies the negative charge of the antiquark.

2.2.2.2 $n+2 \to n$ transition

For the $n+2 \to n$ term, as in Fig. 2.5(b), a quark and an antiquark from the initial state annihilate into a photon, thus the electromagnetic current matrix element takes the form

$$\begin{aligned}
\langle \psi_B(P, j, m_j)|\, J^\mu\, |\psi_A(P', j', m'_j)\rangle_{n+2\to n} &= \sum_n \prod_{i=1}^{n+2} \sum_{s'_i, l'_i} \int_0^z \frac{\mathrm{d}x'_1}{2x'_1} \int_0^1 \frac{\mathrm{d}x'_{i(i\neq 1,2)}}{2x'_i} \int \frac{\mathrm{d}^2 k'_{i\perp}}{(2\pi)^3} 2(2\pi)^3 \\
&\times \delta\left(\sum_{i=1}^{n+2} x'_i - 1\right) \delta^{(2)}\left(\sum_{i=1}^{n+2} \vec{k}'_{i\perp}\right) \psi^{(m_j)*}_{n/B}(\{x_i, \vec{k}_{i\perp}, s_i, l_i\}) j^\mu_{s'_1, s'_2} \psi^{(m'_j)}_{n+2/A}(\{x'_i, \vec{k}'_{i\perp}, s'_i, l'_i\}) \ ,
\end{aligned} \tag{2.46}$$

www.manaraa.com

where the EM current is $j^{\mu}_{s'_1,s'_2} = \bar{v}_{s'_1}(\kappa'_2)\gamma^{\mu}u_{s'_2}(\kappa'_1)$ and the parton coordinates/constraints are

$$\begin{cases} x'_1, \vec{k}'_1, & \text{for the struck quark} \\ x'_2 = z - x'_1, \vec{k}'_2 = -\vec{k}'_1 + \vec{\Delta}_\perp, l'_2 = l'_1, & \text{for the struck antiquark} \\ x'_{i+2} = x_i(1-z), \vec{k}'_{i+2\perp} = \vec{k}_{i\perp} - x_i\vec{\Delta}_\perp, l_i = l'_{i+2}, s_i = s'_{i+2}, & \text{for the spectators}(i = 1, \ldots, n) \ . \end{cases} \tag{2.47}$$

2.2.3 Elastic form factor of the spin-0 particle

The elastic form factor of a (pseudo)scalar ψ_h is the charge form factor $F(q^2)$, defined as

$$\langle \psi_h(P')|J^{\mu}(0)|\psi_h(P)\rangle = (P+P')^{\mu}F(q^2) \ , \tag{2.48}$$

The charge form factor $F(q^2)$ is interpreted as the Fourier transformation of the charge density in the system. For heavy quarkonium, the physical from factor vanishes due to charge conjugation symmetry, so in order to study such issues as dependence on the chosen current component (see below) we calculate the fictitious form factor from the quark current, J^{μ}_q. In the light-front wavefunction representation of the valence Fock sector, the hadron matrix element reads

$$\begin{aligned} \langle \psi_h(P', m'_j)|J^{\mu}_q(0)|\psi_h(P, m_j)\rangle = \sum_{s,s',\bar{s}} \int_0^1 \frac{\mathrm{d}x}{2x(1-x)} \int \frac{\mathrm{d}^2k_\perp}{(2\pi)^3} \frac{1}{x'} \psi^{(m_j)}_{s\bar{s}/h}(\vec{k}_\perp, x)\psi^{(m'_j)*}_{s'\bar{s}/h}(\vec{k}'_\perp, x') \\ \times \bar{u}_{s'}(x'P'^+, \vec{k}'_\perp + x'\vec{P}'_\perp)\gamma^{\mu}u_s(xP^+, \vec{k}_\perp + x\vec{P}_\perp) \ , \end{aligned} \tag{2.49}$$

where $x' = (P'^+ - (1-x)P^+)/P'^+$ and $\vec{k}'_\perp = \vec{k}_\perp + (1-x)(P^+\vec{P}'_\perp - P'^+\vec{P}_\perp)/P'^+$. This is essentially the same as Eq. (2.41). We rewrite x' and $\vec{k}'_\perp$ in terms of the two boost invariants we have defined in Section 2.2.1, z and $\vec{\Delta}_\perp$, as

$$x' = x + z(1-x), \qquad \vec{k}'_\perp = \vec{k}_\perp + (1-x)\vec{\Delta}_\perp \ .$$

The transferred momentum square q^2 can be written according to Eq. (2.30) with $m_A = m_B = m_h$,

$$q^2 = -(z^2m_h^2 + \vec{\Delta}_\perp^2)/(1-z) \ . \tag{2.50}$$

Note that $q^2 \leq 0$.

www.manaraa.com

One could extract the form factor with different current components. The $+$, $\perp$ and $-$ hadron matrix elements can be related through the transverse Lorentz boost specified by the velocity vector $\vec{\beta}_\perp$,

$$v^+ \to v^+, \quad \vec{v}_\perp \to \vec{v}_\perp + v^+\vec{\beta}_\perp, \quad v^- \to v^- + 2\vec{\beta}_\perp \cdot \vec{v}_\perp + \vec{\beta}_\perp^2 v^+ \ . \tag{2.51}$$

The hadron matrix elements are thereby related through,

$$\begin{aligned}
&\langle\psi_h(P'^+, \vec{P}'_\perp + P'^+\vec{\beta}_\perp)|\vec{J}_\perp|\psi_h(P^+, \vec{P}_\perp + P^+\vec{\beta}_\perp)\rangle \\
&\qquad = \langle\psi_h(P')|\vec{J}_\perp|\psi_h(P)\rangle + \vec{\beta}_\perp \langle\psi_h(P')|J^+|\psi_h(P)\rangle \ , \\
&\langle\psi_h(P'^+, \vec{P}'_\perp + P'^+\vec{\beta}_\perp)|J^-|\psi_h(P^+, \vec{P}_\perp + P^+\vec{\beta}_\perp)\rangle \\
&\qquad = \langle\psi_h(P')|J^-|\psi_h(P)\rangle + 2\vec{\beta}_\perp \cdot \langle\psi_h(P')|\vec{J}_\perp|\psi_h(P)\rangle + \vec{\beta}_\perp^2 \langle\psi_h(P')|J^+|\psi_h(P)\rangle \ .
\end{aligned} \tag{2.52}$$

This relation implies that the form factors extracted from different current components should be equivalent. One can verify it by substituting Eq. (2.48) into Eq. (2.52). We would like to know if this is still true in the valence Fock sector, and write out the form factor with different current components in the valence light-front wavefunction representation.

Using the J^+ current,

$$\begin{aligned}
F(q^2)\big|_{J^+} &= \langle\psi_h(P')|J_q^+(0)|\psi_h(P)\rangle\,/(P^+ + P'^+) \\
&= \sum_{s,\bar{s}} \int_0^1 \frac{\mathrm{d}x}{2x(1-x)} \int \frac{\mathrm{d}^2k_\perp}{(2\pi)^3} \frac{1}{x'} \psi_{s\bar{s}/h}(\vec{k}_\perp, x)\psi^*_{s\bar{s}/h}(\vec{k}'_\perp, x')2\sqrt{x'P'^+xP^+}/(P^+ + P'^+) \\
&= \sum_{s,\bar{s}} \int_0^1 \frac{\mathrm{d}x}{2x(1-x)} \int \frac{\mathrm{d}^2k_\perp}{(2\pi)^3} \frac{2}{2-z} \sqrt{\frac{x(1-z)}{x+z(1-x)}} \psi_{s\bar{s}/h}(\vec{k}_\perp, x)\psi^*_{s\bar{s}/h}(\vec{k}'_\perp, x') \ .
\end{aligned} \tag{2.53}$$

In the second line, the form factor is written as a function of $(z, \vec{\Delta}_\perp)$, dependence on P or P' is eliminated. The normalization of the form factor at $q^2 = 0$ follows as the result of the normalization of the hadron wavefunction,

$$F(0)\big|_{J^+} = \sum_{s,\bar{s}} \int_0^1 \frac{\mathrm{d}x}{2x(1-x)} \int \frac{\mathrm{d}^2k_\perp}{(2\pi)^3} \psi_{s\bar{s}/h}(\vec{k}_\perp, x)\psi^*_{s\bar{s}/h}(\vec{k}_\perp, x) = 1 \ . \tag{2.54}$$

Now we turn to the transverse current. Assuming that the rotational symmetry on the transverse plane is preserved, using J^x or J^y component or linear combinations of the two should be equivalent. Here we use $J^R \equiv J^x + iJ^y$ and $J^L \equiv J^x - iJ^y$ as the transverse currents. For any transverse vector $\vec{k}_\perp$, which is expressed

www.manaraa.com

as (k^x, k^y) in the Cartesian coordinate or $(k_\perp, \theta)$ in the polar coordinate, we will write its complex form as $k^R \equiv k^x + ik^y = k_\perp e^{i\theta}$ and $k^L \equiv k^x - ik^y = k_\perp e^{-i\theta}$. The elastic form factor extracted from the J^R current reads,

$$\begin{aligned}
F(q^2)\big|_{J^R} =& \langle \psi_h(P')|J_q^R(0)|\psi_h(P)\rangle /(P^R + P'^R) \\
=& \frac{z}{(2-z)q^R - 2\Delta^R} \sum_{\bar{s}} \int_0^1 \frac{\mathrm{d}x}{2x(1-x)} \int \frac{\mathrm{d}^2k_\perp}{(2\pi)^3} \\
& \times \Bigg\{ \psi_{\uparrow\bar{s}/h}(\vec{k}_\perp, x)\psi^*_{\uparrow\bar{s}/h}(\vec{k}'_\perp, x') \left[\frac{2}{\sqrt{x(1-z)[x+z(1-x)]}}(k^R - \frac{x}{z}\Delta^R) + \frac{2}{z}\sqrt{\frac{x(1-z)}{x+z(1-x)}}q^R \right] \\
& + \psi_{\downarrow\bar{s}/h}(\vec{k}_\perp, x)\psi^*_{\uparrow\bar{s}/h}(\vec{k}'_\perp, x') \frac{2m_q z}{\sqrt{x(1-z)[x+z(1-x)]^3}} \\
& + \psi_{\downarrow\bar{s}/h}(\vec{k}_\perp, x)\psi^*_{\downarrow\bar{s}/h}(\vec{k}'_\perp, x') \left[\frac{2\sqrt{x(1-z)}}{\sqrt{[x+z(1-x)]^3}}(k^R - \frac{x}{z}\Delta^R) + \frac{2}{z}\sqrt{\frac{x(1-z)}{x+z(1-x)}}q^R \right] \Bigg\} .
\end{aligned} \tag{2.55}$$

The second term with spin flip ($s' = -s$) vanishes by considering the symmetry among different spin components of spin-0 particle h_0,

$$\psi_{\uparrow\uparrow/h_0}(\vec{k}_\perp, x) = \psi_{\downarrow\downarrow/h_0}(\vec{k}_\perp, x), \qquad \psi_{\uparrow\downarrow/h_0}(\vec{k}_\perp, x) = -\psi_{\downarrow\uparrow/h_0}(\vec{k}_\perp, x) . \tag{2.56}$$

The first and the third terms have the same wavefunction products and could be combined into one term.

$$\begin{aligned}
F(q^2)\big|_{J^R} =& \langle \psi_h(P')|J_q^R(0)|\psi_h(P)\rangle /(P^R + P'^R) \\
=& \frac{z}{(2-z)q^R - 2\Delta^R} \sum_{s\bar{s}} \int_0^1 \frac{\mathrm{d}x}{2x(1-x)} \int \frac{\mathrm{d}^2k_\perp}{(2\pi)^3} \psi_{s\bar{s}/h}(\vec{k}_\perp, x)\psi^*_{s\bar{s}/h}(\vec{k}'_\perp, x') \\
& \times \frac{1}{\sqrt{x(1-z)[x+z(1-x)]^3}} \Big\{ [z+2x(1-z)](k^R - \frac{x}{z}\Delta^R) + \frac{2}{z}x(1-z)[x+z(1-x)]q^R \Big\} \\
=& F(q^2)\big|_{J^+} + \frac{1}{P^R + P'^R} \sum_{s\bar{s}} \int_0^1 \frac{\mathrm{d}x}{2x(1-x)} \int \frac{\mathrm{d}^2k_\perp}{(2\pi)^3} \psi_{s\bar{s}/h}(\vec{k}_\perp, x)\psi^*_{s\bar{s}/h}(\vec{k}'_\perp, x') \\
& \times \frac{1}{\sqrt{x(1-z)[x+z(1-x)]^3}} \Big\{ [z+2x(1-z)]k^R + \frac{x}{2-z}(2-2x-3z+2xz)\Delta^R \Big\} .
\end{aligned} \tag{2.57}$$

We see that $F(q^2)\big|_{J^R}$ and $F(q^2)\big|_{J^+}$ are different by the second term in the last line of Eq. (2.57). Moreover, this second term depends on $P^R + P'^R$ in the $(z, \vec{\Delta}_\perp)$ parameter space. This indicates that fixing $(z, \vec{\Delta}_\perp)$ is not sufficient to unambiguously determine a frame in this case. However, in the Drell-Yan and the longitudinal

www.manaraa.com

frames, it can be proved that this term actually vanishes, leaving $F(q^2)\big|_{J^R} = F(q^2)\big|_{J^+}$.

$$\begin{aligned} F(q^2)\big|_{J^R,\mathrm{DY}} =& \langle\psi_h(P')|J_q^R(0)|\psi_h(P)\rangle/(P^R+P'^R) \\ =& F(q^2)\big|_{J^+,\mathrm{DY}} \\ &+ \frac{1}{P^R+P'^R}\sum_{s\bar{s}}\int_0^1\frac{\mathrm{d}x}{2x(1-x)}\int\frac{\mathrm{d}^2k_\perp}{(2\pi)^3}\psi_{s\bar{s}/h}(\vec{k}_\perp,x)\psi^*_{s\bar{s}/h}(\vec{k}'_\perp,x')\frac{1}{x}[2k^R+(1-x)q^R] \\ =& F(q^2)\big|_{J^+,\mathrm{DY}}\,. \end{aligned} \tag{2.58}$$

The second term vanishes under the transverse integral with $\vec{k}'_\perp = \vec{k}_\perp + (1-x)q^R$ in the Drell-Yan frame. Now, in the longitudinal frame:

$$\begin{aligned} F(q^2)\big|_{J^R,\mathrm{long}} =& \langle\psi_h(P')|J_q^R(0)|\psi_h(P)\rangle/(P^R+P'^R) \\ =& F(q^2)\big|_{J^+,\mathrm{long}} + \frac{1}{P^R+P'^R}\sum_{s\bar{s}}\int_0^1\frac{\mathrm{d}x}{2x(1-x)}\int\frac{\mathrm{d}^2k_\perp}{(2\pi)^3}\psi_{s\bar{s}/h}(\vec{k}_\perp,x)\psi^*_{s\bar{s}/h}(\vec{k}'_\perp,x') \\ &\times\frac{[z+2x(1-z)]k^R}{\sqrt{x(1-z)[x+z(1-x)]^3}} \\ =& F(q^2)\big|_{J^+,\mathrm{long}}\,. \end{aligned} \tag{2.59}$$

Note that $\vec{k}'_\perp = \vec{k}_\perp$ in the longitudinal frame, thus the second term vanishes since the angular integral is zero. As with the J^+ current, $F(0)|_{J^R} = 1$ is guaranteed by the normalization of the hadron wavefunction. At $q^2 = 0$, the terms proportional to k^R in the integral would vanish since the angular integration would be 0.

Using the J^- current,

$$\begin{aligned} F(q^2)\big|_{J^-} =& \langle\psi_h(P')|J_q^-(0)|\psi_h(P)\rangle/(P^-+P'^-) \\ =& \frac{1}{P_\perp^2+m_h^2+(1-z)(P'^2_\perp+m_h^2)}\sum_{s\bar{s}}\int_0^1\frac{\mathrm{d}x}{2x(1-x)}\int\frac{\mathrm{d}^2k_\perp}{(2\pi)^3}\psi_{s\bar{s}/h}(\vec{k}_\perp,x)\psi^*_{s\bar{s}/h}(\vec{k}'_\perp,x') \\ &\times 2\sqrt{\frac{1-z}{x[x+z(1-x)]}}[m_q^2+(\vec{k}_\perp+x\vec{P}_\perp)\cdot(\vec{k}'_\perp+x'\vec{P}'_\perp)]\,. \end{aligned} \tag{2.60}$$

In deriving Eq. (2.60), the spin flip terms vanish by exact cancellations among different spin components. The normalization of the elastic form factor ($F(0) = 1$) with J^- has a nontrivial requirement on the wavefunctions, and this is referred to as a type of Virial theorem [81]. We can see this explicitly in Eq. (2.61). In the truncated Fock space, the light-front J^- current is not conserved and it violates the Ward-Takahashi

www.manaraa.com

identity [82, 83]. The valence Fock sector is not sufficient to extract the elastic form factor with the J^- current.

$$\begin{aligned} F(0)\big|_{J^-} &= \langle\psi_h(P')|J_q^-(0)|\psi_h(P)\rangle\,/(P^- + P'^-) \\ &= \frac{1}{2(P_\perp^2 + m_h^2)} \sum_{s\bar{s}} \int_0^1 \frac{\mathrm{d}x}{2x(1-x)} \int \frac{\mathrm{d}^2k_\perp}{(2\pi)^3} \psi_{s\bar{s}/h}(\vec{k}_\perp, x)\psi^*_{s\bar{s}/h}(\vec{k}_\perp, x)\frac{2}{x}[m_q^2 + (\vec{k}_\perp + x\vec{P}_\perp)^2] \,. \end{aligned} \tag{2.61}$$

A recent work by H.M. Choi, H.Y. Ryu and C.R. Ji [84] implemented a replacement of the meson mass m_h by the invariant mass $m_0^2 = (m_q^2 + \vec{k}_\perp^2)/x + (m_q^2 + \vec{k}_\perp^2)/(1-x)$ in studying the $(\pi^0, \eta, \eta' \to \gamma^*\gamma^*)$ transitions with a manifestly covariant model. Following the format of this treatment, we see that restoring $F(0) = 1$ in Eq. (2.61) would require a replacement of $m_h^2 \to (m_q^2 + \vec{k}_\perp^2)/x - (1-x)\vec{P}_\perp^2$. In the meson rest frame where $\vec{P}_\perp = \vec{0}_\perp$, the expression reduces to $m_h^2 \to (m_q^2 + \vec{k}_\perp^2)/x$, suggesting to replace the meson mass by the invariant mass of the quark, or half of the invariant mass of the meson.

To conclude, the J^+ and $\vec{J}_\perp$ current components could guarantee the normalization of the elastic form factor in the valence Fock sector, but the J^- component could not. Though the elastic form factors extracted from the J^+ and the $\vec{J}_\perp$ components are expected to be the same through a transverse boost, the valence light-front wavefunction representation shows that the two are the same only in the Drell-Yan and the longitudinal frames. In a practical calculation, J^+ and the Drell-Yan frame is often preferred, and the main advantage of this choice is that vacuum pair production/ annihilation is suppressed [85, 86, 72]. A recent study on the frame dependence of the elastic form factor of pseudoscalars using the J^+ current can be found in Ref. [65].

Here we present the form factors of the spin-0 heavy quarkonia using their light-front wavefunctions solved in the valence Fock sector [3]. We carry out the calculation in the Drell-Yan frame using the J^+ or equivalently the $\vec{J}_\perp$ current. Fig. 2.6 shows the numerical results for the spin-0 states of heavy quarkonia below their respective open-flavor thresholds, those states are charmonia $\eta_c(1S)$, $\chi_{c0}(1P)$ and $\eta_c(2S)$, and bottomonia $\eta_b(1S)$, $\chi_{b0}(1P)$, $\eta_b(2S)$ and $\eta_b(3S)$. The results show a good convergence trend as the basis cutoff increases as $N_{\max} = L_{\max} = 8, 16, 24, 32$. We take the largest basis $N_{\max} = L_{\max} = 32$ as the result, and use the range between $N_{\max} = L_{\max} = 24$ and 32 as the uncertainty. The form factors for the radially excited states, $\eta_c(2S)$, $\eta_b(2S)$ and $\eta_b(3S)$ exhibit a tendency to develop a node.

In nonrelativistic quantum mechanics, the root-mean-square charge (mass) radius is the expectation value of the displacement operator that characterizes the charge (mass) distribution of the system. In quan-

www.manaraa.com

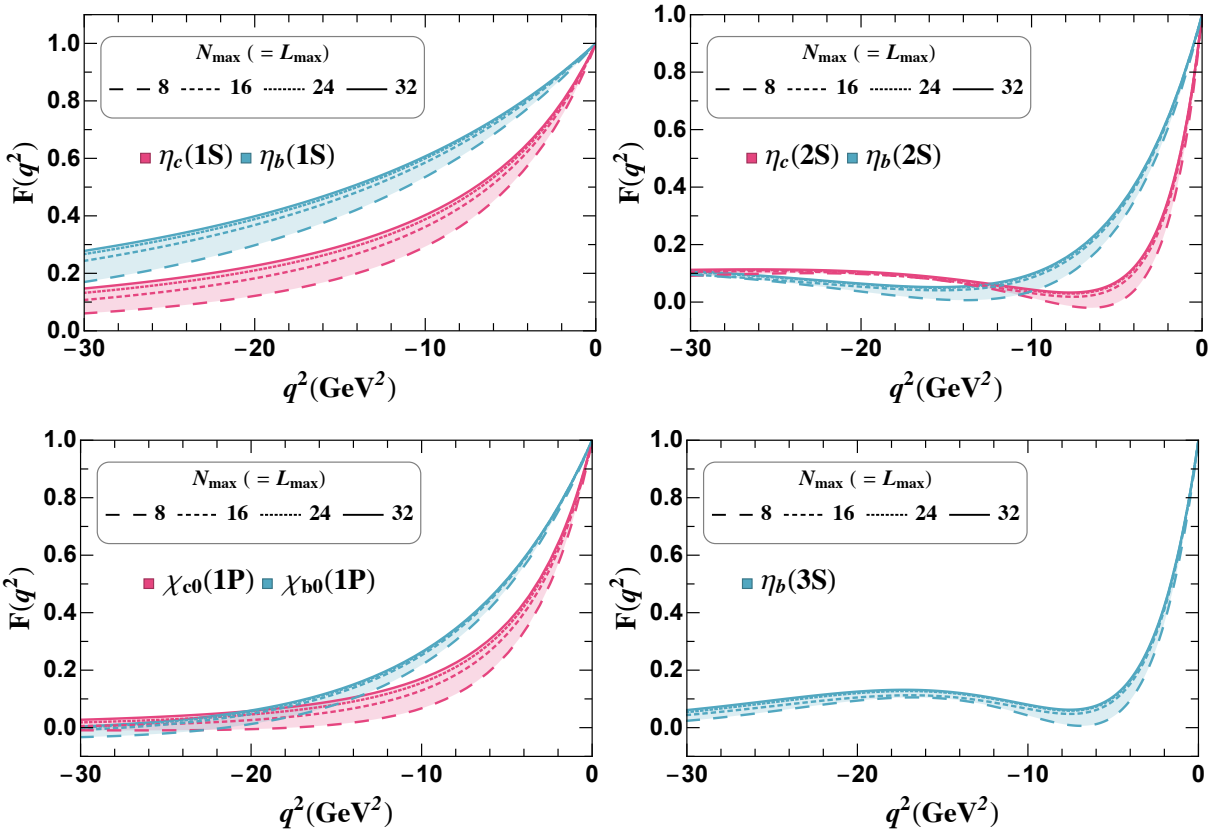

Figure 2.6 The elastic form factor of spin-0 states of heavy quarkonia calculated in the Drell-Yan frame with the J^+ or equivalently the $\vec{J}_\perp$ current, according to Eq. (2.53) with $z = 0$. The light-front wavefunctions used in these results are solved in the BLFQ approach at different basis truncations ($N_{\max} = L_{\max} = 8, 16, 24, 32$) [3].

tum field theory, no such local position operator is allowed and, instead, the charge (mass) radius of the hadron is defined from the charge (gravitational) form factor at small momentum transfer:

$$\langle r_h^2 \rangle = \lim_{q^2 \to 0} -6 \frac{\partial}{\partial q^2} F(q^2) \,. \tag{2.62}$$

The charge radii of spin-0 quarkonia are summarized in Table 2.4. Note that the BLFQ results with running coupling are obtained in a larger basis space which tends to enhance UV effects and generally favors smaller radii.

www.manaraa.com

Table 2.4 The charge mean squared radii $\langle r_h^2 \rangle$ of (pseudo) scalar charmonia and bottomonia [Eq. (2.62)]. The BLFQ results with the running coupling α_s are obtained at $N_{\max} = L_{\max} = 32$. The difference between the $N_{\max} = L_{\max} = 32$ and 24 values are presented as the uncertainty. The BLFQ results with the fixed coupling α_s are obtained at $N_{\max} = L_{\max} = 24$. The difference between the $N_{\max} = L_{\max} = 24$ and 16 values are presented as the uncertainty. We compare our results with those of the Contact Interaction (CI), Lattice and Dyson-Schwinger Equation (DSE) methods.

(fm^2)	η_c	χ_{c0}	η_c'	η_b	χ_{b0}	η_b'	η_b''
BLFQ(running α_s[3])	0.029(1)	0.057(1)	0.120(1)	0.013(0)	0.031(0)	0.051(0)	0.095(1)
BLFQ(fixed α_s[48])[66]	0.043(5)	0.07(1)	0.149(8)	0.016(1)	0.037(1)	0.056(2)	
CI [87, 88, 89]	0.044			0.012			
Lattice [90]	0.063(1)	0.095(6)					
DSE [91, 92]	0.048(4)						

More on Charge Radii

In the Drell-Yan frame, $q^+ = 0$ and $q^2 = -|\vec{q}_\perp|^2$. We can write $\vec{q}_\perp$ in the polar coordinate $\{q, \theta\}$. With a change of variable, $t = q^2$,

$$\begin{aligned}\nabla^2_{\vec{q}_\perp} =& \frac{\partial^2}{\partial q^2} + \frac{1}{q}\frac{\partial}{\partial q} + \frac{1}{q^2}\frac{\partial^2}{\partial \theta^2} \\ =& \frac{\partial^2}{\partial t^2}\left(\frac{\partial t}{\partial q}\right)^2 + \frac{\partial}{\partial t}\left(\frac{\partial^2 t}{\partial q^2}\right) + \frac{1}{\sqrt{t}}\frac{\partial}{\partial t}\frac{\partial t}{\partial q} + \frac{1}{t}\frac{\partial^2}{\partial \theta^2} \\ =& 4t\frac{\partial^2}{\partial t^2} + 4\frac{\partial}{\partial t} + \frac{1}{t}\frac{\partial^2}{\partial \theta^2} \,.\end{aligned} \tag{2.63}$$

At the limit of $q^2 \to 0$, the first term vanishes. Since the form factor does not have angular dependence, the third term vanishes as well. It follows that

$$\left.\frac{\partial}{\partial t}\right|_{t=0} = \frac{1}{4}\nabla^2_{\vec{q}_\perp} \,. \tag{2.64}$$

We can thereby rewrite the charge radius in Eq. (2.62) in terms of the two-dimensional Laplacian of the charge form factor,

$$\langle r_h^2 \rangle = -\frac{3}{2}\nabla^2_{\vec{q}_\perp} F(q^2)\Big|_{q^2=0} \,. \tag{2.65}$$

We have already mentioned that the physical form factors of a hadron should receive contributions from each constituent, $F(q^2) = \sum_f e_f F_f(q^2)$, where f is the constituent (anti)quark with charge e_f. Though for

www.manaraa.com

quarkonium, the physical form factor vanishes due to charge conjugation (see Appendix D.1), we calculate the fictitious form factor contributed from the quark only. For a charged hadron, such as $\pi^{\pm}$ and proton, one should consider its physical form factor that sums over the contributions of all constituent partons. In the following, we will derive the contributions of the quark and the antiquark separately.

- q

  The charge form factor contributed by the quark is calculated as

$$\begin{aligned} F_q(q^2) &= \langle h(P')|\, J_q^+(0)\,|h(P)\rangle\,/(2P^+) \\ &= \sum_{s,\bar{s}} \int_0^1 \frac{\mathrm{d}x}{2x(1-x)} \int \frac{\mathrm{d}^2k_\perp}{(2\pi)^3} \psi_{s,\bar{s}/h}(\vec{k}_\perp, x)\psi^*_{s,\bar{s}/h}(\vec{k}_\perp + (1-x)\vec{q}_\perp, x) \\ &= \sum_{s,\bar{s}} \int_0^1 \frac{\mathrm{d}x}{2x(1-x)} \int \frac{\mathrm{d}^2k_\perp}{(2\pi)^3} \\ &\quad \times \int \mathrm{d}^2r_\perp \int \mathrm{d}^2r'_\perp x(1-x) e^{-i\vec{k}_\perp\cdot\vec{r}_\perp} e^{i(\vec{k}_\perp+(1-x)\vec{q}_\perp)\cdot\vec{r}'_\perp} \tilde{\psi}_{s,\bar{s}/h}(\vec{r}_\perp, x)\tilde{\psi}^*_{s,\bar{s}/h}(\vec{r}'_\perp, x) \\ &= \sum_{s,\bar{s}} \int_0^1 \frac{\mathrm{d}x}{4\pi} \int \mathrm{d}^2r_\perp e^{i(1-x)\vec{q}_\perp\cdot\vec{r}_\perp} \tilde{\psi}_{s,\bar{s}/h}(\vec{r}_\perp, x)\tilde{\psi}^*_{s,\bar{s}/h}(\vec{r}_\perp, x)\,. \end{aligned} \tag{2.66}$$

  $\tilde{\psi}_{s,\bar{s}/h}(\vec{r}_\perp, x)$ is the light-front wavefunction of the spin-0 particle h in coordinate space. The charge radius of the constituent quark is

$$\langle r_h^2\rangle_q = -\frac{3}{2}\nabla^2_{\vec{q}_\perp} F_q(q^2)\Big|_{q^2=0} = \frac{3}{2}\sum_{s,\bar{s}} \int_0^1 \frac{\mathrm{d}x}{4\pi} \int \mathrm{d}^2r_\perp (1-x)^2 \vec{r}_\perp^{\,2} \tilde{\psi}_{s,\bar{s}/h}(\vec{r}_\perp, x)\tilde{\psi}^*_{s,\bar{s}/h}(\vec{r}_\perp, x)\,. \tag{2.67}$$

- $\bar{q}$

  The charge form factor contributed by the antiquark is calculated as

$$\begin{aligned} F_{\bar{q}}(q^2) &\equiv \langle h(P')|\, J_{\bar{q}}^+(0)\,|h(P)\rangle\,/(2P^+) \\ &= \sum_{s,\bar{s}} \int_0^1 \frac{\mathrm{d}x}{2x(1-x)} \int \frac{\mathrm{d}^2k_\perp}{(2\pi)^3} \psi_{s,\bar{s}/h}(\vec{k}_\perp, x)\psi^*_{s,\bar{s}/h}(\vec{k}_\perp - x\vec{q}_\perp, x) \\ &= \sum_{s,\bar{s}} \int_0^1 \frac{\mathrm{d}x}{2x(1-x)} \int \frac{\mathrm{d}^2k_\perp}{(2\pi)^3} \\ &\quad \times \int \mathrm{d}^2r_\perp \int \mathrm{d}^2r'_\perp x(1-x) e^{-i\vec{k}_\perp\cdot\vec{r}_\perp} e^{i(\vec{k}_\perp-x\vec{q}_\perp)\cdot\vec{r}'_\perp} \tilde{\psi}_{s,\bar{s}/h}(\vec{r}_\perp, x)\tilde{\psi}^*_{s,\bar{s}/h}(\vec{r}'_\perp, x) \\ &= \sum_{s,\bar{s}} \int_0^1 \frac{\mathrm{d}x}{4\pi} \int \mathrm{d}^2r_\perp e^{-ix\vec{q}_\perp\cdot\boldsymbol{r}_\perp} \tilde{\psi}_{s,\bar{s}/h}(\vec{r}_\perp, x)\tilde{\psi}^*_{s,\bar{s}/h}(\vec{r}_\perp, x)\,. \end{aligned} \tag{2.68}$$

www.manaraa.com

The charge radius of the constituent anti-quark is

$$\langle r_h^2\rangle_{\bar{q}} = -\frac{3}{2}\nabla^2_{\vec{q}_\perp} F_{\bar{q}}(q^2)\Big|_{q^2=0} = \frac{3}{2}\sum_{s,\bar{s}}\int_0^1 \frac{\mathrm{d}x}{4\pi}\int \mathrm{d}^2 r_\perp x^2 \vec{r}_\perp^{\,2}\tilde{\psi}_{s,\bar{s}/h}(\vec{r}_\perp, x)\tilde{\psi}^*_{s,\bar{s}/h}(\vec{r}_\perp, x) \tag{2.69}$$

As an example, the charge radius of π^+ sums over the contributions from u and $\bar{d}$.

$$\begin{aligned}\langle r^2_{\pi^+}\rangle =& Q_u \langle r^2_{\pi^+}\rangle_u + Q_{\bar{d}}\langle r^2_{\pi^+}\rangle_{\bar{d}} \\ =& \frac{3}{2}\sum_{s,\bar{s}}\int_0^1 \frac{\mathrm{d}x}{4\pi}\int \mathrm{d}^2 r_\perp \Big[\frac{2}{3}(1-x)^2 + \frac{1}{3}x^2\Big]\vec{r}_\perp^{\,2}\tilde{\psi}_{s,\bar{s}/\pi^+}(\vec{r}_\perp, x)\tilde{\psi}^*_{s,\bar{s}/\pi^+}(\vec{r}_\perp, x)\ .\end{aligned} \tag{2.70}$$

The dimensionless fractional charge of the quark is, $Q_u = +2/3$ for the up quark and $Q_{\bar{d}} = +1/3$ for the anti-down quark.

2.2.4 Elastic form factor of the spin-1 particle

In the Lorentz decomposition of the hadron matrix elements for spin-one particles, three Lorentz-invariants arise along with three elastic form factors. A detailed derivation of the Lorentz decomposition can be found in Appendix D.2. The elastic form factors for a spin 1 particle, F_1, F_2 and F_3, are defined as the following,

$$\begin{aligned} I^\mu_{m'_j,m_j} \equiv& \langle\psi_h(P', j=1, m'_j)|\, J^\mu(0)\,|\psi_h(P, j=1, m_j)\rangle \\ =& (P^\mu + P'^\mu)[(e'^*\cdot P)(e\cdot P')F_1(q^2) + (e'^*\cdot e)F_2(q^2)] + [e^\mu(e'^*\cdot P) + e'^{*\mu}(e\cdot P')]F_3(q^2)\ .\end{aligned} \tag{2.71}$$

The polarization vectors of the hadron are $e^\mu = e^\mu(P, m_j)$ and $e'^\mu = e'^\mu(P', m'_j)$. For each current component, $\mu = +, -, 1, 2$, there are nine combinations of the magnetic projections for the initial and the final states, $m_j(m'_j) = 0, \pm 1$. Parity and charge conjugation symmetries on the light front leaves four independent hadron matrix elements, $m_j(m'_j) = 1(-1), 1(1), 1(0), 0(0)$. The rotational invariance of the current should provide another constraint, namely the angular condition, and reduces the number to three, which is in agreement with the number of the form factors. The front-form angular condition for $I^+_{m_j,m'_j}$ could be obtained via Melosh rotation from the instant-form $I^+_{z,z} = I^+_{y,y}$ [93, 94]. In the Breit frame where $P^+ = P'^+$ and $\vec{P}'_\perp = -\vec{P}_\perp$, the angular condition reads as

$$\Delta(q^2) = (1+2\eta)I^+_{1,1} + I^+_{1,-1} - \sqrt{8\eta}I^+_{1,0} - I^+_{0,0} = 0\ , \tag{2.72}$$

www.manaraa.com

where $\eta \equiv -q^2/(4M^2)$ and M is the mass of the hadron, note that $q^2 \leq 0$ in this frame. In the light-front dynamics, the rotations around the x and y axis are dynamical [95], so wavefunctions with a fixed number of constituents no longer retain such covariance, and the angular condition is violated. The breakdown of the rotational symmetry leads to ambiguities in extracting the form factors from the light-front matrix elements $I^+_{m_j,m'_j}$. In the literature, there are different extraction schemes for spin-one form factors [96, 97, 98, 99, 100].

Using the J^+ current component,

$$\begin{aligned}
&\langle\psi_h(P', j=1, m'_j)|\, J^+(0)\,|\psi_h(P, j=1, m_j)\rangle \\
=&2P^+ \begin{cases}
\dfrac{q^4}{4M^2}F_1(q^2) + \left(\dfrac{q^2}{2M^2} - 1\right)F_2(q^2) + \dfrac{q^2}{2M^2}F_3(q^2), & m_j = m'_j = 0 \\
-\dfrac{q^2}{2}F_1(q^2) - F_2(q^2), & m_j = m'_j = \pm 1 \\
e^{\mp i\delta}\left[\dfrac{q^3}{2\sqrt{2}M}F_1(q^2) + \dfrac{q}{\sqrt{2}M}F_2(q^2) + \dfrac{q}{2\sqrt{2}M}F_3(q^2)\right], & m_j = 0(\mp 1),\ m'_j = \pm 1(0) \\
-e^{\mp 2i\delta}\dfrac{q^2}{2}F_1(q^2), & m_j = \mp 1, m'_j = \pm 1
\end{cases}
\end{aligned} \tag{2.73}$$

The phase factor is defined as $\delta \equiv \arg q^\perp$, such that $q^x + iq^y = qe^{i\delta}$. We thereby redefine the helicity amplitudes to get rid of the phase factor as the following

$$I^+_{m'_j,m_j} \equiv \langle\psi_h(P', j=1, m'_j)|\, J^+(0)\,|\psi_h(P, j=1, m_j)\rangle\, e^{i(m'_j - m_j)\delta}/(2P^+)\ .$$

It is often conventional to carry out the calculation in the frame with $P'_x = q_x/2$, $P_x = -q_x/2$ and $P'_y = P_y = q_y = 0$, such that $\delta = 0$ [101, 94, 102]. We adopt the GK prescription [96, 102] to calculate the elastic form factors, namely the charge form factor $G_C(q^2)$, the magnetic form factor $G_M(q^2)$, and the quadruple form factor $G_Q(q^2)$.

$$\begin{aligned}
G_C(q^2) =& \frac{1}{3}[(3-2\eta)I^+_{1,1} + I^+_{1,-1} + 2\sqrt{2\eta}I^+_{1,0}]\ , \\
G_M(q^2) =& 2I^+_{1,1} - \sqrt{\frac{2}{\eta}}I^+_{1,0}\ , \\
G_Q(q^2) =& -\frac{2}{3}\sqrt{2}[\eta I^+_{1,1} + I^+_{1,-1} - \sqrt{2\eta}I^+_{1,0}]\ .
\end{aligned} \tag{2.74}$$

Here we present the form factors of the spin-1 heavy quarkonia using their light-front wavefunctions solved in the valence Fock sector [3]. We carried out the calculation in the Drell-Yan frame using the J^+ current. Fig. 2.7 shows the numerical results of the charge form factors for the spin-1 states of heavy

www.manaraa.com

quarkonia below their respective open-flavor thresholds, those states are charmonia J/ψ, $\psi(2S)$, $\psi(1D)$, $\chi_{c1}(1P)$ and $h_c(1P)$, and bottomonia $\Upsilon(1S)$, $\Upsilon(2S)$, $\Upsilon(3S)$, $\Upsilon(1D)$, $\chi_{b1}(1P)$ and $h_b(1P)$. The magnetic and quadruple form factors of those states are shown in Fig. 2.8 and Fig. 2.9 respectively.

The results show a good convergence trend as the basis cutoff increases as $N_{\max} = L_{\max} = 8, 16, 24, 32$. We take the largest basis $N_{\max} = L_{\max} = 32$ as the result, and use the range between $N_{\max} = L_{\max} = 24$ and 32 as the uncertainty. The comparison between charmonia and bottomonia is also of interest. For comparable states (those plotted on the same graph), the form factors show similarity in their patterns. Bottomonium is associated with a larger mass scale and is broader in momentum space.

The multipole moments of the hadron are defined from the corresponding form factors at small momentum transfer. They are the charge root-mean-squared (rms) radius $\langle r_h^2 \rangle$, the magnetic moment μ, and the quadrupole moment Q [98],

$$\langle r_h^2 \rangle = \lim_{t\to 0} -6\frac{\partial}{\partial t} G_C(q^2), \tag{2.75}$$

$$\mu = \lim_{t\to 0} G_M(q^2), \tag{2.76}$$

$$\mathrm{Q} = \lim_{t\to 0} 3\sqrt{2}\frac{\partial}{\partial t} G_Q(q^2)\ , \tag{2.77}$$

where $t \equiv -q^2$.

Note that for quarkonium, we calculate the fictitious charge radius contributed from the quark only, as done for the charge form factor. But for a charged hadron, one should consider its charge radius that sums over the contributions of all constituent partons, see discussions in Section 2.2.3. The charge radii, magnetic moments and the quadrupole moments of spin-1 quarkonia are summarized in Tables 2.5, 2.6 and 2.7, respectively. In these calculations, we take the light-front wavefunctions calculated from the BLFQ approach with a running coupling on the one-gluon exchange term [3]. The results are close to those calculated with BLFQ light-front wavefunction of the fixed coupling [48, 66].

As shown in Table 2.6, the BLFQ results of the magnetic moments for those mesons are above the canonical value of 2 with the running-coupling LFWF. The canonical magnetic moment is obtained when the overlaps of states of different magnetic projections vanish, i.e. $I^+_{1,0}(q^2 = 0) = I^+_{1,-1}(q^2 = 0) = 0$ in Eqs. (2.74) and (2.76). In our calculation, the deviation from 2 comes from the non-vanishing ratio of the

www.manaraa.com

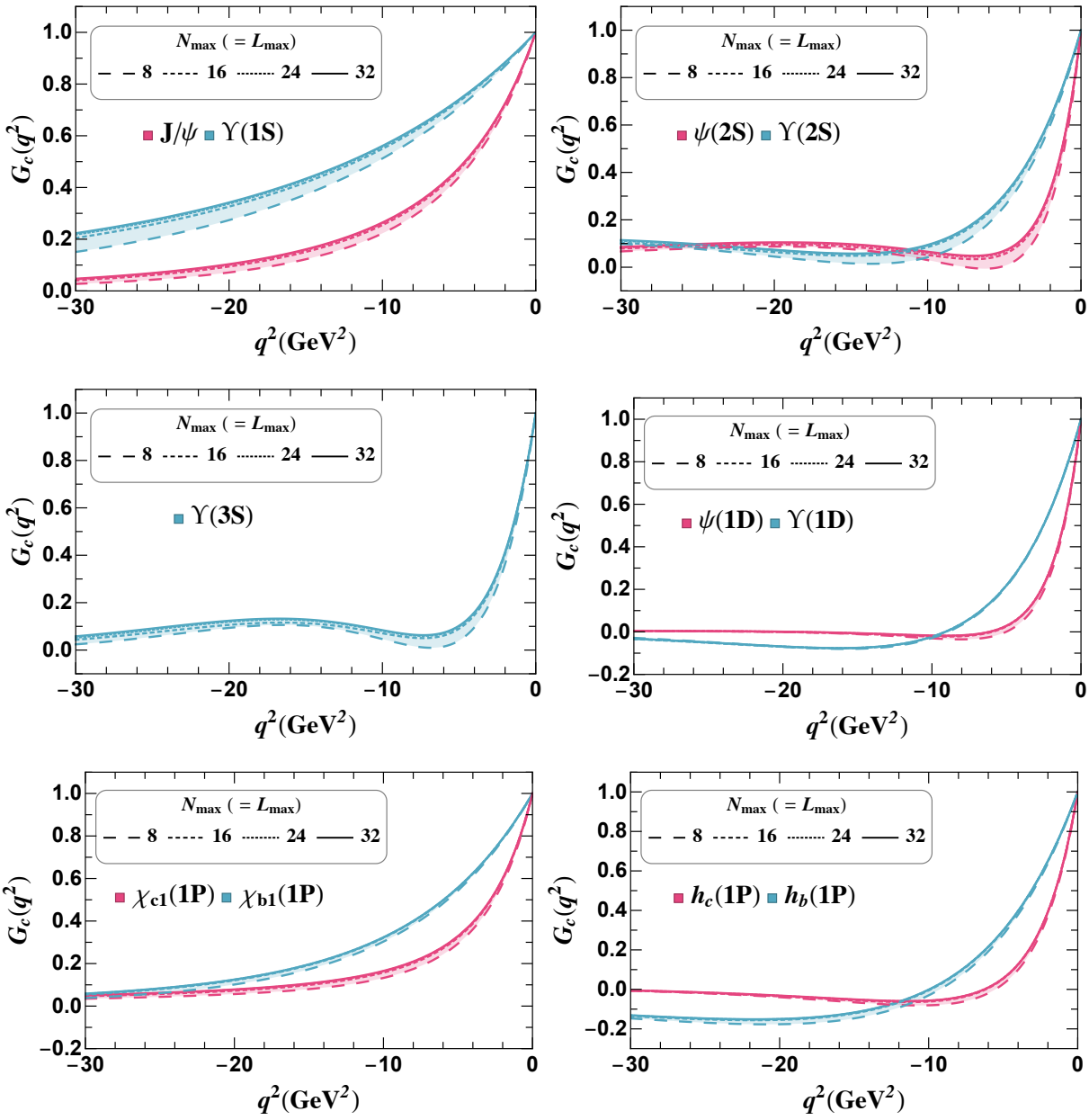

Figure 2.7 The charge form factor of spin-1 states of heavy quarkonia at different basis truncations, $N_{\max} = L_{\max} = 8, 16, 24, 32$. The light-front wavefunctions used in these results are solved in the BLFQ approach at different basis truncations ($N_{\max} = L_{\max} = 8, 16, 24, 32$) [3].

www.manaraa.com

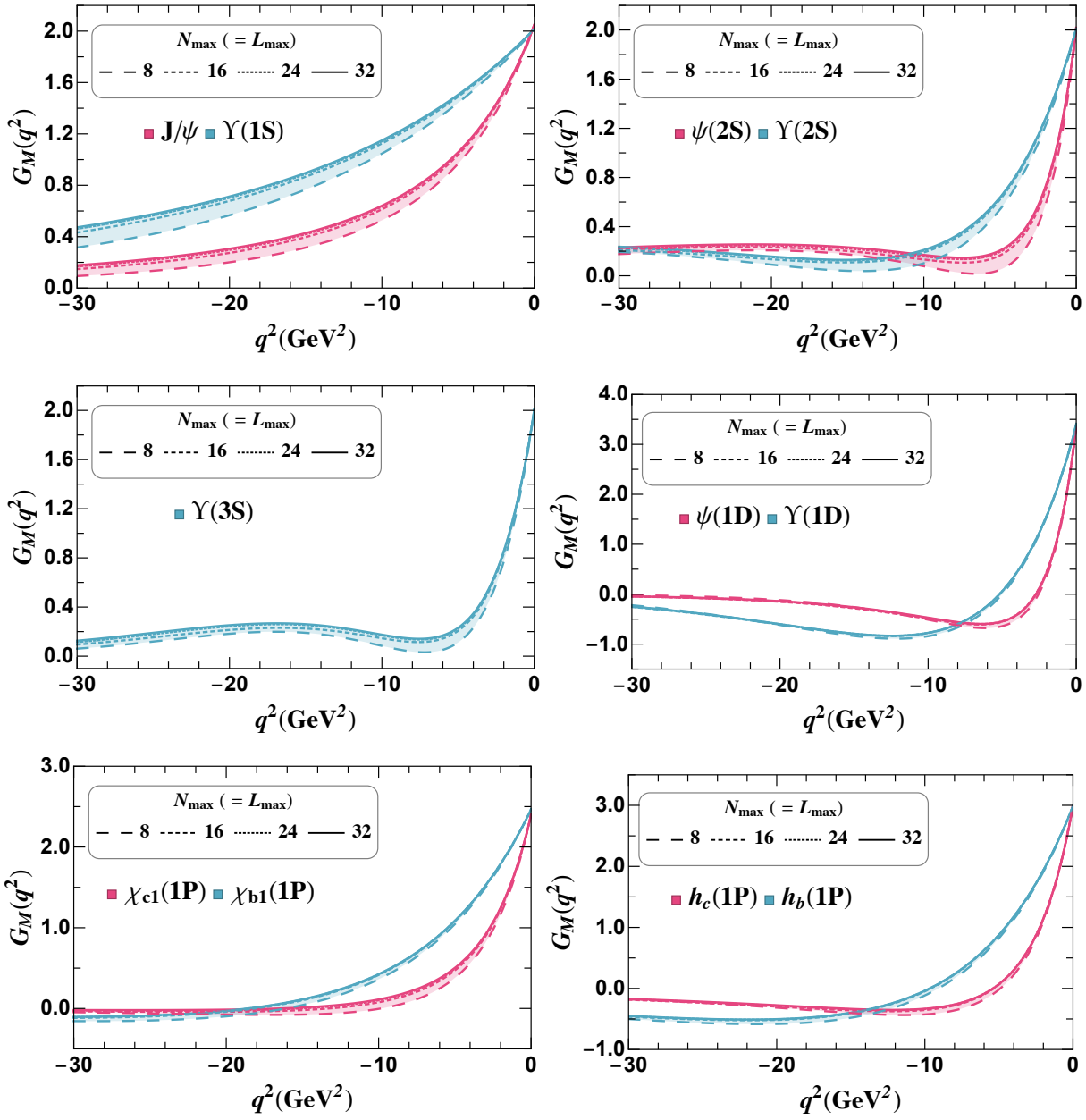

Figure 2.8 The magnetic form factor of spin-1 states of heavy quarkonia at different basis truncations, $N_{\max} = L_{\max} = 8, 16, 24, 32$. The light-front wavefunctions used in these results are solved in the BLFQ approach [3].

www.manaraa.com

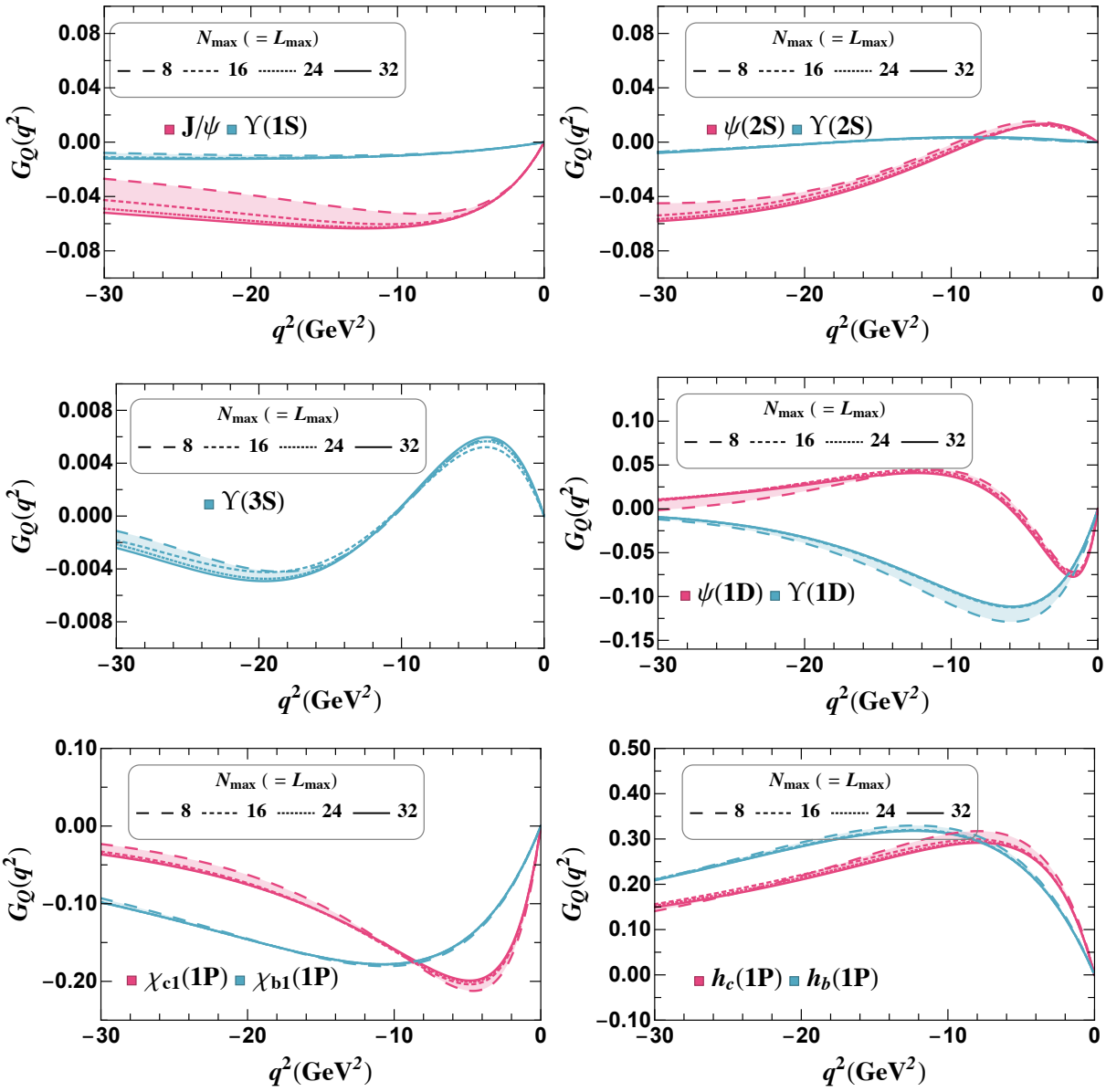

Figure 2.9 The quadruple form factor of spin-1 states of heavy quarkonia at different basis truncations, $N_{\max} = L_{\max} = 8, 16, 24, 32$. The light-front wavefunctions used in these results are solved in the BLFQ approach [3].

www.manaraa.com

Table 2.5 The charge mean squared radii $\langle r_h^2 \rangle$ [Eq. (2.75)] for spin-1 charmonia and bottomonia. The difference between the $N_{\max} = L_{\max} = 24$ and 32 values are presented as the uncertainty in the BLFQ results.

(fm^2)	BLFQ (running-α_s [3]) this work	BLFQ (fixed-α_s [48]) [66]	CI [89]	Lattice [90]	DSE [91, 92]
J/ψ	0.0402(2)	0.045(3)	0.068	0.066(2)	0.052(3)
χ_{c1}	0.066(0)	0.075(2)			
$h_c(1P)$	0.106(1)				
ψ'	0.13(0)	0.15(1)			
$\psi(1D)$	0.13(0)				
Υ	0.015(0)	0.016(1)	0.038		
χ_{b1}	0.028(0)	0.0270(4)			
$h_b(1P)$	0.048(0)				
Υ'	0.053(0)	0.057(3)			
$\Upsilon(1D)$	0.06(0)				
Υ''	0.097(0)				

Table 2.6 The magnetic moment μ [Eq. (2.76)] for spin-1 charmonia and bottomonia. The difference between the $N_{\max} = L_{\max} = 24$ and 32 values are presented as the uncertainty in the BLFQ results.

	BLFQ (running-α_s [3]) this work	BLFQ (fixed-α_s [48]) [66]	CI [89]	Lattice [90]	DSE [91, 92]
J/ψ	2.05(0)	1.952(3)	2.047	2.10(3)	2.13(4)
χ_{c1}	2.40(0)				
$h_c(1P)$	2.99(1)				
ψ'	2.02(0)	2.05(2)			
$\psi(1D)$	3.36(0)				
Υ	3.38(0)	1.985(1)	2.012		
χ_{b1}	2.46(0)				
$h_b(1P)$	2.99(0)				
Υ'	2.01(1)	1.992(1)			
$\Upsilon(1D)$	3.38(0)				
Υ''	2.01(0)				

www.manaraa.com

off-diagonal hadron matrix element to q, $I^{+}_{1,0}(q^2)/q$, at $q^2 = 0$ according to Eq. (2.74). This value thereby reflects the subtle structure of the mesons. Meanwhile, one should be aware that different values of the magnetic moments could be obtained when a different prescription is chosen in extracting the elastic form factors (cf. the GK prescription in Eq. (2.74)) [101].

Table 2.7 The quadrupole moments $\mathrm{Q} \times M^2$ [Eq. (2.77)] for spin-1 charmonia and bottomonia. M is the mass of the corresponding meson, which are taken from PDG [2] if available, and the $\Upsilon(1D)$ mass is taken from Ref. [3]. The difference between the $N_{\max} = L_{\max} = 24$ and 32 values are presented as the uncertainty in the BLFQ results.

	BLFQ (running-α_s [3]) this work	BLFQ (fixed-α_s [48]) [66]	CI [89]	Lattice [90]	DSE [91, 92]
J/ψ	-0.816(4)	-0.78(2)	-0.748	-0.23(2)	-0.28(1)
χ_{c1}	-6.74(6)				
$h_c(1P)$	6.45(0)				
ψ'	0.45(7)	0.2(2)			
$\psi(1D)$	-7.3(2)				
Υ	-0.668(2)	-0.731(9)	-0.704		
χ_{b1}	-19.7(0)				
$h_b(1P)$	31.1(0)				
Υ'	0.25(4)	0.1(1)			
$\Upsilon(1D)$	-22.5(0)				
Υ''	1.5(1)				

Table 2.7 shows that the meson states with orbital excitations have rather large quadrupole moments from the BLFQ calculation, such as χ_{b1} and $\Upsilon(1D)$. The quadrupole moment describes the effective shape of the ellipsoid of the charge distribution. A large magnetic moment indicates a strong deviation from the spherically symmetry, which is expected for states assigned as P-waves and D-waves.

2.3 Radiative transitions

The electromagnetic (EM) transition between quarkonium states, which occurs via emission of a photon, $\psi_A \to \psi_B \gamma$, offers insights into the internal structure and the dynamics of such systems. The magnetic dipole (M1) transition, which takes place between pseudoscalar and vector mesons ($\psi_A, \psi_B = \mathcal{V}, \mathcal{P}$ or $\mathcal{P}, \mathcal{V}$), has been detected with strong signals [2] and stimulates various theoretical investigations [103, 14, 6, 7, 104].

www.manaraa.com

Similarly, the EM Dalitz decay [105], $\psi_A \to \psi_B l^+ l^-$, can be treated by coupling a virtual photon to the final lepton pair. The Dalitz decay, also known as the leptonic conversion decay, provides additional information about the meson structure owing to the virtual photon kinematics. Though widely observed in the light meson sector, such as $\phi \to \pi^0 e^+ e^-$ [106], $\phi \to \eta e^+ e^-$ [107, 108], and $\omega \to \pi^0 e^+ e^-$ [109, 110], only a few such decays have been detected in the heavy sector. The observed Dalitz decays of quarkonium are decays to a light meson plus a lepton pair, such as $J/\psi \to \eta e^+ e^-$, $J/\psi \to \eta' e^+ e^-$ [111], and $\psi(3686) \to \eta' e^+ e^-$ [112]. We investigate the M1 EM Dalitz decay with initial and final mesons both being heavy quarkonia, in the hope of providing another probe of the interaction of quarkonium states with photons.

2.3.1 Transition form factor and decay width

The Lorentz covariant decomposition for the electromagnetic transition matrix element between a vector meson ($\mathcal{V}$) and a pseudoscalar ($\mathcal{P}$) is [90],

$$I^{\mu}_{m_j} \equiv \langle \mathcal{P}(P)| J^{\mu}(0) |\mathcal{V}(P', m_j)\rangle = \frac{2V(q^2)}{m_{\mathcal{P}} + m_{\mathcal{V}}} \epsilon^{\mu\alpha\beta\sigma} P_{\alpha} P'_{\beta} e_{\sigma}(P', m_j) \,, \tag{2.78}$$

where $q^{\mu} = P'^{\mu} - P^{\mu}$ represents the momentum transfer between the two mesons. $V(q^2)$ is the transition form factor. $m_{\mathcal{P}}$ and $m_{\mathcal{V}}$ are the masses of the pseudoscalar and the vector, respectively. e_{σ} is the polarization vector of the vector meson, and $m_j = 0, \pm 1$ is the magnetic projection. A detailed derivation of the Lorentz decomposition can be found in Appendix D.3.

In the physical process of $\mathcal{V} \to \mathcal{P} + \gamma$, the photon is on shell ($q^2 = 0$). The transition amplitude is:

$$\mathcal{M}_{m_j,\lambda} = \langle \mathcal{P}(P)| J^{\mu}(0) |\mathcal{V}(P', m_j)\rangle \, \epsilon^{*}_{\mu,\lambda}(q)|_{q^2=0} \,, \tag{2.79}$$

where $\epsilon_{\mu,\lambda}$ is the polarization vector of the final-state photon with its spin projection $\lambda = \pm 1$. The decay width is usually measured in the rest frame of the initial particle, as such, the momenta of the initial meson, final meson, and the photon read (see Appendix A.1 for the convention of ordering the 4-vector components in light-front coordinates),

$$\begin{aligned} P' &= (m_{\mathcal{V}}, m_{\mathcal{V}}, 0, 0) \,, \\ P &= (\sqrt{m_{\mathcal{P}}^2 + k^2}, \sqrt{m_{\mathcal{P}}^2 + k^2}, k, 0) \,, \\ q &= P' - P = (k, k, -k, 0) \,. \end{aligned}$$

www.manaraa.com

The momentum of the photon is determined by energy-momentum conservation, $|\vec{q}| = k = (m_{\mathcal{V}}^2 - m_{\mathcal{P}}^2)/2m_{\mathcal{V}}$. The transition amplitudes for different polarizations are,

$$\mathcal{M}_{m_j,\lambda} = \frac{4V(q^2)}{m_{\mathcal{P}} + m_{\mathcal{V}}} \begin{cases} \mp\dfrac{im_{\mathcal{V}}k}{2\sqrt{2}}, & m_j = 0, \lambda = \pm 1 \\ -\dfrac{im_{\mathcal{V}}k}{4}, & m_j = 1, \lambda = \pm 1 \\ \dfrac{im_{\mathcal{V}}k}{4}, & m_j = -1, \lambda = \pm 1 \end{cases} . \tag{2.80}$$

The decay width of $\mathcal{V} \to \mathcal{P} + \gamma$ follows by averaging over the initial polarization and summing over the final polarization.

$$\Gamma(\mathcal{V} \to \mathcal{P} + \gamma) = \int \mathrm{d}\Omega_q \frac{1}{32\pi^2} \frac{|\vec{q}|}{m_{\mathcal{V}}^2} \frac{1}{2J_{\mathcal{V}} + 1} \sum_{m_j,\lambda} |\mathcal{M}_{m_j,\lambda}|^2 = \frac{(m_{\mathcal{V}}^2 - m_{\mathcal{P}}^2)^3}{(2m_{\mathcal{V}})^3 (m_{\mathcal{P}} + m_{\mathcal{V}})^2} \frac{|V(0)|^2}{(2J_{\mathcal{V}} + 1)\pi} . \tag{2.81}$$

$J_{\mathcal{V}} = 1$ is the spin of the initial vector meson. To calculate the width of $\mathcal{P} \to \mathcal{V} + \gamma$, exchange $m_{\mathcal{V}}$ and $m_{\mathcal{P}}$, and replace $J_{\mathcal{V}}$ with $J_{\mathcal{P}} = 0$ for the initial pseudoscalar in Eq. (2.81).

The amplitude of the Dalitz decay $\mathcal{V} \to \mathcal{P} + l^+ + l^-$ reads

$$\mathcal{M}_{m_j,\lambda} = \langle \mathcal{V}(P', m_j) | J^\mu(0) | \mathcal{P}(P) \rangle \frac{1}{q^2} \bar{u}\gamma^\mu u, \tag{2.82}$$

where $\bar{u}\gamma^\mu u$ is the leptonic current.

For the Dalitz decay $\psi_A \to \psi_B l^+ l^-$ ($\psi_A, \psi_B = \mathcal{V}, \mathcal{P}$ or $\mathcal{P}, \mathcal{V}$), the physical region of interest is $4m_l^2 \le q^2 \le (m_A - m_B)^2$. The effective mass spectrum of the lepton pair could be derived as [113]:

$$\begin{aligned} \frac{\mathrm{d}\Gamma(\psi_A \to \psi_B l^+ l^-)}{\mathrm{d}q^2 \cdot \Gamma(\psi_A \to \psi_B \gamma)} = \frac{\alpha}{3\pi} \sqrt{1 - \frac{4m_l^2}{q^2}} \left(1 + \frac{2m_l^2}{q^2}\right) \frac{1}{q^2} \\ \times \left[\left(1 + \frac{q^2}{m_A^2 - m_B^2}\right)^2 - \frac{4m_A^2 q^2}{(m_A^2 - m_B^2)^2} \right]^{3/2} \left| \frac{V(q^2)}{V(0)} \right|^2 . \end{aligned} \tag{2.83}$$

2.3.2 Light-front dynamics

In principle, the transition form factor $V(q^2)$ defined in Eq. (2.78) is Lorentz invariant. However, practical calculations usually take place in a finite Fock space, where the Lorentz symmetry is violated. Consequently, two spurious dependences of the transition form factor could emerge, one on the current component and the other on the reference frame. In such situations, knowing the current or frame dependence could

www.manaraa.com

help quantify theoretical uncertainties. One further issue to resolve is whether there exists a preferred current or a preferred frame for calculations in finite Fock space such that the neglected contributions from higher Fock sectors could be minimized. It is the purpose of our work to investigate the violation of the Lorentz symmetry through these two effects.

Let us first study the transition form factor from different current components ($\mu = +, -, x, y$) and different magnetic projections ($m_j = 0, \pm 1$) of the vector meson, without choosing any specific frame. As in the calculation for the elastic form factors in Section 2.2, we use $J^R \equiv J^x + iJ^y$ and $J^L \equiv J^x - iJ^y$ as the transverse currents. From the vector decomposition in Eq. (2.78), we obtain the following formulas,

$$I^+_{m_j} = \frac{2V(q^2)}{m_{\mathcal{P}} + m_{\mathcal{V}}} \begin{cases} 0, & m_j = 0 \\ \dfrac{i}{\sqrt{2}} P^+ P'^+ \left[\dfrac{P^R}{P^+} - \dfrac{P'^R}{P'^+}\right], & m_j = 1 \\ -\dfrac{i}{\sqrt{2}} P^+ P'^+ \left[\dfrac{P^L}{P^+} - \dfrac{P'^L}{P'^+}\right], & m_j = -1 \end{cases} \tag{2.84}$$

$$I^-_{m_j} = \frac{2V(q^2)}{m_{\mathcal{P}} + m_{\mathcal{V}}} \begin{cases} im_{\mathcal{V}} \dfrac{P'^R P^L - P'^L P^R}{P'^+}, & m_j = 0 \\ \dfrac{i}{\sqrt{2}} \left[\dfrac{m_{\mathcal{P}}^2 P'^R + P'^R P^R P^L}{P^+} - \dfrac{m_{\mathcal{V}}^2 P^R + P'^R P'^R P^L}{P'^+}\right], & m_j = 1 \\ -\dfrac{i}{\sqrt{2}} \left[\dfrac{m_{\mathcal{P}}^2 P'^L + P'^L P^R P^L}{P^+} - \dfrac{m_{\mathcal{V}}^2 P^L + P'^L P'^L P^R}{P'^+}\right], & m_j = -1 \end{cases} \tag{2.85}$$

$$I^R_{m_j} = \frac{2V(q^2)}{m_{\mathcal{P}} + m_{\mathcal{V}}} \begin{cases} -im_{\mathcal{V}} P^+ \left[\dfrac{P^R}{P^+} - \dfrac{P'^R}{P'^+}\right], & m_j = 0 \\ \dfrac{i}{\sqrt{2}} P'^R P^+ \left[\dfrac{P^R}{P^+} - \dfrac{P'^R}{P^+}\right], & m_j = 1 \\ -\dfrac{i}{\sqrt{2}} P'^+ \left[P^+ \left(\dfrac{m_{\mathcal{P}}^2}{(P^+)^2} - \dfrac{m_{\mathcal{V}}^2}{(P'^+)^2}\right) + P^R \left(\dfrac{P^L}{P^+} - \dfrac{P'^L}{P'^+}\right)\right], & m_j = -1 \end{cases} \tag{2.86}$$

$$I^L_{m_j} = \frac{2V(q^2)}{m_{\mathcal{P}} + m_{\mathcal{V}}} \begin{cases} im_{\mathcal{V}} P^+ \left[\dfrac{P^L}{P^+} - \dfrac{P'^L}{P'^+}\right], & m_j = 0 \\ \dfrac{i}{\sqrt{2}} P'^+ \left[P^+ \left(\dfrac{m_{\mathcal{P}}^2}{(P^+)^2} - \dfrac{m_{\mathcal{V}}^2}{(P'^+)^2}\right) + P^L \left(\dfrac{P^R}{P^+} - \dfrac{P'^R}{P'^+}\right)\right], & m_j = 1 \\ -\dfrac{i}{\sqrt{2}} P'^L P^+ \left[\dfrac{P^L}{P^+} - \dfrac{P'^L}{P'^+}\right], & m_j = -1 \end{cases} \tag{2.87}$$

www.manaraa.com

Those matrix elements are related through the Lorentz transformation, and all the non-vanishing 11 out of the 12 different formulas in Equations (2.84) to (2.87) should lead to the same $V(q^2)$. The hadron matrix elements of different current components but with the same m_j can be related through the transverse Lorentz boost as written in Eq. (2.51). In terms of the +, $\perp$ and $-$ hadron matrix elements, we get,

$$\begin{aligned}
&\langle \mathcal{P}(P^+, \vec{P}_\perp + P^+\vec{\beta}_\perp)|\vec{J}_\perp|\mathcal{V}(P'^+, \vec{P}'_\perp + P'^+\vec{\beta}_\perp, m_j)\rangle \\
&\qquad = \langle \mathcal{P}(P^+, \vec{P}_\perp)|\, \vec{J}_\perp\, |\mathcal{V}(P'^+, \vec{P}'_\perp, m_j)\rangle + \vec{\beta}_\perp \langle \mathcal{P}(P^+, \vec{P}_\perp)|\, J^+\, |\mathcal{V}(P'^+, \vec{P}'_\perp, m_j)\rangle \ . \\
&\langle \mathcal{P}(P^+, \vec{P}_\perp + P^+\vec{\beta}_\perp)|J^-|\mathcal{V}(P'^+, \vec{P}'_\perp + P'^+\vec{\beta}_\perp, m_j)\rangle \\
&\qquad = \langle \mathcal{P}(P^+, \vec{P}_\perp)|\, J^-\, |\mathcal{V}(P'^+, \vec{P}'_\perp, m_j)\rangle + 2\vec{\beta}_\perp \cdot \langle \mathcal{P}(P^+, \vec{P}_\perp)|\, \vec{J}_\perp\, |\mathcal{V}(P'^+, \vec{P}'_\perp, m_j)\rangle \\
&\qquad\quad + \vec{\beta}_\perp^2 \langle \mathcal{P}(P^+, \vec{P}_\perp)|\, J^+\, |\mathcal{V}(P'^+, \vec{P}'_\perp, m_j)\rangle \ .
\end{aligned} \tag{2.88}$$

The above relations imply that, for each m_j state of the vector meson, using J^+, J^R, J^L and J^- should give the same $V(q^2)$. One exception is that with $m_j = 0$, $V(q^2)$ cannot be extracted from J^+. One can verify it by applying Eq. (2.88) to Eqs. (2.84), (2.85), (2.86) and (2.87). Though this transformation itself is kinematic and survives the Fock space truncation, the current operator J^μ is not complete in the truncated Fock space.

Results from different current components may be different due to violations of Lorentz symmetry introduced by the Fock sector truncation as well as by the modeling of systems. These approximations have led to extensive discussions in the literature [70, 71, 72, 75, 73]. The "+" component, known as the "good current", is typically used, together with the Drell-Yan frame ($q^+ = 0$), to avoid contributions from pair production/annihilation in vacuum. This is also our choice in calculating the elastic form factors in Section 2.2. The transverse components have been shown to be consistent with the "+" component in the limit of zero momentum transfer in certain theories, such as the ϕ^3 theory [72] and the spin-0 two-fermion systems [73]. We have also shown in Section 2.2 that in calculating the charge form factor of the spin-0 particles, however only in the Drell-Yan or the longitudinal frames, using the transverse current would lead to the same results with the plus current. Another option, the "-" component, is known as the "bad current", due to its association with the zero-mode contributions.

The question then arises: to what extent is the Lorentz symmetry violated by Fock sector truncation? To be more concrete, for calculations in the valence Fock sector, are we expecting 11 different results (from Equations (2.84) to (2.87)) or less?

www.manaraa.com

First, we expect that the results from different m_j states of the vector meson might be different, since the ladder operator relating those states is dynamic and cannot be preserved in the valence Fock sector. Considering the symmetry between the $m_j = 1$ and $m_j = -1$ states, there are at least two different results, one with $m_j = 0$ and the other with $m_j = \pm 1$. Then, we know that for each m_j value, using different current components could make a difference if the transverse boost in Eq. (2.88) is not guaranteed. But the two transverse currents, J^R and J^L, should give the same results since rotations in the transverse plane should be preserved in the valence Fock sector. Then, there are three different results for each m_j state, from J^+, $J^\perp$, or J^-. Therefore, in total, there are five (not six, since the combination of J^+ and $m_j = 0$ is not available) different extractions of the transition form factors with different current components and different m_j in the valence Fock sector.

We summarize the formulas of extracting the transition form factor $V(q^2)$ from different current components and different m_j states of the vector meson in Table. 2.8. To simplify the expression, we take the two variables defined in Sec. 2.2.1, $z \equiv (P'^+ - P^+)/P'^+$ and $\vec{\Delta}_\perp \equiv \vec{q}_\perp - z\vec{P}'_\perp$. This also prepares us to study the frame dependence. The five independent extractions in a truncated Fock space are indicated by five different colors in Table. 2.8.

In the valence Fock sector, the five independent hadron matrix elements overdetermine the transition form factor. In practice, the different prescriptions of extracting the same transition form factor could provide a test of violation of the Lorentz symmetry in the calculation. But more importantly, we would like to know if there is a preferred choice such that the result is closer to the true result that would emerge from a full Fock space basis.

Working in the valence Fock sector, we take the impulse approximation, in which the interaction of the external current with the meson is the summation of its coupling to the quark and to the antiquark, as illustrated in Fig. 2.10. The vertex dressing as well as pair creation/annihilation from higher order diagrams are neglected. The hadron matrix element can be written accordingly as a sum of the quark term and the antiquark term:

$$\langle \mathcal{P}(P')| J^\mu(0) |\mathcal{V}(P, m_j)\rangle = eQ_f \langle \mathcal{P}(P')| J^\mu_q(0) |\mathcal{V}(P, m_j)\rangle - eQ_f \langle \mathcal{P}(P')| J^\mu_{\bar{q}}(0) |\mathcal{V}(P, m_j)\rangle \ . \tag{2.89}$$

www.manaraa.com

Table 2.8 The formulas of extracting the transition form factor $V(q^2)$ from different current components and different m_j states of the vector meson, derived from Eqs. (2.84), (2.85), (2.86) and (2.87). The five independent extractions in a truncated Fock space are indicated in five different colors: orange, green, red, blue and brown.

$\frac{2V(q^2)}{m_{\mathcal{P}}+m_{\mathcal{V}}}$	$m_j=0$	$m_j=1$	$m_j=-1$
J^+	-	$\frac{i\sqrt{2}I_1^+}{P'^+\Delta^R}$	$\frac{-i\sqrt{2}I_{-1}^+}{P'^+\Delta^L}$
J^R	$\frac{-iI_0^R}{m_{\mathcal{V}}\Delta^R}$	$\frac{i\sqrt{2}I_1^R}{P'^R\Delta^R}$	$\frac{i\sqrt{2}(1-z)I_{-1}^R}{(m_{\mathcal{P}}^2-(1-z)^2m_{\mathcal{V}}^2-P^R\Delta^L)}$
J^L	$\frac{iI_0^L}{m_{\mathcal{V}}\Delta^L}$	$\frac{-i\sqrt{2}(1-z)I_1^L}{(m_{\mathcal{P}}^2-(1-z)^2m_{\mathcal{V}}^2-P^L\Delta^R)}$	$\frac{-i\sqrt{2}I_{-1}^L}{P'^L\Delta^L}$
J^-	$\frac{-iP^+I_0^-}{m_{\mathcal{V}}(\Delta^RP^L-\Delta^LP^R)}$	$\frac{-i\sqrt{2}P^+P'^+I_1^-}{P'^+P'^R(m_{\mathcal{P}}^2-P^L\Delta^R)-P^+P^Rm_{\mathcal{V}}^2}$	$\frac{i\sqrt{2}P^+P'^+I_{-1}^-}{P'^+P'^L(m_{\mathcal{P}}^2-P^R\Delta^L)-P^+P^Lm_{\mathcal{V}}^2}$

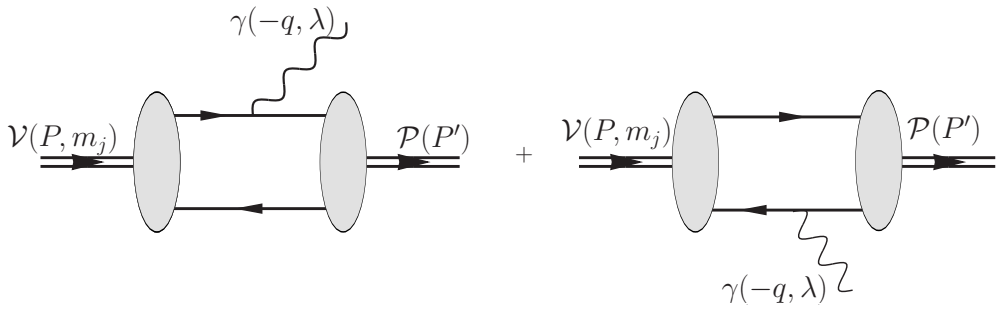

Figure 2.10 Radiative transition from vector to pseudoscalar meson in $|q\bar{q}\rangle$ Fock space representation within the impulse approximation. In these figures light-front time x^+ flows to the right. The double-lines represent the hadrons. The solid lines represent the quark or the antiquark. The wavy lines represent the probing photon. The shaded areas represent the light-front wavefunctions. (Figure adapted from Ref. [9].)

www.manaraa.com

Bu restoring the quark charges, the current operator reads $J^\mu(x) = e\sum_f Q_f\overline{\psi}_f(x)\gamma^\mu\psi_f(x)$ where $\psi_f(x)$ is the quark field operator with flavor f ($f = u, d, s, c, b, t$). J_q and $J_{\bar{q}}$ are the normal ordered pure quark ($b^\dagger b$) and antiquark ($d^\dagger d$) part of J^μ, respectively, where b (d) is the quark (antiquark) annihilation operator. The dimensionless fractional charge of the quark is, $Q_f = Q_c = +2/3$ for the charm quark and $Q_f = Q_b = -1/3$ for the bottom quark. The electric charge $e = \sqrt{4\pi\alpha_{\rm EM}}$. For quarkonium, due to the charge conjugation symmetry, the antiquark gives the same contribution as the quark to the total hadronic current. So, for our purpose, we calculate the hadron matrix element for the quark part. As such, we compute $\hat{V}(q^2)$ which is related to $V(q^2)$ by

$$V(q^2) = 2eQ_f\hat{V}(q^2)\ .$$

We can then write out the hadron matrix elements in the valence light-front wavefunction representation from the quark current, as in Eqs. (2.90) to (2.93).

$$I^+_{m_j} = \sum_{s,\bar{s}}\int_0^1\frac{\mathrm{d}x}{2x(1-x)}\int\frac{\mathrm{d}^2\vec{k}_\perp}{(2\pi)^3}\frac{1}{x'}2\sqrt{x'P'^+xP^+}\psi^*_{s\bar{s}/\mathcal{P}}(\vec{k}_\perp,x)\psi^{(m_j)}_{s\bar{s}/\mathcal{V}}(\vec{k}'_\perp,x')\ . \tag{2.90}$$

$$\begin{aligned}I^-_{m_j} = &\sum_{\bar{s}}\int_0^1\frac{\mathrm{d}x}{2x(1-x)}\int\frac{\mathrm{d}^2\vec{k}_\perp}{(2\pi)^3}\frac{1}{x'}\frac{2}{\sqrt{x'P'^+xP^+}}\\
&\times\Big[\psi^*_{\uparrow\bar{s}/\mathcal{P}}(\vec{k}_\perp,x)\psi^{(m_j)}_{\uparrow\bar{s}/\mathcal{V}}(\vec{k}'_\perp,x')[m_q^2+(k'^R+x'P'^R)(k^L+xP^L)]\\
&+\psi^*_{\uparrow\bar{s}/\mathcal{P}}(\vec{k}_\perp,x)\psi^{(m_j)}_{\downarrow\bar{s}/\mathcal{V}}(\vec{k}'_\perp,x')m_q(k^L+xP^L-k'^L-x'P'^L)\\
&+\psi^*_{\downarrow\bar{s}/\mathcal{P}}(\vec{k}_\perp,x)\psi^{(m_j)}_{\uparrow\bar{s}/\mathcal{V}}(\vec{k}'_\perp,x')m_q(k'^R+x'P'^R-k^R-xP^R)\\
&+\psi^*_{\downarrow\bar{s}/\mathcal{P}}(\vec{k}_\perp,x)\psi^{(m_j)}_{\downarrow\bar{s}/\mathcal{V}}(\vec{k}'_\perp,x')[m_q^2+(k'^L+x'P'^L)(k^R+xP^R)]\Big]\ ,\end{aligned} \tag{2.91}$$

$$\begin{aligned}I^R_{m_j} = &\sum_{\bar{s}}\int_0^1\frac{\mathrm{d}x}{2x(1-x)}\int\frac{\mathrm{d}^2\vec{k}_\perp}{(2\pi)^3}\frac{1}{x'}\frac{2}{\sqrt{x'P'^+xP^+}}\\
&\times\Big[\psi^*_{\uparrow\bar{s}/\mathcal{P}}(\vec{k}_\perp,x)\psi^{(m_j)}_{\uparrow\bar{s}/\mathcal{V}}(\vec{k}'_\perp,x')xP^+(k'^R+x'P'^R)\\
&+\psi^*_{\uparrow\bar{s}/\mathcal{P}}(\vec{k}_\perp,x)\psi^{(m_j)}_{\downarrow\bar{s}/\mathcal{V}}(\vec{k}'_\perp,x')m_q(xP^+-x'P'^+)\\
&+\psi^*_{\downarrow\bar{s}/\mathcal{P}}(\vec{k}_\perp,x)\psi^{(m_j)}_{\downarrow\bar{s}/\mathcal{V}}(\vec{k}'_\perp,x')x'P'^+(k^R+xP^R)\Big]\ ,\end{aligned} \tag{2.92}$$

www.manaraa.com

$$
\begin{aligned}
I^L_{m_j} = &\sum_{\bar{s}} \int_0^1 \frac{\mathrm{d}x}{2x(1-x)} \int \frac{\mathrm{d}^2\vec{k}_\perp}{(2\pi)^3} \frac{1}{x'} \frac{2}{\sqrt{x'P'^+ xP^+}} \\
&\times \Big[\psi^*_{\uparrow\bar{s}/\mathcal{P}}(\vec{k}_\perp, x) \psi^{(m_j)}_{\uparrow\bar{s}/\mathcal{V}}(\vec{k}'_\perp, x') x' P'^+ (k^L + xP^L) \\
&+ \psi^*_{\downarrow\bar{s}/\mathcal{P}}(\vec{k}_\perp, x) \psi^{(m_j)}_{\uparrow\bar{s}/\mathcal{V}}(\vec{k}'_\perp, x') m_q (x' P'^+ - xP^+) \\
&+ \psi^*_{\downarrow\bar{s}/\mathcal{P}}(\vec{k}_\perp, x) \psi^{(m_j)}_{\downarrow\bar{s}/\mathcal{V}}(\vec{k}'_\perp, x') xP^+ (k'^L + x' P'^L) \Big] ,
\end{aligned}
\tag{2.93}
$$

Now let us analyze the transition form factors extracted from these hadron matrix elements. There are five groups of combinations of the current component and the magnetic projection according to Table 2.8.

1. J^+ and $m_j = \pm 1$

   The light-front wavefunction representation of the transition form factor reads,

$$
\begin{aligned}
\hat{V}|_{J^+, m_j=1}(q^2) =& \frac{i(m_\mathcal{V} + m_\mathcal{P})}{\sqrt{2} P'^+ \Delta^R} \langle \mathcal{P}(P) | J^+_q(0) | \mathcal{V}(P', m_j = 1) \rangle \\
=& \frac{i\sqrt{2}(m_\mathcal{V} + m_\mathcal{P})}{\Delta^R} \sum_{s,\bar{s}} \int_0^1 \frac{\mathrm{d}x}{2x(1-x)} \int \frac{\mathrm{d}^2\vec{k}_\perp}{(2\pi)^3} \sqrt{\frac{x(1-z)}{x + z(1-x)}} \\
&\times \psi^*_{s\bar{s}/\mathcal{P}}(\vec{k}_\perp, x) \psi^{(m_j=1)}_{s\bar{s}/\mathcal{V}}(\vec{k}'_\perp, x') \, .
\end{aligned}
\tag{2.94}
$$

   Note that the $m_j = -1$ state would lead to the same result, considering the symmetry of the $m_j = \pm 1$ light-front wavefunctions. According to Eq. (2.94), the transition form factor can be evaluated as a function of z and $\Delta_\perp$. It is evident from this expression that the overlapped spin components of the two wavefunctions indicate no spin-flip (between spin-triplet and spin-singlet), which may appear counter-intuitive for the M1 transition.

2. $J^{R/L}$ and $m_j = 0$

   Using J^R and J^L current components should give the same result with the $m_j = 0$ state of the vector

www.manaraa.com

meson. Here we present the expression derived from J^R,

$$
\begin{aligned}
&\hat{V}|_{J^R,m_j=0}(q^2) \\
&= -i\frac{m_{\mathcal{V}}+m_{\mathcal{P}}}{2m_{\mathcal{V}}\Delta^R}\langle\mathcal{P}(P)|\,J_q^R(0)\,|\mathcal{V}(P',m_j=0)\rangle \\
&= -i\frac{m_{\mathcal{V}}+m_{\mathcal{P}}}{2m_{\mathcal{V}}\Delta^R}\sum_{\bar{s}}\int_0^1\frac{\mathrm{d}x}{2x(1-x)}\int\frac{\mathrm{d}^2\vec{k}_\perp}{(2\pi)^3} \\
&\quad\times\Big\{\psi^*_{\uparrow\bar{s}/\mathcal{P}}(\vec{k}_\perp,x)\psi^{(m_j=0)}_{\uparrow\bar{s}/\mathcal{V}}(\vec{k}'_\perp,x')\Big\{\frac{2\sqrt{x(1-z)}}{\sqrt{[x+z(1-x)]^3}}(k^R-\frac{x}{z}\Delta^R)+\frac{2}{z}\sqrt{\frac{x(1-z)}{x+z(1-x)}}q^R\Big\} \\
&\quad+\psi^*_{\uparrow\bar{s}/\mathcal{P}}(\vec{k}_\perp,x)\psi^{(m_j=0)}_{\downarrow\bar{s}/\mathcal{V}}(\vec{k}'_\perp,x')\frac{2m_q z}{\sqrt{x(1-z)[x+z(1-x)]^3}} \\
&\quad+\psi^*_{\downarrow\bar{s}/\mathcal{P}}(\vec{k}_\perp,x)\psi^{(m_j=0)}_{\downarrow\bar{s}/\mathcal{V}}(\vec{k}'_\perp,x')\Big\{\frac{2}{\sqrt{x(1-z)[x+z(1-x)]}}(k^R-\frac{x}{z}\Delta^R)+\frac{2}{z}\sqrt{\frac{x(1-z)}{x+z(1-x)}}q^R\Big\}\Big\}
\end{aligned}
\tag{2.95}
$$

We can further simplify the expression by taking advantage of the symmetries in the light-front wave-functions,

$$
\begin{aligned}
&\psi^{(m_j=0)}_{\uparrow\uparrow/\mathcal{V}}(\vec{k}_\perp,x)=-\psi^{(m_j=0)*}_{\downarrow\downarrow/\mathcal{V}}(\vec{k}_\perp,x), \qquad \psi_{\uparrow\uparrow/\mathcal{P}}(\vec{k}_\perp,x)=\psi^*_{\downarrow\downarrow/\mathcal{P}}(\vec{k}_\perp,x), \\
&\psi^{(m_j=0)}_{\uparrow\downarrow/\mathcal{V}}(\vec{k}_\perp,x)=\psi^{(m_j=0)}_{\downarrow\uparrow/\mathcal{V}}(\vec{k}_\perp,x), \qquad \psi_{\uparrow\downarrow/\mathcal{P}}(\vec{k}_\perp,x)=-\psi_{\downarrow\uparrow/\mathcal{P}}(\vec{k}_\perp,x)\,.
\end{aligned}
\tag{2.96}
$$

This leads to a partial cancellation of the first and the third terms in Eq. (2.95) and reduces it to,

$$
\begin{aligned}
&\hat{V}|_{J^R,m_j=0}(q^2) \\
&= -i\frac{m_{\mathcal{V}}+m_{\mathcal{P}}}{2m_{\mathcal{V}}\Delta^R}\sum_{\bar{s}}\int_0^1\frac{\mathrm{d}x}{2x(1-x)}\int\frac{\mathrm{d}^2\vec{k}_\perp}{(2\pi)^3}\frac{2}{\sqrt{x(1-z)[x+z(1-x)]^3}} \\
&\quad\times\Big[\psi^*_{\uparrow\bar{s}/\mathcal{P}}(\vec{k}_\perp,x)\psi^{(m_j=0)}_{\uparrow\bar{s}/\mathcal{V}}(\vec{k}'_\perp,x')(zk^R-x\Delta^R)+\psi^*_{\uparrow\bar{s}/\mathcal{P}}(\vec{k}_\perp,x)\psi^{(m_j=0)}_{\downarrow\bar{s}/\mathcal{V}}(\vec{k}'_\perp,x')m_q z\Big] \\
&= -i\frac{m_{\mathcal{V}}+m_{\mathcal{P}}}{2m_{\mathcal{V}}\Delta^R}\int_0^1\frac{\mathrm{d}x}{2x(1-x)}\int\frac{\mathrm{d}^2\vec{k}_\perp}{(2\pi)^3}\frac{2}{\sqrt{x(1-z)[x+z(1-x)]^3}} \\
&\quad\times\Big[[\frac{1}{2}\psi^*_{\uparrow\downarrow-\downarrow\uparrow/\mathcal{P}}(\vec{k}_\perp,x)\psi^{(m_j=0)}_{\uparrow\downarrow+\downarrow\uparrow/\mathcal{V}}(\vec{k}'_\perp,x')+\psi^*_{\uparrow\uparrow/\mathcal{P}}(\vec{k}_\perp,x)\psi^{(m_j=0)}_{\uparrow\uparrow/\mathcal{V}}(\vec{k}'_\perp,x')](zk^R-x\Delta^R) \\
&\quad+\frac{1}{\sqrt{2}}[\psi^*_{\uparrow\uparrow/\mathcal{P}}(\vec{k}_\perp,x)\psi^{(m_j=0)}_{\uparrow\downarrow+\downarrow\uparrow/\mathcal{V}}(\vec{k}'_\perp,x')+\psi^*_{\uparrow\downarrow-\downarrow\uparrow/\mathcal{P}}(\vec{k}_\perp,x)\psi^{(m_j=0)}_{\downarrow\downarrow/\mathcal{V}}(\vec{k}'_\perp,x')]m_q z\Big]\,.
\end{aligned}
\tag{2.97}
$$

In the second equality, we adopt the notations of spin configurations as $\psi_{\uparrow\downarrow\pm\downarrow\uparrow}\equiv(\psi_{\uparrow\downarrow}\pm\psi_{\downarrow\uparrow})/\sqrt{2}$. This would be convenient to study the non-relativistic limit. According to Eq. (2.97), the transition form factor can be evaluated as a function of z and $\Delta_\perp$.

www.manaraa.com

3. $J^{R/L}$ and $m_j = \pm 1$

According to our discussion, these four choices should give the same result based on the symmetry in the transverse plane. However, this "equivalence" is not very explicit in the light-front wavefunction representation, and we see two pairs of choices.

The first pair contains these two extractions: (J^R and $m_j = 1$) and (J^L and $m_j = -1$).

$$
\begin{aligned}
&\hat{V}|_{J^R,m_j=1}(q^2) \\
=&\frac{i(m_{\mathcal{V}}+m_{\mathcal{P}})}{\sqrt{2}P'^R\Delta^R}\langle\mathcal{P}(P)|\,J_q^R(0)\,|\mathcal{V}(P',m_j=1)\rangle \\
=&\frac{i(m_{\mathcal{V}}+m_{\mathcal{P}})}{\sqrt{2}P'^R\Delta^R}\sum_{\bar{s}}\int_0^1\frac{\mathrm{d}x}{2x(1-x)}\int\frac{\mathrm{d}^2\vec{k}_\perp}{(2\pi)^3} \\
&\times\left\{\psi^*_{\uparrow\bar{s}/\mathcal{P}}(\vec{k}_\perp,x)\psi^{(m_j=1)}_{\uparrow\bar{s}/\mathcal{V}}(\vec{k}'_\perp,x')\frac{2}{\sqrt{x(1-z)[x+z(1-x)]}}(k^R+(1-x)\Delta^R+[x+z(1-x)]P'^R)\right. \\
&+\psi^*_{\downarrow\bar{s}/\mathcal{P}}(\vec{k}_\perp,x)\psi^{(m_j=1)}_{\uparrow\bar{s}/\mathcal{V}}(\vec{k}'_\perp,x')\frac{2m_q z}{\sqrt{x(1-z)[x+z(1-x)]^3}} \\
&\left.+\psi^*_{\downarrow\bar{s}/\mathcal{P}}(\vec{k}_\perp,x)\psi^{(m_j=1)}_{\downarrow\bar{s}/\mathcal{V}}(\vec{k}'_\perp,x')\frac{2\sqrt{x(1-z)}}{\sqrt{[x+z(1-x)]^3}}(k^R+x(1-z)P'^R-x\Delta^R)\right\}.
\end{aligned}
\tag{2.98}
$$

Unlike extracting the transition from factor with the first two choices as in Eqs. (2.94) and (2.97), fixing the values of z and $\Delta_\perp$ could not uniquely determine the transition form factor in Eq. (2.98). There is an extra dependence on the transverse momentum, $\vec{P}_\perp$, or equivalently on $\vec{P'}_\perp$ or $\vec{q}_\perp$. This implies that the transition form factor extracted this way is not invariant under the transverse boost.

To investigate such dependence, we calculate the transition form factor of $J/\psi \to \eta_c\gamma$ by letting $z = 0$ (this is the same as choosing the Drell-Yan frame, see the definition of frames in Section 2.2.1) and varying the value of P^R. Note that by setting $z = 0$, $\vec{\Delta}_\perp$ becomes $\vec{q}_\perp$, and q^2 should be determined directly from the value of $\vec{\Delta}_\perp$ as $q^2 = -|\vec{\Delta}_\perp|^2$. For convenience, we define the transverse momentum fraction ξ such that $P'^R = \xi\Delta^R$. Note that ξ can be any complex number, and here we consider its real domain of $-\infty < \xi < +\infty$ for simplicity. We could thereby extract the transition form factor numerically as a function of q^2 and ξ according to Eq. (2.98). It is noticeable that in the limit of $\xi \to \pm\infty$, Eq. (2.98) reduces to Eq. (2.94), that is to say, $\lim_{\xi\to\pm\infty}\hat{V}|_{J^R,m_j=1}(q^2) = \hat{V}|_{J^+,m_j=1}(q^2)$. From the results in Fig. 2.11, we see a dramatic dependence of $\hat{V}|_{J^R,m_j=1}(q^2)$ on ξ. This might imply that

www.manaraa.com

the extraction $\hat{V}|_{J^R,m_j=1}(q^2)$ is heavily affected by the Fock space truncation and should not be used in practical calculations.

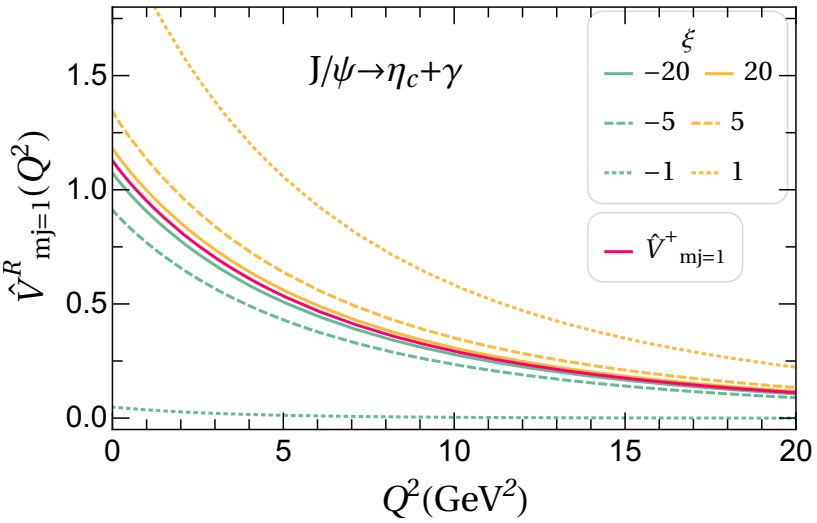

Figure 2.11 The transition form factor of $J/\psi \to \eta_c(1S) + \gamma$ calculated according to Eq. (2.98) at $z = 0$ with different values of $\xi = P^R/\Delta^R$. In this plot, $Q^2 \equiv -q^2 = -|\vec{\Delta}_\perp|^2$, and $\hat{V}|_{J^R,m_j=1}$ ($\hat{V}|_{J^+,m_j=1}$) is labeled as $\hat{V}^R_{m_j=1}$ ($\hat{V}^+_{m_j=1}$). In the limit of $\xi \to \pm\infty$, $\hat{V}|_{J^R,m_j=1}(q^2)$ reduces to $\hat{V}|_{J^+,m_j=1}(q^2)$, and it is shown in the red solid line. The light-front wavefunctions used in this calculation are obtained through the BLFQ approach in Ref. [3].

The second pair contains (J^R and $m_j = -1$) and (J^L and $m_j = 1$).

$$
\begin{aligned}
&\hat{V}|_{J^R,m_j=-1}(q^2) \\
&= \frac{i\sqrt{2}(1-z)}{m_{\mathcal{P}}^2 - (1-z)^2 m_{\mathcal{V}}^2 - P^R\Delta^L} \langle \mathcal{P}(P)| J_q^R(0) |\mathcal{V}(P', m_j = -1)\rangle \\
&= \frac{i\sqrt{2}(1-z)}{m_{\mathcal{P}}^2 - (1-z)^2 m_{\mathcal{V}}^2 - ((1-z)P'^R - \Delta^R)\Delta^L} \sum_{\bar{s}} \int_0^1 \frac{\mathrm{d}x}{2x(1-x)} \int \frac{\mathrm{d}^2\vec{k}_\perp}{(2\pi)^3} \\
&\times \Big\{ \psi^*_{\uparrow\bar{s}/\mathcal{P}}(\vec{k}_\perp, x)\psi^{(m_j=-1)}_{\uparrow\bar{s}/\mathcal{V}}(\vec{k}'_\perp, x')(k^R + (1-x)\Delta^R + [x + z(1-x)]P'^R) \\
&+ \psi^*_{\downarrow\bar{s}/\mathcal{P}}(\vec{k}_\perp, x)\psi^{(m_j=-1)}_{\uparrow\bar{s}/\mathcal{V}}(\vec{k}'_\perp, x') \frac{2m_q z}{\sqrt{x(1-z)[x + z(1-x)]^3}} \\
&+ \psi^*_{\downarrow\bar{s}/\mathcal{P}}(\vec{k}_\perp, x)\psi^{(m_j=-1)}_{\downarrow\bar{s}/\mathcal{V}}(\vec{k}'_\perp, x')(k^R + x(1-z)P'^R - x\Delta^R) \Big\}
\end{aligned}
\tag{2.99}
$$

www.manaraa.com

This formalism of extracting the transition form factor also has the problematic dependence on P'^R, and is therefore not practical to use.

4. J^- and $m_j = 0$

In this combination, the light-front wavefunction representation of the transition form factor reads,

$$\begin{aligned}\hat{V}|_{J^-,m_j=0}(q^2) =& \frac{-iP^+}{m_{\mathcal{V}}(\Delta^R P^L - \Delta^L P^R)} \sum_{\bar{s}} \int_0^1 \frac{\mathrm{d}x}{2x(1-x)} \int \frac{\mathrm{d}^2\vec{k}_\perp}{(2\pi)^3} \frac{1}{x'} \frac{2}{\sqrt{x'P'^+ xP^+}} \\ &\times \Big[\psi^*_{\uparrow\bar{s}/\mathcal{P}}(\vec{k}_\perp, x)\psi^{(m_j=0)}_{\uparrow\bar{s}/\mathcal{V}}(\vec{k}'_\perp, x')[m_q^2 + (k'^R + x'P'^R)(k^L + xP^L)] \\ &+ \psi^*_{\uparrow\bar{s}/\mathcal{P}}(\vec{k}_\perp, x)\psi^{(m_j=0)}_{\downarrow\bar{s}/\mathcal{V}}(\vec{k}'_\perp, x')m_q(k^L + xP^L - k'^L - x'P'^L) \\ &+ \psi^*_{\downarrow\bar{s}/\mathcal{P}}(\vec{k}_\perp, x)\psi^{(m_j=0)}_{\uparrow\bar{s}/\mathcal{V}}(\vec{k}'_\perp, x')m_q(k'^R + x'P'^R - k^R - xP^R) \\ &+ \psi^*_{\downarrow\bar{s}/\mathcal{P}}(\vec{k}_\perp, x)\psi^{(m_j=0)}_{\downarrow\bar{s}/\mathcal{V}}(\vec{k}'_\perp, x')[m_q^2 + (k'^L + x'P'^L)(k^R + xP^R)]\Big],\end{aligned} \tag{2.100}$$

We can simplify this expression by applying the symmetries in the light-front wavefunctions in Eq. (2.96).

$$\begin{aligned}\hat{V}|_{J^-,m_j=0}(q^2) =& \frac{-i}{m_{\mathcal{V}}(\Delta^R P^L - \Delta^L P^R)} \sum_{\bar{s}} \int_0^1 \frac{\mathrm{d}x}{2x(1-x)} \int \frac{\mathrm{d}^2\vec{k}_\perp}{(2\pi)^3} \frac{2\sqrt{1-z}}{\sqrt{x[x+z(1-x)]^3}} \\ &\times \Big[\psi^*_{\uparrow\bar{s}/\mathcal{P}}(\vec{k}_\perp, x)\psi^{(m_j=0)}_{\uparrow\bar{s}/\mathcal{V}}(\vec{k}'_\perp, x')2i[(k'^y + x'P'^y)(k^x + xP^x) - (k'^x + x'P'^x)(k^y + xP^y)] \\ &+ \psi^*_{\uparrow\bar{s}/\mathcal{P}}(\vec{k}_\perp, x)\psi^{(m_j=0)}_{\downarrow\bar{s}/\mathcal{V}}(\vec{k}'_\perp, x')(-2i)m_q(k^y + xP^y - k'^y - x'P'^y)\Big],\end{aligned} \tag{2.101}$$

As in Eq. (2.98), fixing the values of z and $\Delta_\perp$ could not uniquely determine the transition form factor in Eq. (2.98). There is an extra dependence on the transverse momentum of the initial state, $\vec{P}'_\perp$. This implies that the transition form factor extracted this way is not invariant under the transverse boost.

5. J^- and $m_j = \pm 1$

With this combination, we see the extra dependence of the transition form factor on the transverse

www.manaraa.com

momentum, again.

$$\begin{aligned}\hat{V}|_{J^-,m_j=1}(q^2) =& \frac{-i\sqrt{2}P^+P'^+}{P'^+P'^R(m_{\mathcal{P}}^2 - P^L\Delta^R) - P^+P^Rm_{\mathcal{V}}^2}\sum_{\bar{s}}\int_0^1\frac{\mathrm{d}x}{2x(1-x)}\int\frac{\mathrm{d}^2\vec{k}_\perp}{(2\pi)^3}\frac{1}{x'}\frac{2}{\sqrt{x'P'^+xP^+}}\\ &\times\Big[\psi^*_{\uparrow\bar{s}/\mathcal{P}}(\vec{k}_\perp,x)\psi^{(m_j=1)}_{\uparrow\bar{s}/\mathcal{V}}(\vec{k}'_\perp,x')[m_q^2+(k'^R+x'P'^R)(k^L+xP^L)]\\ &+\psi^*_{\uparrow\bar{s}/\mathcal{P}}(\vec{k}_\perp,x)\psi^{(m_j=1)}_{\downarrow\bar{s}/\mathcal{V}}(\vec{k}'_\perp,x')m_q(k^L+xP^L-k'^L-x'P'^L)\\ &+\psi^*_{\downarrow\bar{s}/\mathcal{P}}(\vec{k}_\perp,x)\psi^{(m_j=1)}_{\uparrow\bar{s}/\mathcal{V}}(\vec{k}'_\perp,x')m_q(k'^R+x'P'^R-k^R-xP^R)\\ &+\psi^*_{\downarrow\bar{s}/\mathcal{P}}(\vec{k}_\perp,x)\psi^{(m_j=1)}_{\downarrow\bar{s}/\mathcal{V}}(\vec{k}'_\perp,x')[m_q^2+(k'^L+x'P'^L)(k^R+xP^R)]\Big],\end{aligned}\tag{2.102}$$

To summarize, only two combinations of the current component and the magnetic projection of the vector meson could unambiguously extract the transition form factor from the valence hadron matrix element: they are $\hat{V}|_{J^{R/L},m_j=0}(q^2)$ in Eq. (2.95) and $\hat{V}|_{J^+,m_j=\pm1}(q^2)$ in Eq. (2.94). The other choices are not invariant under the transverse boost, and are therefore not very useful for calculating the transition form factor.

2.3.2.1 The nonrelativistic limit of $\hat{V}|_{J^R,m_j=0}$ and $\hat{V}|_{J^+,m_j=1}$

From the above discussions, we see that using J^R with $m_j = 0$ and using J^+ with $m_j = 1$ are the two possible choices of extracting the transition form factor in the valence Fock space. Though, in principle, these two choices should be equivalent due to Lorentz covariance, adoption of certain approximations in the model may lead to violation of the Lorentz symmetry that would be evident through nonequivalent results. In this section, we will further study these two choices and in particular their nonrelativistic limits.

In nonrelativistic quantum mechanics, magnetic moments and transitions can only be extracted from the *current density* $\vec{J} = (J^x, J^y, J^z)$ rather than the *charge density* J^0. Therefore one may expect that for the M1 transitions in nonrelativistic systems such as heavy quarkonia, the transverse current density $\vec{J}_\perp$ could be better than the charge density J^+. Indeed, $\hat{V}|_{J^+,m_j=1}$ does not involve spin-flip between the initial and final states, as in Eq. (2.94), while $\hat{V}|_{J^R,m_j=0}$ includes such contribution as in Eq. (2.95).

In the nonrelativistic limit, the M1 transition with the same radial and angular quantum numbers (e.g. $\mathcal{V}(nS) \to \mathcal{P}(nS) + \gamma$), is often referred to as *allowed*, for which the transition amplitude is large and $\hat{V}(0) \to 2$ as a result of the similarity between the spatial wavefunctions of the vector and the pseudoscalar mesons with the same spatial quantum numbers; whereas the transition between states with different radial

www.manaraa.com

or angular excitations is referred to as *hindered*, for which the transition amplitude is zero and $\hat{V}(0) \to 0$ at the leading order due to the orthogonality of the wavefunctions [114, 103, 115, 116]. The deviations of experimentally measured results from those nonrelativistic limits indicate relativistic effects [2]. For a heavy quarkonium system, which is close to the nonrelativistic domain, such deviations are expected to be small but nonzero.

The wavefunctions of heavy quarkonia, treated as relativistic bound states, are dominated by those components that are non-vanishing and reduce to the nonrelativistic wavefunction in the nonrelativistic limit. These wavefunction components are therefore referred to as the *dominant* components. It is necessary to emphasize that despite the correspondence between the dominant spin components and the nonrelativistic wavefunctions, the former carries relativistic contributions when solved in a relativistic formalism. There are also wavefunction components of purely relativistic origin, which vanish in the nonrelativistic limit and are therefore *subdominant*.

In practice, the dominant components tend to be better constrained, while the subdominant ones are more sensitive to the model and numerical uncertainties. For the pseudoscalar states resembling S-waves (in particular n^1S_0), $\eta_c(nS)$ and $\eta_b(nS)$, their dominant components are the spin-singlets $\psi_{\uparrow\downarrow-\downarrow\uparrow/\mathcal{P}}$, while relativistic treatments would also allow them to have subdominant components, such as $\psi_{\uparrow\uparrow/\mathcal{P}} = \psi^*_{\downarrow\downarrow/\mathcal{P}}$. Analogously, for the vector states of heavy quarkonia resembling S-waves (in particular n^3S_1), $\psi(nS)$ and $\Upsilon(nS)$, the dominant components are the spin-triplets, $\psi^{m_j=0}_{\uparrow\downarrow+\downarrow\uparrow/\mathcal{V}}$, $\psi^{m_j=1}_{\uparrow\uparrow/\mathcal{V}}$ and $\psi^{m_j=-1}_{\downarrow\downarrow/\mathcal{V}}$. For those vector states identified as D-waves, $\psi(n^3D_1)$ and $\Upsilon(n^3D_1)$, where orbital excitations occur, all the spin-triplet components $\psi^{m_j=0,\pm1}_{\uparrow\downarrow+\downarrow\uparrow/\mathcal{V}}$, $\psi^{m_j=0,\pm1}_{\uparrow\uparrow/\mathcal{V}}$ and $\psi^{m_j=0,\pm1}_{\downarrow\downarrow/\mathcal{V}}$ exist in the nonrelativistic limit and are considered dominant, and only the spin-singlet components $\psi^{m_j=0,\pm1}_{\uparrow\downarrow-\downarrow\uparrow/\mathcal{V}}$ are subdominant. In detail, the spin components with larger orbital angular momentum projection $m_\ell = m_j - s - \bar{s}$, $\psi^{m_j=0}_{\uparrow\uparrow/\mathcal{V}} = -\psi^{*m_j=0}_{\downarrow\downarrow/\mathcal{V}}(m_\ell = \pm1)$ and $\psi^{m_j=1}_{\downarrow\downarrow/\mathcal{V}}(m_\ell = 2)$, have the largest occupancy. The less occupied components, $\psi^{m_j=0}_{\uparrow\downarrow+\downarrow\uparrow/\mathcal{V}}(m_\ell = 0)$, $\psi^{m_j=1}_{\uparrow\downarrow+\downarrow\uparrow/\mathcal{V}}(m_\ell = 1)$ and $\psi^{m_j=1}_{\uparrow\uparrow/\mathcal{V}}(m_\ell = 0)$, could also exist in the nonrelativistic limit. Moreover, the spin components with $m_\ell = 0$ admit the admixtures of S-waves, though the actual amount of such admixtures is small and sensitive to both the model parameters and the truncation. For example, the $\psi(3770)$ [$\psi(1D)$] state, though primarily a 1^3D_1 state, has contributions from n^3S_1 states (notably 2^3S_1) [117, 118, 119, 120], and these S-wave admixtures are responsible for the

www.manaraa.com

$nD \to n'S + \gamma$ transitions [121, 122, 123, 116]. In order to have a more intuitive view of the dominant and subdominant spin components for those states, we take the LFWFs from Ref. [3] to show in Fig. 2.12 the proportions of those dominant and subdominant components of heavy quarkonia. For all those pseudoscalar and vector states, the dominant terms could each occupy 88% $\sim$ 100% of the whole LFWF, suggesting that the heavy quarkonium indeed resembles a nonrelativistic system. The comparison between the same states of the charmonium and those of the bottomonium also reveals that the dominant component is more pronounced in the heavier, and less relativistic, system.

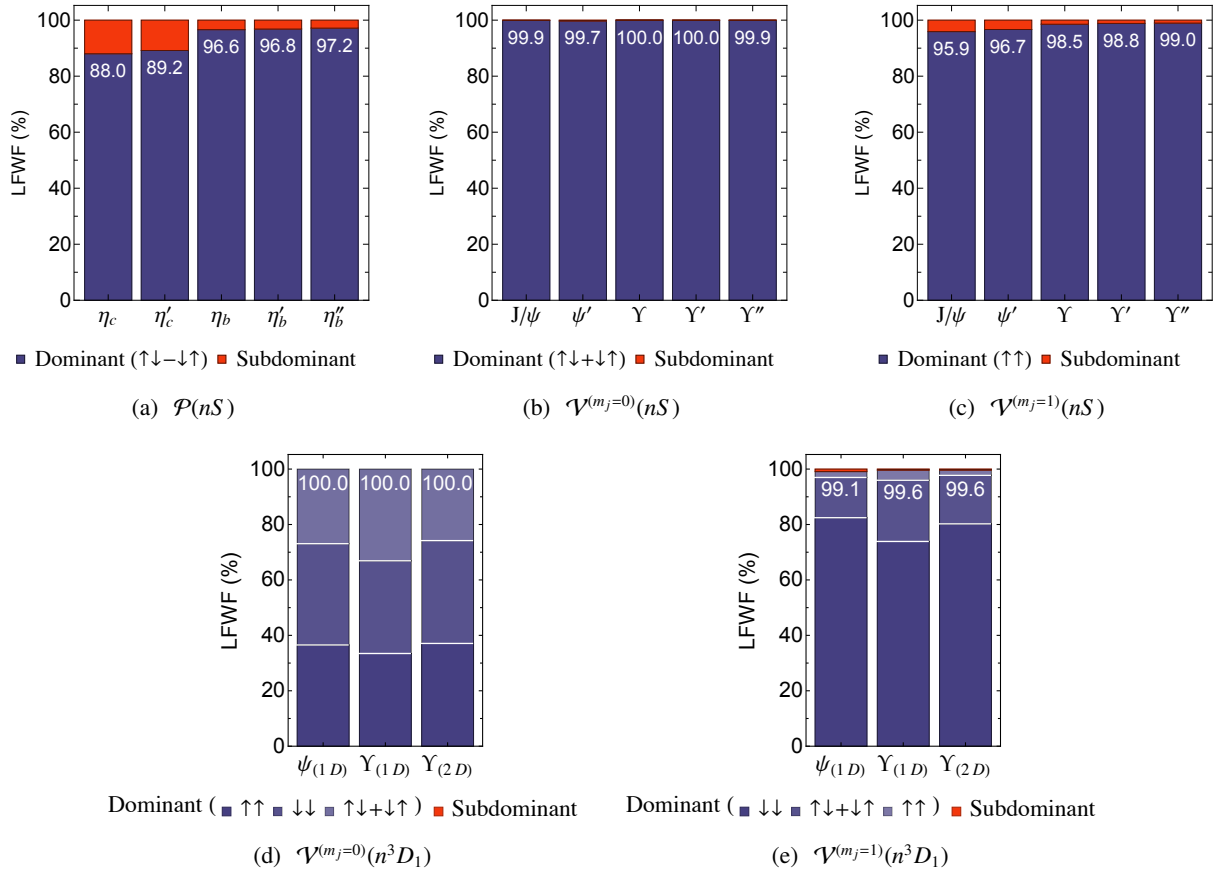

(a) $\mathcal{P}(nS)$ (b) $\mathcal{V}^{(m_j=0)}(nS)$ (c) $\mathcal{V}^{(m_j=1)}(nS)$

(d) $\mathcal{V}^{(m_j=0)}(n^3D_1)$ (e) $\mathcal{V}^{(m_j=1)}(n^3D_1)$

Figure 2.12 Comparison of dominant and subdominant LFWF components for pseudoscalar and vector systems in heavy quarkonia. Single (double) apostrophe stands for the radial excited 2S (3S) state. LFWFs are taken from the $N_{\max} = L_{\max} = 32$ result of Ref. [3]. The numbers in white suggest the occupancy of the dominant spin components for each state. (Figure adopted from Ref. [9].)

www.manaraa.com

It follows that in calculating the transition form factors, we can examine the two procedures, $\hat{V}|_{J^R,m_j=0}(q^2)$ presented in Eq. (2.95) and $\hat{V}|_{J^+,m_j=1}(q^2)$ presented in Eq. (2.94), in terms of their proximities to the nonrelativistic domain. The result of $\hat{V}|_{J^R,m_j=0}(q^2)$ mainly comes from the overlap of the dominant components, $\psi^{(m_j=0)}_{\uparrow\downarrow+\downarrow\uparrow/\mathcal{V}}\psi^*_{\uparrow\downarrow-\downarrow\uparrow/\mathcal{P}}$, whereas even the major part of $\hat{V}|_{J^+,m_j=1}(q^2)$ involves the subdominant components, such as $\psi^{(m_j=1)}_{\uparrow\uparrow/\mathcal{V}}\psi^*_{\uparrow\uparrow/\mathcal{P}}$ and $\psi^{(m_j=1)}_{\uparrow\downarrow-\downarrow\uparrow/\mathcal{V}}\psi^*_{\uparrow\downarrow-\downarrow\uparrow/\mathcal{P}}$. In heavy quarkonium, the dominant components tend to be better constrained than the subdominant ones which suggests that $\hat{V}|_{J^R,m_j=0}(q^2)$ is more robust than $\hat{V}|_{J^+,m_j=1}(q^2)$.

The nonrelativistic limit at $q^2 = 0$ can be achieved for $\hat{V}|_{J^R,m_j=0}(q^2)$ by adopting nonrelativistic wavefunctions where only the dominant spin components exist. However, with $\hat{V}|_{J^+,m_j=1}(q^2)$, simply taking the nonrelativistic wavefunction would always lead to zero since the expression in Eq. (2.94) involves the subdominant terms. To be specific, we examine the transition form factors at $q^2 = 0$ by taking $z = 0$ and $\vec{\Delta}_\perp = \vec{0}_\perp$, where they can be interpreted as the overlaps of wavefunctions in coordinate space $[\tilde{\psi}^{(m_j)}_{s\bar{s}}(\vec{r}_\perp, x)]$, shown in Eqs. (2.103) and (2.104). Though equivalent to Eqs. (2.95) and (2.94) at $q^2 = 0$ respectively, Eqs. (2.103) and (2.104) do not have the complicating factor of $1/\Delta^R$, and are therefore more intuitive for the purpose of illustration.

$$\begin{aligned}\hat{V}|_{J^R,m_j=0}(0) = \int_0^\infty \mathrm{d}r_\perp \Big\{ &\frac{m_\mathcal{P} + m_\mathcal{V}}{4\pi m_\mathcal{V}} \int_0^1 \mathrm{d}x \int_0^{2\pi} \mathrm{d}\theta \, \frac{r_\perp}{x} \\ &\times [-\frac{1}{2}\tilde{\psi}^{(m_j=0)}_{\uparrow\downarrow+\downarrow\uparrow/\mathcal{V}}(r_\perp,\theta,x)\tilde{\psi}^*_{\uparrow\downarrow-\downarrow\uparrow/\mathcal{P}}(r_\perp,\theta,x) - \tilde{\psi}^{(m_j=0)}_{\uparrow\uparrow/\mathcal{V}}(r_\perp,\theta,x)\tilde{\psi}^*_{\uparrow\uparrow/\mathcal{P}}(r_\perp,\theta,x)]\Big\}\end{aligned} \tag{2.103}$$

$$\begin{aligned}\hat{V}|_{J^+,m_j=1}(0) = \int_0^\infty \mathrm{d}r_\perp \Big\{ &\frac{\sqrt{2}(m_\mathcal{P} + m_\mathcal{V})}{4\pi} \int_0^1 \mathrm{d}x \int_0^{2\pi} \mathrm{d}\theta \, (1-x) r_\perp^2 \cos\theta \\ &\times \sum_{s,\bar{s}} \tilde{\psi}^{(m_j=1)}_{s\bar{s}/\mathcal{V}}(r_\perp,\theta,x)\tilde{\psi}^*_{s\bar{s}/\mathcal{P}}(r_\perp,\theta,x)\Big\}\end{aligned} \tag{2.104}$$

Note that in the nonrelativistic limit, the wavefunctions of the respective pseudoscalar and vector states with the same radial and angular numbers are identical in their spatial dependence, and they only differ in their spin structures. For the allowed transition, $\hat{V}|_{J^R,m_j=0}(0) \to 2$ due to the normalization of the spatial wavefunctions, which can be seen from Eq. (2.103) along with taking $x \to 1/2 + k_z/(2m_q)$ [3] and small hyperfine splitting $m_\mathcal{P} \approx m_\mathcal{V}$. For the hindered transition, $\hat{V}|_{J^R,m_j=0}(0) \to 0$ due to the orthogonality of the two wavefunctions. Such a nonrelativistic reduction that takes advantage of the near orthonormality of wavefunctions is reminiscent of the nonrelativistic quark model (see Refs. [114, 103, 115]). However, for $\hat{V}|_{J^+,m_j=1}(0)$, the realization of the nonrelativistic limits depends strongly on the details of the subdominant wavefunctions

www.manaraa.com

which are less constrained in the parameter fitting. For the hindered transition, where cancellation occurs, this leads to a strong sensitivity to the truncations and to the model parameters. Fig. 2.13 presents the integrands (those inside $\{\ldots\}$) of $\hat{V}|_{J^R,m_j=0}(0)$ and $\hat{V}|_{J^+,m_j=1}(0)$ according to Eqs. (2.103) and (2.104) for an allowed ($1S \to 1S + \gamma$) as well as a hindered ($2S \to 1S + \gamma$) transition. In the left panel of Fig. 2.13, the integrands of the allowed transition have no nodes resulting from the coherent overlaps of the two wavefunctions. On the other hand, the right panel of Fig. 2.13 shows significant cancellations of contributions from the integrands which change sign due to nodes in the $2S$ wavefunctions.

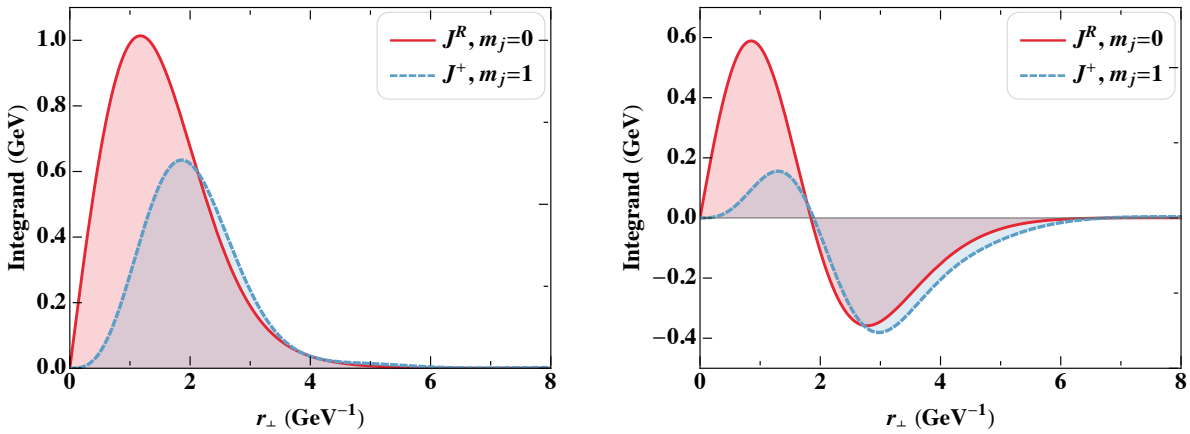

(a) $J/\psi(1S) \to \eta_c(1S) + \gamma$ (b) $\eta_c(2S) \to J/\psi(1S) + \gamma$

Figure 2.13 Integrands of $\hat{V}(0)$ according to Eqs. (2.103) ($J^R, m_j = 0$) and (2.104) ($J^+, m_j = 1$). As a representative of the allowed ($nS \to nS + \gamma$) transitions, the integrand in (a) has the same sign in the entire $r_\perp$ region. On the other hand, (b) involves a transition with radial excitation, which is sensitive to small changes in the cancellations between positive and negative contributions. (Figure adapted from Ref. [9])

Based on these lines of reasoning, we suggest using the transverse current with $m_j = 0$, i.e. $\hat{V}|_{J^R,m_j=0}(q^2)$ as in Eq. (2.95), to evaluate the transition form factors for heavy quarkonia in the valence Fock space. In general, such as for light mesons, one could calculate both $\hat{V}|_{J^R,m_j=0}(q^2)$ and $\hat{V}|_{J^+,m_j=1}(q^2)$ and use the difference of the two as an certainty to quantify the violation of the Lorentz symmetry.

www.manaraa.com

2.3.2.2 Results: applications to heavy quarkonia

Now we apply the formalism of calculating the M1 transition form factor to the heavy quarkonia system. We adopt wavefunctions of heavy quarkonia from the work of Ref. [3] using the BLFQ approach [1]. The numerical calculations in this section are carried out with $z = 0$, i.e. in the Drell-Yan frame. We will study the effects of the reference frames in the next section.

We first compare the two choices of extracting the transition form factors, $\hat{V}|_{J^R,m_j=0}$ and $\hat{V}|_{J^+,m_j=1}$. Fig. 2.14 shows the numerical results of four representative transitions in the charmonia system. There are noticeable differences between the two ways of extracting the transition form factor, especially for the hindered transitions. As already mentioned, we expect the calculation from $\hat{V}|_{J^R,m_j=0}$ to be more robust, since it depends on the dominant components of the wavefunctions.

We then present our results for selected pseudoscalar-vector transition form factors for charmonia and bottomonia below their respective open flavor thresholds with the preferred procedure $\hat{V}|_{J^R,m_j=0}(q^2)$ as in Eq. (2.95). Fig. 2.15 shows our numerical results of the transition form factors in three groups, the allowed transition $nS \to nS + \gamma$, the radial excited transition $nS \to n'S + \gamma$ $(n \neq n')$ and the angular excited transition $nD \to n'S + \gamma$, through a progression from upper to lower panels. As already discussed in the previous section, for the allowed transitions we find $\hat{V}(0) \approx 2$, whereas for the hindered transitions involving either radial or angular excitations we have $\hat{V}(0) \approx 0$. Transitions involving higher radial excited states feature more wiggles in the curve, which is especially evident in the $nS \to nS + \gamma$ transitions as n increases. This is because the radial excited states have transverse nodes. As a result, the transition form factors, in the form of their convolutions [see Eq. (2.95)], are not monotonic. The comparison between charmonia and bottomonia is also of interest. For comparable transition modes, the transition form factors show similarity in their patterns as well as their behavior as a function of $N_{\max}$. Furthermore, as illustrated in the second row of panels in Fig. 2.15, one observes that the $\mathcal{P}(nS) \to \mathcal{V}(n'S) + \gamma$ transition form factors are very similar to the $\mathcal{V}(nS) \to \mathcal{P}(n'S) + \gamma$ form factors for $n > n'$.

Comparisons of $\hat{V}(0)$ from our calculations, with experiments (compiled by PDG [4]) and with other models (Lattice QCD [11, 12, 13, 14, 15], Quark Model [6, 7, 8]) are collected in Table 2.9 and visualized in Fig. 2.16. Most calculations, as well as available experimental data, give a value of the the order of 2 for the

www.manaraa.com

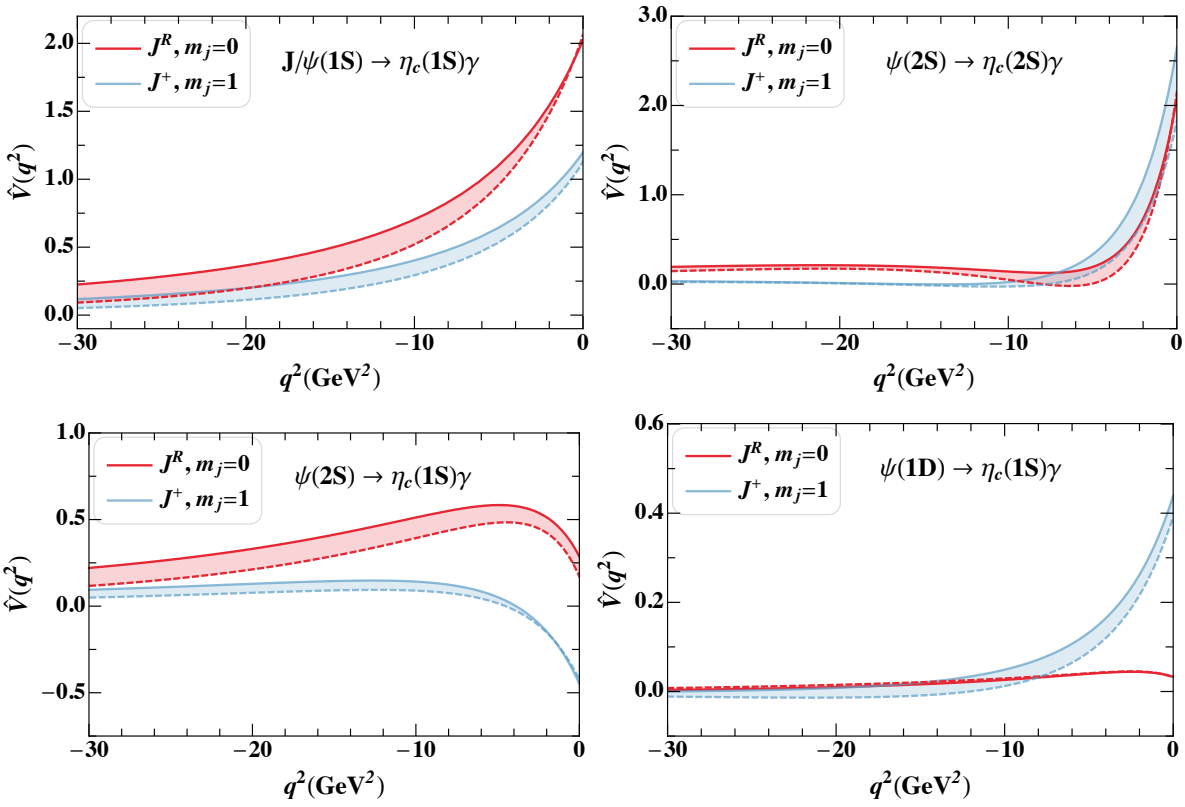

Figure 2.14 Transition form factors calculated from light-front wavefunctions [3] according to Eqs. (2.95) ($J^R, m_j = 0$) and (2.94) ($J^+, m_j = 1$). The dashed and solid curves are calculated with light-front wavefunctions at $N_{\max} = L_{\max} = 8$ and $N_{\max} = L_{\max} = 32$ respectively. The shaded areas in between indicates the numerical uncertainty from basis truncation.

www.manaraa.com

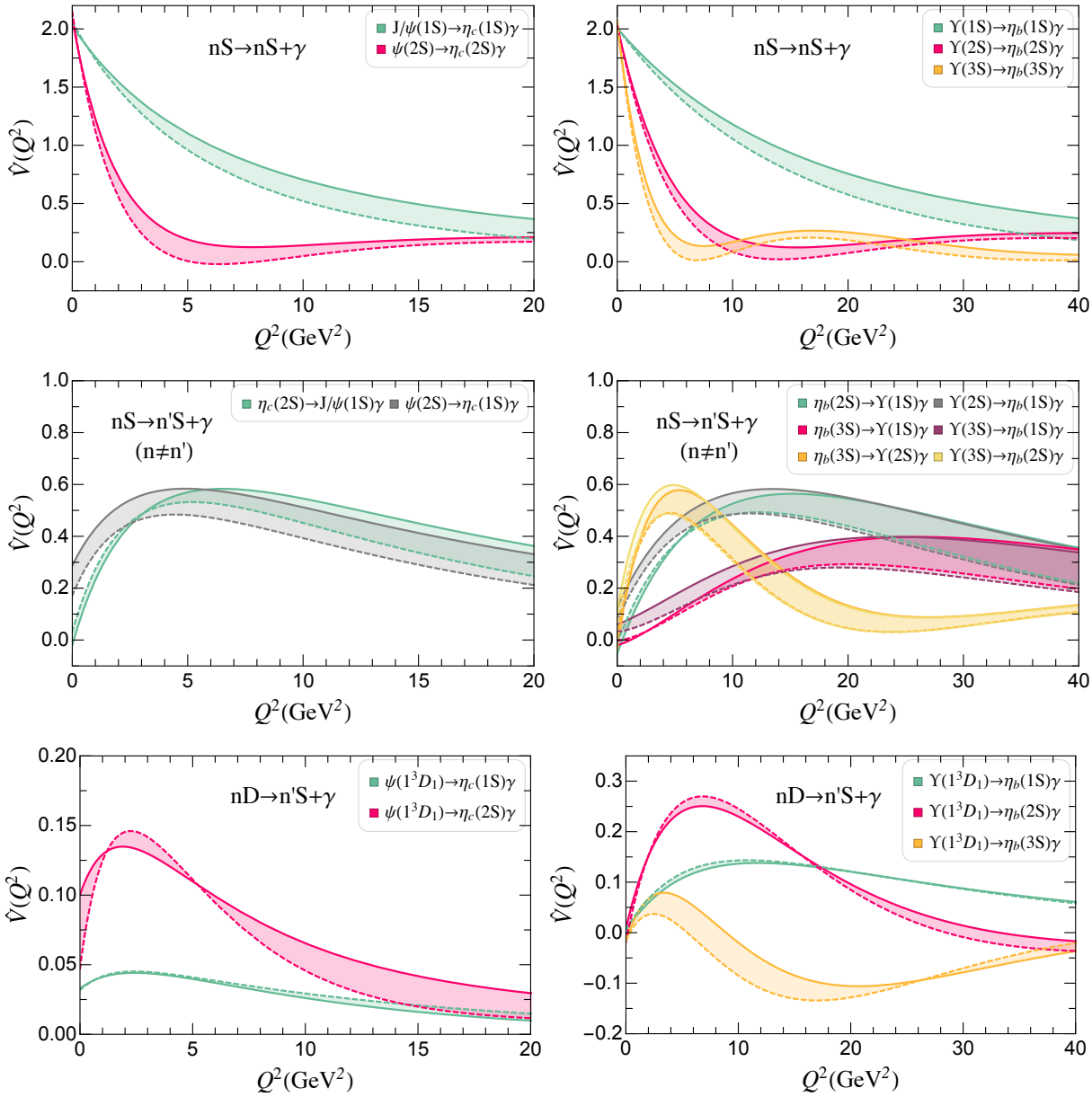

Figure 2.15 Transition form factors for charmonia (left) and bottomonia (right) are calculated from the BLFQ light-front wavefunctions [3] according to Eq. (2.95). In these plots, $Q^2 = -q^2$. The first row shows the allowed transitions, the second row shows transitions between different radial excitations, and the third row presents those involving angular excitations. The dashed and solid curves are calculated with light-front wavefunctions at $N_{\max} = L_{\max} = 8$ and $N_{\max} = L_{\max} = 32$ respectively. The shaded areas in between indicates the numerical uncertainty from basis truncation. As a consequence of the UV cutoff from the basis, the largest $Q^2(\simeq \Lambda^2_{\rm UV})$ at $N_{\max} = 32$ truncation is 31 GeV^2 (44 GeV^2) for charmonia (bottomonia). (Figure adopted from Ref. [9])

www.manaraa.com

allowed transitions $nS \to nS + \gamma$: All such data in Table 2.9 are between 1.5 and 2.5 with only one exception, the relativistic quark model calculation of $J/\psi \to \eta_c + \gamma$. This is in agreement with the vector $\mathcal{V}(nS)$ and the pseudoscalar $\mathcal{P}(nS)$ mesons possessing very similar spatial wavefunctions, but different spin structures. On the other hand, there is a significant spread in the theoretical results of the hindered transitions. This is expected because the hindered transitions involve changes in radial quantum numbers and/or orbital angular motions and are sensitive to delicate cancellations as discussed above. Considering the fact that only two free parameters are employed by the model for quarkonia in Ref. [3] and the fact that we did not adjust any parameters in our calculation for the transitions, the qualitative agreement with experiment and results from other methods is encouraging.

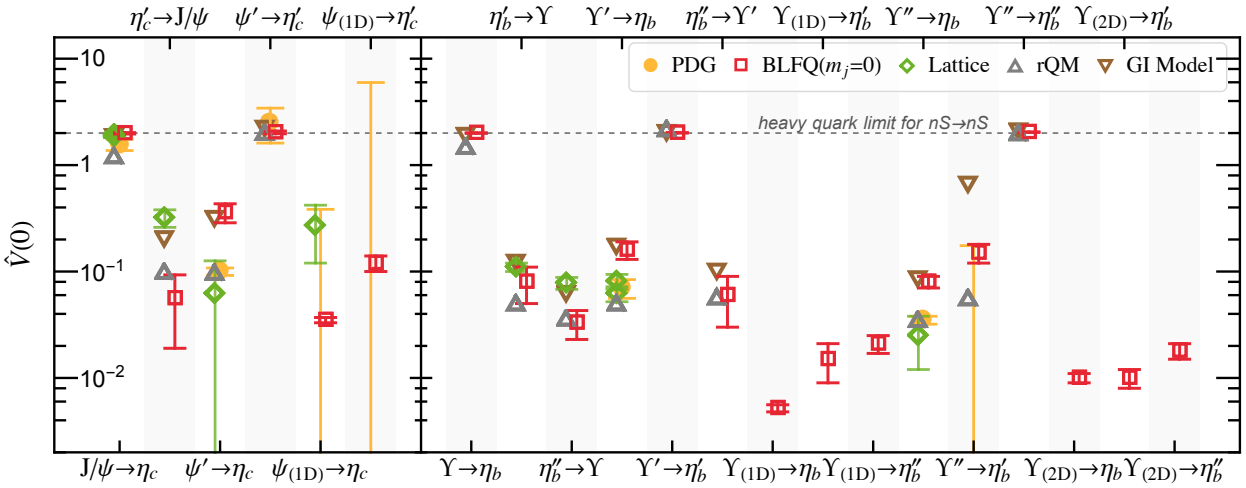

Figure 2.16 $\hat{V}(0)$ of charmonia and bottomonia transitions, calculated from Eq. (2.95) and summarized in Table. 2.9. Extrapolations are made from $N_{\max} = L_{\max} = 8, 16, 24, 32$ using second-order polynomials in $N_{\max}^{-1}$. We use the difference between the extrapolated and the $N_{\max} = 32$ results to quantify numerical uncertainty which is indicated by the vertical error bars on the BLFQ results (sometimes smaller than the symbols). We do not include any systematic uncertainty. Quarkonia in the initial and final states are labeled on the top and bottom of the figure. Single (double) apostrophe stands for the radial excited 2S (3S) state. The D-wave states are identified as n^3D_1. The heavy quark limit $\hat{V}(0) = 2$ of the allowed ($nS \to nS + \gamma$) transition is shown in the dashed line. Results from PDG [4], Lattice QCD [11, 12, 13, 14] and Lattice NRQCD [15, 5], the relativistic quark model (rQM) [6] and the Godfrey-Isgur (GI) model [7, 8] are also presented for comparison. (Figure adopted from Ref. [9])

www.manaraa.com

Table 2.9 $\hat{V}(0)$ for radiative decay between 0^{-+} and 1^{--} charmonia (bottomonia) below the $D\overline{D}$ ($B\overline{B}$) threshold. Values from PDG [4] are converted from their decay widths according to Eq. (2.81). Note that the uncertainties of meson masses propagate into that of $\hat{V}(0)$. The BLFQ results are from Eq. (2.95). For these results, all meson masses are taken from PDG [4], except that $\Upsilon(1^3D_1)$, $\Upsilon(2^3D_1)$ and $\eta_b(3S)$ masses are taken from Ref. [3]. Extrapolations for BLFQ are made from $N_{\max} = L_{\max} = 8, 16, 24, 32$ using second-order polynomials in $N_{\max}^{-1}$. We use the difference between the extrapolated and the $N_{\max} = 32$ results to quantify numerical uncertainty, which does not include any systematic uncertainty. Uncertainties are quoted in parenthesis and apply to the least significant figures of the result. Some lattice results are quoted with more than one source of uncertainty. The lattice nonrelativistic QCD (NRQCD) [5] results are converted from their three-point matrix elements with meson masses from PDG [4]. Values from the relativistic quark model (rQM) [6] and the Godfrey-Isgur (GI) model [7, 8] are converted from their decay widths according to Eq. (2.81) with their suggested meson masses, respectively. These results are plotted in Fig. 2.16. (Table adapted from Ref. [9])

$\hat{V}(0)$	PDG [4]	BLFQ	Lattice [11, 12, 13, 14, 15, 5]				Quark Model	
			Dudek	Bečirević	HPQCD	NRQCD	rQM	GI
$J/\psi(1S) \to \eta_c(1S)\gamma$	1.56(19)	1.99(3)	1.89(3)	1.92(3)(2)	1.90(7)(1)		1.21	1.82
$\eta_c(2S) \to J/\psi(1S)\gamma$		0.056(38)		0.32(6)(2)			0.099	0.20
$\psi(2S) \to \eta_c(1S)\gamma$	0.100(8)	0.360(74)	0.062(64)				0.097	0.31
$\psi(2S) \to \eta_c(2S)\gamma$	2.52(91)	2.03(6)					2.01	2.18
$\psi(1^3D_1) \to \eta_c(1S)\gamma$	< 0.377	0.035(2)	0.27(15)					
$\psi(1^3D_1) \to \eta_c(2S)\gamma$	< 5.84	0.121(21)						
$\Upsilon(1S) \to \eta_b(1S)\gamma$		2.00(1)					1.48	1.87
$\eta_b(2S) \to \Upsilon(1S)\gamma$		0.080(27)				0.11(1)	0.050	0.12
$\eta_b(3S) \to \Upsilon(1S)\gamma$		0.033(12)				0.078(10)	0.036	0.061
$\Upsilon(2S) \to \eta_b(1S)\gamma$	0.070(14)	0.156(30)			0.081(13)	0.062(10)	0.050	0.17
$\Upsilon(2S) \to \eta_b(2S)\gamma$		2.01(1)					2.17	1.99
$\eta_b(3S) \to \Upsilon(2S)\gamma$		0.059(27)					0.057	0.099
$\Upsilon(1^3D_1) \to \eta_b(1S)\gamma$		0.0052(4)						
$\Upsilon(1^3D_1) \to \eta_b(2S)\gamma$		0.0148(61)						
$\Upsilon(1^3D_1) \to \eta_b(3S)\gamma$		0.021(4)						
$\Upsilon(3S) \to \eta_b(1S)\gamma$	0.035(3)	0.079(10)				0.025(13)	0.035	0.084
$\Upsilon(3S) \to \eta_b(2S)\gamma$	< 0.167	0.145(33)					0.056	0.65
$\Upsilon(3S) \to \eta_b(3S)\gamma$		2.04(1)					1.99	2.06
$\Upsilon(2^3D_1) \to \eta_b(1S)\gamma$		0.010(1)						
$\Upsilon(2^3D_1) \to \eta_b(2S)\gamma$		0.010(2)						
$\Upsilon(2^3D_1) \to \eta_b(3S)\gamma$		0.018(3)						

www.manaraa.com

We also compare the two choices of extracting the transition form factors, $\hat{V}|_{J^R,m_j=0}$ and $\hat{V}|_{J^+,m_j=1}$ through $\hat{V}(0)$. The ratios of $\hat{V}|_{J^+,m_j=1}(0)$ over $\hat{V}|_{J^R,m_j=0}(0)$ are presented in Fig. 2.17. The hindered transitions have a much larger fluctuation than the allowed transition, due to their sensitivity to the subdominant components in one of the two spatial wavefunctions with different radial quantum numbers and/or different orbital motions. The results with the J^+ current, $\hat{V}|_{J^+,m_j=1}(0)$, differ by up to 2 orders of magnitude from the more reliable results with the transverse component of the current, $\hat{V}|_{J^R,m_j=0}(0)$.

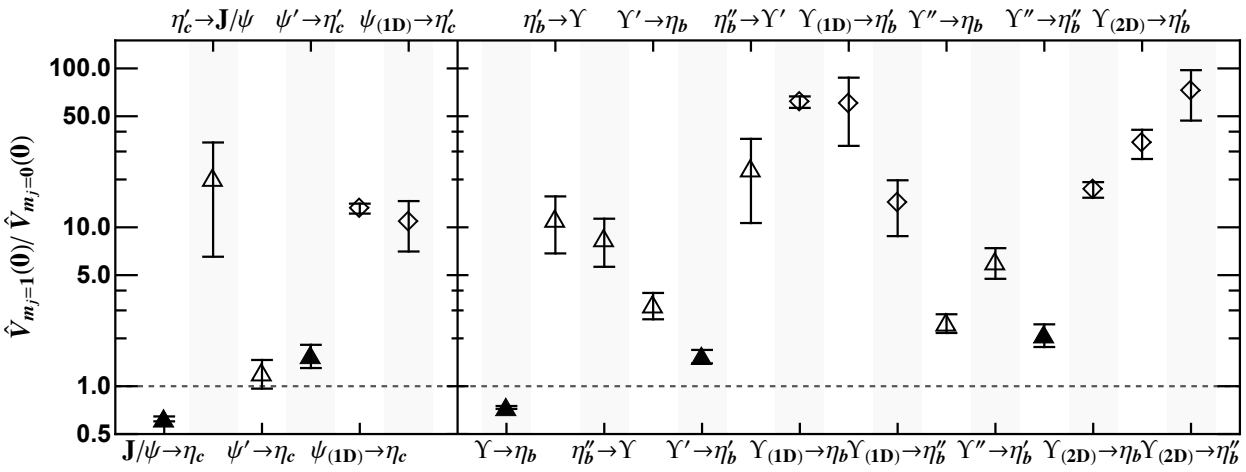

Figure 2.17 Ratio of $\hat{V}|_{J^+,m_j=1}(0)$ over $\hat{V}|_{J^R,m_j=0}(0)$, calculated from Eq. (2.94) and Eq. (2.95) respectively. The results are extrapolated to $N_{\max}=\infty$ from $N_{\max}=L_{\max}=8,16,24,32$ using second-order polynomials in $N_{\max}^{-1}$. We use the difference between the extrapolated and the $N_{\max}=32$ results to quantify the numerical uncertainty (indicated by vertical error bars). The allowed transitions are shown as filled triangles, whereas the hindered transitions, involving radial/angular excitations, are shown as open diamonds. (Figure adopted from Ref. [9])

2.3.3 Frame dependence of the transition form factor

The dependence of the transition form factor on the current components and on the reference frame are two typical measures of the violation of the Lorentz covariance in light-front dynamics. In Section 2.3.2, we have shown that for calculations with light-front wavefunctions in the valence Fock sector, using the transverse current J^R with the $m_j=0$ state of the vector meson is preferred for the transition form factor

www.manaraa.com

$V(q^2)$, as in Eq. (2.95). We will take this choice for the purpose of studying the frame dependence in this section.

Studies in the literature have revealed that the elastic and transition form factors could have different results when evaluated in different reference frames [124, 72, 125, 78, 65]. Such frame dependence is closely related to the Fock-space truncation that omits the non-valence contributions. In Sec. 2.2.1, we have defined a parameter space of $(z, \vec{\Delta}_\perp)$ to describe frames. There, different choices of $(z, \vec{\Delta}_\perp)$ for the same q^2 could characterize different frames. We will therefore calculate the frame dependence of the transition form factor through a dense sampling on the $(z, \vec{\Delta}_\perp)$ space.

Let us first analyze the potential effects of choosing different frames by looking into the light-front wavefunction representation of the hadron matrix elements, which are derived in Section 2.2.2. We immediately find that z is the lower bound of the range of x_1' for the $n \to n$ matrix element in Eq. 2.35. As a consequence, increasing the value of z would reduce the overlap region of the two wavefunctions in the longitudinal direction. We illustrate this effect in Fig. 2.18 by visualizing the convoluted valence wavefunctions [3] at different $(z, \vec{\Delta}_\perp)$ with the same q^2 for the transition $J/\psi \to \eta_c + \gamma^{(*)}$. In the valence Fock sector, the light-front wavefunction can be written in the form of $\psi^{(m_j)}_{s\bar{s}/h}(\vec{k}_\perp, x)$ where $(x, \vec{k}_\perp)$ is the relative coordinates of the quark. s represents the fermion spin projection in the x^- direction. Both the initial and final wavefunctions are plotted in the same $(x, \vec{k}_\perp)$ space, where the initial state wavefunction would appear as being reshaped due to momentum transfer. We can see that the information from the wavefunction in the longitudinal direction is preserved best at minimal z.

For the $n + 2 \to n$ term, as in Fig. 2.5(b), a quark and an antiquark from the initial state annihilate into a photon. The light-front wavefunction representation of the hadron matrix element is in Eq. (2.46). The frame parameter z is now the upper bound of the range of x_1', suggesting that decreasing the value of z might reduce the contribution of the $n + 2 \to n$ transition to the full transition form factor. However, even at $z = 0$, this parton-number-non-conserving term may yield a non-zero value, by generating zero-mode $\delta(x)$ terms [126, 81, 71, 72]. In the space-like region, the Drell-Yan frame always has the minimal $z = 0$. In the time-like region, it is the longitudinal-II frame that takes the smallest z. When the $n + 2 \to n$ contribution is not accessible, which happens when the light-front wavefunctions are solved in a truncated Fock space, using

www.manaraa.com

those minimal-z frames seems advantageous in suppressing the parton-number-non-conserving contribution. This observation suggests optimal frames for our meson systems solved from light-front Hamiltonian in the valence Fock sector.

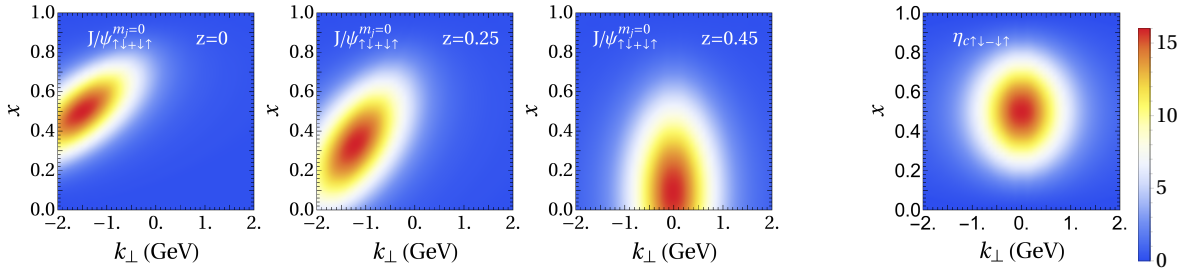

(a) $\psi^{(m_j=0)}_{\uparrow\downarrow+\downarrow\uparrow/J/\psi}(x' = x + z(1-x), \vec{k}'_\perp = \vec{k}_\perp + (1-x)\vec{\Delta}_\perp)$ (b) $\psi^{(m_j=0)}_{\uparrow\downarrow-\downarrow\uparrow/\eta_c}(x, \vec{k}_\perp)$

Figure 2.18 The valence light-front wavefunctions of mesons as they contribute (see Eq. (2.35)) to the convolution in the transition $J/\psi \to \eta_c + \gamma^{(*)}$ at $q^2 = -3\,\mathrm{GeV}^2$ in different frames. According to Eq. (2.35), in this $2 \to 2$ parton-number-conserving term, the initial state wavefunction of J/ψ would appear shifted and stretched to overlap with the final state wavefunction of η_c, when plotted on the $(x, \vec{k}_\perp)$ space. Shown in (a), the wavefunction of J/ψ is shaped differently at different $(z, \vec{\Delta}_\perp)$, i.e. in different frames. The longitudinal dimension is preserved most in the Drell-Yan frame where $z = 0$. At larger z, the information in the longitudinal region is reduced, and the transverse shift becomes smaller. The largest z is achieved when $\Delta_\perp = 0$ in the longitudinal frame, in this case, $z = 0.45$. Plotted in (b) is the wavefunction of η_c. All light-front wavefunctions what we employ are calculated by Ref. [3] and here we only plot the dominant spin components for the purpose of illustration. (Figure adapted from Ref. [10])

2.3.3.1 Results: applications to heavy quarkonia

We adopt light-front wavefunctions of heavy quarkonia from recent works [48, 3] in the BLFQ approach [1]. We calculate the frame dependence of the transition form factor through a dense sampling on the $(z, \vec{\Delta}_\perp)$ space.

Figures 2.19, 2.20 and 2.21 show numerical results for selected pseudoscalar-vector transition form factors for charmonia and bottomonia below their respective open-flavor thresholds. Those lowest states are the primary foci of several investigations [127, 15, 14, 12, 114, 8]. They have been measured in experiments [2], and their transitions are more readily detected with good statistics than higher excited states. Moreover, with

www.manaraa.com

their experimental masses, we have an entire landscape of frames in the $(z, \vec{\Delta}_\perp)$ parameter space according to Eq. (2.30). The solid curve represents the Drell-Yan frame, the dotted and the dashed curves represent the two branches of the longitudinal frame, longitudinal I and longitudinal II respectively. The shaded areas represent all other frames with different z and $\Delta_\perp$. We also compare $\hat{V}(0)$ obtained in different frames with available experimental data from the Particle Data Group (PDG) [2] in Table. 2.10.

Table 2.10 Comparison of $\hat{V}(0)$ from available experimental data and the BLFQ calculations in the limiting frames. Values from PDG [2] are converted from their decay widths according to Eq. (2.81). The BLFQ results are calculated using meson wavefunctions obtained at $N_{\max} = L_{\max} = 32$. The Drell-Yan/longitudinal II is the preferred result, and the difference between it and the longitudinal I quantifies the uncertainty resulting from frame dependence. (Table adapted from Ref. [10])

$\hat{V}(0)$	PDG [2]	BLFQ	
		Drell-Yan/long-II	long-I
$J/\psi(1S) \to \eta_c(1S)\gamma$	1.56(19)	2.02	2.12
$\eta_c(2S) \to J/\psi(1S)\gamma$	···	−0.019	0.29
$\psi(2S) \to \eta_c(1S)\gamma$	0.100(8)	0.29	0.46
$\psi(2S) \to \eta_c(2S)\gamma$	2.52(91)	2.09	2.14
$\psi(1D) \to \eta_c(1S)\gamma$	< 0.377	0.033	0.44
$\Upsilon(1S) \to \eta_b(1S)\gamma$	···	2.01	2.03
$\eta_b(2S) \to \Upsilon(1S)\gamma$	···	−0.052	0.20
$\Upsilon(2S) \to \eta_b(1S)\gamma$	0.070(14)	0.13	0.35
$\Upsilon(2S) \to \eta_b(2S)\gamma$	···	2.02	2.03
$\Upsilon(1D) \to \eta_b(1S)\gamma$	···	0.0048	0.19

For the transition form factor of the *allowed* transition, i.e. $\psi_A(nS) \to \psi_B(nS)\gamma$, $(\psi_A, \psi_B = \mathcal{V}, \mathcal{P}$ or $\mathcal{P}, \mathcal{V})$, as in Fig. 2.19, there are no crossings between the curves of the longitudinal frame and the Drell-Yan frame. In these cases, the results from all other frames are represented by the enclosed shaded area. The frame

www.manaraa.com

dependence is relatively small, no more than a 5% spread at $q^2 = 0$, as in Table. 2.10. For the transition form factor of the *hindered* transitions, i.e. $\psi_A(nS) \to \psi_B(n'S)\gamma(n' \neq n)$, $(\psi_A, \psi_B = \mathcal{V}, \mathcal{P}$ or $\mathcal{P}, \mathcal{V})$, as in Fig. 2.20, the curves of the longitudinal frame and the Drell-Yan frame cross each other, and their joined lower bound forms the lower bound for the results from all other frames. The upper bound, however, envelops the Drell-Yan and the longitudinal results. The frame dependence of these hindered transitions is very strong, indicating major sensitivity to the Lorentz symmetry breaking. This sensitivity seems understandable since these weaker transitions result from cancellations coming from different regions of integration. Transition form factors of the *hindered* transitions with angular excitations, $\mathcal{V}(1D) \to \mathcal{P}(1S)\gamma$ is shown in Fig. 2.21.

We also compare charmonia and bottomonia at corresponding transition modes in Figures 2.19, 2.20 and 2.21. Such comparisons suggest that the frame dependence tends to be reduced for heavier systems, presumably due to the overall reduction in relativistic effects.

It is natural to ask how frame dependence may be sensitive to the BLFQ basis truncation applied to these valence Fock space calculations. For this purpose, we present transition form factors from different basis truncations in Fig. 2.22. A trend towards convergence with increasing basis cutoff is observed in both the Drell-Yan and the longitudinal frames. The frame dependence indicated by the shaded regions is shrinking slightly with increasing basis cutoff but Lorentz symmetry breaking effects remain visible even at the highest basis cutoffs.

From those results, we observe that the frame dependence of the transition form factor can be characterized by the two limits, the Drell-Yan and the longitudinal frames. Transitions with excitations in the lighter system (e.g. $\eta_c(2S) \to J/\psi(1S)\gamma$) admit the largest frame dependence, implying a stronger sensitivity to the Fock sector truncation. Our suggested frames for the calculation in the valence Fock sector, the Drell-Yan and the longitudinal-II frames, provide values of $\hat{V}(0)$ that are closer to the experimental data, as seen in Table. 2.10.

www.manaraa.com

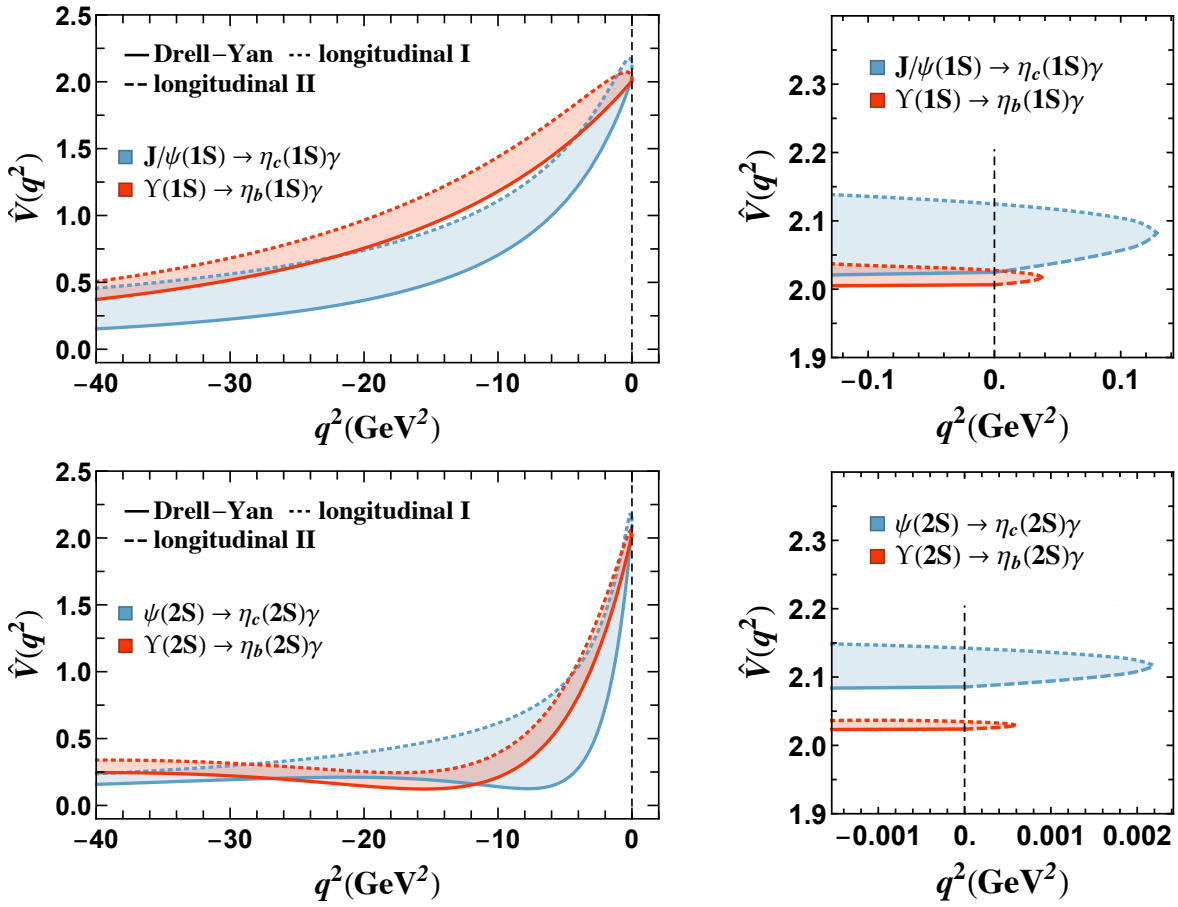

Figure 2.19 The transition form factor of the transition $\mathcal{V}(nS) \to \mathcal{P}(nS)\gamma$ of charmonia (blue curves/shades) and bottomonia (red curves/shades), calculated with light-front wavefunctions at $N_{\max} = L_{\max} = 32$ basis truncation. Meson masses are taken from experimental data [2] in defining the frames according to Eq. (2.30). The solid curves represent the Drell-Yan frame while the other curves represent the longitudinal I (dotted lines) and II (dashed lines) frames. The shaded areas represent the results from all other frames. The left panel shows the transition form factor at a larger scale of q^2, and the right panel focuses on the small q^2 region. (Figure adapted from Ref. [10])

www.manaraa.com

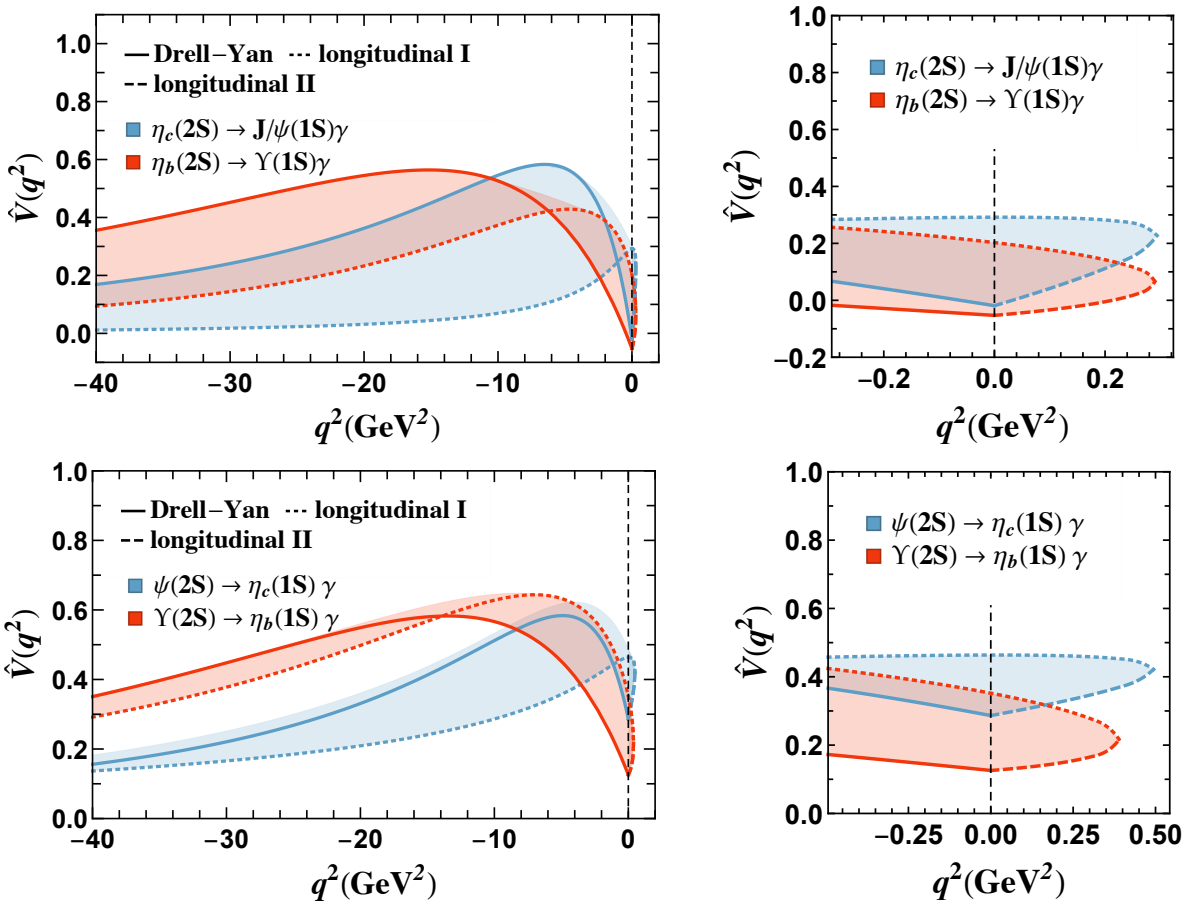

Figure 2.20 The transition form factor of the transition $\psi_A(2S) \to \psi_B(1S)\gamma$ ($\psi_A, \psi_B = \mathcal{V}, \mathcal{P}$ or $\mathcal{P}, \mathcal{V}$) of charmonia (blue curves/shades) and bottomonia (red curves/shades), calculated with light-front wavefunctions at $N_{\max} = L_{\max} = 32$ basis truncation. Meson masses are taken from experimental data [2] for defining the frames according to Eq. (2.30). The solid curves represent the Drell-Yan frame while the other curves represent the longitudinal I (dotted lines) and II (dashed lines) frames. The shaded areas represent the results from all other frames. The left panel shows the transition form factor at a larger scale of q^2, and the right panel focuses on the small q^2 region. (Figure adapted from Ref. [10])

www.manaraa.com

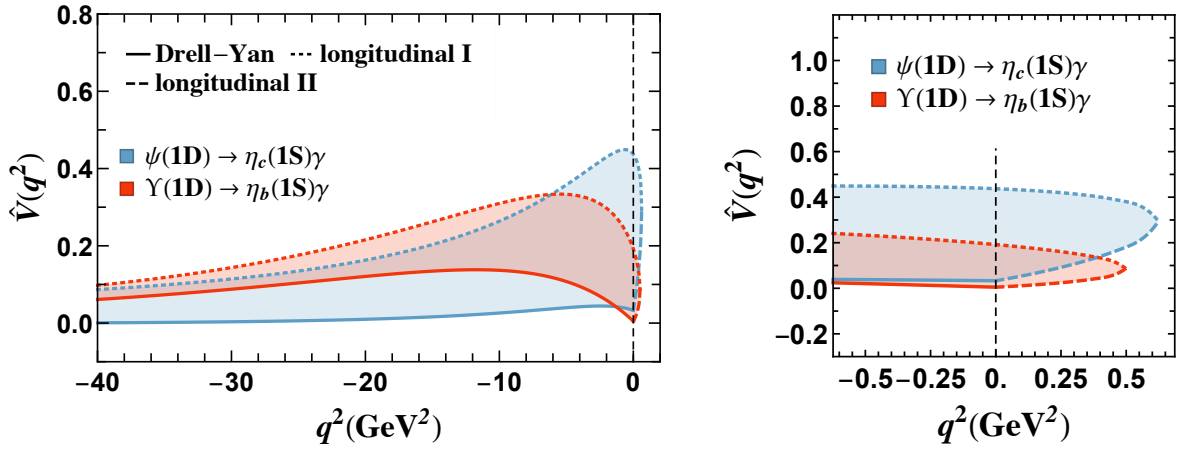

Figure 2.21 The transition form factor of the transition $\mathcal{V}(1D) \to \mathcal{P}(1S)\gamma$ of charmonia (blue curves/shades) and bottomonia (red curves/shades), calculated with light-front wavefunctions at $N_{\max} = L_{\max} = 32$ basis truncation. Meson masses are taken from experimental data [2] for defining the frames according to Eq. (2.30). The solid curves represent the Drell-Yan frame while the other curves represent the longitudinal I (dotted lines) and II (dashed lines) frames. The shaded areas represent the results from all other frames. The left panel shows the transition form factor at a larger scale of q^2, and the right panel focuses on the small q^2 region.

www.manaraa.com

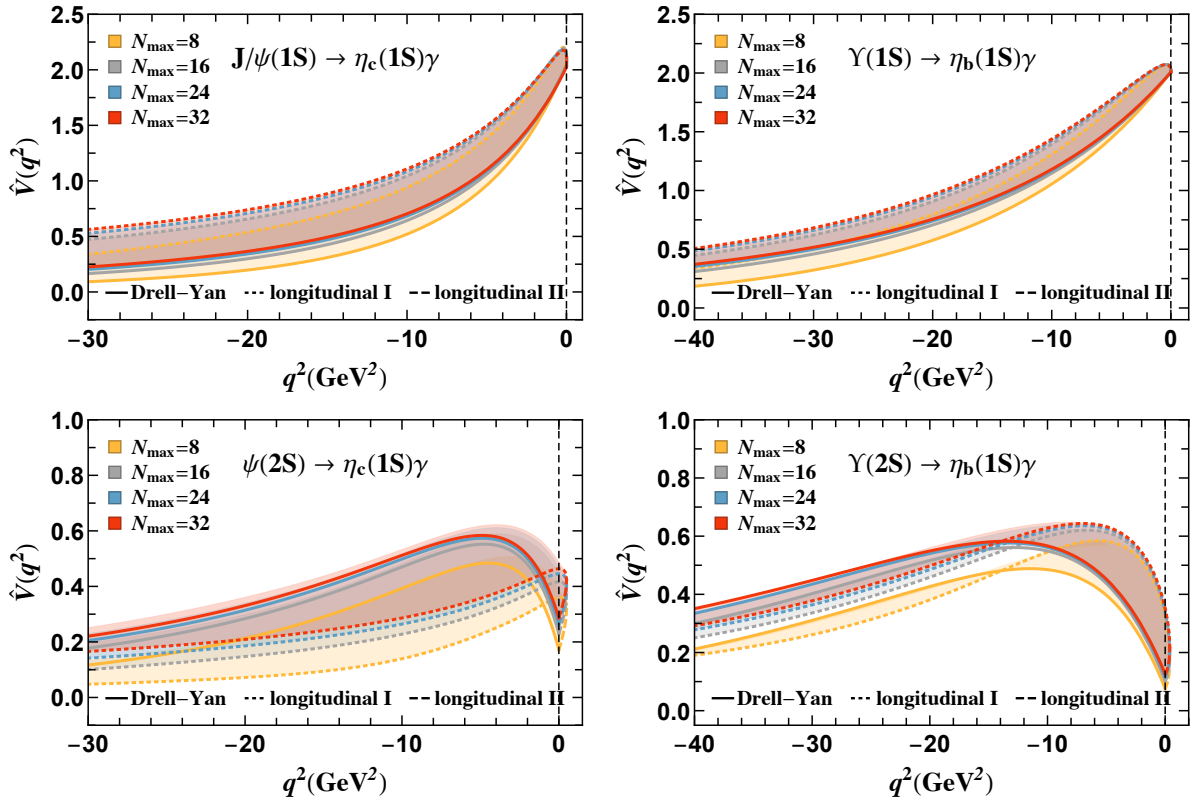

Figure 2.22 The transition form factors for charmonia (left panels) and bottomonia (right panels) with different basis truncations. Meson masses are taken from experimental data [2] in defining the frames according to Eq. (2.30). The solid curves represent the Drell-Yan frame while the other curves represent the longitudinal I (dotted lines) and II (dashed lines) frames. The shaded areas represent the results from all other frames. (Figure adapted from Ref. [10])

2.3.4 The electromagnetic Dalitz decay

The effective mass spectrum of the lepton pair in the Dalitz decay can be obtained from the corresponding transition form factor according to Eqs. (2.81) and (2.83). The results of $\mathrm{d}\Gamma(\psi_A \to \psi_B l^+ l^-)/\,\mathrm{d}q^2$ for eight selected decays are shown in Fig. 2.23. The frame dependence is barely visible in the allowed transitions as in the top four panels, but very substantial in the hindered transitions as in the bottom four panels. Such different sensitivities to frames can be expected in light of the sensitivities observed for the transition form factors in the time-like region. The allowed transitions are between states with similar spatial wavefunctions (e.g. $J/\psi(1S) \to \eta_c(1S)e^+e^-$), whereas the hindered transitions are between states with nearly orthogonal

www.manaraa.com

spatial parts (e.g. $\psi(2S) \to \eta_c(1S)e^+e^-$). Therefore in the latter cases, the transition form factors and thus the leptonic widths would admit strong cancellations between positive and negative contributions, and thus become more sensitive to the finer details of light-front wavefunctions.

2.3.5 Covariant light-front formalism

So far we have been using the standard light-front approach to calculate the transition form factor. In this section, we will study the transition form factor with a different approach, the covariant formulation of light-front dynamics [70]. In the explicitly covariant light-front dynamics, the hadron wavefunctions are defined on the general plane $\omega \cdot x = 0$, where ω is an arbitrary four-vector restricted to the condition $\omega^2 = 0$. The standard light-front approach is recovered as a particular case for $\omega = (\omega^0, \omega^1, \omega^2, \omega^3) = (1, 0, 0, -1)$, where the wavefunction is defined on the plane of $x^+ = 0$. The dynamical dependence of the wavefunction on the light-front plane results in their dependence on ω. The electromagnetic form factors should not depend on a particular choice of orientation of the light-front plane in an exact calculation or in a given order of perturbation theory. However, in approximate calculations, the non-physical dependence on ω would arise in the electromagnetic vertex. The covariant light-front formalism provides a method to extract the physical form factors from such vertices.

The amplitude of the M1 transition is written in its explicitly covariant form as

$$I^{\mu}_{m_j}(P, P') \equiv \langle \mathcal{P}(P')| J^{\mu} |\mathcal{V}(P, m_j)\rangle = \frac{2}{m_{\mathcal{P}} + m_{\mathcal{V}}} F^{\mu\nu} e_{\nu}(P, m_j) \,, \tag{2.105}$$

where the tensor $F^{\mu\nu}$ is decomposed on the general invariant amplitudes as

$$\begin{aligned} F^{\mu\nu} =& \epsilon^{\mu\nu\alpha\beta} P'_{\alpha} P_{\beta} V(q^2) + \epsilon^{\mu\nu\alpha\beta} P'_{\alpha} \omega_{\beta} B_1(q^2) + \epsilon^{\mu\nu\alpha\beta} P_{\alpha} \omega_{\beta} B_2(q^2) + (W^{\mu} P'^{\nu} + W^{\nu} P'^{\mu}) B_3(q^2) \\ &+ (W^{\mu}\omega^{\nu} + W^{\nu}\omega^{\mu}) B_4(q^2) + \frac{1}{\omega \cdot P}(W^{\mu} P^{\nu} + W^{\nu} P^{\mu}) B_5(q^2) \,, \end{aligned} \tag{2.106}$$

with $W^{\mu} = \epsilon^{\mu\rho\sigma\lambda} \omega_{\rho} P'_{\sigma} P_{\lambda}$. $V(q^2)$ is the physical transition form factor, and $B_{1,2,3,4,5}$ are non-physical form factors arising from the ω-dependent parts. Note that in the exact calculation, the ω-dependent parts cancel each other and the standard Lorentz covariant decomposition as in Eq. (2.78) follows.

From Eq. (2.106), the physical form factor V can be obtained as,

$$V(Q^2) = \frac{1}{2Q^2(\omega \cdot P)} \epsilon^{\mu\nu\rho\sigma} F_{\mu\nu} q_{\rho} \omega_{\sigma}, \tag{2.107}$$

www.manaraa.com

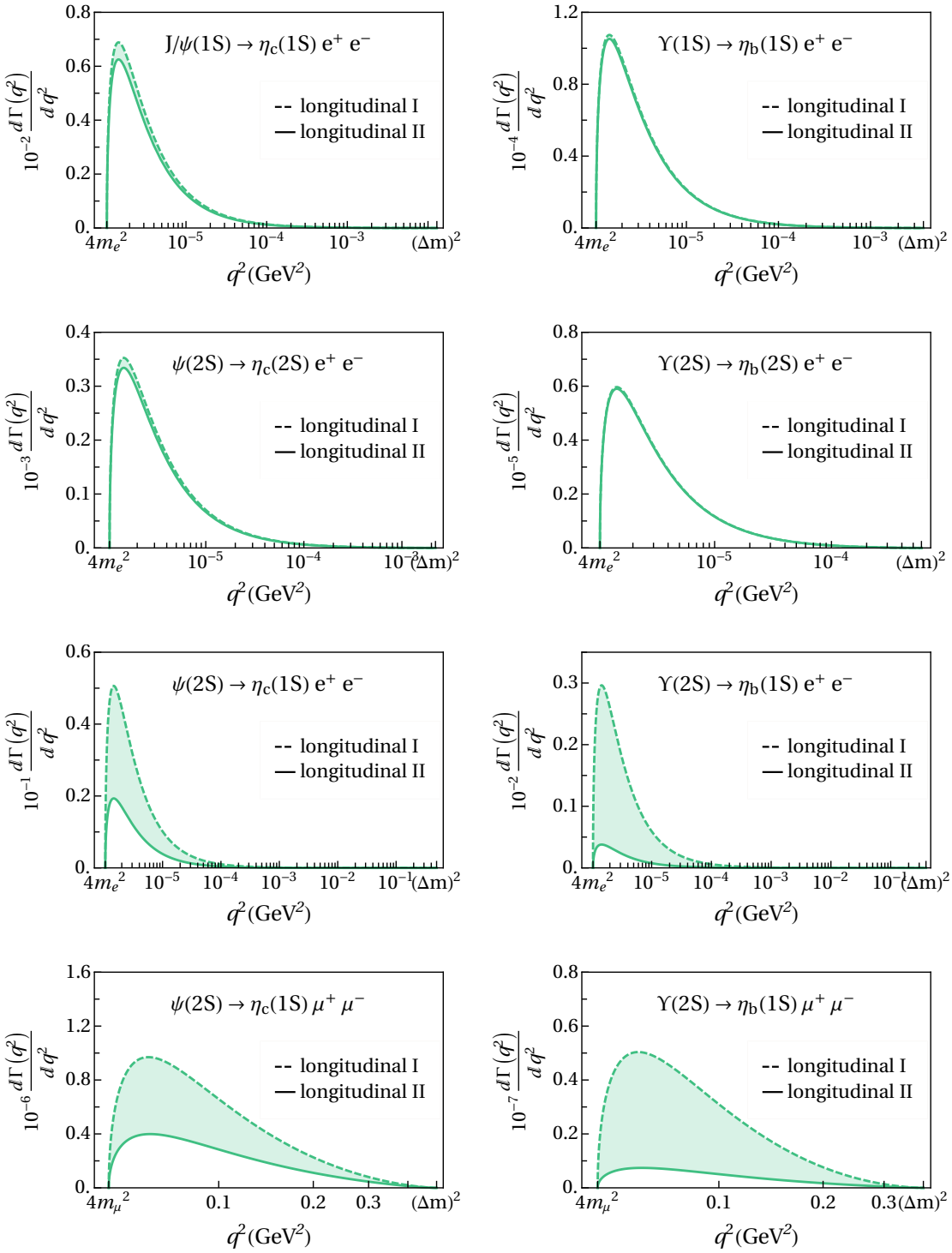

Figure 2.23 The effective mass spectrum of the lepton pairs in the Dalitz decays for charmonia (left panels) and bottomonia (right panels). The dashed and solid curves represent the longitudinal I and II frames respectively. The shaded areas represent the results from all other frames. $\Delta m^2 = (m_A - m_B)^2$ is the square of the mass difference between the initial and the final mesons. Meson masses are taken from experimental data [2]. (Figure adapted from Ref. [10])

www.manaraa.com

where $q = P' - P$ and $Q^2 \equiv -q^2$. We follow the light-front graph technique presented in Ref. [70] to calculate the amplitude. In the impulse approximation, $F^{\mu\nu}$ can be written as the sum of two contributions $F^{\mu\nu} = F_q^{\mu\nu} + F_{\bar{q}}^{\mu\nu}$, in which the photon coupled to the quark as $F_q^{\mu\nu}$ and the photon coupled to the antiquark as $F_{\bar{q}}^{\mu\nu}$. We will derive the transition form factor from $F_q^{\mu\nu}$. The diagrammatic representation of the radiative transition from a vector meson $\phi_{\mathcal{V}}$ to a pseudoscalar meson $\phi_{\mathcal{P}}$ is shown in Fig. 2.24. The spurions represented as dashed lines are the fictitious particles responsible for taking the intermediate states off the energy shell.

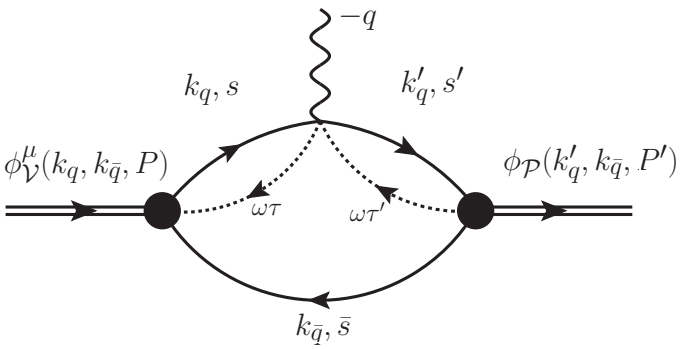

Figure 2.24 Diagrammatic representation of the radiative transition from a vector meson $\phi_{\mathcal{V}}$ to a pseudoscalar meson $\phi_{\mathcal{P}}$. $q = P' - P$. The dashed lines correspond to the spurions. The wavy line represents the photon and it is coupled to the quark line.

It follows that

$$F_q^{\mu\nu} = \int_0^1 \frac{\mathrm{d}x}{2x(1-x)} \int \frac{\mathrm{d}^2\vec{k}_\perp}{(2\pi)^3} \mathrm{Tr}[\phi^*_{\mathcal{P}}(k'_q, k_{\bar{q}}, P')(\not{k}'_q + m_q)\gamma^\mu(\not{k}_q + m_q)\phi^\nu_{\mathcal{V}}(k_q, k_{\bar{q}}, P)(\not{k}_{\bar{q}} - m_{\bar{q}})] \,. \tag{2.108}$$

The 'slash' notation is defined as $\not{a} \equiv a^\mu\gamma_\mu$. The valence Fock sector light-front wavefunctions relate to $\phi^\nu_{\mathcal{V}}$ and $\phi_{\mathcal{P}}$ as

$$\begin{aligned} \psi^{(m_j)}_{s\bar{s}/\mathcal{V}}(x, \vec{k}_\perp) &= e_\mu(P, m_j)\bar{u}_s(k_q)\phi^\mu_{\mathcal{V}}(k_q, k_{\bar{q}}, P)v_{\bar{s}}(k_{\bar{q}}) \,, \\ \psi_{s'\bar{s}/\mathcal{P}}(x', \vec{k}'_\perp) &= \bar{u}_{s'}(k'_q)\phi_{\mathcal{P}}(k'_q, k_{\bar{q}}, P')v_{\bar{s}}(k_{\bar{q}}) \,. \end{aligned} \tag{2.109}$$

www.manaraa.com

$\phi^{\nu}_{\mathcal{V}}$ and $\phi_{\mathcal{P}}$ are subject to Lorentz structure decomposition,

$$\begin{aligned}\phi^{\mu}_{\mathcal{V}}(k_q,k_{\bar{q}},P) =&\frac{1}{2m_q}(k_q-k_{\bar{q}})^{\mu}g_1(x,\vec{k}_{\perp})+\gamma^{\mu}g_2(x,\vec{k}_{\perp})\\ &+\frac{m_q\omega^{\mu}}{\omega\cdot P}g_3(x,\vec{k}_{\perp})+\frac{(k_q-k_{\bar{q}})^{\mu}\not{\omega}}{2\omega\cdot P}g_4(x,\vec{k}_{\perp})\\ &-\frac{i}{m_q\omega\cdot P}\gamma^5\epsilon^{\mu\nu\rho\sigma}k_{q\nu}k_{\bar{q}\rho}\omega_{\sigma}g_5(x,\vec{k}_{\perp})+\frac{m_q^2\omega^{\mu}\not{\omega}}{(\omega\cdot P)^2}g_6(x,\vec{k}_{\perp})\,,\\ \phi_{\mathcal{P}}(k'_q,k_{\bar{q}},P') =&\gamma^5 f_1(x',\vec{k}'_{\perp})+\not{\omega}\gamma^5 f_2(x',\vec{k}'_{\perp})\,.\end{aligned} \tag{2.110}$$

One can thereby extract the structure functions $g_{1,\ldots,6}$ and $f_{1,2}$ from the light-front wavefunctions. The expressions are in Eqs. (2.111) and (2.112). Note that we do not present g_3 and g_6 below since their expressions are rather tedious and more importantly, they do not contribute to the transition form factor $V(Q^2)$ as we will see later.

$$\begin{aligned}f_1(x',\vec{k}'_{\perp}) =&-\frac{\sqrt{x'(1-x')}}{(k')^L}\psi_{\uparrow\uparrow/\mathcal{P}}(x',\vec{k}'_{\perp})\\ f_2(x',\vec{k}'_{\perp}) =&\frac{1}{2P'^{+}\sqrt{x'(1-x')}(k')^L}\left[(k')^L\psi_{\uparrow\downarrow/\mathcal{P}}(x',\vec{k}'_{\perp})+m_q\psi_{\uparrow\uparrow/\mathcal{P}}(x',\vec{k}'_{\perp})\right]\end{aligned} \tag{2.111}$$

$$\begin{aligned}g_1(x,\vec{k}_{\perp}) =&\frac{m_q\sqrt{x(1-x)}}{\sqrt{2}k^Rk^R(m_q^2+k^Rk^L)}\Big[-k^Rk^R\psi^{(m_j=1)}_{\uparrow\uparrow/\mathcal{V}}(x,\vec{k}_{\perp})+(2m_q^2+k^Rk^L)\psi^{(m_j=1)}_{\downarrow\downarrow/\mathcal{V}}(x,\vec{k}_{\perp})\\ &-m_qk^R[\psi^{(m_j=1)}_{\uparrow\downarrow/\mathcal{V}}(x,\vec{k}_{\perp})-\psi^{(m_j=1)}_{\downarrow\uparrow/\mathcal{V}}(x,\vec{k}_{\perp})]\Big]\\ g_2(x,\vec{k}_{\perp}) =&\frac{\sqrt{x(1-x)}}{\sqrt{2}k^Rk^R(m_q^2+k^Rk^L)}\Big[m_qk^L\psi^{(m_j=1)}_{\downarrow\downarrow/\mathcal{V}}(x,\vec{k}_{\perp})+m_qk^R\psi^{(m_j=1)}_{\uparrow\uparrow/\mathcal{V}}(x,\vec{k}_{\perp})\\ &-k^Rk^L[\psi^{(m_j=1)}_{\uparrow\downarrow/\mathcal{V}}(x,\vec{k}_{\perp})-\psi^{(m_j=1)}_{\downarrow\uparrow/\mathcal{V}}(x,\vec{k}_{\perp})]\Big]\\ g_3(x,\vec{k}_{\perp}) =&\ldots\\ g_4(x,\vec{k}_{\perp}) =&\frac{1}{\sqrt{2}\sqrt{x(1-x)}k^Rk^R}\Big[-(1-x)k^R\psi^{(m_j=1)}_{\uparrow\downarrow/\mathcal{V}}(x,\vec{k}_{\perp})-xk^R\psi^{(m_j=1)}_{\downarrow\uparrow/\mathcal{V}}(x,\vec{k}_{\perp})-(1-2x)m_q\psi^{(m_j=1)}_{\downarrow\downarrow/\mathcal{V}}(x,\vec{k}_{\perp})\Big]\\ g_5(x,\vec{k}_{\perp}) =&-\frac{m_q(P^+)^2\sqrt{x(1-x)}}{2\sqrt{2}(m_q^2+k^Rk^L)[2(P^+)^2k^R-P^R(P^Rk^L-P^Lk^R)]}\Big[k^R\psi^{(m_j=1)}_{\uparrow\uparrow/\mathcal{V}}(x,\vec{k}_{\perp})+k^L\psi^{(m_j=1)}_{\downarrow\downarrow/\mathcal{V}}(x,\vec{k}_{\perp})\\ &+m_q[\psi^{(m_j=1)}_{\downarrow\uparrow/\mathcal{V}}(x,\vec{k}_{\perp})-\psi^{(m_j=1)}_{\uparrow\downarrow/\mathcal{V}}(x,\vec{k}_{\perp})]\Big]\\ g_6(x,\vec{k}_{\perp}) =&\ldots\end{aligned} \tag{2.112}$$

www.manaraa.com

We assign momenta $\omega\tau$ and $\omega\tau'$ to the fictitious spurions in the initial and final particles respectively, as indicated in Fig. 2.24. The conservation law reads,

$$P = k_q + k_{\bar{q}} - \omega\tau, \qquad P' = k'_q + k_{\bar{q}} - \omega\tau' \ . \tag{2.113}$$

In the Drell-Yan frame, $q^+ = P'^+ - P^+$. It follows that $x' = x$, $\vec{k}'_\perp = \vec{k}_\perp + (1-x)\vec{q}_\perp$ and $Q^2 = \vec{q}_\perp^{\,2}$. The transition form factor follows by plugging Eqs. (2.110) and (2.108) in Eq. (2.107). One would need to compute the following scalar products during the derivation. Scalar products of the mesons' momenta,

$$\begin{aligned}
&P^2 = m_{\mathcal{V}}^2, \qquad P'^2 = m_{\mathcal{P}}^2, \\
&q^2 = (P' - P)^2 \equiv -Q^2, \\
&P \cdot P' = (m_{\mathcal{V}}^2 + m_{\mathcal{P}}^2 + Q^2)/2, \\
&P \cdot q = P \cdot (P' - P) = (-m_{\mathcal{V}}^2 + m_{\mathcal{P}}^2 + Q^2)/2, \\
&P' \cdot q = P' \cdot (P' - P) = (-m_{\mathcal{V}}^2 + m_{\mathcal{P}}^2 - Q^2)/2 \ .
\end{aligned} \tag{2.114}$$

Scalar products of the fermions' momenta,

$$\begin{aligned}
&k_q^2 = k'^2_q = k_{\bar{q}}^2 = m_q^2, \qquad k_q \cdot k'_q = (2m_q^2 + Q^2)/2, \\
&k_q \cdot k_{\bar{q}} = (s - 2m_q^2)/2, \qquad k'_q \cdot k_{\bar{q}} = (s' - 2m_q^2)/2.
\end{aligned} \tag{2.115}$$

s and s' are defined as

$$\begin{aligned}
s &\equiv (k_q + k_{\bar{q}})^2 = m_{\mathcal{V}}^2 + 2P^+\tau, \\
s' &\equiv (k'_q + k_{\bar{q}})^2 = m_{\mathcal{P}}^2 + 2P^+\tau'.
\end{aligned} \tag{2.116}$$

In terms of the relative coordinates, they take the forms of

$$s = \frac{\vec{k}_\perp^{\,2} + m_q^2}{x} + \frac{\vec{k}_\perp^{\,2} + m_q^2}{1-x}, \qquad s' = \frac{\vec{k}'^2_\perp + m_q^2}{x} + \frac{\vec{k}'^2_\perp + m_q^2}{1-x} \ . \tag{2.117}$$

Finally the scalar products between the fermions' and the mesons' momenta,

$$\begin{aligned}
&k_q \cdot P = \frac{x}{2} m_{\mathcal{V}}^2 + \frac{1-x}{2} s, \qquad k_{\bar{q}} \cdot P = \frac{1-x}{2} m_{\mathcal{V}}^2 + \frac{x}{2} s, \\
&k'_q \cdot P' = \frac{x}{2} m_{\mathcal{P}}^2 + \frac{1-x}{2} s', \qquad k_{\bar{q}} \cdot P' = \frac{1-x}{2} m_{\mathcal{P}}^2 + \frac{x}{2} s', \\
&k_q \cdot q = [(k_q + q)^2 - k_q^2 - q^2]/2 = \frac{1}{2}Q^2 + \frac{x}{2}(s - s' - m_{\mathcal{V}}^2 + m_{\mathcal{P}}^2) \ , \\
&k'_q \cdot q = -Q^2/2 + xP^+(\tau - \tau') = -\frac{1}{2}Q^2 + \frac{x}{2}(s - s' - m_{\mathcal{V}}^2 + m_{\mathcal{P}}^2) \ , \\
&k_q \cdot P' = k_q \cdot (P + q), k'_q \cdot P = k'_q \cdot (P' - q), k_{\bar{q}} \cdot q = k_{\bar{q}} \cdot (P' - P) \ .
\end{aligned} \tag{2.118}$$

www.manaraa.com

We then arrive at

$$
\begin{aligned}
V_q(Q^2) = \int_0^1 \frac{\mathrm{d}x}{2x(1-x)} \int \frac{\mathrm{d}^2\vec{k}_\perp}{(2\pi)^3} \times \frac{i}{Q^2 2m_q x(1-x)} \Big\{ \\
& Q^2 f_1 \Big[g_1 \Big(\vec{k}_\perp^2 + (2x-1)[(1-x)\vec{k}_\perp \cdot \vec{q}_\perp + m_q^2(2x-1)] \Big) + 2m_q^2(x-1)x[4g_2 + g_4(2x-1)] \Big] \\
& + 2Q^2 f_2 m_q P^+ (x-1)x \Big[g_1(1-2x)^2 + 2(x-1)x[2g_2 + g_4(2x-1)] \Big] \\
& + 2\vec{k}_\perp \cdot \vec{q}_\perp \Big[f_1 g_1 (x-1)\vec{k}_\perp \cdot \vec{q}_\perp - 2 f_1 g_5 x(\vec{k}_\perp^2 + (1-x)\vec{k}_\perp \cdot \vec{q}_\perp + m_q^2) + 4 f_2 m_q P^+ (x-1)x^2(g_2 - g_5) \Big] \Big\}.
\end{aligned}
\tag{2.119}
$$

We see that g_3 and g_6 do not contribute to $V(Q^2)$. Two weight functions appear to depend on the momentum of the mesons, f_2 and g_5. However, in the transition form factor, f_2 always appears in the product of $f_2 P^+$, which cancels out the P dependence. In the denominator of g_5, $(P^R k^L - P^L k^R)$ would be zero if we ignore the imaginary part, leaving g_5 independent of P. From Eq. (2.119), one could proceed the calculation with light-front wavefunctions, such as from BLFQ [3].

This procedure extracts the transition form factor by considering all the four current components and all three m_j states of the vector meson, as opposed to the standard light-front calculation discussed in Section 2.3.2. It might shed additional light on the Lorentz symmetry violations arising from Fock sector truncation.

2.4 Decay constant

The decay constant of the vector meson is defined with the same electromagnetic current operator as the elastic and the transition form factors, via the local vacuum-to-hadron matrix elements. The decay constant of the pseudoscalar is defined with the axial current $J_5^\mu = \bar{\Psi}\gamma^\mu\gamma^5\Psi$.

$$
\begin{aligned}
\langle 0|\, \bar{\Psi}(0)\gamma^\mu\gamma^5\Psi(0)\, |\mathcal{P}(P)\rangle &= iP^\mu f_\mathcal{P} \,, \\
\langle 0|\, \bar{\Psi}(0)\gamma^\mu\Psi(0)\, |\mathcal{V}(P,m_j)\rangle &= m_\mathcal{V} e^\mu(P,m_j) f_\mathcal{V} \,.
\end{aligned}
\tag{2.120}
$$

Here $m_\mathcal{V}$ is the mass of the vector meson $\mathcal{V}$. $f_\mathcal{P}$ and $f_\mathcal{V}$ are the decay constants for the pseudoscalar and the vector respectively. Those decay constants can be accesses through various processes by experiment.

For a charged pseudoscalar, the decay constant is related to its decay via a virtual W^+ into a $l^+\nu_l$ final state, as in Fig. 2.25. To the lowest order, the decay width is related to the psudoscalar decay constant

www.manaraa.com

as [128]

$$\Gamma_{P\to\nu_l} = \frac{G_F^2}{8\pi} f_{\mathcal{P}}^2 m_l^2 m_{\mathcal{P}}^2 \left(1 - \frac{m_l^2}{m_{\mathcal{P}}^2}\right)^2 |V_{q_1q_2}|^2 \ . \tag{2.121}$$

$m_{\mathcal{P}}$ is the mass of the pseudoscalar meson $\mathcal{P}$. m_l is the mass of the lepton l, $V_{q_1q_2}$ is the Cabibbo-Kobayashi-Maskawa (CKM) matrix element between the constituent quarks $q_1\bar{q}_2$ in $\mathcal{P}$, and G_F is the Fermi coupling constant.

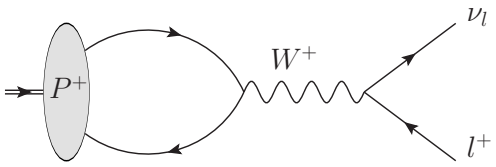

Figure 2.25 The annihilation process for a charged pseudoscalar P^+ (such as π^+, K^+ and D^+) decays into a $l^+\nu_l$ state. This diagram also indicates the process for the charge-conjugate particle as $P^- \to W^- \to l^-\bar{\nu}_l$.

For a neutral pseudoscalar, its decay constant can be accessed via the two photon decay, as in Fig. 2.26. Its relation to the decay width can be derived through a single pole fit to the transition form factor $F_{P\gamma}$ [129, 130], and the leading order approximation is

$$\Gamma_{P\to\gamma\gamma} = 4\pi Q_f^4 \alpha_{em}^2 \frac{f_{\mathcal{P}}^2}{m_{\mathcal{P}}} \ . \tag{2.122}$$

Q_f is the dimensionless fractional charge of the constituent quarks, $Q_c = +2/3$ for the charm quark and $Q_b = -1/3$ for the bottom quark.

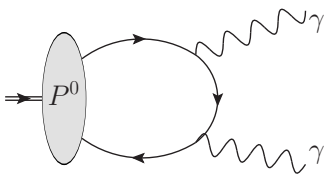

Figure 2.26 A neutral pseudoscalar P^0 (such as η, η_c and η_b) decays into two photons.

For a vector meson, the decay constant can be accessed via its dilepton decay, as in Fig. 2.27. It relates to the experimental decay width as [129, 130],

$$\Gamma_{V\to l^+l^-} = \frac{4\pi}{3} Q_f^2 \alpha_{em}^2 \frac{f_{\mathcal{V}}^2}{m_{\mathcal{V}}} \ . \tag{2.123}$$

www.manaraa.com

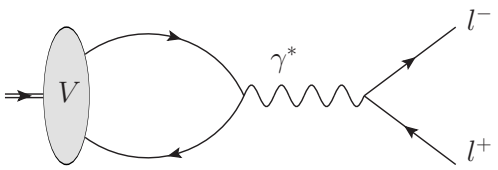

Figure 2.27 A vector meson V (such as J/ψ, Υ) decays into dileptons.

Since only the absolute value of decay constants matter when relating to decay width, I will drop the i in the following calculation for convenience. The light-front wavefunction representations of the matrix elements read,

$$\begin{aligned}
\langle 0|\,\bar{\Psi}(0)\gamma^{\mu}\gamma^{5}\Psi(0)\,|\mathcal{P}(P)\rangle &= \sqrt{N_c}\sum_{s,\bar{s}}\int_0^1 \frac{\mathrm{d}x}{2x(1-x)}\int\frac{\mathrm{d}^2k_{\perp}}{(2\pi)^3}\psi_{s\bar{s}/\mathcal{P}}(\vec{k}_{\perp},x)\\
&\quad \bar{v}_{\bar{s}}((1-x)P^{+},-\vec{k}_{\perp}+(1-x)\vec{P}_{\perp})\gamma^{\mu}\gamma^{5}u_{s}(xP^{+},\vec{k}_{\perp}+x\vec{P}_{\perp})\,,\\
\langle 0|\,\bar{\Psi}(0)\gamma^{\mu}\Psi(0)\,|\mathcal{V}(P,m_j)\rangle &= \sqrt{N_c}\sum_{s,\bar{s}}\int_0^1 \frac{\mathrm{d}x}{2x(1-x)}\int\frac{\mathrm{d}^2k_{\perp}}{(2\pi)^3}\psi^{(m_j)}_{s\bar{s}/\mathcal{V}}(\vec{k}_{\perp},x)\\
&\quad \bar{v}_{\bar{s}}((1-x)P^{+},-\vec{k}_{\perp}+(1-x)\vec{P}_{\perp})\gamma^{\mu}u_{s}(xP^{+},\vec{k}_{\perp}+x\vec{P}_{\perp})\,.
\end{aligned} \tag{2.124}$$

The derivation is very similar to that of the hadron matrix elements in Section 2.2.2. Calculations of the spinor part are included in Appendix A.3.

In the discussion of the transition form factors, we see that differences could arise when different magnetic projections of the vector mesons are used, in combination with different components of the electromagnetic current operator. It is then interesting to know how the decay constant would reflect such differences. The decay constant is defined with the same current operator as the transition form factor, but it features the simplicity of involving only one light-front wavefunction instead of convoluting two light-front wavefunctions. It therefore could provide a pathway for examining more specific information on the rotational symmetry of light-front wavefunctions.

www.manaraa.com

2.4.1 Decay constant of the pseudoscalar

1. J_5^+

$$\begin{aligned} f_{\mathcal{P}}|_{J^+} &= \sqrt{N_c}\int_0^1 \frac{\mathrm{d}x}{\sqrt{x(1-x)}}\int \frac{\mathrm{d}^2k_\perp}{(2\pi)^3}[\psi_{\uparrow\downarrow/\mathcal{P}}(\vec{k}_\perp,x)-\psi_{\downarrow\uparrow/\mathcal{P}}(\vec{k}_\perp,x)] \\ &= \sqrt{2N_c}\int_0^1 \frac{\mathrm{d}x}{\sqrt{x(1-x)}}\int \frac{\mathrm{d}^2k_\perp}{(2\pi)^3}\psi_{\uparrow\downarrow-\downarrow\uparrow/\mathcal{P}}(\vec{k}_\perp,x)\ , \end{aligned} \tag{2.125}$$

In the second equality, we adopt the notations of spin configurations as $\psi_{\uparrow\downarrow\pm\downarrow\uparrow} \equiv (\psi_{\uparrow\downarrow} \pm \psi_{\downarrow\uparrow})/\sqrt{2}$. This would be convenient to study the non-relativistic limit.

2. $J_5^\perp$

Without loss of generality, we use $J^R = J^x + iJ^y$ as the transverse current to calculate the decay constant. The calculation with $J^L = J^x - iJ^y$ is very similar and leads to the same result.

$$\begin{aligned} f_{\mathcal{P}}|_{J^R} =& \frac{1}{P^R}\sqrt{N_c}\int_0^1 \frac{\mathrm{d}x}{2x(1-x)}\int \frac{\mathrm{d}^2k_\perp}{(2\pi)^3}\frac{2}{\sqrt{x(1-x)}} \\ & [-(-k^R+(1-x)P^R)x\psi_{\downarrow\uparrow/\mathcal{P}}(\vec{k}_\perp,x)+(k^R+xP^R)(1-x)\psi_{\uparrow\downarrow/\mathcal{P}}(\vec{k}_\perp,x) \\ & + m_q(1-2x)\psi_{\downarrow\downarrow/\mathcal{P}}(\vec{k}_\perp,x)] \\ =& \sqrt{N_c}\int_0^1 \frac{\mathrm{d}x}{\sqrt{x(1-x)}}\int \frac{\mathrm{d}^2k_\perp}{(2\pi)^3}[\psi_{\uparrow\downarrow/\mathcal{P}}(\vec{k}_\perp,x)-\psi_{\downarrow\uparrow/\mathcal{P}}(\vec{k}_\perp,x)] \\ =& f_{\mathcal{P}}|_{J^+}\ . \end{aligned} \tag{2.126}$$

In the second equation, $\psi_{\downarrow\downarrow/\mathcal{P}}$ and $k^R\psi_{\uparrow\downarrow/\downarrow\uparrow/\mathcal{P}}$ vanish under the angular integration. We then get exactly the same result from $\mu = +$, as in Eq (2.125).

www.manaraa.com

3. J_5^-

$$
\begin{aligned}
f_{\mathcal{P}}|_{J^-} =& \frac{1}{P^-}\sqrt{N_c}\int_0^1 \frac{\mathrm{d}x}{2x(1-x)}\int \frac{\mathrm{d}^2k_\perp}{(2\pi)^3}\frac{2}{\sqrt{x(1-x)}P^+} \\
&\Big\{m_q(-k^R+(1-x)P^R-k^R-xP^R)\psi_{\uparrow\uparrow/\mathcal{P}}(\vec{k}_\perp,x) \\
&+[-m_q^2-(-k^R+(1-x)P^R)(k^L+xP^L)]\psi_{\downarrow\uparrow/\mathcal{P}}(\vec{k}_\perp,x) \\
&+[m_q^2+(-k^L+(1-x)P^L)(k^R+xP^R)]\psi_{\uparrow\downarrow/\mathcal{P}}(\vec{k}_\perp,x) \\
&+m_q(-k^L+(1-x)P^L-k^L-xP^L)\psi_{\downarrow\downarrow/\mathcal{P}}(\vec{k}_\perp,x)]\Big\} \\
=& \frac{1}{m_{\mathcal{P}}^2+\vec{P}_\perp^2}\sqrt{N_c}\int_0^1 \frac{\mathrm{d}x}{[x(1-x)]^{3/2}}\int \frac{\mathrm{d}^2k_\perp}{(2\pi)^3}\Big\{-2m_qk^R\psi_{\uparrow\uparrow/\mathcal{P}}(\vec{k}_\perp,x) \\
&-2m_qk^L\psi_{\downarrow\downarrow/\mathcal{P}}(\vec{k}_\perp,x)+[m_q^2-\vec{k}_\perp^2+x(1-x)\vec{P}_\perp^2][\psi_{\uparrow\downarrow/\mathcal{P}}(\vec{k}_\perp,x)-\psi_{\downarrow\uparrow/\mathcal{P}}(\vec{k}_\perp,x)]\Big\}\,.
\end{aligned}
\tag{2.127}
$$

In the second equation, $\psi_{\uparrow\uparrow/\downarrow\downarrow/\mathcal{P}}$ and $k^{R/L}\psi_{\uparrow\downarrow/\downarrow\uparrow/\mathcal{P}}$ vanish under the angular integration. The decay constant from the J^- current component has an dependence on the meson's momentum $\vec{P}_\perp$, so we could not unambiguously determine its value. To match it with the extraction from the J^+ or the $J^\perp$ current, one would need to drop the subdominant wavefunction $\psi_{\uparrow\uparrow/\downarrow\downarrow/\mathcal{P}}$ and replace the meson mass by $m_{\mathcal{P}}^2 \to (m_q^2-\vec{k}_\perp^2)/[x(1-x)]$. The first condition is satisfied in the nonrelativistic limit. The second condition implies nontrivial requirement on the wavefunction and the associated mass eigenvalue. Note that the replacement is different from the invariant mass of $m_0^2 = m_{\mathcal{P}}^2 \to (m_q^2+\vec{k}_\perp^2)/[x(1-x)]$.

To summarize, in calculating the decay constant of the pseudoscalar, using the J^+ and the $J^\perp$ current components are equivalent. The calculation with the J^- current has dependence on the meson's momentum and agrees with the two only under some nontrivial conditions. We suggest using J^+ or $J^\perp$ to calculate the decay constant, $f_{\mathcal{P}} = f_{\mathcal{P}}|_{J^+} = f_{\mathcal{P}}|_{J^\perp}$.

2.4.2 Decay constant of the vector

1. J^+

Since $e^+(P,m_j=\pm1)=0$, with the "+" component of the current the decay constant can only be

www.manaraa.com

extracted from $m_j = 0$,

$$\begin{aligned} f_{\mathcal{V}}|_{J^+,m_j=0} &= \sqrt{N_c}\int_0^1 \frac{\mathrm{d}x}{\sqrt{x(1-x)}}\int \frac{\mathrm{d}^2k_\perp}{(2\pi)^3}[\psi^{(m_j=0)}_{\uparrow\downarrow/\mathcal{V}}(\vec{k}_\perp,x)+\psi^{(m_j=0)}_{\downarrow\uparrow/\mathcal{V}}(\vec{k}_\perp,x)] \\ &= \sqrt{2N_c}\int_0^1 \frac{\mathrm{d}x}{\sqrt{x(1-x)}}\int \frac{\mathrm{d}^2k_\perp}{(2\pi)^3}\psi^{(m_j=0)}_{\uparrow\downarrow+\downarrow\uparrow/\mathcal{V}}(\vec{k}_\perp,x)\,. \end{aligned} \tag{2.128}$$

2. $J^\perp$

With the transverse current, the decay constant can be extracted from both the $m_j = 0$ state and the $m_j = \pm 1$ state. For the calculation with the $m_j = 0$ state, though we use the J^R current in derivation, using J^L would lead to the same result.

$$\begin{aligned} f_{\mathcal{V}}|_{J^\perp,m_j=0} =& \frac{1}{P^R}\sqrt{N_c}\int_0^1 \frac{\mathrm{d}x}{[x(1-x)]^{3/2}}\int \frac{\mathrm{d}^2k_\perp}{(2\pi)^3}[(-k^R+(1-x)P^R)x\psi^{(m_j=0)}_{\downarrow\uparrow/\mathcal{V}}(\vec{k}_\perp,x) \\ &+(k^R+xP^R)(1-x)\psi^{(m_j=0)}_{\uparrow\downarrow/\mathcal{V}}(\vec{k}_\perp,x)+m_q\psi^{(m_j=0)}_{\downarrow\downarrow/\mathcal{V}}(\vec{k}_\perp,x)] \\ =& \sqrt{2N_c}\int_0^1 \frac{\mathrm{d}x}{\sqrt{x(1-x)}}\int \frac{\mathrm{d}^2k_\perp}{(2\pi)^3}\psi^{(m_j=0)}_{\uparrow\downarrow+\downarrow\uparrow/\mathcal{V}}(\vec{k}_\perp,x) \\ =& f_{\mathcal{V}}|_{J^+,m_j=0}\,. \end{aligned} \tag{2.129}$$

In the second line, $\psi^{(m_j=0)}_{\downarrow\downarrow/\mathcal{V}}$ and $k^R\psi^{(m_j=0)}_{\uparrow\downarrow/\downarrow\uparrow/\mathcal{V}}$ vanish under the angular integration. We get the same result with that from J^+, as in Eq (2.128). This should not come as a surprise. Recall that the "+" and the transverse matrix elements with the same m_j can be related through a transverse Lorentz boost [see Eq. (2.88)].

To extract the decay constant with the $m_j = 1$ state, we use J^L and note that J^R is not available since $e^R(P, m_j = 1) = 0$.

$$\begin{aligned} f_{\mathcal{V}}|_{J^L,m_j=1} =& \frac{\sqrt{N_c}}{\sqrt{2}m_{\mathcal{V}}}\int_0^1 \frac{\mathrm{d}x}{[x(1-x)]^{3/2}}\int \frac{\mathrm{d}^2k_\perp}{(2\pi)^3}[-k^Lx\psi^{(m_j=1)}_{\uparrow\downarrow/\mathcal{V}}(\vec{k}_\perp,x) \\ &+k^L(1-x)\psi^{(m_j=1)}_{\downarrow\uparrow/\mathcal{V}}(\vec{k}_\perp,x)-m_q\psi^{(m_j=1)}_{\uparrow\uparrow/\mathcal{V}}(\vec{k}_\perp,x)]\,. \end{aligned} \tag{2.130}$$

To extract the decay constant with the $m_j = -1$ state, we use J^R and note that J^L is not available since $e^L(P, m_j = -1) = 0$.

$$\begin{aligned} f_{\mathcal{V}}|_{J^R,m_j=-1} =& \frac{\sqrt{N_c}}{\sqrt{2}m_{\mathcal{V}}}\int_0^1 \frac{\mathrm{d}x}{[x(1-x)]^{3/2}}\int \frac{\mathrm{d}^2k_\perp}{(2\pi)^3}[-k^Rx\psi^{(m_j=-1)}_{\downarrow\uparrow/\mathcal{V}}(\vec{k}_\perp,x) \\ &+k^R(1-x)\psi^{(m_j=-1)}_{\uparrow\downarrow/\mathcal{V}}(\vec{k}_\perp,x)+m_q\psi^{(m_j=-1)}_{\downarrow\downarrow/\mathcal{V}}(\vec{k}_\perp,x)]\,. \end{aligned} \tag{2.131}$$

www.manaraa.com

Eqs. (2.130) and (2.131) are equivalent by an overall minus sign. Considering that we take the absolute value as the decay constant, it is safe to write $f_{\mathcal{V}}|_{J^\perp,m_j=\pm1} = f_{\mathcal{V}}|_{J^L,m_j=1} = f_{\mathcal{V}}|_{J^R,m_j=-1}$.

3. J^-

With the "-" current, the decay constant can be extracted from both the $m_j = 0$ state and the $m_j = \pm1$ state.

$$
\begin{aligned}
f_{\mathcal{V}}|_{J^-,m_j=0} =& \frac{P^+}{\vec{P}_\perp^2 - m_{\mathcal{V}}^2}\sqrt{N_c}\int_0^1 \frac{\mathrm{d}x}{[x(1-x)]^{3/2}}\int\frac{\mathrm{d}^2k_\perp}{(2\pi)^3}\frac{1}{P^+} \\
& [-m_q^2 - k^R k^L + (1-x)xP^R P^L][\psi^{(m_j=0)}_{\uparrow\downarrow/\mathcal{V}}(\vec{k}_\perp,x) + \psi^{(m_j=0)}_{\downarrow\uparrow/\mathcal{V}}(\vec{k}_\perp,x)] \\
=& \frac{1}{\vec{P}_\perp^2 - m_{\mathcal{V}}^2}\sqrt{2N_c}\int_0^1 \frac{\mathrm{d}x}{\sqrt{x(1-x)}}\int\frac{\mathrm{d}^2k_\perp}{(2\pi)^3}\left[\vec{P}_\perp^2 - \frac{m_q^2+\vec{k}_\perp^2}{x(1-x)}\right]\psi^{(m_j=0)}_{\uparrow\downarrow+\downarrow\uparrow/\mathcal{V}}(\vec{k}_\perp,x)\ .
\end{aligned}
\tag{2.132}
$$

In deriving the above equation, $\psi^{(m_j=0)}_{\uparrow\uparrow/\downarrow\downarrow/\mathcal{V}}$ and $k^{R/L}\psi^{(m_j=0)}_{\uparrow\downarrow/\downarrow\uparrow/\mathcal{V}}$ vanish under the angular integration. The troubling dependence on the meson momentum appear again for the J^- current. By comparing to the calculation with the J^+ and $J^\perp$ currents, Eq. (2.128) or Eq. (2.129), we see that the substitution of the meson mass to the invariant mass ($m_{\mathcal{V}}^2 \to m_0^2 = (m_q^2 + \vec{k}_\perp^2)/[x(1-x)]$) would bring J^- calculation equal to J^+ and $J^\perp$.

For $m_j = 1$, $\psi^{(m_j=1)}_{\uparrow\downarrow/\downarrow\uparrow/\mathcal{V}}$ and $\psi^{(m_j=1)}_{\downarrow\downarrow/\mathcal{V}}$ vanish under the angular integration.

$$
\begin{aligned}
f_{\mathcal{V}}|_{J^-,m_j=1} =& \frac{P^+}{\sqrt{2}m_{\mathcal{V}}P^R}\sqrt{N_c}\int_0^1\frac{\mathrm{d}x}{[x(1-x)]^{3/2}}\int\frac{\mathrm{d}^2k_\perp}{(2\pi)^3}\frac{1}{P^+}\Big\{-m_q P^R\psi^{(m_j=1)}_{\uparrow\uparrow/\mathcal{V}}(\vec{k}_\perp,x) \\
& + (1-x)P^R k^L\psi^{(m_j=1)}_{\downarrow\uparrow/\mathcal{V}}(\vec{k}_\perp,x) - xP^R k^L\psi^{(m_j=1)}_{\uparrow\downarrow/\mathcal{V}}(\vec{k}_\perp,x)\Big\} \\
=& \frac{\sqrt{N_c}}{\sqrt{2}m_{\mathcal{V}}}\int_0^1\frac{\mathrm{d}x}{[x(1-x)]^{3/2}}\int\frac{\mathrm{d}^2k_\perp}{(2\pi)^3}[-k^L x\psi^{(m_j=1)}_{\uparrow\downarrow/\mathcal{V}}(\vec{k}_\perp,x) \\
& + k^L(1-x)\psi^{(m_j=1)}_{\downarrow\uparrow/\mathcal{V}}(\vec{k}_\perp,x) - m_q\psi^{(m_j=1)}_{\uparrow\uparrow/\mathcal{V}}(\vec{k}_\perp,x)] \\
=& f_{\mathcal{V}}|_{J^L,m_j=1}\ .
\end{aligned}
\tag{2.133}
$$

www.manaraa.com

For $m_j = -1$, $\psi^{(m_j=-1)}_{\uparrow\downarrow/\downarrow\uparrow/\mathcal{V}}$ and $\psi^{(m_j=-1)}_{\uparrow\uparrow/\mathcal{V}}$ vanish under the angular integration.

$$\begin{aligned} f_{\mathcal{V}}|_{J^-,m_j=-1} =& \frac{P^+}{\sqrt{2}m_{\mathcal{V}}P^L}\sqrt{N_c}\int_0^1 \frac{\mathrm{d}x}{[x(1-x)]^{3/2}}\int \frac{\mathrm{d}^2k_\perp}{(2\pi)^3}\frac{1}{P^+}\Big\{m_q P^L \psi^{(m_j=-1)}_{\downarrow\downarrow/\mathcal{V}}(\vec{k}_\perp,x) \\ & - xk^R P^L \psi^{(m_j=-1)}_{\downarrow\uparrow/\mathcal{V}}(\vec{k}_\perp,x) + (1-x)P^L k^R \psi^{(m_j=-1)}_{\uparrow\downarrow/\mathcal{V}}(\vec{k}_\perp,x)\Big\} \\ =& \frac{\sqrt{N_c}}{\sqrt{2}m_{\mathcal{V}}}\int_0^1 \frac{\mathrm{d}x}{[x(1-x)]^{3/2}}\int \frac{\mathrm{d}^2k_\perp}{(2\pi)^3}[-k^R x\psi^{(m_j=-1)}_{\downarrow\uparrow/\mathcal{V}}(\vec{k}_\perp,x) \\ & + k^R(1-x)\psi^{(m_j=-1)}_{\uparrow\downarrow/\mathcal{V}}(\vec{k}_\perp,x) + m_q\psi^{(m_j=-1)}_{\downarrow\downarrow/\mathcal{V}}(\vec{k}_\perp,x)] \\ =& f_{\mathcal{V}}|_{J^R,m_j=-1}\ . \end{aligned} \tag{2.134}$$

In calculating the decay constant of the vector meson with the $m_j = \pm 1$ states, using the J^- and the $J^\perp$ currents agree.

To summarize, in calculating the decay constant of the vector, there are two choices on the magnetic projection of the particle state, $m_j = 0$ and $m_j = \pm 1$. For $m_j = 0$, using the J^+ and the $J^\perp$ current components are equivalent, and the calculation with the J^- current agrees with the two by substituting the meson mass with the invariant mass of the constituents. The calculation of $f_{\mathcal{V}}|_{m_j=0} = f_{\mathcal{V}}|_{J^+/J^\perp,m_j=0}$ should follow Eq. (2.135), which is equivalent to Eq. (2.128) or Eq. (2.129). For $m_j = \pm 1$, the J^+ is not available, and the $J^\perp$ and the J^- currents give the same result. The calculation of $f_{\mathcal{V}}|_{m_j=\pm1} = f_{\mathcal{V}}|_{J^-/J^\perp,m_j=\pm1}$ should follow Eq. (2.136), which is equivalent to Eq. (2.131), (2.130), (2.133) and (2.134).

$$f_{\mathcal{V}}|_{m_j=0} = \sqrt{2N_c}\int_0^1 \frac{\mathrm{d}x}{\sqrt{x(1-x)}}\int \frac{\mathrm{d}^2k_\perp}{(2\pi)^3}\psi^{(m_j=0)}_{\uparrow\downarrow+\downarrow\uparrow/\mathcal{V}}(\vec{k}_\perp,x)\ , \tag{2.135}$$

$$\begin{aligned} f_{\mathcal{V}}|_{m_j=\pm1} =& \frac{\sqrt{N_c}}{\sqrt{2}m_{\mathcal{V}}}\int_0^1 \frac{\mathrm{d}x}{[x(1-x)]^{3/2}}\int \frac{\mathrm{d}^2k_\perp}{(2\pi)^3}[-m_q\psi^{(m_j=1)}_{\uparrow\uparrow/\mathcal{V}}(\vec{k}_\perp,x) - k^L x\psi^{(m_j=1)}_{\uparrow\downarrow/\mathcal{V}}(\vec{k}_\perp,x) \\ & + k^L(1-x)\psi^{(m_j=1)}_{\downarrow\uparrow/\mathcal{V}}(\vec{k}_\perp,x)]\ . \end{aligned} \tag{2.136}$$

In the non-relativistic(NR) limit of $x \to 1/2 + k_z/(2m_q)$, $m_q \to m_{\mathcal{V}}/2$ and $m_q >> k_z$, only the dominant spin components of the wavefunction, $\psi^{(m_j=0)}_{\uparrow\downarrow+\downarrow\uparrow/\mathcal{V}}$, $\psi^{(m_j=-1)}_{\downarrow\downarrow/\mathcal{V}}$ and $\psi^{(m_j=1)}_{\uparrow\uparrow/\mathcal{V}}$, survive as the NR wavefunction $\psi^{NR}_{\mathcal{V}}$. The two choices of extracting the decay constants reduce to the same form, i.e. $f^{NR}_{\mathcal{V}}|_{m_j=0} = f^{NR}_{\mathcal{V}}|_{m_j=\pm1}$ as in Eqs. (2.137) and (2.138). Alternatively, we can write the NR limit of the decay constant in the coordinate space, as in Eqs. (2.139) and (2.140). In both cases, the leading order approximation of the decay constant is proportional to the wavefunction at the origin $\vec{r} = 0$. Note that the derivation of the NR limit in Eqs. (2.137)

www.manaraa.com

and (2.139) also apply to the pseudoscalar as in Eq. (2.125).

$$
\begin{aligned}
f_{\mathcal{V}}^{NR}|_{m_j=0} &\to \sqrt{2N_c}\int \frac{\mathrm{d}^3\vec{k}}{(2\pi)^3 2m_q}[(\frac{1}{2}+\frac{k_z}{2m_q})(\frac{1}{2}-\frac{k_z}{2m_q})]^{-1/2}\psi_{\mathcal{V}}^{NR}(\vec{k}) \\
&= \sqrt{2N_c}\int \frac{\mathrm{d}^3\vec{k}}{(2\pi)^3}\frac{1}{m_q[1-k_z^2/m_q^2]^{1/2}}\psi_{\mathcal{V}}^{NR}(\vec{k}) \\
&\to \sqrt{2N_c}\int \frac{\mathrm{d}^3\vec{k}}{(2\pi)^3}\frac{1}{m_q}\psi_{\mathcal{V}}^{NR}(\vec{k})\ .
\end{aligned}
\tag{2.137}
$$

$$
\begin{aligned}
f_{\mathcal{V}}^{NR}|_{m_j=\pm1} &= \frac{\sqrt{N_c}}{\sqrt{2}(2m_q)}\int \frac{\mathrm{d}^3\vec{k}}{(2\pi)^3 2m_q}[(\frac{1}{2}+\frac{k_z}{2m_q})(\frac{1}{2}-\frac{k_z}{2m_q})]^{-3/2}m_q\psi_{\mathcal{V}}^{NR}(\vec{k}) \\
&= \frac{\sqrt{N_c}}{2\sqrt{2}}\int \frac{\mathrm{d}^3\vec{k}}{(2\pi)^3}\frac{4}{m_q[1-k_z^2/m_q^2]^{3/2}}\psi_{\mathcal{V}}^{NR}(\vec{k}) \\
&\to \sqrt{2N_c}\int \frac{\mathrm{d}^3\vec{k}}{(2\pi)^3}\frac{1}{m_q}\psi_{\mathcal{V}}^{NR}(\vec{k})\ .
\end{aligned}
\tag{2.138}
$$

The non-relativisitic limits are also found in terms of the non-relativistic wavefunction in the the coordinate space,

$$
\begin{aligned}
f_{\mathcal{V}}^{NR}|_{m_j=0} &= \frac{\sqrt{2N_c}}{m_q}\int \frac{\mathrm{d}^3\vec{k}}{(2\pi)^3}[1+\frac{1}{2}(\frac{k_z}{m_q})^2+\frac{3}{8}(\frac{k_z}{m_q})^4+\ldots]\psi_{\mathcal{V}}^{NR}(\vec{k}) \\
&= \frac{\sqrt{2N_c}}{m_q}[\tilde{\psi}_{\mathcal{V}}^{NR}(\vec{r}=0)-\frac{1}{2m_q^2}\tilde{\psi}_{\mathcal{V}}^{\prime\prime NR}(\vec{r}=0)+\frac{3}{8m_q^4}\tilde{\psi}_{\mathcal{V}}^{\prime\prime\prime\prime NR}(\vec{r}=0)+\ldots]\ .
\end{aligned}
\tag{2.139}
$$

$$
\begin{aligned}
f_{\mathcal{V}}^{NR}|_{m_j=\pm1} &= \frac{\sqrt{2N_c}}{m_q}\int \frac{\mathrm{d}^3\vec{k}}{(2\pi)^3}[1+\frac{3}{2}(\frac{k_z}{m_q})^2+\frac{15}{8}(\frac{k_z}{m_q})^4+\ldots]\psi_{\mathcal{V}}^{NR}(\vec{k}) \\
&= \frac{\sqrt{2N_c}}{m_q}[\tilde{\psi}_{\mathcal{V}}^{NR}(\vec{r}=0)-\frac{3}{2m_q^2}\tilde{\psi}_{/\mathcal{V}}^{\prime\prime NR}(\vec{r}=0)+\frac{15}{8m_q^4}\tilde{\psi}_{\mathcal{V}}^{\prime\prime\prime\prime NR}(\vec{r}=0)+\ldots]\ .
\end{aligned}
\tag{2.140}
$$

In calculations with the light-front wavefunctions solved by treating the mesons as relativistic bound states, the difference between $f_{\mathcal{V}}|_{m_j=0}$ and $f_{\mathcal{V}}|_{m_j=\pm1}$ could help examine the violation of rotational symmetry in the modeling of the bound state system. This test is in the same spirit of examining the deviations of the mass eigenvalues associated with different m_j.

For vector meson states identified as S-wave states, both $f_{\mathcal{V}}|_{m_j=0}$ and $f_{\mathcal{V}}|_{m_j=\pm1}$ arise primarily from the dominant spin components of light-front wavefunctions, which relate to the nonrelativistic wavefunctions. Moreover, the two expressions reduce to the same form in the nonrelativistic limit as we have found above. For vector meson states identified as D-wave states, both $f_{\mathcal{V}}|_{m_j=0}$ and $f_{\mathcal{V}}|_{m_j=\pm1}$ are calculated mainly from the

www.manaraa.com

dominant but less occupied spin components of light-front wavefunctions (see Sec. 2.3.2.1 for discussions of spin components for D-wave states). The two resulting small values are sensitive to model and numerical uncertainties, and could reveal differences. Nevertheless, for the S-wave states of heavy quarkonia, we expect to find robust results when either $m_j = 0$ or $m_j = \pm 1$ is used to calculate $f_{\mathcal{V}}$. The parameters $m_{\mathcal{V}}$ and m_q involved in $f_{\mathcal{V}}|_{m_j=\pm 1}$ might result in additional uncertainty but the resulting fluctuation should be small for heavy systems.

We use both Eqs. (2.135) and (2.136) to calculate the decay constants for the lowest three charmonium and five bottomonium vector states below their open flavor thresholds. We take the same light-front wavefunctions as we have used in calculating the elastic form factor and the transition form factor in the previous sections. The wavefunction is solved by the BLFQ formalism which extends the holographic QCD [61] by introducing the one-gluon exchange interaction with a running coupling [3]. The results are presented in Fig. 2.28, where basis truncations are chosen to match the UV cutoffs $\Lambda_{\rm UV} \simeq \kappa \sqrt{N_{\rm max}} \approx 1.7 m_q$ [3]. The two sets of results, $f_{\mathcal{V}}|_{m_j=0}$ and $f_{\mathcal{V}}|_{m_j=\pm 1}$, are all within each others' uncertainties for the five S-wave states in Fig. 2.28. Such consistency implies that the rotational symmetry is reasonably preserved in these light-front wavefunctions we adopted. For the D-wave states, the decay constants are small but differences between $f_{\mathcal{V}}|_{m_j=0}$ and $f_{\mathcal{V}}|_{m_j=\pm 1}$ can be noticed since each result depends on different small components. By implication, the transition form factor $\hat{V}(q^2)|_{J^R, m_j=0}$ calculated using the transverse current, with its overlapping dominant components of both the initial and the final light-front wavefunctions, is further indicated as a robust result.

www.manaraa.com

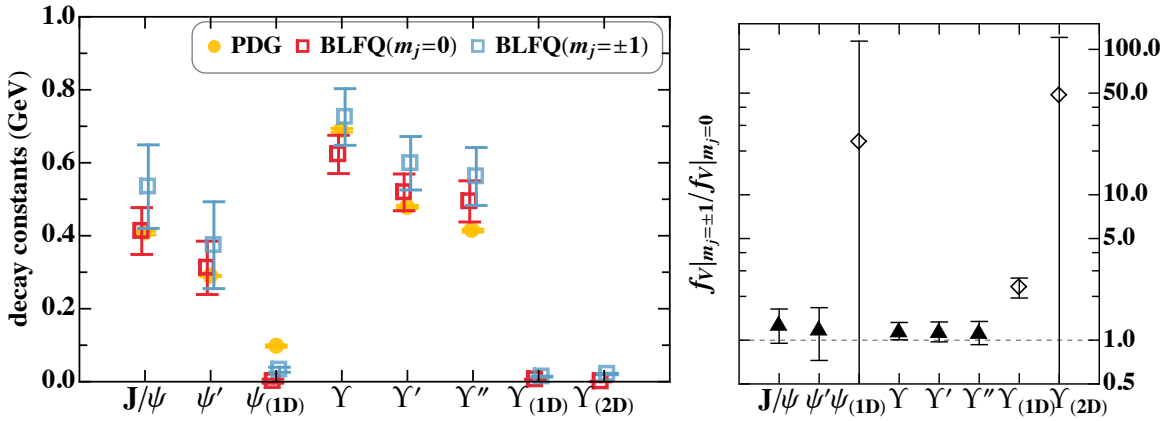

Figure 2.28 Decay constants of vector heavy quarkonia, calculated from Eqs. (2.135) and (2.136). Single (double) apostrophe stands for the radial excited 2S (3S) state. The D-wave states are identified as n^3D_1. The results are obtained with $N_{\max} = L_{\max} = 8$ with error bars $\Delta f_{c\bar{c}} = |f_{c\bar{c}}(N_{\max} = 8) - f_{c\bar{c}}(N_{\max} = 16)|$ for charmonium, and $N_{\max} = L_{\max} = 32$ with error bars $\Delta f_{b\bar{b}} = 2|f_{b\bar{b}}(N_{\max} = 32) - f_{b\bar{b}}(N_{\max} = 24)|$ for bottomonium. Results from PDG [4] are provided for comparison. The right panel shows the ratio of $f_V|_{m_j=\pm1}$ to $f_V|_{m_j=0}$, where the S-wave states are shown in filled triangles and the D-wave states are shown in open diamonds. (Figure adapted from Ref. [9].)

www.manaraa.com

CHAPTER 3. TIME-DEPENDENT BASIS LIGHT-FRONT QUANTIZATION APPROACH TO A SCATTERING PROBLEM

In this chapter, we will study the time-dependent process using the light-front Hamiltonian approach. We first review the formalism for solving the time-dependent problem with an external field in general. We then use this formalism to investigate the scattering of a quark jet on a high-energy nucleus.

3.1 Time-dependent basis light-front quantization

Non-perturbative Hamiltonian light-front quantum field theory offers insights into both the bound state properties and the dynamical scattering processes. We have already discussed the first aspect in Chapter 2 with the basis light-front quantization (BLFQ) approach [1]. BLFQ is based on the light-front quantum field theory and the Hamiltonian formalism. The implementation of the basis function representation allows us to choose a basis with the same symmetries of the system under investigation, and is therefore advantageous in carrying out efficient numerical calculations. It has been applied to solve both the QED bound state system of positronium [45] and the QCD bound states of heavy and light mesons [48, 3, 49, 50]. Time-dependent basis light-front quantization (tBLFQ) is a natural extension of the BLFQ formalism to investigate non-perturbative time-evolution problems. It was first introduced in Ref. [37] to solve the nonlinear Compton scattering, and later applied to the interaction of an electron with intense electromagnetic fields in Ref. [38]. We will study its application to the quark nucleus scattering in the next section.

The light-front Hamiltonian could be derived from the Lagrangian through the standard Legendre transformation [33]. The QCD Lagrangian with an external field reads

$$\mathcal{L} = -\frac{1}{4} F^{\mu\nu}{}_a F^a_{\mu\nu} + \overline{\psi}(i\gamma^\mu \boldsymbol{D}_\mu - \boldsymbol{m})\psi \ , \tag{3.1}$$

where $\boldsymbol{D}^\mu \equiv \partial_\mu \boldsymbol{I} + ig\boldsymbol{C}^\mu$ and $\boldsymbol{C}^\mu$ is the sum of the quantum gauge fields $\boldsymbol{A}^\mu$ and the external field $\mathcal{A}^\mu$. In general, the background field should also be included in the field tensor, such that $F^{\mu\nu}_a \equiv \partial^\mu C^\nu_a - \partial^\nu C^\mu_a - gf^{abc}C^\mu_b C^\nu_c$. The full light-front Hamiltonian P^- is obtained in the light cone gauge $A^+ = 0$, and the detailed

www.manaraa.com

derivation can be found in Appendix B. The evolution of quantum states is governed by the Shrödinger equation

$$i\frac{\partial}{\partial x^+}\left|\psi; x^+\right\rangle = \frac{1}{2}P^-(x^+)\left|\psi; x^+\right\rangle \ , \tag{3.2}$$

where $|\psi; x^+\rangle$ is the state at light-front time x^+. The Hamiltonian contains two parts: P^-_{QCD} which is the full light-front Hamiltonian of QCD as in Eq. (1.9), and V which contains interaction terms introduced by the background field, so $P^-(x^+) = P^-_{QCD} + V(x^+)$. This interaction term, in general, contains an explicit time dependence. It is therefore natural to use an interaction picture to solve the evolution equation,

$$i\frac{\partial}{\partial x^+}\left|\psi; x^+\right\rangle_I = \frac{1}{2}V_I(x^+)\left|\psi; x^+\right\rangle_I \ , \tag{3.3}$$

where $V_I(x^+) = e^{i\frac{1}{2}P^-_{QCD}x^+}V(x^+)e^{-i\frac{1}{2}P^-_{QCD}x^+}$ is the interaction Hamiltonian in the interaction picture. The solution of Eq. (3.3) describes the state at a given light-front time x^+,

$$\left|\psi; x^+\right\rangle_I = \mathcal{T}_+ \exp[-\frac{i}{2}\int_0^{x^+} \mathrm{d}z^+ V_I(z^+)]\left|\psi; 0\right\rangle_I \ , \tag{3.4}$$

where $\mathcal{T}_+$ is the light-front time ordering. In the perturbative calculations, the time-ordered exponential is written as the Taylor series expansion, and only the leading terms are retained. However, in cases where the external fields are strong, a perturbative treatment may not be sufficient. It is our interest to solve the problem through a non-perturbative approach. We decompose the time-evolution operator into many small steps in the light-front time x^+,

$$\begin{aligned}\mathcal{T}_+ \exp[-\frac{i}{2}\int_0^{x^+} \mathrm{d}z^+ V_I(z^+)] =& \mathcal{T}_+ \lim_{n\to\infty}\prod_{k=1}^{n}[1 - \frac{i}{2}V_I(x_k^+)\frac{x^+}{n}] \\ =& \lim_{n\to\infty}[1 - \frac{i}{2}V_I(x_n^+)\delta x^+]\ldots[1 - \frac{i}{2}V_I(x_1^+)\delta x^+] \ .\end{aligned} \tag{3.5}$$

The step size is $\delta x^+ \equiv x^+/n$, and the intermediate time is $x_k^+ = k\delta x^+ (k = 1, 2, \ldots, n)$. This product expansion is exact in the continuum limit of $n \to \infty$. In practical calculations, the value of n could be determined as to achieve a desired convergence on the final state. There are various numerical schemes in implementing Eq. (3.5). The most straight forward implementation is to use a finite difference approximation,

$$\begin{aligned} i\frac{\left|\psi; x^+ + \delta x^+\right\rangle_I - \left|\psi; x^+\right\rangle_I}{\delta x^+} &\approx \frac{1}{2}V_I(x^+)\left|\psi; x^+\right\rangle_I \ , \\ \Rightarrow \left|\psi; x^+ + \delta x^+\right\rangle_I &\approx [1 - \frac{i}{2}V_I(x_1^+)\delta x^+]\left|\psi; x^+\right\rangle_I \ . \end{aligned} \tag{3.6}$$

www.manaraa.com

The resulting method is known as the explicit Euler method. The second-order approximation, also known as the explicit midpoint method, has a faster convergence rate,

$$\begin{aligned} i\frac{|\psi; x^+ + \delta x^+\rangle_I - |\psi; x^+ - \delta x^+\rangle_I}{2\delta x^+} &\approx \frac{1}{2} V_I(x^+) |\psi; x^+\rangle_I \ , \\ \Rightarrow |\psi; x^+ + \delta x^+\rangle_I &\approx -iV_I(x_1^+)\delta x^+ |\psi; x^+\rangle_I + |\psi; x^+ - \delta x^+\rangle_I \ . \end{aligned} \tag{3.7}$$

We are interested in how eigenstates of the QCD Hamiltonian, P^-_{QCD}, evolve due to interactions with a background field. To begin, let us first identify the eigenstates $|\beta\rangle$ and eigenvalues P^-_β of P^-_{QCD}, such that

$$P^-_{QCD} |\beta\rangle = P^-_\beta |\beta\rangle \ . \tag{3.8}$$

We could then expand the physical state as a summation over the QCD eigenstates,

$$|\psi; x^+\rangle_I = \sum_\beta c_\beta(x^+) |\beta\rangle \ , \tag{3.9}$$

where $c_\beta(x^+) \equiv \langle\beta|\psi; x^+\rangle_I$ are the basis coefficients. The initial state at $x^+ = 0$ can be specified by $c_\beta(0)$ as a column vector, and the solution of Eq. (3.4) can be written in the QCD eigenstate basis as

$$c(x^+) = \mathcal{T}_+ \exp\Big(- i \int_0^{x^+} \mathrm{d}z^+ \mathcal{M}(z^+)\Big) c(0) \ , \tag{3.10}$$

where the matrix element is defined as $\mathcal{M}_{\beta\beta'}(x^+) \equiv \langle\beta|V_I(x^+)/2|\beta'\rangle$. Once we know the wavefunction of the state via $c(x^+)$, it is straightforward to evaluate observables from it.

A physical state can be expanded into the Fock space of infinite sectors. The coefficients of the Fock expansion are the complete set of n-particle light-front wavefunctions. In practical calculations, Fock sector truncation is needed and one usually implements basis truncation by assuming that higher Fock sectors give decreasing contributions. In solving phenomenological bound state problem, basis truncation is also taken as part of the model [61, 48, 3, 49, 50]. The time-dependent physical processes are also related to the Fock space truncation. In the recent work on the nonlinear Compton scattering process [37], the Fock space is truncated as $|e_{\text{phys}}\rangle \approx a|e\rangle + b|e\gamma\rangle$, thereby the excitation of the electron and the photon emission by the background field are studied. In analogy to physical bound states, here we consider the single dressed quark state as an expansion in the Fock space,

$$|q_{\text{dressed}}\rangle = a|q\rangle + b|qg\rangle + c|qgg\rangle + d|qq\bar{q}\rangle + \cdots \ . \tag{3.11}$$

www.manaraa.com

This series includes the bare quark and its dressed states with gluons and sea quarks. We start our investigation of a single quark evolution with the leading Fock sector contribution. In the future, we will add the $|qg\rangle$ sector and study the gluon emission.

Within each Fock sector, the Fock particle has an infinite number of degrees of freedom, and truncations of the basis space is also necessary. An optimal basis should preserve the symmetry of the system and approximate the eigenfunctions of the Hamiltonian. One well-known basis is the discretized momentum representation, where one expands the fields into plane waves. The discretized light-cone quantization (DLCQ) approach takes this treatment [43, 131]. This basis choice is also advantageous for our study of the single quark state, since the momentum state becomes the eigenstate of the QCD Hamiltonian, P^-_{QCD}. We therefore carry out our calculation in the momentum basis. One other popular choice is the two-dimensional harmonic oscillator (2D-HO) function. It preserves the rotational symmetry in the transverse plane and has been taken in various applications of the BLFQ approach, including the positronium bound states [45], the electron scatterings [37, 38] and the meson systems [48, 3, 49, 50].

3.2 Quark jet scattering off the Color Glass Condensate

We consider the quark-nucleus scattering at high rapidity, and treat it as a fundamental process of the more complicated ep, eA, pp, pA and AA collisions at high energy. In the dipole picture of the electron-nucleus deep inelastic scattering, a virtual photon fluctuates into a quark-antiquark pair, and subsequently the quark dipole scatters off the nucleus [132, 133, 134, 135, 136]. In the proton-nucleus collisions, the quark-nucleus scattering cross section may be related to the single inclusive hadron cross section through the collinear factorization of the proton [137]. It is from this standpoint, we apply the tBLFQ approach to solve the time evolution of a quark jet through a nuclear field.

We start by considering scattering of a high-energy quark moving in the positive z direction, on a high-energy nucleus moving in the negative z direction, as shown in Fig. 3.1. The quark has momentum p^μ and $p^+ >> p^-, p_\perp$ whereas the nucleus has momentum P^μ and $P^- >> P^+, P_\perp$. We treat the quark state as the system of interest, and the target as an external background field. The quark encounters the nuclear field at $x^+ = 0$ and leaves the field at $x^+ = \Delta x^+$. The internal structure of the nucleus at the quark-gluon

www.manaraa.com

level has drawn tremendous efforts. In this work, we take its description by the Color Glass Condensate model [138, 139, 140].

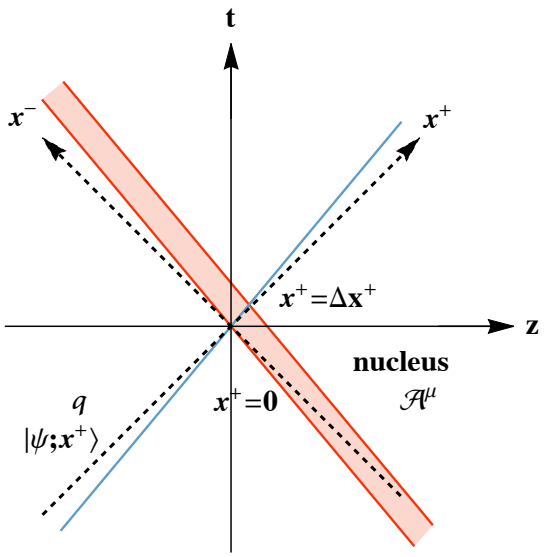

Figure 3.1 An illustration of a quark scattering on a nucleus in the spacetime diagram. The quark is moving along the positive-z direction and the nucleus along the negative-z direction. The blue line is the worldline of the quark, $z = \beta_q t$ with β_q the speed of the quark. The red band are worldlines of the nucleus, $z = -\beta_A t$ for one end and $z = -\beta_A t + d'$ for the other end. β_A is the speed of the nucleus and $d' = d\sqrt{1-\beta_A^2}$ with d the width of the nucleus in its rest frame. In the ultrarelativistic limit of $\beta_A \to 1$, the red band in the diagram shrinks to a single line aligned with $x^+ = 0$.

3.2.1 Background gluon field as the Color Glass Condensate

The CGC formalism takes into account the dynamics of large gluon densities at the small-x kinematic region. The underlying approximation involved in the CGC effective theory of high energy scattering is the eikonal approximation, i.e. small angle deflection of a high energy projectile traversing a medium. This is a good approximation if the transverse momentum of the scattered parton is small. In the McLerran-Venugopalan (MV) model [138, 139, 140], the classical small-x gluon field can be solved from the Yang-Mills equation

$$D_\mu \mathcal{F}^{\mu\nu} = J^\nu \,, \tag{3.12}$$

www.manaraa.com

$\mu, \nu = +, -, x, y$ (see definitions of the light-front variables in the Appendix A.1). $J^\nu = J^\nu_a T_a$ $(a = 1, 2, \ldots, 8)$ is the color current, where T_a are the color tensors. It has only one large component, $J^\nu_a = \delta^{\nu-}\rho_a(\vec{x}_\perp, x^+)$, where $\rho_a(\vec{x}_\perp, x^+)$ is the density of color charges of the large-x partons. $\rho_a(\vec{x}_\perp, x^+)$ does not depend on its time x^- because of time dilation. Moreover, due to Lorentz contraction of the target, the x^+ dependence is peaked around $x^+ = 0$, and the field is often treated as a delta function at $x^+ = 0$. Here we keep the x^+ dependence to allow for an extended target. The valence charges are treated as stochastic variables satisfying the correlation relation,

$$\langle \rho_a(\vec{x}_\perp, x^+)\rho_b(\vec{y}_\perp, y^+)\rangle = [g\mu(x^+)]^2\delta_{ab}\delta^2(\vec{x}_\perp - \vec{y}_\perp)\delta(x^+ - y^+) \,. \tag{3.13}$$

The dependence of the charge density in the x^+ dimension is encoded in $\mu(x^+)$, and we will take it as a constant (i.e. $\mu(x^+) = \mu$) in the range of the source. This correlation relation could be achieved by taking the color charge density $\rho_a(\vec{x}_\perp, x^+)$ to be a stochastic random variable with a local Gaussian distribution [138, 139],

$$f[\rho^2_a(\vec{x}_\perp, x^+)] = \exp\Big[-\frac{1}{(g\mu)^2}\int \mathrm{d}^2x_\perp \rho^2_a(\vec{x}_\perp, x^+)\Big] \,.$$

The Gaussian form is reasonable when the color charges at high rapidity are uncorrelated and random [141, 142]. Any observable O should be evaluated as a configuration average over ρ,

$$\langle O\rangle = \int \mathcal{D}\rho O[\rho] f[\rho^2] \,. \tag{3.14}$$

In covariant gauge $\partial^\mu \mathcal{A}_\mu = 0$,the field is solved as

$$(m_g^2 - \nabla^2_\perp)\mathcal{A}^-_a(\vec{x}_\perp, x^+) = \rho_a(\vec{x}_\perp, x^+) \,. \tag{3.15}$$

The gluon mass m_g is introduced to regularize the infrared (IR) divergence in the field, which imposes color neutrality on the source distribution [143]. The field solved from this regularized Poisson equation can be expressed in terms of the Green's function

$$\mathcal{A}^-_a(\vec{x}_\perp, x^+) = \int \mathrm{d}^2y_\perp G_0(\vec{x}_\perp - \vec{y}_\perp)\rho_a(\vec{y}_\perp, x^+) \,, \tag{3.16}$$

where

$$G_0(\vec{x}_\perp - \vec{y}_\perp) = -\int \frac{\mathrm{d}^2k_\perp}{(2\pi)^2}\frac{e^{-i\vec{k}_\perp\cdot(\vec{x}_\perp - \vec{y}_\perp)}}{m_g^2 + \vec{k}^2_\perp} \,. \tag{3.17}$$

www.manaraa.com

The field is logarithmically ultraviolet (UV) divergent. The divergence corresponds to the large momentum modes in the nuclei wavefunction, which are the degrees of freedom not meant to be included in the classical field. It is then natural to introduce a UV regulator [144]. In numerical calculations, there are several ways to implement the UV cutoff. First, discretization of the transverse space would introduce a UV cutoff automatically, as we will do in this work. Second, one can introduce an additional parameter Λ_{UV} when solving the gluon field as in Eq. (3.17), and the integral measure becomes $\int^{\Lambda_{UV}^2} \mathrm{d}^2 k_\perp$ [145]. Third, instead of regulating the gluon field, one could impose the UV cutoff on the phase space of the quark.

Note that there is no x-evolution in the MV model, and the saturation scale is a constant for a fixed charge density $g^2\mu$ and L_η, the extension of the field along x^+ [137, 146],

$$Q_s^2 = \frac{(g^2\mu)^2 L_\eta}{2\pi^2} \,. \tag{3.18}$$

This differs from more elaborate methods where the saturation scale is related to the gluon structure function of the nucleus and depends on x [147, 148].

One could estimate the duration of the field L_η through experimental energy scales. Consider the quark moves along the positive-a direction with speed β_q and the nucleus moves along the negative-a direction with speed $-\beta_A$, as illustrated in Fig. 3.1. The starting point of the quark-nucleus interaction is at $t_{start} = 0, z_{start} = 0$, i.e. $x^+_{start} = 0$. The end point of their interaction is at $t_{end} = d\sqrt{(1-\beta_A\beta_q)^2/(\beta_A+\beta_q)^2 - 1}, z_{end} = \beta_q t_{start}$. Thereby,

$$\Delta x^+ = (t_{end} + z_{end}) - (t_{start} + z_{start}) = d(\beta_q + 1)\frac{\sqrt{(1-\beta_A^2)(1-\beta_q^2)}}{\beta_A + \beta_q} \,. \tag{3.19}$$

d is the width of the nucleus in its rest frame. If we consider a gold beam at the RHIC energy of $\sqrt{s} = 100A$ GeV, and estimate its velocity according to $\gamma_A = 1/\sqrt{1-\beta_A^2} = \sqrt{s}/m = 100$ with m the mass of gold nucleus, thereby $\beta_A = 0.9999$. Its rest width is $d = 2R \approx 74\,\mathrm{GeV}^{-1}$. Assuming that the quark has the same speed, i.e. $\beta_q = \beta_A$, we get $\Delta x^+ \approx 0.015\,\mathrm{GeV}^{-1}$, which is small just as we expected. However the color field generated by the nucleus is identified as the small momentum degrees of freedom in the nucleus, and should admit a smaller longitudinal momentum scaled by Bjorken-x, $p^- = xP^-$. The resulting Lorentz factor is also scaled as $\gamma = x\gamma_A$. At $x = 0.1$, $\Delta x^+ \approx 1.48\,\mathrm{GeV}^{-1}$, and at $x = 0.015$, $\Delta x^+ \approx 71\,\mathrm{GeV}^{-1}$. We will take $L_\eta = 50\ \mathrm{GeV}^{-1}$ as the duration of the color field along x^+ in our calculations.

www.manaraa.com

3.2.2 Basis construction

3.2.2.1 Discretization of the fields

We have shown the canonical quantization of the QCD fields on the light front in Section 1.3. Here we want to write out the interaction vertex in the discretized momentum basis. Imagine that the system is contained in a box of finite volume $\Omega = 2L(2L_\perp)^2$. We have introduced two artificial length parameters, L in longitudinal direction and $L_\perp$ in transverse directions. The discretization is achieved by imposing the periodic boundary condition for bosons and the anti-periodic boundary condition for fermions in the coordinate space of a finite volume. Written explicitly, $-L \le x^- \le L$, $-L_\perp \le x^1, x^2 \le L_\perp$, and the normalization volume is $\Omega = 2L(2L_\perp)^2$. Correspondingly, in the momentum space,

$$p^+ = \begin{cases} \dfrac{2\pi}{2L} n, \text{ with } n = \dfrac{1}{2}, \dfrac{3}{2}, \ldots, \infty \text{ for fermions} , \\ \dfrac{2\pi}{2L} n, \text{ with } n = 1, 2, \ldots, \infty \text{ for bosons} , \end{cases} \tag{3.20}$$

$$p^i = \frac{2\pi}{2L_\perp} n^i, \text{ with } n^1, n^2 = 1, 2, \ldots, \infty . \tag{3.21}$$

The free fields are expanded as

$$\tilde{\Psi}_c^{\text{Box}}(x) = \sum_{\bar{\alpha}} \frac{1}{2p^+ 2L(2L_\perp)^2} [b_{\bar{\alpha},c} u(p,\lambda) e^{-ip\cdot x} + d^\dagger_{\bar{\alpha},c} v(p,\lambda) e^{ip\cdot x}] \tag{3.22}$$

$$\tilde{A}_{\mu,a}^{\text{Box}}(x) = \sum_{\bar{\alpha}} \frac{1}{2p^+ 2L(2L_\perp)^2} [a_{\bar{\alpha},a} \epsilon_\mu(p,\lambda) e^{-ip\cdot x} + a^\dagger_{\bar{\alpha},a} \epsilon^*_\mu(p,\lambda) e^{ip\cdot x}] \tag{3.23}$$

The creation operators $b^\dagger_{\bar{\alpha}}$, $d^\dagger_{\bar{\alpha}}$ and $a^\dagger_{\bar{\alpha}}$ create quarks, antiquarks and gluons with quantum numbers $\bar{\alpha}$ respectively. Each single particle state $\bar{\alpha}$ is specified by four quantum numbers, $\bar{\alpha} = \{n, n^1, n^2, \lambda\}$, where λ is the spin projection. They obey the following commutation and anti-commutation relations.

$$\{b_{\bar{\alpha},c}, b^\dagger_{\bar{\alpha}',c'}\} = \{d_{\bar{\alpha},c}, d^\dagger_{\bar{\alpha}',c'}\} = 2p^+ 2L(2L_\perp)^2 \delta_{\bar{\alpha},\bar{\alpha}'} \delta_{c,c'}, \qquad [a_{\bar{\alpha}}, a^\dagger_{\bar{\alpha}'}] = 2p^+ 2L(2L_\perp)^2 \delta_{\bar{\alpha},\bar{\alpha}'} \delta_{a,a'} \tag{3.24}$$

The commutation relation for the fermion fields in the box follows,

$$\begin{aligned} \{\tilde{\Psi}_c^{\text{Box}}(x), \tilde{\Psi}^{\dagger\text{Box}}_{c'}(y)\} = \sum_{\bar{\alpha},\bar{\alpha}'} \frac{1}{4p^+ q^+ \left(2L(2L_\perp)^2\right)^2} [\{b_{\bar{\alpha},c}, b^\dagger_{\bar{\alpha}',c'}\} u(p,\lambda) \bar{u}(q,\lambda') \gamma^0 e^{-ip\cdot x + iq\cdot y} \\ + \{d^\dagger_{\bar{\alpha},c}, d_{\bar{\alpha}',c'}\} v(p,\lambda) \bar{v}(q,\lambda') \gamma^0 e^{ip\cdot x - iq\cdot y}] \\ = \sum_{p^+, p_\perp} \frac{1}{2p^+ 2L(2L_\perp)^2} [(\not{p} + m)\gamma^0 e^{-ip\cdot(x-y)} + (\not{p} - m)\gamma^0 e^{ip\cdot(x-y)}] \delta_{c,c'} \end{aligned} \tag{3.25}$$

www.manaraa.com

3.2.2.2 The time evolution operator

To start, we consider the single quark Fock sector, $|q\rangle$. The light-front Hamiltonian, $P^-(x^+) = P^-_{QCD} + V(x^+)$, consists of two terms. The QCD part is the kinetic energy of the quark field and we neglet the kinetic energy of the background field,

$$P^-_{QCD} = \int \mathrm{d}x^- \, \mathrm{d}^2x_\perp \, \frac{1}{2}\bar{\tilde{\Psi}}\gamma^+ \frac{m^2 - \nabla^2_\perp}{i\partial^+}\tilde{\Psi} \, . \tag{3.26}$$

In the $|q\rangle$ sector, the V term contains the interactions between the quark field and the background field.

$$V = \int \mathrm{d}x^- \, \mathrm{d}^2x_\perp \left\{ g\bar{\tilde{\Psi}}\gamma^\mu T^a \tilde{\Psi}\mathcal{A}^a_\mu + \frac{g^2}{2}\bar{\tilde{\Psi}}\gamma^i \mathcal{A}_i \frac{\gamma^+}{i\partial^+}\gamma^j \mathcal{A}_j \tilde{\Psi} \right\} . \tag{3.27}$$

The background field is solved in the covariant gauge of $\partial^\mu \mathcal{A}_\mu = 0$, and $\mathcal{A}^\mu = \delta^{\mu-}\mathcal{A}^\mu$, as discussed in Section 3.2.1. The solution of the background field is consistent with the assumption that $\mathcal{A}^+ = 0$ in deriving the light-front Hamiltonian in Appendix B. The interaction term becomes

$$V = \int \mathrm{d}x^- \, \mathrm{d}^2x_\perp g\bar{\tilde{\Psi}}\gamma^+ T^a \tilde{\Psi}\mathcal{A}^a_+ \, . \tag{3.28}$$

In the discretized momentum basis, the vertex interaction reads

$$\begin{aligned} V =& \frac{g}{\left(2L(2L_\perp)^2\right)^2 4p_1^+ p_2^+} \sum_{\alpha_1,\alpha_2}\sum_{c_1,c_2}\int \mathrm{d}x^- \, \mathrm{d}^2x_\perp b^\dagger_{\alpha_2,c_2}\bar{u}(p_2,\lambda_2)e^{ip_2\cdot x}\gamma^+ b_{\alpha_1,c_1}u(p_1,\lambda_1)e^{-ip_1\cdot x} \\ & T^a_{c_2,c_1}\mathcal{A}^a_+(x_\perp,x^+) \\ =& \frac{g}{\left(2L(2L_\perp)^2\right)^2 2\sqrt{p_1^+p_2^+}} \sum_{\alpha_1,\alpha_2}\sum_{c_1,c_2}\int \mathrm{d}x^- \, \mathrm{d}^2x_\perp b^\dagger_{\alpha_2,c_2}e^{ip_2\cdot x}b_{\alpha_1,c_1}e^{-ip_1\cdot x}T^a_{c_2,c_1}\mathcal{A}^a_+(x_\perp,x^+)\delta_{\lambda_1,\lambda_2} \, . \end{aligned} \tag{3.29}$$

The spinor part is calculated in Appendix A.3. Integrate out x^- first,

$$V = \frac{g}{\left(2L(2L_\perp)^2\right)^2 2\sqrt{p_1^+p_2^+}} \sum_{\alpha_1,\alpha_2}\sum_{c_1,c_2}\int \mathrm{d}^2x_\perp 2L\delta_{p_2^+,p_1^+}e^{i(p_2^\perp - p_1^\perp)\cdot x_\perp}b^\dagger_{\alpha_2,c_2}T^a_{c_2,c_1}\mathcal{A}^a_+(x_\perp,x^+)\delta_{\lambda_1,\lambda_2} \, . \tag{3.30}$$

The integration over $x_\perp$ performs a Fourier transformation on the background field, $\int \mathrm{d}^2x_\perp \mathcal{A}^a_+(\vec{x}_\perp,x^+)e^{-i\vec{k}_\perp\cdot\vec{x}_\perp} = \tilde{\mathcal{A}}^a_+(\vec{k}_\perp,x^+)$, thereby

$$V = \frac{g}{2L(2L_\perp)^4 2\sqrt{p_1^+p_2^+}} \sum_{\alpha_1,\alpha_2}\sum_{c_1,c_2}\delta_{p_2^+,p_1^+}b^\dagger_{\alpha_2,c_2}b_{\alpha_1,c_1}T^a_{c_2,c_1}\tilde{\mathcal{A}}^a_+(\vec{p}_2^\perp - \vec{p}_1^\perp,x^+)\delta_{\lambda_1,\lambda_2} \, . \tag{3.31}$$

www.manaraa.com

The matrix element of the operator reads

$$
\begin{aligned}
&\langle\psi_q(p_f,\lambda_f,c_f)|V|\psi_q(p_i,\lambda_i,c_i)\rangle \\
&\quad=\frac{g}{2L(2L_\perp)^4 2\sqrt{p_1^+p_2^+}}\sum_{\alpha_1,\alpha_2}\sum_{c_1,c_2}\langle 0|\,b(p_f,\lambda_f,c_f)\sqrt{2L(2L_\perp)^2 2p_f^+}\delta_{p_2^+,p_1^+}\delta_{\lambda_1,\lambda_2} \\
&\quad T^a_{c_2,c_1}\tilde{\mathcal{A}}^a_+(\vec{p}_2^{\,\perp}-\vec{p}_1^{\,\perp},x^+)b^\dagger(p_2,\lambda_2,c_2)b(p_1,\lambda_1,c_1)\sqrt{2L(2L_\perp)^2 2p_i^+}b^\dagger(p_i,\lambda_i,c_i)\,|0\rangle \qquad (3.32)\\
&\quad=\frac{g}{(2L_\perp)^2}\sum_{\alpha_1,\alpha_2}\sum_{c_1,c_2}\delta_{p_2^+,p_1^+}\delta_{\lambda_1,\lambda_2}T^a_{c_2,c_1}\tilde{\mathcal{A}}^a_+(\vec{p}_2^{\,\perp}-\vec{p}_1^{\,\perp},x^+)\delta_{p_f,p_2}\delta_{\lambda_f,\lambda_2}\delta_{c_f,c_2}\delta_{p_1,p_i}\delta_{\lambda_1,\lambda_i}\delta_{c_1,c_i} \\
&\quad=\frac{g}{(2L_\perp)^2}\delta_{p_f^+,p_i^+}\delta_{\lambda_f,\lambda_i}T^a_{c_f,c_i}\tilde{\mathcal{A}}^a_+(\vec{p}_2^{\,\perp}-\vec{p}_1^{\,\perp},x^+)\,.
\end{aligned}
$$

We can see immediately that the interaction with this background field could change the transverse momentum and the color of the quark, but it leaves the longitudinal momentum and the spin configuration unchanged.

3.2.3 Numerical scheme

In the numerical calculation, the fields are color SU(3) matrices on the sites of a 3-dimensional discrete space. The 2-dimensional transverse space is a lattice extending from $-L$ to L for each side. The number of transverse lattice sites is $2N$ given the lattice spacing $a = L/N$. As such, a vector $\vec{r}_\perp = (r_x, r_y)$ would read as,

$$r_i = n_i a\ (i = x, y), \quad n_i = -N, -N+1, \ldots, N-1.$$

This space satisfies periodic boundary conditions. As such, the lattice point at the far boundary $L = Na$ is taken as the same as the one at the boundary $-L$. It follows that in the momentum space, for any vector, $\vec{p}_\perp = (p_x, p_y)$,

$$p_i = k_i d_p\ (i = x, y), \quad k_i = -N, -N+1, \ldots, N-1,$$

where $d_p \equiv \pi/L$ is the resolution in momentum space. The momentum space extends from $-\pi/a$ to π/a. Therefore, the transverse lattice introduces a pair of IR and UV cutoffs, $\lambda_{IR} = \pi/L$ and $\lambda_{UV} = N\pi/L$.

The longitudinal dimension of the field x^+ (note that this is the light-front time of the struck quark) is discretized into a number of N_η layers. If the field extends L_η along x^+, each layer would have an expansion of $\tau = L_\eta/N_\eta$. For example, the k-th ($k = 1, 2, \ldots, N_\eta$) layer extends as $x^+ = [(k-1)\tau, k\tau]$.

To summarize, our calculation depends on the following numerical parameters.

www.manaraa.com

- $g^2\mu$, color charge density. We take different values and study how observables depend on it.
- m_g, screening mass, the IR regulator. We will take $m_g = 0.1$ GeV for most calculations and use various values when studying the resulting effects.
- The transverse lattice: size L, number N and spacing $a = L/N$. In most cases, we take $L = 50\,\text{GeV}^{-1}$(= 9.87 fm) as estimated from the radius of the gold nucleus.
- The x^+ direction: duration L_η, the number of layers N_η and interval $\tau = L_\eta/N_\eta$. We take $L_\eta = 50\,\text{GeV}^{-1}$ and study the convergence on N_η.

In this discretized space, the correlation relation of the color charge as defined in Eq. (3.13) also takes a discrete form as,

$$\left\langle \rho_a(n_x, n_y, k)\rho_b(n'_x, n'_y, k')\right\rangle = (g\mu)^2\delta_{ab}\frac{\delta_{n_x,n'_x}\delta_{n_y,n'_y}}{a^2}\frac{\delta_{k,k'}}{\tau}\ . \tag{3.33}$$

Note that the Kronecker delta dividing the discrete resolution replaces the Dirac delta in Eq. (3.13), and they converge in the continuous limit of $a \to 0$ and $\tau \to 0$.

3.3 Observables

In this section, we study various observables in the quark-nucleus sacttering obtained from the tBLFQ formalism. We first study the total and elastic cross sections, and justify our calculation by comparing to predictions in the eikonal limit. We then study the differential cross section and look into the time evolution of the quark's distribution in transverse coordinate space and color space. We further relax the eikonal condition and explore sub-eikonal effects with finite p^+.

3.3.1 The cross section

The cross section for an individual event can be calculated as the sum of transition amplitude square [34], and it reads,

$$\frac{\mathrm{d}\sigma}{\mathrm{d}^2b} = \sum_{\phi_f}|M(\phi_f;\psi_i)|^2 = \sum_{\phi_f}|{}_{out}\langle\phi_f|S|\psi_i\rangle_{in} - {}_{out}\langle\phi_f|\psi_i\rangle_{in}|^2\ . \tag{3.34}$$

www.manaraa.com

ψ_i stands for the initial state, and ϕ_f is the final state, $\sum_{\phi_f}$ sums over the phase space of the final state. The S in the equation is the evolution operator from the initial state to the final through a finite time transition, and is different from the case where one takes the infinite time limit. In evaluating the cross section, one should average over the color charge density ρ as in Eq. (3.14). This would give us the total cross section by definition,

$$\frac{\mathrm{d}\sigma_{\mathrm{tot}}}{\mathrm{d}^2 b} = \langle \sum_{\phi_f} |M(\phi_f;\psi_i)|^2 \rangle \ . \tag{3.35}$$

The total cross section is the summation of the elastic $2 \to 2$ contribution and the inelastic contributions ($2 \to 3$, $2 \to 4$, etc.), $\sigma_{tot} = \sigma_{els} + \sigma_{inels}$. To calculate the elastic cross section, one need to carry out the configuration average on the amplitude level to get the elastic scattering amplitude first, and afterwards square it [149].

$$\frac{\mathrm{d}\sigma_{\mathrm{els}}}{\mathrm{d}^2 b} = \sum_{\phi_f} |\langle M(\phi_f;\psi_i)\rangle|^2 \ . \tag{3.36}$$

3.3.1.1 The eikonal limit of the cross sections

In the eikonal limit, the longitudinal momentum of the quark is infinite, $p^+ = \infty$, thus the phase factor $e^{\pm i p^- x^+/2}$ (see text associated with Eq. (3.3)) is 1 and $V_I(x^+)$ reduces to $V(x^+)$. In this limit, the cross sections can be evaluated analytically as a function of the charge density $g^2\mu$, the interaction duration L_η (for which the background field exists for $x^+ = [0, L_\eta]$), and the IR and UV cutoffs of the gluon field, $\lambda_{IR} = m_g$ and Λ_{UV}. In this limit, the evolution operator is diagonal in the transverse coordinate space, and it is essentially the Wilson line of the quark.

$$\begin{aligned}
\lim_{p^+=\infty} \langle \vec{x}'_\perp | \mathcal{T}_+ \exp[-\frac{i}{2}\int_0^{L_\eta} \mathrm{d}x^+ V_I(x^+)] | \vec{x}_\perp \rangle =& \mathcal{T}_+ \exp[-\frac{i}{2}\int_0^{L_\eta} \mathrm{d}x^+ V(x^+, \vec{x}_\perp)] \delta^2(\vec{x}_\perp - \vec{x}'_\perp) \\
=& \mathcal{T}_+ \exp\Big(- ig \int_0^{L_\eta} \mathrm{d}x^+ \mathcal{A}_a^-(\vec{x}_\perp, x^+) T_a \Big) \delta^2(\vec{x}_\perp - \vec{x}'_\perp) \\
\equiv& U(\vec{x}_\perp) \delta^2(\vec{x}_\perp - \vec{x}'_\perp) \ .
\end{aligned} \tag{3.37}$$

www.manaraa.com

The physical observable such as the cross section is related to the configuration average of the Wilson line, $\langle U(\vec{x}_\perp)\rangle$. The Taylor expansion of the time-ordered exponential function leads to

$$\begin{aligned}\langle U(\vec{x}_\perp)\rangle = \sum_{n=0}^{\infty}(-ig)^n \int \prod_{i=1}^{n} \mathrm{d}^2 z_{i\perp} G_0(x_\perp - z_{i\perp}) \int_0^{L_\eta} dz_1^+ \int_{z_1^+}^{L_\eta} dz_2^+ \cdots \int_{z_{n-1}^+}^{L_\eta} dz_n^+ \\ \langle \rho_{a_1}(z_1^+, z_{1\perp})\rho_{a_2}(z_2^+, z_{2\perp})\cdots\rho_{a_n}(z_n^+, z_{n\perp})\rangle T_{a_1} T_{a_2}\cdots T_{a_n}\ .\end{aligned} \tag{3.38}$$

We can decompose the product of multiple charge densities $\langle \rho_1\rho_2...\rho_n\rangle$ into all possible contractions in the case of the Gaussian average, according to the correlation function of ρ given in Eq. (3.13). It follows that the configuration average of the odd number product of the charge densities, $\langle \rho_1\rho_2...\rho_{2j+1}\rangle$ would vanish, and that of the even number product, $\langle \rho_1\rho_2...\rho_{2j}\rangle$, sums over all possible permutations

$$\begin{aligned}&\langle \rho_{a_1}(z_1^+, z_{1\perp})\cdots\rho_{a_n}(z_n^+, z_{n\perp})\rangle \\ =&\begin{cases} 0, & n \text{ is odd} \\ \langle \rho_{a_1}(z_1^+, z_{1\perp})\rho_{a_2}(z_2^+, z_{2\perp})\rangle\cdots\langle \rho_{a_{n-1}}(z_{n-1}^+, z_{n-1\perp})\rho_{a_n}(z_n^+, z_{n\perp})\rangle + \text{permutations}, & n \text{ is even} \end{cases}.\end{aligned} \tag{3.39}$$

For the even number product, only the adjacent contractions survive under the time-ordered integrals. The other two types of contractions, nesting and overlapping, all vanish.

$$\langle \rho_{a_1}(z_1^-, z_{1\perp})\cdots\rho_{a_n}(z_n^-, z_{n\perp})\rangle \to \langle \rho_{a_1}(z_1^-, z_{1\perp})\rho_{a_2}(z_2^-, z_{2\perp})\rangle\cdots\langle \rho_{a_{n-1}}(z_{n-1}^-, z_{n-1\perp})\rho_{a_n}(z_n^-, z_{n\perp})\rangle\ .$$

We can see this in the simplest nontrivial case, the four source contraction. The nesting contraction vanishes because of the delta function in Eq. (3.40).

$$\begin{aligned}&\int_0^{L_\eta} \mathrm{d}z_1^+ \int_{z_1^+}^{L_\eta} \mathrm{d}z_2^+ \int_{z_2^+}^{L_\eta} \mathrm{d}z_3^+ \int_{z_3^+}^{L_\eta} \mathrm{d}z_4^+ \langle \rho_{a_1}(z_1^+, z_{1\perp})\rho_{a_4}(z_4^+, z_{4\perp})\rangle \langle \rho_{a_2}(z_2^+, z_{2\perp})\rho_{a_3}(z_3^+, z_{3\perp})\rangle \\ =&\int_0^{L_\eta} \mathrm{d}z_1^+ \int_{z_1^+}^{L_\eta} \mathrm{d}z_2^+ \int_{z_2^+}^{L_\eta} \mathrm{d}z_3^+ \int_{z_3^+}^{L_\eta} \mathrm{d}z_4^+ \delta_{a_1a_4}[g\mu(z_1^+)]^2\delta^2(z_{1\perp} - z_{4\perp})\delta(z_1^+ - z_4^+) \\ &\times \delta_{a_2a_3}[g\mu(z_2^+)]^2\delta^2(z_{2\perp} - z_{3\perp})\delta(z_2^+ - z_3^+) \\ =&0\ .\end{aligned} \tag{3.40}$$

www.manaraa.com

The overlapping contraction also vanishes as in Eq. (3.41)

$$\begin{aligned}
&\int_0^{L_\eta} \mathrm{d}z_1^+ \int_{z_1^+}^{L_\eta} \mathrm{d}z_2^+ \int_{z_2^+}^{L_\eta} \mathrm{d}z_3^+ \int_{z_3^+}^{L_\eta} \mathrm{d}z_4^+ \left\langle \rho_{a_1}(z_1^+, z_{1\perp}) \rho_{a_3}(z_3^+, z_{3\perp}) \right\rangle \left\langle \rho_{a_2}(z_2^+, z_{2\perp}) \rho_{a_4}(z_4^+, z_{4\perp}) \right\rangle \\
=& \int_0^{L_\eta} \mathrm{d}z_1^+ \int_{z_1^+}^{L_\eta} \mathrm{d}z_2^+ \int_{z_2^+}^{L_\eta} \mathrm{d}z_3^+ \int_{z_3^+}^{L_\eta} \mathrm{d}z_4^+ \delta_{a_1 a_3} [g\mu(z_1^+)]^2 \delta^2(z_{1\perp} - z_{3\perp}) \delta(z_1^+ - z_3^+) \\
&\times \delta_{a_2 a_4} [g\mu(z_2^+)]^2 \delta^2(z_{2\perp} - z_{4\perp}) \delta(z_2^+ - z_4^+) \\
=& 0 \, .
\end{aligned} \tag{3.41}$$

Only the adjacent contraction survives as in Eq. (3.42)

$$\begin{aligned}
&\int_0^{L_\eta} \mathrm{d}z_1^+ \int_{z_1^+}^{L_\eta} \mathrm{d}z_2^+ \int_{z_2^+}^{L_\eta} \mathrm{d}z_3^+ \int_{z_3^+}^{L_\eta} \mathrm{d}z_4^+ \left\langle \rho_{a_1}(z_1^+, z_{1\perp}) \rho_{a_2}(z_2^+, z_{2\perp}) \right\rangle \left\langle \rho_{a_3}(z_3^+, z_{3\perp}) \rho_{a_4}(z_4^+, z_{4\perp}) \right\rangle \\
=& \int_0^{L_\eta} \mathrm{d}z_1^+ \int_{z_1^+}^{L_\eta} \mathrm{d}z_2^+ \delta_{a_1 a_2} [g\mu(z_1^+)]^2 \delta^2(z_{1\perp} - z_{2\perp}) \delta(z_1^+ - z_2^+) \\
&\times \int_{z_2^+}^{L_\eta} \mathrm{d}z_3^+ \int_{z_3^+}^{L_\eta} \mathrm{d}z_4^+ \delta_{a_3 a_4} [g\mu(z_3^+)]^2 \delta^2(z_{3\perp} - z_{4\perp}) \delta(z_3^+ - z_4^+) \\
=& \int_0^{L_\eta} \mathrm{d}z_1^+ \int_{z_1^+}^{L_\eta} \mathrm{d}z_3^+ \delta_{a_1 a_2} \frac{[g\mu(z_1^+)]^2}{2} \delta^2(z_{1\perp} - z_{2\perp}) \delta_{a_3 a_4} \frac{[g\mu(z_3^+)]^2}{2} \delta^2(z_{3\perp} - z_{4\perp}) \, .
\end{aligned} \tag{3.42}$$

By decomposing the multiple point correlator into two point correlators, the Wilson line in Eq. (3.38) follows as,

$$\begin{aligned}
\left\langle U(\vec{x}_\perp) \right\rangle =& \sum_{n=0}^{\infty} (-ig^2)^n \int \prod_{i=1}^{n/2} \mathrm{d}^2 z_{2i\perp} G_0^2(\vec{x}_\perp - \vec{z}_{2i\perp}) \\
&\times \frac{1}{2} \int_0^{L_\eta} \mathrm{d}z_1^+ \mu^2(z_1^+) \frac{1}{2} \int_{z_1^+}^{L_\eta} \mathrm{d}z_3^+ \mu^2(z_3^+) \cdots \frac{1}{2} \int_{z_{n-3}^+}^{L_\eta} \mathrm{d}z_{n-1}^+ \mu^2(z_{n-1}^+) T_{a_1}^2 T_{a_3}^2 \cdots T_{a_{n-1}}^2 \\
=& \sum_{n=0}^{\infty} \frac{1}{(n/2)!} \left[\frac{-g^4}{2} \int \mathrm{d}^2 z_\perp G_0^2(x_\perp - z_\perp) \int_0^{L_\eta} \mathrm{d}z^+ \mu^2(z^+) T_a^2 \right]^{n/2} .
\end{aligned} \tag{3.43}$$

www.manaraa.com

The Green function is written explicitely in Eq. (3.17). By introducing an UV cutoff Λ_{UV}, the transverse integral becomes

$$\begin{aligned}\int \mathrm{d}^2 z_\perp G_0^2(x_\perp - z_\perp) &= \int \mathrm{d}^2 z_\perp \Big[- \int^{\Lambda_{UV}} \frac{\mathrm{d}^2 k_\perp}{(2\pi)^2} \frac{e^{-i\vec{k}_\perp\cdot(\vec{x}_\perp - \vec{z}_\perp)}}{m_g^2 + \vec{k}_\perp^2} \Big]^2 \\ &= \int \mathrm{d}^2 z_\perp \int^{\Lambda_{UV}} \frac{\mathrm{d}^2 k_\perp}{(2\pi)^2} \frac{e^{-i\vec{k}_\perp\cdot(\vec{x}_\perp - \vec{z}_\perp)}}{m_g^2 + \vec{k}_\perp^2} \int^{\Lambda_{UV}} \frac{\mathrm{d}^2 l_\perp}{(2\pi)^2} \frac{e^{i\vec{l}_\perp\cdot(\vec{x}_\perp - \vec{z}_\perp)}}{m_g^2 + \vec{l}_\perp^2} \\ &= (2\pi)^2 \delta^2(\vec{k}_\perp - \vec{l}_\perp) \int^{\Lambda_{UV}} \frac{\mathrm{d}^2 k_\perp}{(2\pi)^2} \frac{e^{-i\vec{k}_\perp\cdot\vec{x}_\perp}}{m_g^2 + \vec{k}_\perp^2} \int^{\Lambda_{UV}} \frac{\mathrm{d}^2 l_\perp}{(2\pi)^2} \frac{e^{i\vec{l}_\perp\cdot\vec{x}_\perp}}{m_g^2 + \vec{l}_\perp^2} \\ &= \int^{\Lambda_{UV}} \frac{\mathrm{d}^2 k_\perp}{(2\pi)^2} \frac{1}{(m_g^2 + \vec{k}_\perp^2)^2} \\ &= \int_0^{2\pi} \mathrm{d}\theta \int_0^{\Lambda_{UV}} \frac{k_t\, \mathrm{d}k_t}{(2\pi)^2} \frac{1}{(m_g^2 + k_t^2)^2} \\ &= \frac{1}{4\pi}\Big[\frac{1}{m_g^2} - \frac{1}{\Lambda_{UV}^2 + m_g^2}\Big] .\end{aligned} \tag{3.44}$$

Though the background field admits an UV divergence in the transverse momentum space, the two point correlation does not. By taking $\Lambda_{UV} \to \infty$, we have $\int \mathrm{d}^2 z_\perp G_0^2(x_\perp - z_\perp) = 1/(4\pi m_g^2)$. The Wilson line then follows as

$$\langle U(\vec{x}_\perp)\rangle = \exp\Big[\frac{-(N_c^2-1)}{16\pi m_g^2 N_c} \int_0^{L_\eta} \mathrm{d}z^+ g^4 \mu^2(z^+)\Big] . \tag{3.45}$$

Note that the result is diagonal in the color space of the quark, by taking $T_a^2 = (N_c^2 - 1)/N_c I_3$. In the cases with constant color charge strength in the $x^+ = [0, L_\eta]$ duration, i.e. $\mu(x^+) = \mu$, the Wilson line reads

$$\langle U(\vec{x}_\perp)\rangle = \exp\Big[\frac{-g^4\mu^2(N_c^2-1)L_\eta}{16\pi m_g^2 N_c}\Big] . \tag{3.46}$$

The derivation of the configuration average of the Wilson line correlator is similar,

$$\langle U(\vec{x}_\perp) U^\dagger(\vec{x}'_\perp)\rangle = \exp\Big[\frac{-g^4\mu^2(N_c^2-1)L_\eta}{4N_c} 2 \int \frac{\mathrm{d}^2 k_\perp}{(2\pi)^2} \frac{1}{(m_g^2 + \vec{k}_\perp^2)^2} [1 - e^{-i\vec{k}_\perp\cdot(\vec{x}_\perp - \vec{x}'_\perp)}]\Big] . \tag{3.47}$$

The amplitude of the transition from a quark state with momentum $\vec{p}_\perp$ to a state with momentum $\vec{q}_\perp$ reads,

$$M(\vec{q}_\perp; \vec{p}_\perp) = {}_{out}\langle \vec{q}_\perp | S | \vec{p}_\perp\rangle_{in} - {}_{out}\langle \vec{q}_\perp | I | \vec{p}_\perp\rangle_{in} = \int \mathrm{d}^2 x_\perp [U(\vec{x}_\perp) - 1] e^{i(\vec{q}_\perp - \vec{p}_\perp)\cdot\vec{x}_\perp} \tag{3.48}$$

www.manaraa.com

The total cross section is calculated as

$$\begin{aligned}
\sigma_{tot} &= \langle \int \frac{\mathrm{d}^2 q_\perp}{(2\pi)^2} |M(\vec{q}_\perp;\vec{p}_\perp)|^2 \rangle \\
&= \langle \int \frac{\mathrm{d}^2 q_\perp}{(2\pi)^2} \int \mathrm{d}^2 x_\perp [U(\vec{x}_\perp)-1] e^{i(\vec{q}_\perp-\vec{p}_\perp)\cdot\vec{x}_\perp} \int \mathrm{d}^2 x'_\perp [U(\vec{x}'_\perp)-1] e^{-i(\vec{q}_\perp-\vec{p}_\perp)\cdot\vec{x}'_\perp} \rangle \\
&= \langle \int \mathrm{d}^2 x_\perp [U(\vec{x}_\perp)-1] e^{-i\vec{p}_\perp\cdot\vec{x}_\perp} \int \mathrm{d}^2 x'_\perp [U(\vec{x}'_\perp)-1] e^{i\vec{p}_\perp\cdot\vec{x}'_\perp} \delta^2(\vec{x}_\perp-\vec{x}'_\perp) \rangle \\
&= \langle \int \mathrm{d}^2 x_\perp [U(\vec{x}_\perp)-1]^2 \rangle \\
&= \int \mathrm{d}^2 x_\perp \Big(\langle U(\vec{x}_\perp) U^\dagger(\vec{x}_\perp) \rangle - \langle U(\vec{x}_\perp) \rangle - \langle U^\dagger(\vec{x}_\perp) \rangle + 1 \Big) \\
&= \int \mathrm{d}^2 x_\perp 2\Big(1 - \langle U(\vec{x}_\perp) \rangle \Big) .
\end{aligned} \tag{3.49}$$

Since the averaged Wilson does not have dependence on the transverse coordinate as in Eq. (3.47), the resulting cross section is proportional to the area of transverse space. It would be more convenient to study the cross section as a ratio to the transverse space,

$$\frac{\mathrm{d}\sigma_{tot}}{\mathrm{d}^2 b} = 2\left\{1 - \exp\left[\frac{-g^4\mu^2(N_c^2-1)L_\eta}{16\pi m_g^2 N_c}\right]\right\} . \tag{3.50}$$

The last line also implies the optical theorem,

$$\sigma_{tot} = \int \mathrm{d}^2 x_\perp 2\mathrm{Im}A(\vec{x}_\perp) , \tag{3.51}$$

by recognizing the forward scattering amplitude as

$$A(\vec{x}_\perp) = i[1 - \langle U(\vec{x}_\perp) \rangle] . \tag{3.52}$$

The elastic cross section can be calculated from the forward scattering amplitude as

$$\sigma_{els} = \int \mathrm{d}^2 x_\perp |A(\vec{x}_\perp)|^2 = \int \mathrm{d}^2 x_\perp [1 - \langle U(\vec{x}_\perp) \rangle]^2 . \tag{3.53}$$

www.manaraa.com

This result is equivalent to that obtained by taking the configuration average of the transition amplitude first and afterwards square it,

$$\begin{aligned}\sigma_{els} &= \int \frac{\mathrm{d}^2 q_\perp}{(2\pi)^2} |\langle M(\vec{q}_\perp;\vec{p}_\perp)\rangle|^2 \\ &= \int \frac{\mathrm{d}^2 q_\perp}{(2\pi)^2} \int \mathrm{d}^2 x_\perp [\langle U(\vec{x}_\perp)\rangle - 1] e^{i(\vec{q}_\perp - \vec{p}_\perp)\cdot\vec{x}_\perp} \int \mathrm{d}^2 x'_\perp [\langle U^\dagger(\vec{x}'_\perp)\rangle - 1] e^{-i(\vec{q}_\perp - \vec{p}_\perp)\cdot\vec{x}'_\perp} \\ &= \int \frac{\mathrm{d}^2 q_\perp}{(2\pi)^2} \int \mathrm{d}^2 x_\perp [\langle U(\vec{x}_\perp)\rangle - 1] e^{i(\vec{q}_\perp - \vec{p}_\perp)\cdot\vec{x}_\perp} [\langle U^\dagger(\vec{x}'_\perp)\rangle - 1] 2\pi^2 \delta^2(\vec{q}_\perp - \vec{p}_\perp) \\ &= \int \mathrm{d}^2 x_\perp [\langle U(\vec{x}_\perp)\rangle - 1]^2 \,.\end{aligned} \tag{3.54}$$

Note that since the Wilson line is translation invariant under the configuration average, the integral $\int \mathrm{d}^2 \vec{x}'_\perp$ leads to a delta function of the transverse momenta. The result is the same with that in Eq. (3.53). As for the total cross section, we can write the elastic cross section as a ratio to the transverse area,

$$\frac{\mathrm{d}\sigma_{els}}{\mathrm{d}^2 b} = \left\{1 - \exp\left[\frac{-g^4\mu^2(N_c^2-1)L_\eta}{16\pi m_g^2 N_c}\right]\right\}^2 . \tag{3.55}$$

In the high energy limit, i.e. $g^2\mu \to \infty$ in Eqs. (3.50) and (3.55), the total cross section approaches 2 and the elastic cross section approaches 1, and their ratio $\sigma_{tot}/\sigma_{els} \to 1/2$. This corresponds to the standard 'black disc' limit, enshrined in classical optics as the "Babinet's principle". Consider a disc that is totally 'black' in the sense that everything hitting it is completely absorbed, which gives the inelastic cross section. At the same time this 'absorption' creates a 'hole' in the incoming wave front, leading to an elastic scattering which has the same cross section. Therefore in this limit, $\sigma_{tot} = \sigma_{els} + \sigma_{inels} = 2\sigma_{els}$.

3.3.1.2 Numerical results

We first calculate the total and elastic cross sections in the eikonal limit and compare our results with the eikonal expectations in Eqs. (3.50) and (3.55). We also study the sensitivity of the cross sections to the parameters, N, L, N_η, and m_g. We then relax the eikonal condition to finite p^+, and explore potential effects. The light-front kinetic energy of the quark is calculated as $p^- = (\vec{p}_\perp^2 + m_q^2)/p^+$, we use $m_q = 0.15\,\mathrm{GeV}$ in the presented results. We have checked that using a quark mass in the range of $m_q = 0.05 - 4.50\,\mathrm{GeV}$ does not make noticeable changes on the results with the current setting.

We then check the dependence of the cross sections on the lattice by varying N and L. Note that a reasonable numerical grid should cover the physical range of interest. In this case, we should make sure

www.manaraa.com

that the numerical IR cutoff ($\lambda_{IR} = \pi/L$) is much smaller than the physical IR cutoff, $\Lambda_{IR} = m_g$, and the numerical UV cutoff ($\lambda_{UV} = N\pi/L$) much bigger than Λ_{IR}. Thus a suitable grid for our investigation should satisfy:

$$\frac{\pi}{L} \ll m_g \ll N\frac{\pi}{L} \,. \tag{3.56}$$

Fig. 3.2 represents the total and elastic cross sections as functions of $g^2\mu$ at different N for a fixed L. The results show a convergence on increasing N. We take the standard deviation of the 100 averaged configurations as the uncertainty. Such uncertainty is smaller at larger N. This is not hard to imagine, since with more sites on the lattice, the fluctuation of each configuration is more likely to smooth out when averaged over an equal number of events. Most importantly, there is a good agreement between the tBLFQ results and the eikonal analytical expectations calculated from Eqs. (3.50) and (3.55). This agreement helps verify our formalism.

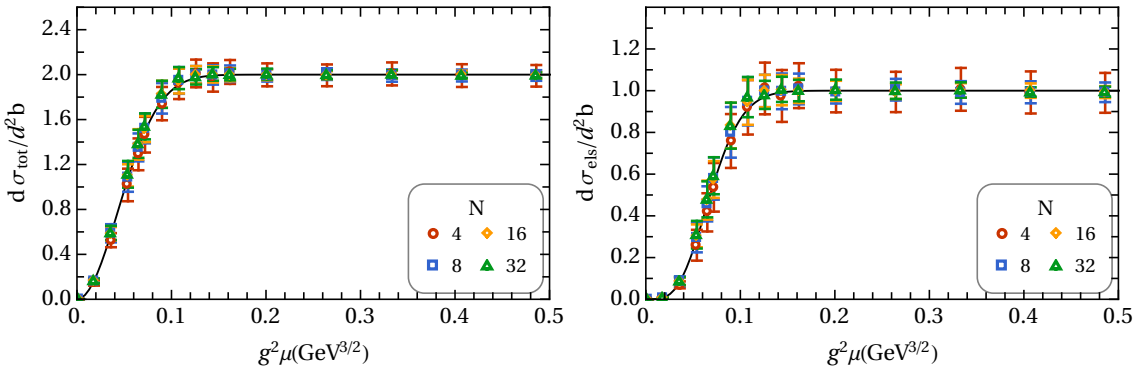

Figure 3.2 The dependence on the transverse grid number N of the cross sections at $L = 50\,\mathrm{GeV}^{-1}$. The cross sections are calculated as functions of $g^2\mu$ with $L_\eta = 50\,\mathrm{GeV}^{-1}$, $N_\eta = 4$ and $p^+ = \infty$. The left panel is the total cross section and the right panel is the elastic cross section. The solid lines are the eikonal predictions as calculated from Eqs. (3.50) and (3.55). Each data point results from an average over 100 configurations, and the standard deviation is taken as the uncertainty.

The dependence of the cross sections on the grid size L is also checked and shown in Fig. 3.3. The total and elastic cross sections are calculated as functions of $g^2\mu$ at different L for a fixed lattice spacing $a = L/N = 6.25\ \mathrm{GeV}^{-1}$. The results show agreements with the eikonal analytical expectations from Eqs. (3.50)

www.manaraa.com

and (3.55). We again observe that the lattice with a larger number of grids has smaller uncertainties. The cross sections are not sensitive to the grid size.

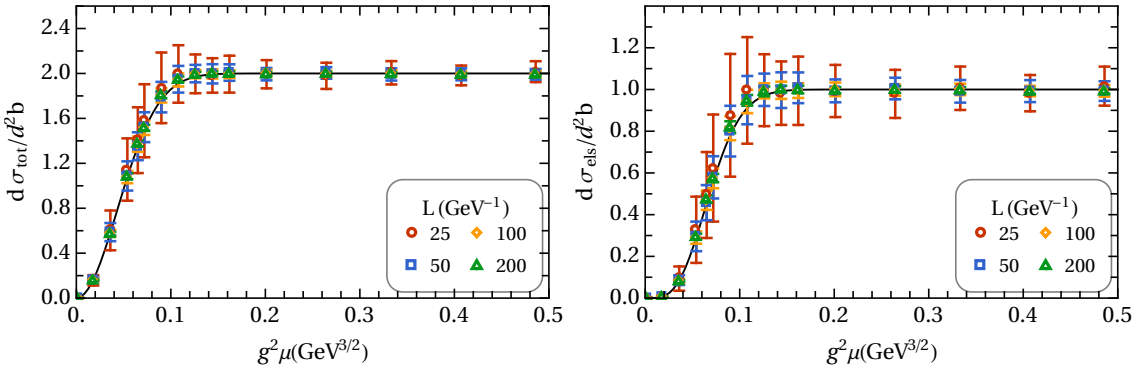

Figure 3.3 The dependence on the transverse grid length L of the cross sections. The lattice spacing is fixed as $a = L/N = 6.25\ \mathrm{GeV}^{-1}$ for these results. The cross sections of the quark are plotted as functions of $g^2\mu$ at $L_\eta = 50\,\mathrm{GeV}^{-1}$, $N_\eta = 4$ and $p^+ = \infty$. The solid lines are the eikonal predictions as calculated from Eqs. (3.50) and (3.55). Results for each data point are averaged over 100 configurations, and the standard deviation is taken as the uncertainty.

We next show in Fig. 3.4 the dependence of the cross sections on the number of layers in the longitudinal direction, N_η. An interesting "oscillation" pattern is observed when $N_\eta = 1$. At $N_\eta = 1$, the source and therefore the gluon field along x^+ is constant, this breaks one necessary ingredient for the CGC field: sources are uncorrelated along x^+, as in Eq. (3.13). It follows that in deriving the analytical expression of the cross section, the contraction of multiple sources is no longer preserved, causing a nontrivial "oscillation". In our calculation, the $x^+ = [0, L_\eta]$ duration is divided into N_η layers, each lasting equally for $\tau = L_\eta/N_\eta$. The color charges from different layers belong to different nucleons, so they are uncorrelated with each other, as in Eq. (3.33). Within each layer, the field is constant along x^+. The continuum limit is restored at $N_\eta \to \infty$, as in Eq. (3.57).

$$\begin{aligned}\int_{-\infty}^{+\infty}\mathrm{d}x^+\int_{-\infty}^{+\infty}\mathrm{d}y^+\,\langle\rho_a(x^+,x_\perp)\rho_b(y^+,y_\perp)\rangle &= g^2\mu^2\delta_{ab}\delta^2(\vec{x}_\perp-\vec{y}_\perp)\int_{-\infty}^{+\infty}\mathrm{d}x^+\int_{-\infty}^{+\infty}\mathrm{d}y^+\frac{\delta_{k,k'}}{\tau}\\ &= g^2\mu^2\delta_{ab}\delta^2(\vec{x}_\perp-\vec{y}_\perp)(\sum_{k=1}^{N_\eta}\tau^2)\frac{1}{\tau}\\ &= g^2\mu^2\delta_{ab}\delta^2(\vec{x}_\perp-\vec{y}_\perp)L_\eta\end{aligned} \tag{3.57}$$

www.manaraa.com

This "oscillation" gets strongly suppressed when $N_\eta = 2$, and for larger $N_\eta (\geq 4)$, the physical results converge to the analytical expectation and depend very little on N_η, as shown in Fig. 3.4.

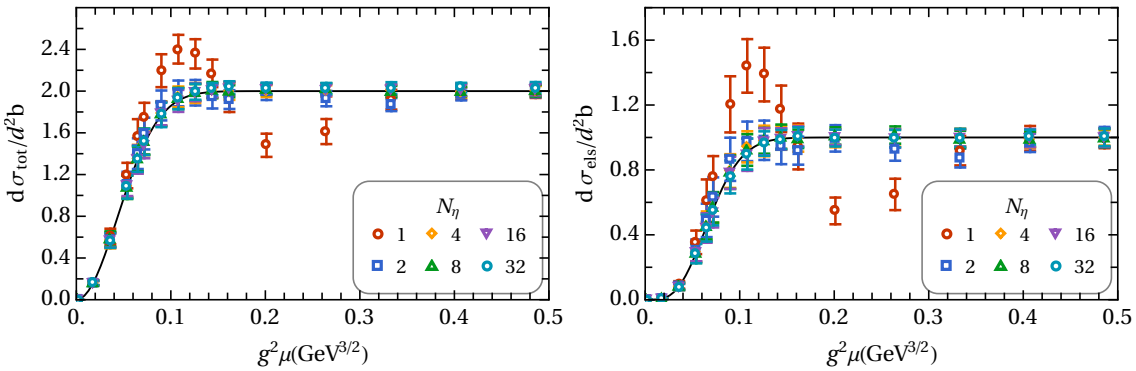

Figure 3.4 The dependence on N_η of the cross sections. Parameters for those results: $L = 50\ \text{GeV}^{-1}$, $N = 8$, $L_\eta = 50\ \text{GeV}^{-1}$ and $p^+ = \infty$. The left panel is the total cross section and the right panel is the elastic cross section. The solid lines are the eikonal predictions as calculated from Eqs. (3.50) and (3.55). Each data point is averaged over 100 configurations, and the standard deviation is taken as the uncertainty.

Another dependence of the cross sections comes from the IR cutoff $\Lambda_{IR} = m_g$. Fig. 3.5 presents the cross sections evaluated at different m_g on the same grid. These m_g values are covered by the grid range (see Eq. (3.56) and the associated discussion), and the cross sections agree well with the analytical eikonal expectation. Though not shown in the figure, we found that when the m_g value falls out of the accessible range of the grid, the results would start to deviate from the expectations.

We have seen that the cross sections in the eikonal limit agree with the analytical expectations. We now relax the condition to have finite p^+ and see if this could affect the cross section. Fig. 3.6 presents the cross sections at different p^+ values. It turns out that even for very small p^+, the cross section does not show noticeable differences from the $p^+ = \infty$ case.

We have seen that the calculated cross sections from tBLFQ agree well with the analytical eikonal expectations in the eikonal limit. Our results also show good numerical convergences on the various parameters. We did not observe noticeable differences by relaxing the eikonal condition. To study differences from the eikonal limit, we will investigate other observables that depend on additional kinematic variables in the following.

www.manaraa.com

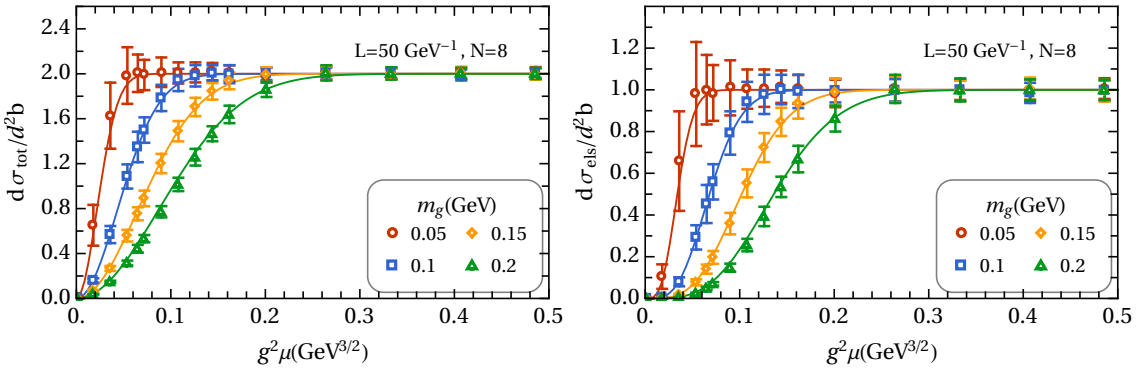

Figure 3.5 The dependence of the cross sections on m_g. Parameters for those panels are: $N = 8$,$L = 50$ GeV^{-1}, $L_\eta = 50$ GeV^{-1}, $N_\eta = 4$ and $p^+ = \infty$. The transverse grid parameters introduce a numerical IR cutoff $\lambda_{IR} = \pi/L \approx 0.06$ GeV and UV cutoff $\lambda_{UV} = N\pi/L \approx 0.5$ GeV to the momentum space. The physical IR cutoff m_g should be inside the numerical range to obtain a valid result. The solid lines are the eikonal predictions as calculated from Eqs. (3.50) and (3.55). Each data point is averaged over 100 configurations, and the standard deviation is taken as the uncertainty.

3.3.2 The differential cross section

The differential cross section $\mathrm{d}\sigma/(\mathrm{d}^2b\,\mathrm{d}^2p_\perp)$ is also of great interest to study. The $p + A \to h + X$ cross section can be obtained by convoluting the total qA cross section with the distribution function of the quark in the proton at factorization scales.

In Fig. 3.7, we present the tBLFQ calculations and compare with perturbative approximations. For a weaker field, the leading order and next-to-leading order perturbations agree with our results. For stronger fields and at small-$p_\perp$ region, the perturbation approximation breaks down, whereas our results provide a non-perturbative prediction.

We also check the dependence of the differential cross section on the grid parameters, N and L. Like the total and the elastic cross sections, the dependence is not noticeable for grids covering the physical range. The result is also not sensitive to the longitudinal resolution, N_η, as in Fig. 3.8. Unlike the cross sections, no "oscillation" pattern appears even at $N_\eta = 1$.

www.manaraa.com

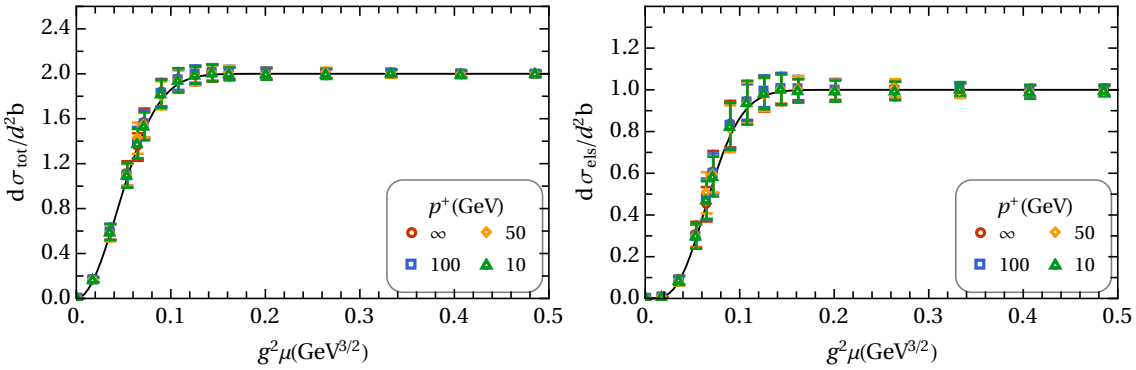

Figure 3.6 The dependence on p^+ of the cross sections at $L = 50\ \text{GeV}^{-1}$ and $N = 18$. The cross sections of the quark as functions of $g^2\mu$ for $L_\eta = 50\ \text{GeV}^{-1}$ with $N_\eta = 4$. The solid lines are the eikonal predictions ($p^+ = \infty$). Results for each data point are averaged over 100 configurations, and the standard deviation is taken as the uncertainty bar.

3.3.3 The evolution of the quark state

By carrying out the explicit time-evolution of the quark, we are able to access the intermediate states and investigate the process of the quark-nucleus scattering. In particular, we study how the quark evolves in two regimes, the transverse coordinate space and the color space.

To explore how the quark state evolves in the transverse coordinate space, we let the initial state of the quark be a Gaussian packet $Ce^{-|\vec{r}_\perp|^2/(0.2R_0)^2}$, where $R_0 = 50\ \text{GeV}^{-1} = 9.87$ fm and C is the normalization coefficient. Snapshots of the quark's transverse coordinate distribution at a sequence of light-front times are presented in Fig. 3.9. In the eikonal limit, i.e. $p^+ = \infty$, the quark does not change its transverse location. But with finite values of p^+, the quark admits changes in its transverse coordinate distribution. In the plot of a single event as of Fig. 3.9(b), the quark dissipates with a random pattern, which is related to the randomly generated field. In the plot of averaged event as of Fig. 3.9(c), the quark spreads out more evenly, as expected by averaging the field configurations.

We know that even without an external field, the quark should dissipate in the coordinate space with a finite p^+. Figure. 3.10 shows the evolution of the quark's transverse coordinate distribution when no external field exists. The quark spreads out slower with a more isotropic pattern compared with cases

www.manaraa.com

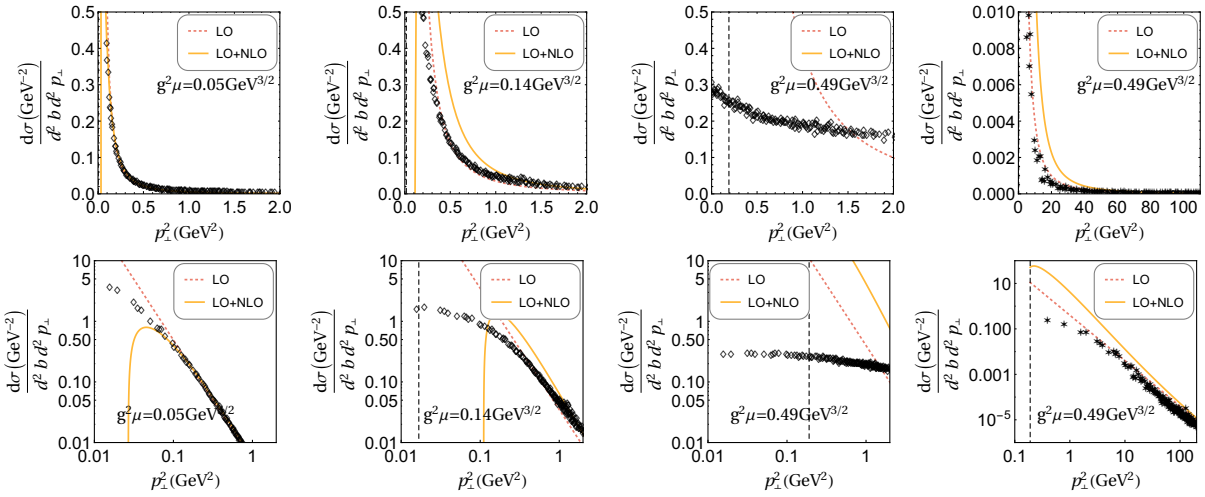

Figure 3.7 The differential cross section of the qA scattering at different $g^2\mu$. The tBLFQ results are plotted as empty diamonds. The presented data are averaged over 50 events. Parameters for those panels, $N = 18$, $L = 50\ \mathrm{GeV}^{-1}$, $m_g = 0.1\ \mathrm{GeV}$, $L_\eta = 50\ \mathrm{GeV}^{-1}$ and $N_\eta = 4$. $g^2\mu = 0.05, 0.14, 0.49\ \mathrm{GeV}^{3/2}$ for the first three panels from left to right. The fourth panel presents the results calculated at the same $g^2\mu = 0.49\ \mathrm{GeV}^{3/2}$ as in the third panel, but it is evaluated on the lattice of $N = 18$, $L = 5\ \mathrm{GeV}^{-1}$ to reveal the large $p_\perp^2$ range. The top panels are plotted on a linear scale, and the bottom panels are on log-log scales. The vertical dashed line is at the saturation scale $Q_s^2 = (g^2\mu)^2 L_\eta/(2\pi^2)$. LO (NLO) is the leading (next-to leading) order expansion on $Q_s^2/p_\perp^2$.

where the external field participates. To study the effect of the external field quantitatively, we calculate the expectation value of the quark's transverse coordinate $|\vec{r}_\perp|$ in cases with and without external fields.

We first show how the energy scale of the quark, p^+, affects the evolution. Fig. 3.11 presents the expectation value of the quark's transverse coordinate as a function of light-front time at various p^+. It shows that the CGC field promotes the quark's dissipation in the transverse plane compared with the no-field case ($g^2\mu = 0$). The quark spreads faster with smaller p^+.

We also check the sensitivity of the quark's evolution to grid parameters. Results at different lattice size L with a fixed lattice spacing of $a = L/N = 5\ \mathrm{GeV}^{-1} = 0.99$ fm are compared in Fig. 3.12. We find that the evolution is not very sensitive to the lattice size over the range investigated here.

We study the dependence on the grid number N in Fig. 3.13. When the external field is absent or weak, the evolution of $|r_\perp|$ agrees among cases with different N. However, with a strong external field, the

www.manaraa.com

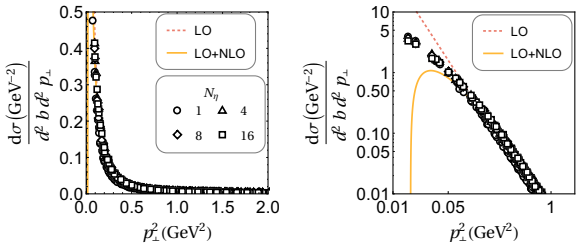

Figure 3.8 The differential cross section of the qA scattering with different N_η. The presented data are averaged over 50 events. Parameters for those panels: $N = 18$, $L = 50$ GeV^{-1}, $m_g = 0.1$ GeV, $L_\eta = 50$ GeV^{-1} and $g^2\mu = 0.05$ GeV$^{3/2}$. The left panel is plotted on a linear scale, and the right panel is on log-log scales. The vertical dashed line is at the saturation scale $Q_s^2 = (g^2\mu)^2 L_\eta/(2\pi^2) \approx 0.006\,\text{GeV}^2$. LO (NLO) is the leading (next-to leading) order expansion on $Q_s^2/p_\perp^2$.

evolution of $|r_\perp|$ diverges, as seen in Fig. 3.13(a). This divergence is expected from the ultraviolet divergent gluon field, as discussed in text associated with Eq. (3.17). We verify this source of divergence by imposing a UV cutoff on the gluon field. The results become better converged with the UV cutoff, as presented in Fig. 3.13(b).

The quark admits changes in the transverse coordinate at finite p^+, and this is achieved through the phase factor $e^{\pm i\frac{1}{2}p^- x^+}$ with $p^- = (\vec{p}_\perp^2 + m_q^2)/p^+$. One may then expect that using different values of the quark mass might also affect this effect. We show that the influence from the quark mass is very small by testing with $m_q = 0.05, 0.15, 0.3$ and 4.5 GeV in Fig. 3.14.

In the color space, the quark evolves toward a uniformly distributed state, $|\psi_c|^2 \to 1/3, (c = 1, 2, 3)$. This is shown in Fig. 3.15. The quark evolves faster in the color space with larger $g^2\mu$. This is expected since the background field generated from the source with a larger $g^2\mu$ is also stronger, therefore applies more influence to the quark.

3.3.4 The profiled CGC field

The CGC field we adopt so far is uniform in the transverse plane. In reality, the field generated from a large nucleus could be stronger at the center than on the perimeter. We take this into consideration by using a Gaussian profile and a Woods-Saxon profile to scale the CGC field in the transverse coordinate space. In

www.manaraa.com

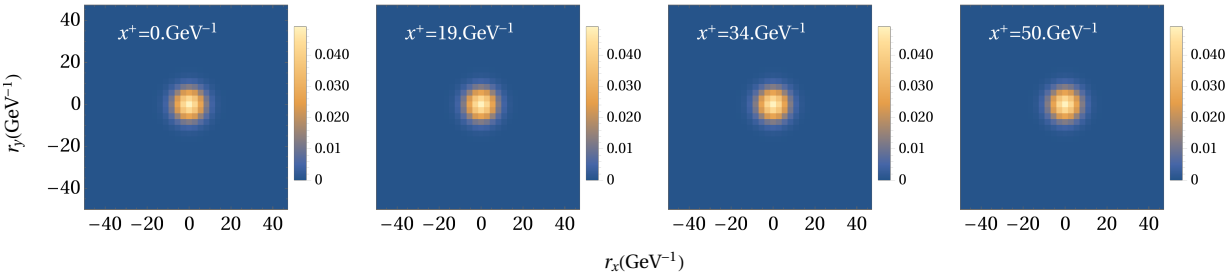

(a) Evolution of the quark's transverse coordinate distribution at $p^+ = \infty$

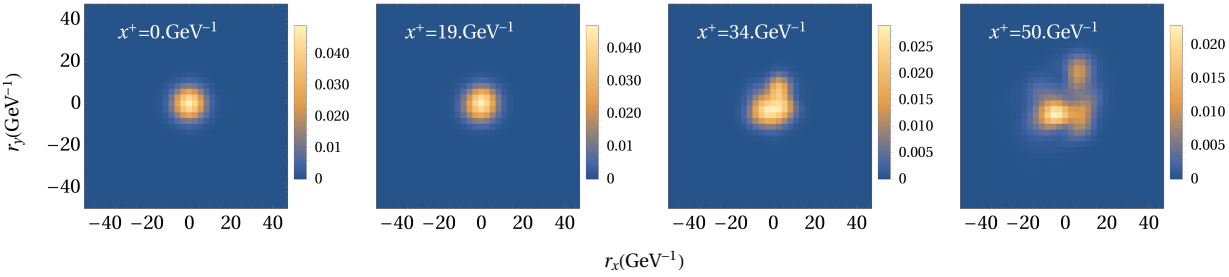

(b) Single event evolution of the quark's transverse coordinate distribution at $p^+ = 10\,\mathrm{GeV}$

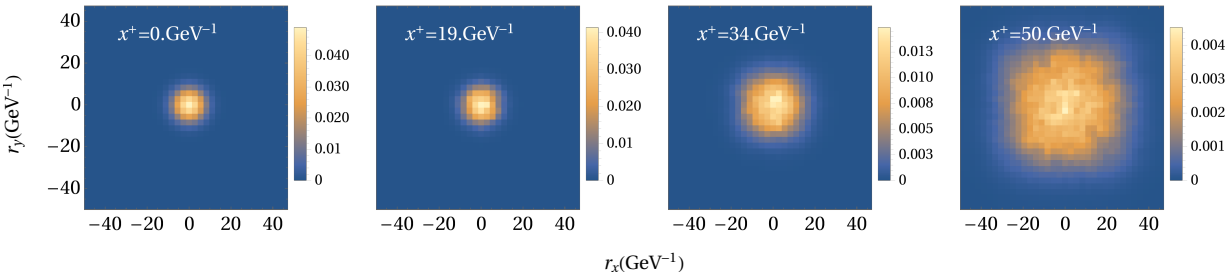

(c) Evolution of the quark's transverse coordinate distribution at $p^+ = 10\,\mathrm{GeV}$, averaged over 50 events

Figure 3.9 The evolution of the quark's transverse coordinate distribution. The initial state of the quark is distributed as $Ce^{-|\vec{r}_\perp|^2/(0.2L)^2}$, where C is the normalization coefficient. From left to right, the transverse coordinate distribution of the quark is shown at a sequential interaction time calculated by tBLFQ. Parameters in those panels: $L_\eta = 50\,\mathrm{GeV}^{-1}$, $N_\eta = 4$, $m_g = 0.1\,\mathrm{GeV}$, $N = 18$, $L = 50\mathrm{GeV}^{-1}$, $g^2\mu = 0.486\,\mathrm{GeV}^{-3/2}$. Top row: $p^+ = \infty$, bottom two rows: $p^+ = 10\,\mathrm{GeV}$. The second row shows the result of a single event. The third row shows the average result of 50 events.

www.manaraa.com

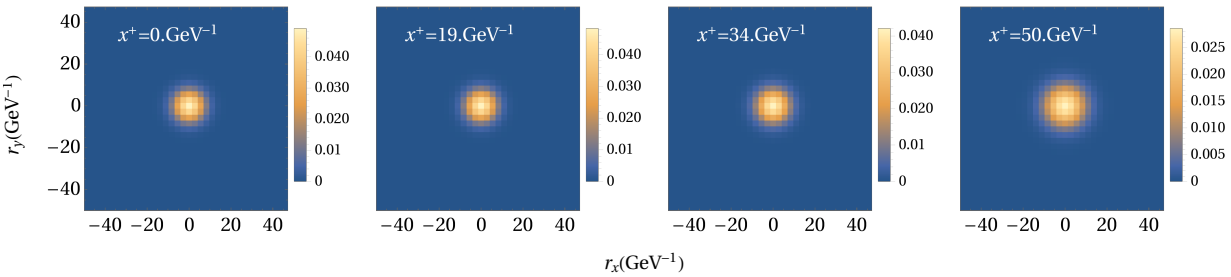

Figure 3.10 The evolution of the quark's transverse coordinate distribution when no source exists. The initial state of the quark is distributed as $Ce^{-|\vec{r}_\perp|^2/(0.2L)^2}$, where C is the normalization coefficient. From left to right, the transverse coordinate distributions of the quark are shown at a sequential interaction time calculated by tBLFQ. Parameters in those panels: $L_\eta = 50\,\mathrm{GeV}^{-1}$, $N_\eta = 4$, $m_g = 0.1\,\mathrm{GeV}$, $N = 18$, $L = 50\mathrm{GeV}^{-1}$, $p^+ = 10\,\mathrm{GeV}$.

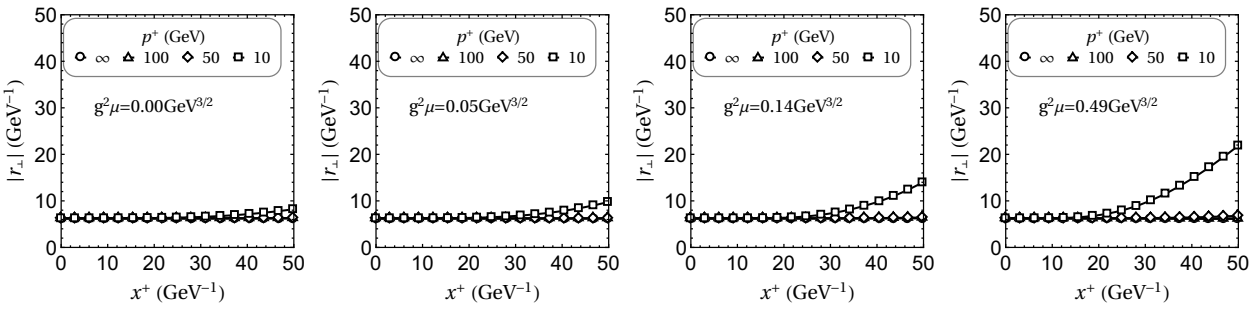

Figure 3.11 The evolution of the expectation value of the quark's transverse coordinate at different p^+. The initial state of the quark is distributed as $Ce^{-|\vec{r}_\perp|^2/(0.2L)^2}$, where C is the normalization coefficient. From left to right, the first panel is calculated without an external field while the following three panels are calculated with increasing color charge density $g^2\mu$. The results are averaged over 10 events. Parameters in those panels: $L_\eta = 50\mathrm{GeV}^{-1}$, $N_\eta = 4$, $m_g = 0.1\mathrm{GeV}$, $N = 18$, $L = 50\mathrm{GeV}^{-1}$.

www.manaraa.com

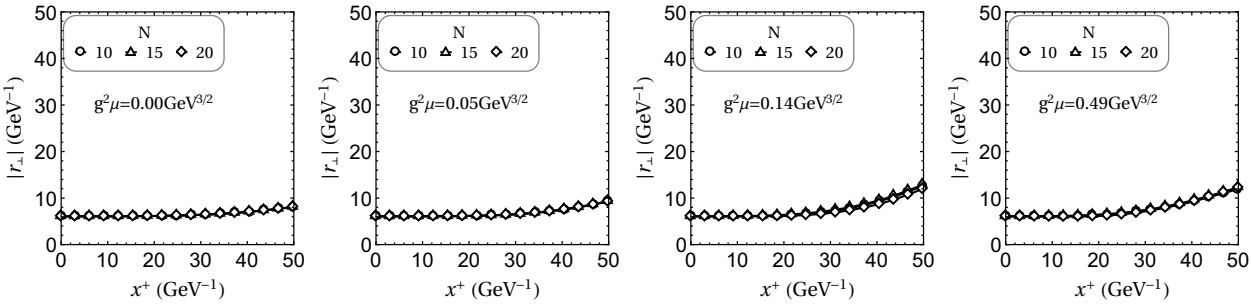

Figure 3.12 The evolution of the expectation value of the quark's transverse coordinate at different lattice size with a fixed lattice spacing of $a = L/N = 5\,\mathrm{GeV}^{-1}$. Parameters in those panels: $L_\eta = 50\mathrm{GeV}^{-1}$, $N_\eta = 4$, $m_g = 0.1\mathrm{GeV}$, $p^+ = 10\,\mathrm{GeV}$. The initial state of the quark is distributed as $Ce^{-|\vec{r}_\perp|^2/(0.2*50\,\mathrm{GeV}^{-1})^2}$, where C is the normalization coefficient. From left to right, the first panel is calculated without an external field while the following three panels are calculated with increasing color charge density $g^2\mu$. The results are averaged over 10 events.

the Gaussian form, the scale factor reads

$$f_{\text{Gaussian}}(\vec{r}_\perp) = e^{-(r_\perp/R_0)^2}\ , \tag{3.58}$$

where R_0 is taken as the nuclear radius. For the gold nucleus, $R_0 = 37\ \mathrm{GeV}^{-1}$. In the Woods-Saxon form, the scale factor reads

$$f_{\text{Woods-Saxon}}(\vec{r}_\perp) = \frac{1}{1 + e^{(r_\perp - R_0)/s}}\ . \tag{3.59}$$

We use the usual parametrization, where R_0 is taken as the nuclear radius and $s = 3.2\ \mathrm{GeV}^{-1}$ is the surface diffuseness [150]. An example of the source charge distribution in the transverse plane $\vec{r}_\perp$ with different transverse profiles is obtained by single event simulation, and is presented in Fig. 3.16.

We revisited the quark's evolution, the cross section and the $p_\perp$-dependent differential cross section in Figs. 3.17, 3.18 and 3.19. We see that there is not much difference in the total cross section and the evolution of $|r_\perp|$. The differential cross section is more peaked around $p_\perp = 0$ when the fields are scaled as may be expected due to reduced scattering in the peripheral regions.

www.manaraa.com

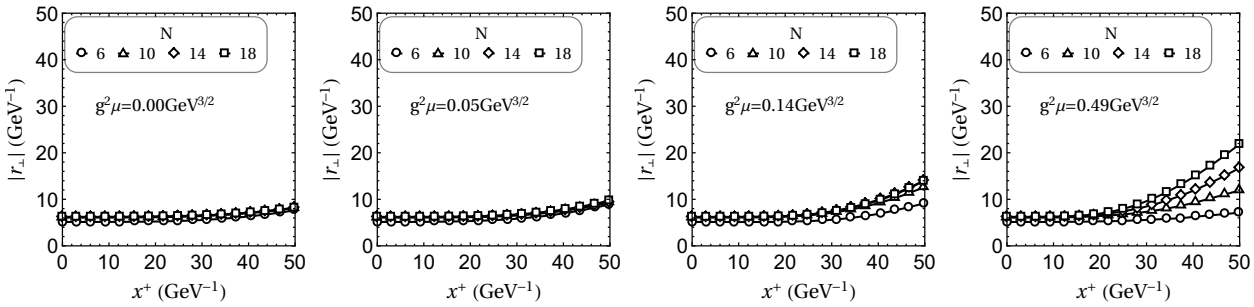

(a) $\Lambda_{UV} = \infty$

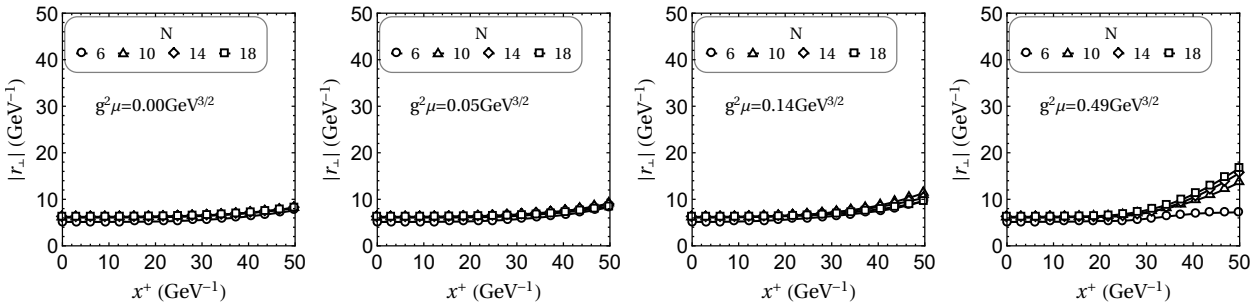

(b) $\Lambda_{UV} = 0.2$ GeV

Figure 3.13 The evolution of the expectation value of the quark's transverse coordinate at $L = 50\,\mathrm{GeV}^{-1}$. The initial state of the quark is $Ce^{-|\vec{r}_\perp|^2/(0.2L)^2}$, where C is the normalization coefficient. From left to right, the first panel is calculated without an external field while the following three panels are calculated with increasing color charge density $g^2\mu$. The results are averaged over 10 events. Parameters in those panels: $L_\eta = 50\mathrm{GeV}^{-1}$, $N_\eta = 4$, $m_g = 0.1\,\mathrm{GeV}$, $p^+ = 10\,\mathrm{GeV}$. In the bottom row, we impose a UV cutoff when solving the gluon field by setting $\tilde{A}(\vec{k}_\perp) = 0$ for $|\vec{k}_\perp| \geq \Lambda_{UV} = 0.2\,\mathrm{GeV}$.

www.manaraa.com

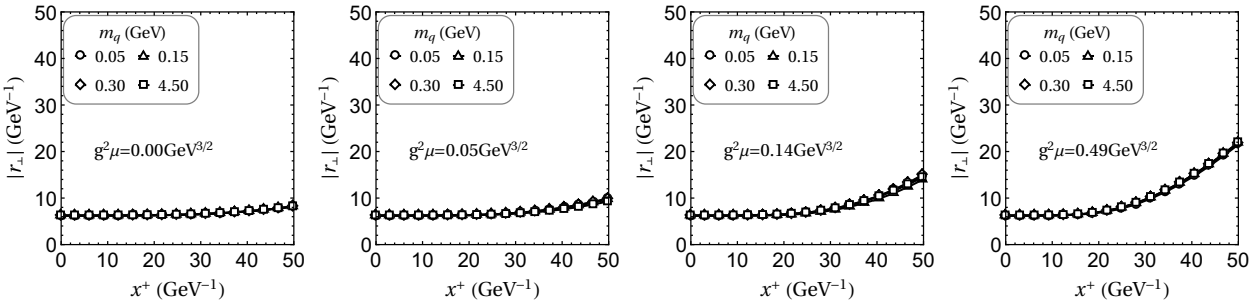

Figure 3.14 The evolution of the expectation value of the quark's transverse coordinate with different quark mass and charge densities. Parameters in those panels: $L = 50\ \mathrm{GeV}^{-1}$, $N = 18$, $L_\eta = 50\mathrm{GeV}^{-1}$, $N_\eta = 4$, $m_g = 0.1$ GeV, $p^+ = 10\,\mathrm{GeV}$. The initial state of the quark is distributed as $Ce^{-|\vec{r}_\perp|^2/(0.2*50\,\mathrm{GeV}^{-1})^2}$, where C is the normalization coefficient. From left to right, the first panel is calculated without an external field while the following three panels are calculated with increasing color charge density $g^2\mu$. The results are averaged over 10 events.

3.4 Conclusions and outlook

In this Chapter, we have made the first attempt of the tBFLQ approach to a QCD problem, the quark-nucleus scattering. We are able to access the wavefunction of the quark at any intermediate time during the evolution. This provides us with an opportunity to carry out detailed studies of the time-dependent process.

Our results of the total and cross sections are in good agreement with the analytical expectations under the eikonal condition $p^+ = \infty$. In the sub-eikonal case with a finite p^+, the cross sections do not show noticeable deviation from the eikonal limit. However, there are clear sub-eikonal effects shown from the distribution of the quark's transverse coordinate. At finite p^+, the quark admits changes in its transverse coordinate distribution.

We take the Color Glass Condensate model as the background field of the nucleus, and keep the dominant field component ($\mathcal{A}^-$) in our calculation. In the future, we expect to include the transverse component of the color field ($\mathcal{A}_\perp$) and investigate its effect on the spin of the quark. We also plan to extend the Fock space to $|q\rangle + |qg\rangle$ and study the gluon radiation.

We foresee more applications of the tBLFQ approach to scattering processes in the future, especially the dipole-nucleus scattering and meson productions in heavy-ion collisions.

www.manaraa.com

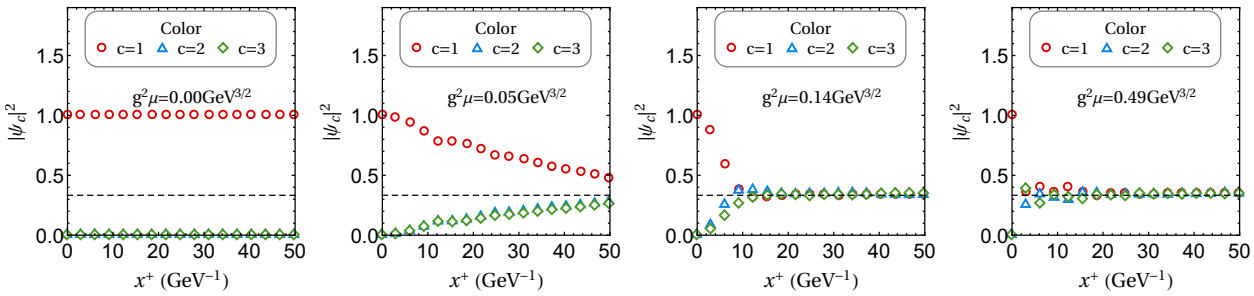

(a) Evolution of the quark's color distribution at $p^+ = \infty$

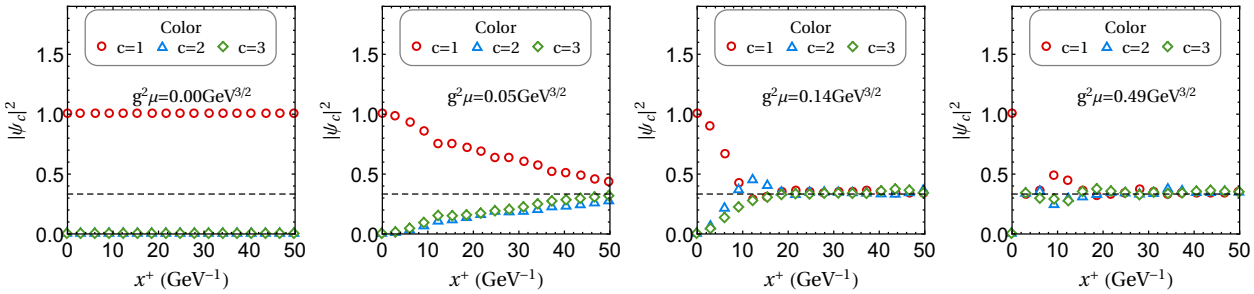

(b) Evolution of the quark's color distribution at $p^+ = 10\,\mathrm{GeV}$

Figure 3.15 The evolution of the quark's distribution in the color space. The results are averaged over 50 events. Parameters in those panels: $N = 18$, $L = 50\,\mathrm{GeV}^{-1}$, $L_\eta = 50\,\mathrm{GeV}^{-1}$, $N_\eta = 4$, $m_g = 0.1\,\mathrm{GeV}$. From left to right, the first panel is calculated without an external field while the following three panels are calculated with increasing color charge density $g^2\mu$. The top panels are results obtained in the eikonal limit ($p^+ = \infty$), the bottom row is obtained wtih $p^+ = 10\,\mathrm{GeV}$. The initial state of the quark is a single color state ($c = 1$) with space distribution as $Ce^{-|\vec{r}_\perp|^2/(0.2L)^2}$, where C is the normalization coefficient. The dashed line marks the average probability of the three colors: 0.33.

www.manaraa.com

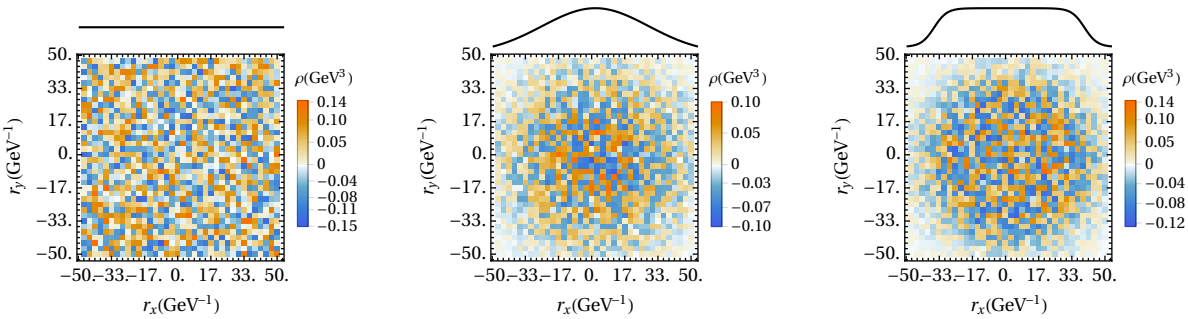

(a) Uniform profile (b) Gaussion profile (c) Woods-Saxon profile

Figure 3.16 Single-event simulation of source charges in the transverse plane $\vec{r}_\perp$ with different transverse profiles. From left to right, the corresponding profiles are uniform, Gaussion and Woods-Saxon. See Eqs. (3.58) and (3.59) and associated text for more information. Parameters in those panels: $N = 18$, $L = 50\,\mathrm{GeV}^{-1}$, $L_\eta = 50\ \mathrm{GeV}^{-1}$ and $g^2\mu = 0.14\ \mathrm{GeV}^{3/2}$.

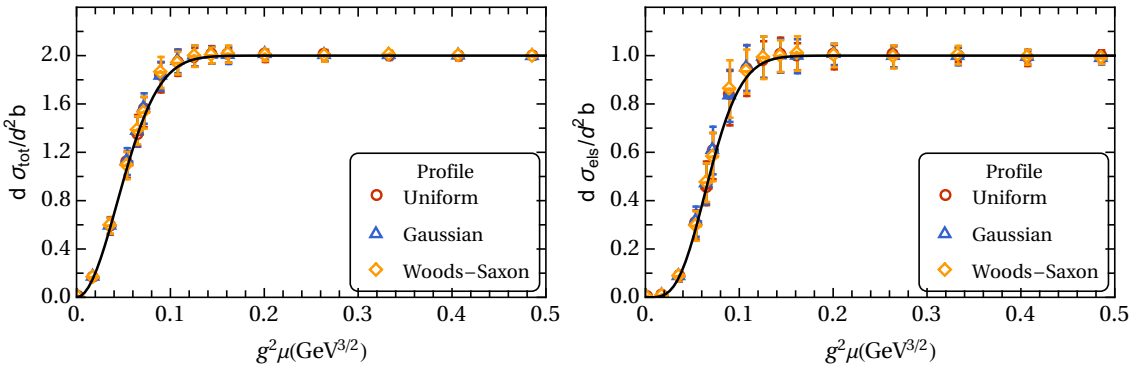

Figure 3.17 The total and elastic cross sections at the CGC fields with different profiles. the initial state of the quark as $\vec{p}_\perp = \vec{0}_\perp$. The results are averaged over 100 events. Parameters in those panels: $N = 18$, $L = 50\,\mathrm{GeV}^{-1}$, $L_\eta = 50\ \mathrm{GeV}^{-1}$, $N_\eta = 4$, $m_g = 0.1\mathrm{GeV}$, $p^+ = 10\mathrm{GeV}$.

www.manaraa.com

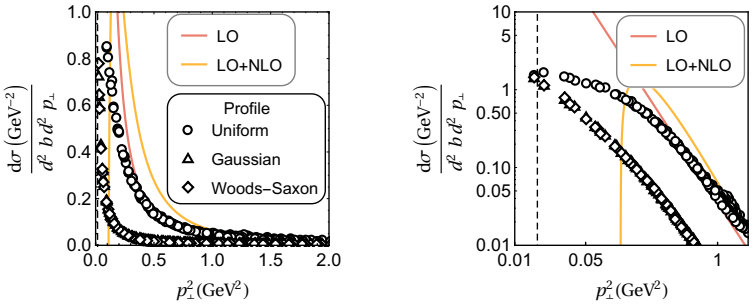

Figure 3.18 The differential cross sections at the CGC fields with different profiles. The initial state of the quark is $\vec{p}_\perp = \vec{0}_\perp$. The results are averaged over 100 events. Parameters in those panels: $N = 18$, $L = 50\,\mathrm{GeV}^{-1}$, $L_\eta = 50\ \mathrm{GeV}^{-1}$, $N_\eta = 4$, $m_g = 0.1\mathrm{GeV}$, $p^+ = 10\mathrm{GeV}$, and $g^2\mu = 0.14\ \mathrm{GeV}^{3/2}$.

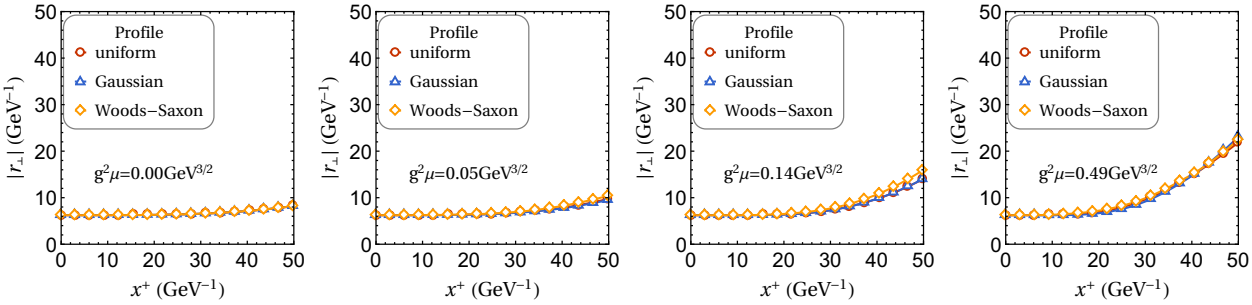

Figure 3.19 The evolution of the expectation value of the quark's transverse coordinate at different profiles. The initial state of the quark is $Ce^{-|\vec{r}_\perp|^2/(0.2L)^2}$, where C is the normalization coefficient. The results are averaged over 100 events. Parameters in those panels: $N = 18$, $L = 50\,\mathrm{GeV}^{-1}$, $L_\eta = 50\ \mathrm{GeV}^{-1}$, $N_\eta = 4$, $m_g = 0.1\mathrm{GeV}$, $p^+ = 10\mathrm{GeV}$.

www.manaraa.com

CHAPTER 4. SUMMARY AND OUTLOOK

In this thesis, we have investigated quantum chromodynamics in the non-perturbative regime with the light-front Hamiltonian formalism. Our explorations are from two aspects, the hadron bound states and the high energy scattering.

We have reviewed the formalism of solving the quarkonium system with the effective Hamiltonian approach and discussed how one could extend the calculation from the valence Fock sector to higher Fock space. We then studied the properties of the quarkonium through electromagnetic processes, via the elastic form factors, the radiative transition form factors and the decay widths. In light-front dynamics, the electromagnetic transition amplitudes between mesons are usually computed with the "+" current and in the Drell-Yan frame for simplicity. Though in principle, calculations of the Lorentz invariant form factors should not depend on the choice of current components or reference frames, practical calculations could receive such spurious dependence when rotational symmetry is broken by Fock space truncation. We were therefore motivated to make a complete study by analyzing all four current components, with all possible magnetic projections of the states, and in a general reference frame. Based on our analysis, we made suggestions on choosing the preferred currents and frames in calculating the elastic form factor, the M1 transition form factor, and the decay constants. We also carried out numerical calculations of those quantities with light-front wavefunctions calculated from the valence Fock sector and compared with experimental data and other theoretical calculations. The formalism of our investigations could also apply to light mesons and can be extended to baryons.

The scattering of a light projectile, proton or electron with large nuclei helps us understand QCD dynamics from a dynamical viewpoint. Intrigued by the strong interaction between the fast quarks and the nucleus, we studied the process of a quark jet scattering off a nuclear field. We treat the nuclear field as a background using the Color Glass Condensate model. We carry out an explicit evolution for the quark by decomposing the time-evolution operator into small time increments. In this way, we calculate the cross

www.manaraa.com

section, and moreover, we get access to the intermediate states and witness the dynamical processes such as color rotation and momentum transfer. By relaxing the longitudinal momentum of the quark to finite values, we also revealed the sub-eikonal effect on the quark's transverse location. The framework in this study also shows exciting possibilities for future applications of time-dependent approaches in the non-perturbative quantum field theory.

The two studies in this thesis together investigate the non-perturbative quantum field theory on the light front. We foresee future developments in two directions. The first direction is to include higher Fock sectors in our calculations. We have outlined the framework of solving the heavy quarkonium system in the $|q\bar{q}\rangle$ + $|q\bar{q}q\bar{q}\rangle$ sectors with the BLFQ approach. Its realization will not only result in more realistic representations of quantum states, but also allow for a more complete treatment of a variety of processes, especially the radiative transition and the strong decay. For the quark-nucleus scattering, inclusion of higher Fock sectors such as the $|qg\rangle$ sector would allow us study the gluon emission from the non-perturbative aspect. The second direction is to extend the range of applications. Following the initial efforts on positronium and heavy quarkonium, the works on heavy-light mesons, light mesons, baryons and glueballs are underway. We also hope to apply the time-dependent light-front Hamiltonian approach to address strong scattering problems such as the dipole-nucleus scattering and particle production in the fields of two colliding nuclei.

www.manaraa.com

BIBLIOGRAPHY

[1] J. P. Vary, H. Honkanen, Jun Li, P. Maris, S. J. Brodsky, A. Harindranath, G. F. de Teramond, P. Sternberg, E. G. Ng, and C. Yang. Hamiltonian light-front field theory in a basis function approach. *Phys. Rev.*, C81:035205, 2010.

[2] M. Tanabashi et al. Review of Particle Physics. *Phys. Rev.*, D98(3):030001, 2018.

[3] Yang Li, Pieter Maris, and James P. Vary. Quarkonium as a relativistic bound state on the light front. *Phys. Rev.*, D96(1):016022, 2017.

[4] C. Patrignani et al. Review of Particle Physics. *Chin. Phys.*, C40(10):100001, 2016.

[5] Randy Lewis and R. M. Woloshyn. More about excited bottomonium radiative decays. *Phys. Rev.*, D86:057501, 2012.

[6] D. Ebert, R. N. Faustov, and V. O. Galkin. Properties of heavy quarkonia and B_c mesons in the relativistic quark model. *Phys. Rev.*, D67:014027, 2003.

[7] T. Barnes, S. Godfrey, and E. S. Swanson. Higher charmonia. *Phys. Rev.*, D72:054026, 2005.

[8] Stephen Godfrey and Kenneth Moats. Bottomonium Mesons and Strategies for their Observation. *Phys. Rev.*, D92(5):054034, 2015.

[9] Meijian Li, Yang Li, Pieter Maris, and James P. Vary. Radiative transitions between 0^{-+} and 1^{--} heavy quarkonia on the light front. *Phys. Rev.*, D98(3):034024, 2018.

[10] Meijian Li, Yang Li, Pieter Maris, and James P. Vary. Frame dependence of transition form factors in light-front dynamics. 2019.

[11] Jozef J. Dudek, Robert Edwards, and Christopher E. Thomas. Exotic and excited-state radiative transitions in charmonium from lattice QCD. *Phys. Rev.*, D79:094504, 2009.

[12] Damir Bečirević and Francesco Sanfilippo. Lattice QCD study of the radiative decays $J/\psi \to \eta_c\gamma$ and $h_c \to \eta_c\gamma$. *JHEP*, 01:028, 2013.

[13] Damir Bečirević, Michael Kruse, and Francesco Sanfilippo. Lattice QCD estimate of the $\eta_c(2S) \to J/\psi\gamma$ decay rate. *JHEP*, 05:014, 2015.

[14] G. C. Donald, C. T. H. Davies, R. J. Dowdall, E. Follana, K. Hornbostel, J. Koponen, G. P. Lepage, and C. McNeile. Precision tests of the J/ψ from full lattice QCD: mass, leptonic width and radiative decay rate to η_c. *Phys. Rev.*, D86:094501, 2012.

[15] Ciaran Hughes, Rachel J. Dowdall, Christine T. H. Davies, Ronald R. Horgan, Georg von Hippel, and Matthew Wingate. Hindered M1 Radiative Decay of $\Upsilon(2S)$ from Lattice NRQCD. *Phys. Rev.*, D92:094501, 2015.

www.manaraa.com

[16] A. Zee. *Quantum field theory in a nutshell*. 2003.

[17] D. Ebert, H. Reinhardt, and M. K. Volkov. Effective hadron theory of QCD. *Prog. Part. Nucl. Phys.*, 33:1–120, 1994.

[18] L. J. Reinders, H. Rubinstein, and S. Yazaki. Hadron Properties from QCD Sum Rules. *Phys. Rept.*, 127:1, 1985.

[19] Kenneth G. Wilson. Confinement of Quarks. *Phys. Rev.*, D10:2445–2459, 1974. [,319(1974)].

[20] C. T. H. Davies et al. High precision lattice QCD confronts experiment. *Phys. Rev. Lett.*, 92:022001, 2004.

[21] F. J. Dyson. The S matrix in quantum electrodynamics. *Phys. Rev.*, 75:1736–1755, 1949.

[22] Julian S. Schwinger. On the Green's functions of quantized fields. 1. *Proc. Nat. Acad. Sci.*, 37:452–455, 1951.

[23] Craig D. Roberts and Anthony G. Williams. Dyson-Schwinger equations and their application to hadronic physics. *Prog. Part. Nucl. Phys.*, 33:477–575, 1994.

[24] Reinhard Alkofer and Lorenz von Smekal. The Infrared behavior of QCD Green's functions: Confinement dynamical symmetry breaking, and hadrons as relativistic bound states. *Phys. Rept.*, 353:281, 2001.

[25] Pieter Maris and Craig D. Roberts. Dyson-Schwinger equations: A Tool for hadron physics. *Int. J. Mod. Phys.*, E12:297–365, 2003.

[26] Steven Weinberg. *The Quantum theory of fields. Vol. 1: Foundations*. Cambridge University Press, 2005.

[27] Alberto Candel. *Foliations / Alberto Candel, Lawrence Conlon.* Graduate studies in mathematics v. 23, 60. American Mathematical Society, Providence, R.I., 2000.

[28] Paul A. M. Dirac. Forms of Relativistic Dynamics. *Rev. Mod. Phys.*, 21:392–399, 1949.

[29] Elmar P. Biernat, Wolfgang Schweiger, Kajetan Fuchsberger, and William H. Klink. Electromagnetic meson form factor from a relativistic coupled-channel approach. *Phys. Rev.*, C79:055203, 2009.

[30] Elmar P. Biernat, William H. Klink, and Wolfgang Schweiger. Point-Form Hamiltonian Dynamics and Applications. *Few Body Syst.*, 49:149–161, 2011.

[31] Maria Gomez-Rocha and Wolfgang Schweiger. Electroweak form factors of heavy-light mesons: A relativistic point-form approach. *Phys. Rev.*, D86:053010, 2012.

[32] T. Heinzl. Light cone quantization: Foundations and applications. *Lect. Notes Phys.*, 572:55–142, 2001.

[33] Stanley J. Brodsky, Hans-Christian Pauli, and Stephen S. Pinsky. Quantum chromodynamics and other field theories on the light cone. *Phys. Rept.*, 301:299–486, 1998.

www.manaraa.com

[34] Michael E. Peskin and Daniel V. Schroeder. *An Introduction to quantum field theory*. Addison-Wesley, Reading, USA, 1995.

[35] George Leibbrandt. The Light Cone Gauge in Yang-Mills Theory. *Phys. Rev.*, D29:1699, 1984.

[36] Prem P. Srivastava and Stanley J. Brodsky. Light front quantized QCD in light cone gauge. *Phys. Rev.*, D64:045006, 2001.

[37] Xingbo Zhao, Anton Ilderton, Pieter Maris, and James P. Vary. Scattering in Time-Dependent Basis Light-Front Quantization. *Phys. Rev.*, D88:065014, 2013.

[38] Guangyao Chen, Xingbo Zhao, Yang Li, Kirill Tuchin, and James P. Vary. Particle distribution in intense fields in a light-front Hamiltonian approach. *Phys. Rev.*, D95(9):096012, 2017.

[39] S. Dalley. Transverse lattice. *Nucl. Phys. Proc. Suppl.*, 90:227–232, 2000. [,227(2000)].

[40] Stanislaw D. Glazek. Running couplings in Hamiltonians. *Acta Phys. Polon.*, B31:909–930, 2000.

[41] I. Tamm. Relativistic interaction of elementary particles. *J. Phys.(USSR)*, 9:449, 1945.

[42] S. M. Dancoff. Nonadiabatic meson theory of nuclear forces. *Phys. Rev.*, 78:382–385, 1950.

[43] Hans Christian Pauli and Stanley J. Brodsky. Solving Field Theory in One Space One Time Dimension. *Phys. Rev.*, D32:1993, 1985.

[44] J. R. Hiller. Calculations with DLCQ. *Nucl. Phys. Proc. Suppl.*, 90:170–174, 2000. [,170(2000)].

[45] Paul Wiecki, Yang Li, Xingbo Zhao, Pieter Maris, and James P. Vary. Basis Light-Front Quantization Approach to Positronium. *Phys. Rev.*, D91(10):105009, 2015.

[46] Xingbo Zhao, Heli Honkanen, Pieter Maris, James P. Vary, and Stanley J. Brodsky. Electron g-2 in Light-Front Quantization. *Phys. Lett.*, B737:65–69, 2014.

[47] Lekha Adhikari, Yang Li, Xingbo Zhao, Pieter Maris, James P. Vary, and Alaa Abd El-Hady. Form Factors and Generalized Parton Distributions in Basis Light-Front Quantization. *Phys. Rev.*, C93(5):055202, 2016.

[48] Yang Li, Pieter Maris, Xingbo Zhao, and James P. Vary. Heavy Quarkonium in a Holographic Basis. *Phys. Lett.*, B758:118–124, 2016.

[49] Shuo Tang, Yang Li, Pieter Maris, and James P. Vary. B_c mesons and their properties on the light front. *Phys. Rev.*, D98(11):114038, 2018.

[50] Shaoyang Jia and James P. Vary. Basis light front quantization for the charged light mesons with color singlet Nambu–Jona-Lasinio interactions. *Phys. Rev.*, C99(3):035206, 2019.

[51] James P. Vary et al. Trends and Progress in Nuclear and Hadron Physics: a straight or winding road. *Few Body Syst.*, 58(2):56, 2017.

[52] James P. Vary et al. Hadron Spectra, Decays and Scattering Properties Within Basis Light Front Quantization. *Few Body Syst.*, 59(4):56, 2018.

www.manaraa.com

[53] N. Brambilla et al. Heavy Quarkonium: Progress, Puzzles, and Opportunities. *Eur. Phys. J.*, C71:1534, 2011.

[54] Hans-Christian Pauli. On perturbation series for large coupling constants. *Nucl. Phys.*, A369:413–424, 1981.

[55] D. C. Zheng, J. P. Vary, and B. R. Barrett. Exact solutions of model Hamiltonian problems with effective interactions. *Nucl. Phys.*, A560:211–222, 1993.

[56] M. Krautgartner, H. C. Pauli, and F. Wolz. Positronium and heavy quarkonia as testing case for discretized light cone quantization. 1. *Phys. Rev.*, D45:3755–3774, 1992.

[57] Thomas Appelquist, R. Michael Barnett, and Kenneth D. Lane. Charm and Beyond. *Ann. Rev. Nucl. Part. Sci.*, 28:387–499, 1978.

[58] S. Godfrey and Nathan Isgur. Mesons in a Relativized Quark Model with Chromodynamics. *Phys. Rev.*, D32:189–231, 1985.

[59] Andrew C. Tang, Stanley J. Brodsky, and Hans Christian Pauli. Discretized light cone quantization: Formalism for quantum electrodynamics. *Phys. Rev.*, D44:1842–1865, 1991.

[60] David Griffiths. *Introduction to elementary particles*. 2008.

[61] Stanley J. Brodsky, Guy F. de Teramond, Hans Gunter Dosch, and Joshua Erlich. Light-Front Holographic QCD and Emerging Confinement. *Phys. Rept.*, 584:1–105, 2015.

[62] Andreas Karch, Emanuel Katz, Dam T. Son, and Mikhail A. Stephanov. Linear confinement and AdS/QCD. *Phys. Rev.*, D74:015005, 2006.

[63] Guangyao Chen, Yang Li, Pieter Maris, Kirill Tuchin, and James P. Vary. Diffractive charmonium spectrum in high energy collisions in the basis light-front quantization approach. *Phys. Lett.*, B769:477–484, 2017.

[64] Sofia Leitão, Yang Li, Pieter Maris, M. T. Peña, Alfred Stadler, James P. Vary, and Elmar P. Biernat. Comparison of two Minkowski-space approaches to heavy quarkonia. *Eur. Phys. J.*, C77(10):696, 2017.

[65] Yang Li, Pieter Maris, and James P. Vary. Frame dependence of form factors in light-front dynamics. *Phys. Rev.*, D97:054034, Mar 2018.

[66] Lekha Adhikari, Yang Li, Meijian Li, and James P. Vary. Form factors and generalized parton distributions of heavy quarkonia in basis light front quantization. *Phys. Rev.*, C99(3):035208, 2019.

[67] Guangyao Chen, Yang Li, Kirill Tuchin, and James Vary. Heavy quarkonia production at LHC and EIC using Basis Light-Front Quantization wavefunctions. *to be published*, 2018.

[68] Stanley J. Brodsky and Guy F. de Teramond. Ads/qcd, light-front holography, and sublimated gluons, 2011.

[69] Woosung Park and Su Houng Lee. Color spin wave functions of heavy tetraquark states. *Nucl. Phys.*, A925:161–184, 2014.

www.manaraa.com

[70] J. Carbonell, B. Desplanques, V. A. Karmanov, and J. F. Mathiot. Explicitly covariant light front dynamics and relativistic few body systems. *Phys. Rept.*, 300:215–347, 1998.

[71] J. P. B. C de Melo, J. H. O. Sales, T. Frederico, and P. U. Sauer. Pairs in the light front and covariance. *Nucl. Phys.*, A631:574C–579C, 1998.

[72] Stanley J. Brodsky and Dae Sung Hwang. Exact light cone wave function representation of matrix elements of electroweak currents. *Nucl. Phys.*, B543:239–252, 1999.

[73] Dmitri Melikhov and Silvano Simula. Electromagnetic form-factors in the light front formalism and the Feynman triangle diagram: Spin 0 and spin 1 two fermion systems. *Phys. Rev.*, D65:094043, 2002.

[74] Silvano Simula. Comparison among Hamiltonian light front formalisms at $q^+ = 0$ and q^+ not equal to 0: Space - like elastic form-factors of pseudoscalar and vector mesons. *Phys. Rev.*, C66:035201, 2002.

[75] Alfredo Takashi Suzuki, Jorge Henrique Sales, and Luis Alberto Soriano. Zero Mode Effect Generalization for the Electromagnetic Current in the Light Front. *Phys. Rev.*, D88(2):025036, 2013.

[76] Dmitri Melikhov. Form-factors of meson decays in the relativistic constituent quark model. *Phys. Rev.*, D53:2460–2479, 1996.

[77] Wolfgang Jaus. Semileptonic, radiative, and pionic decays of B, B* and D, D* mesons. *Phys. Rev.*, D53:1349, 1996. [Erratum: Phys. Rev.D54,5904(1996)].

[78] Bernard L. G. Bakker, Ho-Meoyng Choi, and Chueng-Ryong Ji. Transition form-factors between pseudoscalar and vector mesons in light front dynamics. *Phys. Rev.*, D67:113007, 2003.

[79] Nathan Isgur and C. H. Llewellyn Smith. The Applicability of Perturbative QCD to Exclusive Processes. *Nucl. Phys.*, B317:526–572, 1989.

[80] Mikolaj Sawicki. Soft charge form-factor of the pion. *Phys. Rev.*, D46:474–477, 1992.

[81] M. Burkardt. The Virial Theorem and the Structure of the Deuteron in (1+1)-dimensional QCD on the Light Cone. *Nucl. Phys.*, A504:762–776, 1989.

[82] J. A. O. Marinho, T. Frederico, and P. U. Sauer. Light-front Ward-Takahashi identity and current conservation. *Phys. Rev.*, D76:096001, 2007.

[83] J. A. O. Marinho, T. Frederico, E. Pace, G. Salme, and P. Sauer. Light-front Ward-Takahashi Identity for Two-Fermion Systems. *Phys. Rev.*, D77:116010, 2008.

[84] Ho-Meoyng Choi, Hui-Young Ryu, and Chueng-Ryong Ji. Doubly virtual $(\pi^0, \eta, \eta') \to \gamma^*\gamma^*$ transition form factors in the light-front quark model. *Phys. Rev.*, D99(7):076012, 2019.

[85] Stanley J. Brodsky, Ralph Roskies, and Roberto Suaya. Quantum Electrodynamics and Renormalization Theory in the Infinite Momentum Frame. *Phys. Rev.*, D8:4574, 1973.

[86] Stanley J. Brodsky and S. D. Drell. The Anomalous Magnetic Moment and Limits on Fermion Substructure. *Phys. Rev.*, D22:2236, 1980.

www.manaraa.com

[87] Marco A. Bedolla, J. J. Cobos-Martínez, and Adnan Bashir. Charmonia in a contact interaction. *Phys. Rev.*, D92(5):054031, 2015.

[88] Marco A. Bedolla, Khépani Raya, J. J. Cobos-Martínez, and Adnan Bashir. η_c elastic and transition form factors: Contact interaction and algebraic model. *Phys. Rev.*, D93(9):094025, 2016.

[89] Khepani Raya, Marco A. Bedolla, J. J. Cobos-Martínez, and Adnan Bashir. Heavy quarkonia in a contact interaction and an algebraic model: mass spectrum, decay constants, charge radii and elastic and transition form factors. *Few Body Syst.*, 59(6):133, 2018.

[90] Jozef J. Dudek, Robert G. Edwards, and David G. Richards. Radiative transitions in charmonium from lattice QCD. *Phys. Rev.*, D73:074507, 2006.

[91] Pieter Maris. Hadron Physics and the Dyson-Schwinger Equations of QCD. *AIP Conf. Proc.*, 892(1):65–71, 2007.

[92] M. S. Bhagwat and P. Maris. Vector meson form factors and their quark-mass dependence. *Phys. Rev.*, C77:025203, 2008.

[93] B. D. Keister and W. N. Polyzou. Relativistic Hamiltonian dynamics in nuclear and particle physics. *Adv. Nucl. Phys.*, 20:225–479, 1991. [,225(1991)].

[94] J. P. B. C de Melo and T. Frederico. Covariant and light front approaches to the rho meson electromagnetic form-factors. *Phys. Rev.*, C55:2043, 1997.

[95] J. M. Namyslowski. LIGHT CONE PERTURBATION THEORY AND ITS APPLICATION TO DIFFERENT FIELDS. *Prog. Part. Nucl. Phys.*, 14:49–104, 1985.

[96] I. L. Grach and L. A. Kondratyuk. ELECTROMAGNETIC FORM-FACTOR OF DEUTERON IN RELATIVISTIC DYNAMICS. TWO NUCLEON AND SIX QUARK COMPONENTS. *Sov. J. Nucl. Phys.*, 39:198, 1984. [Yad. Fiz.39,316(1984)].

[97] L. L. Frankfurt, I. L. Grach, L. A. Kondratyuk, and M. I. Strikman. Is the Structure in the Deuteron Magnetic Form-factor at $Q^2 \approx 2\mathrm{GeV}^2$ a New Evidence for Nuclear Core? *Phys. Rev. Lett.*, 62:387, 1989.

[98] P. L. Chung, W. N. Polyzou, F. Coester, and B. D. Keister. Hamiltonian Light Front Dynamics of Elastic electron Deuteron Scattering. *Phys. Rev.*, C37:2000–2015, 1988.

[99] L. L. Frankfurt, M. Strikman, and T. Frederico. Deuteron form-factors in the light cone quantum mechanics 'good' component approach. *Phys. Rev.*, C48:2182–2189, 1993.

[100] Stanley J. Brodsky and John R. Hiller. Universal properties of the electromagnetic interactions of spin one systems. *Phys. Rev.*, D46:2141–2149, 1992.

[101] V. A. Karmanov. On ambiguities of the spin-1 electromagnetic form-factors in light front dynamics. *Nucl. Phys.*, A608:316–330, 1996.

[102] F. Cardarelli, I. L. Grach, I. M. Narodetsky, G. Salme, and S. Simula. Electromagnetic form-factors of the rho meson in a light front constituent quark model. *Phys. Lett.*, B349:393–399, 1995.

www.manaraa.com

[103] Nora Brambilla, Yu Jia, and Antonio Vairo. Model-independent study of magnetic dipole transitions in quarkonium. *Phys. Rev.*, D73:054005, 2006.

[104] Antonio Pineda and J. Segovia. Improved determination of heavy quarkonium magnetic dipole transitions in potential nonrelativistic QCD. *Phys. Rev.*, D87(7):074024, 2013.

[105] R. H. Dalitz. On an alternative decay process for the neutral pi-meson, Letters to the Editor. *Proc. Phys. Soc.*, A64:667–669, 1951.

[106] A. Anastasi et al. Measurement of the $\phi \to \pi^0 e^+ e^-$ transition form factor with the KLOE detector. *Phys. Lett.*, B757:362–367, 2016.

[107] M. N. Achasov et al. Study of Conversion Decays $phi \to \eta e^+ e^-$ and $\eta \to \gamma e^+ e^-$ in the Experiment with SND Detector at the VEPP-2M Collider. *Phys. Lett.*, B504:275–281, 2001.

[108] D. Babusci et al. Study of the Dalitz decay $\phi \to \eta e^+ e^-$ with the KLOE detector. *Phys. Lett.*, B742:1–6, 2015.

[109] R. R. Akhmetshin et al. Study of the rho and omega meson decays into pseudoscalar meson and e+ e- pair with the CMD-2 detector. *Phys. Lett.*, B613:29–38, 2005.

[110] P. Adlarson et al. Measurement of the $\omega \to \pi^0 e^+ e^-$ and $\eta \to e^+ e^- \gamma$ Dalitz decays with the A2 setup at MAMI. *Phys. Rev.*, C95(3):035208, 2017.

[111] M. Ablikim et al. Observation of electromagnetic Dalitz decays $J/\psi \to P e^+ e^-$. *Phys. Rev.*, D89(9):092008, 2014.

[112] M. Ablikim et al. Observation of $\psi(3686) \to \eta' e^+ e^-$. *Phys. Lett.*, B783:452–458, 2018.

[113] L. G. Landsberg. Electromagnetic Decays of Light Mesons. *Phys. Rept.*, 128:301–376, 1985.

[114] Stephen Godfrey and Jonathan L. Rosner. Production of the eta(b)(n S) states. *Phys. Rev.*, D64:074011, 2001. [Erratum: Phys. Rev.D65,039901(2002)].

[115] Randy Lewis and R. M. Woloshyn. Excited Upsilon Radiative Decays. *Phys. Rev.*, D84:094501, 2011.

[116] Estia Eichten, Stephen Godfrey, Hanna Mahlke, and Jonathan L. Rosner. Quarkonia and their transitions. *Rev. Mod. Phys.*, 80:1161–1193, 2008.

[117] J. M. Richard. Ground State Admixture Into the ψ'' (3.772). *Z. Phys.*, C4:211, 1980.

[118] Jonathan L. Rosner. ψ'' decays to charmless final states. *Annals Phys.*, 319:1–12, 2005.

[119] Estia J. Eichten, Kenneth Lane, and Chris Quigg. Charmonium levels near threshold and the narrow state $X(3872) \to \pi^+ \pi^- J/\psi$. *Phys. Rev.*, D69:094019, 2004.

[120] Estia J. Eichten, Kenneth Lane, and Chris Quigg. New states above charm threshold. *Phys. Rev.*, D73:014014, 2006. [Erratum: Phys. Rev.D73,079903(2006)].

[121] E. Eichten, K. Gottfried, T. Kinoshita, K. D. Lane, and Tung-Mow Yan. Charmonium: The Model. *Phys. Rev.*, D17:3090, 1978. [Erratum: Phys. Rev.D21,313(1980)].

www.manaraa.com

[122] Waikwok Kwong and Jonathan L. Rosner. *D* Wave Quarkonium Levels of the Υ Family. *Phys. Rev.*, D38:279, 1988.

[123] Jonathan L. Rosner. Charmless final states and S D wave mixing in the psi-prime- prime. *Phys. Rev.*, D64:094002, 2001.

[124] Hai-Yang Cheng, Chi-Yee Cheung, and Chien-Wen Hwang. Mesonic form-factors and the Isgur-Wise function on the light front. *Phys. Rev.*, D55:1559–1577, 1997.

[125] Chueng-Ryong Ji and Chad Mitchell. Frame independence of exclusive amplitudes in light front quantization. *Phys. Rev.*, D62:085020, 2000.

[126] Shau-Jin Chang, Robert G. Root, and Tung-Mow Yan. Quantum field theories in the infinite momentum frame. 1. Quantization of scalar and Dirac fields. *Phys. Rev.*, D7:1133–1148, 1973.

[127] Wei-Jun Deng, Hui Liu, Long-Cheng Gui, and Xian-Hui Zhong. Spectrum and electromagnetic transitions of bottomonium. *Phys. Rev.*, D95(7):074002, 2017.

[128] Jonathan L. Rosner, Sheldon Stone, and Ruth S. Van de Water. Leptonic Decays of Charged Pseudoscalar Mesons - 2015. *Submitted to: Particle Data Book*, 2015.

[129] Thorsten Feldmann and Peter Kroll. A Perturbative approach to the eta(c) gamma transition form-factor. *Phys. Lett.*, B413:410–415, 1997.

[130] Damir Bečirević, Goran Duplančić, Bruno Klajn, Blaženka Melić, and Francesco Sanfilippo. Lattice QCD and QCD sum rule determination of the decay constants of η_c, J/ψ and h_c states. *Nucl. Phys.*, B883:306–327, 2014.

[131] Thomas Eller, Hans Christian Pauli, and Stanley J. Brodsky. Discretized Light Cone Quantization: The Massless and the Massive Schwinger Model. *Phys. Rev.*, D35:1493, 1987.

[132] Krzysztof J. Golec-Biernat and M. Wusthoff. Saturation effects in deep inelastic scattering at low Q^2 and its implications on diffraction. *Phys. Rev.*, D59:014017, 1998.

[133] A. M. Stasto, Krzysztof J. Golec-Biernat, and J. Kwiecinski. Geometric scaling for the total $\gamma^* p$ cross-section in the low x region. *Phys. Rev. Lett.*, 86:596–599, 2001.

[134] E. Iancu, K. Itakura, and S. Munier. Saturation and BFKL dynamics in the HERA data at small x. *Phys. Lett.*, B590:199–208, 2004.

[135] Nestor Armesto, Carlos A. Salgado, and Urs Achim Wiedemann. Relating high-energy lepton-hadron, proton-nucleus and nucleus-nucleus collisions through geometric scaling. *Phys. Rev. Lett.*, 94:022002, 2005.

[136] Guillaume Beuf. Dipole factorization for DIS at NLO: Loop correction to the $\gamma^*_{T,L} \to q\bar{q}$ light-front wave functions. *Phys. Rev.*, D94(5):054016, 2016.

[137] Adrian Dumitru and Jamal Jalilian-Marian. Forward quark jets from protons shattering the colored glass. *Phys. Rev. Lett.*, 89:022301, 2002.

www.manaraa.com

[138] Larry D. McLerran and Raju Venugopalan. Computing quark and gluon distribution functions for very large nuclei. *Phys. Rev.*, D49:2233–2241, 1994.

[139] Larry D. McLerran and Raju Venugopalan. Gluon distribution functions for very large nuclei at small transverse momentum. *Phys. Rev.*, D49:3352–3355, 1994.

[140] Larry D. McLerran and Raju Venugopalan. Green's functions in the color field of a large nucleus. *Phys. Rev.*, D50:2225–2233, 1994.

[141] Larry D. McLerran and Raju Venugopalan. Fock space distributions, structure functions, higher twists and small x. *Phys. Rev.*, D59:094002, 1999.

[142] Jamal Jalilian-Marian, Alex Kovner, Larry D. McLerran, and Heribert Weigert. The Intrinsic glue distribution at very small x. *Phys. Rev.*, D55:5414–5428, 1997.

[143] Alex Krasnitz, Yasushi Nara, and Raju Venugopalan. Gluon production in the color glass condensate model of collisions of ultrarelativistic finite nuclei. *Nuclear Physics A*, 717(3):268–290, 2003.

[144] T. Lappi. Energy density of the glasma. *Phys. Lett.*, B643:11–16, 2006.

[145] David Müller. *Simulations of the Glasma in 3+1D*. PhD thesis, TU Vienna, 2019.

[146] Kenji Fukushima and Yoshimasa Hidaka. Light projectile scattering off the color glass condensate. *Journal of High Energy Physics*, 2007(06):040, 2007.

[147] Alfred H. Mueller. Toward equilibration in the early stages after a high-energy heavy ion collision. *Nucl. Phys.*, B572:227–240, 2000.

[148] Dmitri Kharzeev and Marzia Nardi. Hadron production in nuclear collisions at RHIC and high density QCD. *Phys. Lett.*, B507:121–128, 2001.

[149] Yuri V. Kovchegov and Eugene Levin. Quantum chromodynamics at high energy. *Camb. Monogr. Part. Phys. Nucl. Phys. Cosmol.*, 33:1–350, 2012.

[150] Jouni Suhonen. *From Nucleons to Nucleus*. Theoretical and Mathematical Physics. Springer, Berlin, Germany, 2007.

[151] Hans-Christian Pauli, Alex C. Kalloniatis, and Stephen S. Pinsky. Towards solving QCD: The transverse zero modes in light cone quantization. *Phys. Rev.*, D52:1176–1189, 1995.

[152] SK. T. R. Davies and S. J. Krieger . Harmonic-oscillator transformation coefficients. *Can. J. Phys.*, 69:62–69, 1991.

www.manaraa.com

APPENDIX A. CONVENTIONS

A.1 Light-Front coordinates

The contravariant four-vectors of position x^μ are written as $x^\mu = (x^+, x^-, x^1, x^2)$, where $x^+ = x^0 + x^3$ is the light-front time, $x^- = x^0 - x^3$ is the longitudinal coordinate, and $\vec{x}_\perp = (x^1, x^2)$ are the transverse coordinates. We sometimes write the transverse components with subscript x (y) in place of 1 (2), for example $\vec{r}_\perp = (r^x, r^y)$.

The covariant vectors are obtained by $x_\mu = g_{\mu\nu}x^\nu$, with the metric tensors $g_{\mu\nu}$ and $g^{\mu\nu}$. The nonzero components of the metric tensors are,

$$g^{+-} = g^{-+} = 2, \qquad g_{+-} = g_{-+} = \frac{1}{2}, \qquad g^{ii} = g_{ii} = -1 \ (i = 1, 2) \ . \tag{A.1}$$

Scalar products are

$$a \cdot b = a^\mu b_\mu = a^+ b_+ + a^- b_- + a^1 b_1 + a^2 b_2 = \frac{1}{2}(a^+ b^- + a^- b^+) - \vec{a}_\perp \cdot \vec{b}_\perp \ . \tag{A.2}$$

Derivatives are written as

$$\partial_+ = \frac{\partial}{\partial x^+} = \frac{\partial}{2\partial x_-} = \frac{1}{2}\partial^-, \quad \partial_- = \frac{\partial}{\partial x^-} = \frac{\partial}{2\partial x_+} = \frac{1}{2}\partial^+ \ . \tag{A.3}$$

The Levi-Civita tensor is defined as

$$\epsilon^{\mu\nu\rho\sigma} = \frac{1}{\sqrt{-\det g}} \begin{cases} +1, & \text{if } \mu, \nu, \rho, \sigma \text{ is an even permutation of } -, +, 1, 2 \\ -1, & \text{if } \mu, \nu, \rho, \sigma \text{ is an odd permutation of } -, +, 1, 2 \\ 0, & \text{other cases} \end{cases} \tag{A.4}$$

with $\sqrt{-\det g} = \frac{1}{2}$.

The full four-dimensional integral is

$$\int \mathrm{d}^4 x = \int \mathrm{d}x^0 \, \mathrm{d}x^1 \, \mathrm{d}x^2 \, \mathrm{d}x^3 = \frac{1}{2} \int \mathrm{d}x^+ \, \mathrm{d}x^- \, \mathrm{d}^2 x_\perp = \int \mathrm{d}^3 x \, \mathrm{d}x^+ \ , \tag{A.5}$$

www.manaraa.com

where we also define the volume integral as

$$\int \mathrm{d}^3x \equiv \int \mathrm{d}x_+ \, \mathrm{d}^2x^\perp = \frac{1}{2}\int \mathrm{d}x^- \, \mathrm{d}^2x^\perp \, . \tag{A.6}$$

In the momentum space, the Lorentz invariant integral is,

$$\begin{aligned}\int \frac{\mathrm{d}^4p}{(2\pi)^4}\theta(p^+)(2\pi)\delta^2(p^+p^- - \vec{p}_\perp^{\,2} - m^2) &= \frac{1}{2}\int \frac{\mathrm{d}p^+ \, \mathrm{d}p^- \, \mathrm{d}^2p_\perp}{(2\pi)^4}\theta(p^+)(2\pi)\delta^2(p^+p^- - \vec{p}_\perp^{\,2} - m^2) \\ &= \int \frac{\mathrm{d}^2p_\perp \, \mathrm{d}p^+}{(2\pi)^3 2p^+}\theta(p^+)\end{aligned} \tag{A.7}$$

The Fourier transform of a function $f(\vec{r}_\perp)$ and the inverse transform are defined as

$$f(\vec{r}_\perp) = \int \frac{\mathrm{d}^2p_\perp}{(2\pi)^2} e^{i\vec{p}_\perp\cdot\vec{r}_\perp}\tilde{f}(\vec{p}_\perp), \qquad \tilde{f}(\vec{p}_\perp) = \int \mathrm{d}^2\vec{r}_\perp e^{-i\vec{p}_\perp\cdot\vec{r}_\perp} f(\vec{r}_\perp) \, . \tag{A.8}$$

A.2 γ matrices

The Dirac matrices are four unitary traceless 4×4 matrices:

$$\gamma^0 = \beta = \begin{pmatrix} 0 & -i \\ i & 0 \end{pmatrix}, \quad \gamma^+ = \begin{pmatrix} 0 & 0 \\ 2i & 0 \end{pmatrix}, \quad \gamma^- = \begin{pmatrix} 0 & -2i \\ 0 & 0 \end{pmatrix}, \quad \gamma^i = \begin{pmatrix} -i\hat{\sigma}^i & 0 \\ 0 & i\hat{\sigma}^i \end{pmatrix} . \tag{A.9}$$

They are expressed in terms of the 2×2 Pauli matrices,

$$\hat{\sigma}^1 = \sigma^2 = \begin{pmatrix} 0 & -i \\ i & 0 \end{pmatrix}, \quad \hat{\sigma}^2 = -\sigma^1 = \begin{pmatrix} 0 & -1 \\ -1 & 0 \end{pmatrix} . \tag{A.10}$$

Note that $\gamma^3 = \gamma^+ - \gamma^0$. It is also convenient to define $\gamma^R \equiv \gamma^1 + i\gamma^2$ and $\gamma^L \equiv \gamma^1 + i\gamma^2$. The chiral matrix is $\gamma^5 = i\gamma^0\gamma^1\gamma^2\gamma^3$. Some useful relations,

$$\gamma^1\gamma^+\gamma^1 = \gamma^2\gamma^+\gamma^2 = \gamma^+, \quad \gamma^1\gamma^+\gamma^2 = -\gamma^2\gamma^+\gamma^1 = i\gamma^+ \tag{A.11}$$

$$\gamma^0\gamma^\mu = \gamma^{\mu\dagger}\gamma^0, \qquad \{\gamma^\mu, \gamma^\nu\} = 2g^{\mu\nu}\boldsymbol{I} \tag{A.12}$$

$$\alpha^\kappa = \gamma^0\gamma^\kappa, \quad (\alpha^1)^2 = (\alpha^2)^2 = \boldsymbol{I}, \quad \alpha^1\alpha^2 = -\alpha^1\alpha^2 \tag{A.13}$$

www.manaraa.com

Combinations of Dirac matrices as projection operators,

$$\Lambda^{\pm} = \frac{1}{4}\gamma^{\mp}\gamma^{\pm} = \frac{1}{2}\gamma^{0}\gamma^{\pm} = \frac{1}{2}(\boldsymbol{I} \pm \alpha^{3}) \,. \tag{A.14}$$

They have the following properties,

$$\begin{aligned} &\Lambda^{+} + \Lambda^{-} = \boldsymbol{I} \,, \quad (\Lambda^{\pm})^{2} = \Lambda^{\pm} \,, \quad \Lambda^{\pm}\Lambda^{\mp} = 0 \,, \quad (\Lambda^{\pm})^{\dagger} = \Lambda^{\pm} \,, \\ &\alpha^{i}\Lambda^{\pm} = \Lambda^{\mp}\alpha^{i} \,, \quad \gamma^{0}\Lambda^{\pm} = \Lambda^{\mp}\gamma^{0} \,. \end{aligned} \tag{A.15}$$

A.3 Spinors

The u, v spinors are defined as,

$$\begin{aligned} u(p, \lambda = \frac{1}{2}) &= \frac{1}{\sqrt{p^{+}}}(p^{+}, 0, im_{q}, ip^{x} - p^{y})^{\intercal} \,, \\ u(p, \lambda = -\frac{1}{2}) &= \frac{1}{\sqrt{p^{+}}}(0, p^{+}, -ip^{x} - p^{y}, im_{q})^{\intercal} \,, \\ \bar{u}(p, \lambda = \frac{1}{2}) &= \frac{1}{\sqrt{p^{+}}}(m_{q}, p^{x} - ip^{y}, -ip^{+}, 0) \,, \\ \bar{u}(p, \lambda = -\frac{1}{2}) &= \frac{1}{\sqrt{p^{+}}}(-p^{x} - ip^{y}, m_{q}, 0, -ip^{+}) \,, \end{aligned} \tag{A.16}$$

and

$$\begin{aligned} v(p, \lambda = \frac{1}{2}) &= \frac{1}{\sqrt{p^{+}}}(p^{+}, 0, -im_{q}, ip^{x} - p^{y})^{\intercal} \,, \\ v(p, \lambda = -\frac{1}{2}) &= \frac{1}{\sqrt{p^{+}}}(0, p^{+}, -ip^{x} - p^{y}, -im_{q})^{\intercal} \,, \\ \bar{v}(p, \lambda = \frac{1}{2}) &= \frac{1}{\sqrt{p^{+}}}(-m_{q}, p^{x} - ip^{y}, -ip^{+}, 0) \,, \\ \bar{v}(p, \lambda = -\frac{1}{2}) &= \frac{1}{\sqrt{p^{+}}}(-p^{x} - ip^{y}, -m_{q}, 0, -ip^{+}) \,. \end{aligned} \tag{A.17}$$

They satisfy the Dirac equations:

$$\bar{u}(p, \lambda)(\not{p} + m_{q}) = 0, \qquad (\not{p} - m_{q})u(p, \lambda) = 0 \,; \tag{A.18}$$

$$\bar{v}(p, \lambda)(\not{p} - m_{q}) = 0, \qquad (\not{p} + m_{q})v(p, \lambda) = 0 \,. \tag{A.19}$$

They follow normalization relations,

$$u(p, \lambda_{1})\bar{u}(p, \lambda_{2}) = 2m_{q}\delta_{\lambda_{1},\lambda_{2}}, \qquad v(p, \lambda_{1})\bar{v}(p, \lambda_{2}) = -2m_{q}\delta_{\lambda_{1},\lambda_{2}}, \tag{A.20}$$

$$u(p, \lambda_{1})\bar{v}(p, \lambda_{2}) = \bar{v}(p, \lambda_{1})u(p, \lambda_{2}) = 0 \tag{A.21}$$

www.manaraa.com

Gordon identities:

$$2m_q\bar{u}(p',\lambda')\gamma^\mu u(p,\lambda) = \bar{u}(p',\lambda')[(p'+p)^\mu - \frac{1}{2}[\gamma^\mu,\gamma^\nu](p'-p)_\nu]u(p,\lambda) \tag{A.22}$$

A.3.1 spinor part in the quark current

$$\begin{aligned}
&\bar{u}(p_2,\lambda_2)\gamma^+u(p_1,\lambda_1) = 2\sqrt{p_1^+p_2^+}\delta_{\lambda_2,\lambda_1}\\
&\bar{u}(p_2,\lambda_2)\gamma^-u(p_1,\lambda_1) = \frac{2}{\sqrt{p_1^+p_2^+}}\begin{cases} m^2+p_1^Rp_2^L, & \lambda_1=+,\lambda_2=+\\ m(p_2^L-p_1^L), & \lambda_1=-,\lambda_2=+\\ m(p_1^R-p_2^R), & \lambda_1=+,\lambda_2=-\\ m^2+p_1^Lp_2^R, & \lambda_1=-,\lambda_2=- \end{cases}\\
&\bar{u}(p_2,\lambda_2)\gamma^xu(p_1,\lambda_1) = \frac{1}{\sqrt{p_1^+p_2^+}}\begin{cases} p_2^+p_1^R+p_1^+p_2^L, & \lambda_1=+,\lambda_2=+\\ m(p_2^+-p_1^+), & \lambda_1=-,\lambda_2=+\\ m(p_1^+-p_2^+), & \lambda_1=+,\lambda_2=-\\ p_2^+p_1^L+p_1^+p_2^R, & \lambda_1=-,\lambda_2=- \end{cases}\\
&\bar{u}(p_2,\lambda_2)\gamma^yu(p_1,\lambda_1) = \frac{1}{\sqrt{p_1^+p_2^+}}\begin{cases} i(-p_2^+p_1^R+p_1^+p_2^L), & \lambda_1=+,\lambda_2=+\\ -im(p_2^+-p_1^+), & \lambda_1=-,\lambda_2=+\\ -im(p_2^+-p_1^+), & \lambda_1=+,\lambda_2=-\\ i(p_2^+p_1^L-p_1^+p_2^R), & \lambda_1=-,\lambda_2=- \end{cases}
\end{aligned} \tag{A.23}$$

www.manaraa.com

By defining $p^R \equiv p^x + ip^y, p^L \equiv p^x - ip^y$,

$$\bar{u}(p_2,\lambda_2)\gamma^R u(p_1,\lambda_1) = \frac{2}{\sqrt{p_1^+ p_2^+}} \begin{cases} p_2^+ p_1^R, & \lambda_1 = +, \lambda_2 = + \\ m(p_2^+ - p_1^+), & \lambda_1 = -, \lambda_2 = + \\ 0, & \lambda_1 = +, \lambda_2 = - \\ p_1^+ p_2^R, & \lambda_1 = -, \lambda_2 = - \end{cases}$$
$$\bar{u}(p_2,\lambda_2)\gamma^L u(p_1,\lambda_1) = \frac{2}{\sqrt{p_1^+ p_2^+}} \begin{cases} p_1^+ p_2^L, & \lambda_1 = +, \lambda_2 = + \\ 0, & \lambda_1 = -, \lambda_2 = + \\ m(p_1^+ - p_2^+), & \lambda_1 = +, \lambda_2 = - \\ p_2^+ p_1^L, & \lambda_1 = -, \lambda_2 = - \end{cases} \tag{A.24}$$

www.manaraa.com

A.3.2 spinor part in the antiquark current

$$\bar{v}(p_2,\lambda_2)\gamma^+ v(p_1,\lambda_1) = 2\sqrt{p_1^+ p_2^+}\,\delta_{\lambda_2,\lambda_1}$$

$$\bar{v}(p_2,\lambda_2)\gamma^- v(p_1,\lambda_1) = \frac{2}{\sqrt{p_1^+ p_2^+}} \begin{cases} m^2 + p_1^L p_2^R, & \lambda_1 = +, \lambda_2 = + \\ m(p_2^R - p_1^R), & \lambda_1 = -, \lambda_2 = + \\ m(p_1^L - p_2^L), & \lambda_1 = +, \lambda_2 = - \\ m^2 + p_1^R p_2^L, & \lambda_1 = -, \lambda_2 = - \end{cases}$$

$$\bar{v}(p_2,\lambda_2)\gamma^R v(p_1,\lambda_1) = \frac{2}{\sqrt{p_1^+ p_2^+}} \begin{cases} p_1^+ p_2^R, & \lambda_1 = +, \lambda_2 = + \\ 0, & \lambda_1 = -, \lambda_2 = + \\ m(p_1^+ - p_2^+), & \lambda_1 = +, \lambda_2 = - \\ p_2^+ p_1^R, & \lambda_1 = -, \lambda_2 = - \end{cases} \tag{A.25}$$

$$\bar{v}(p_2,\lambda_2)\gamma^L v(p_1,\lambda_1) = \frac{2}{\sqrt{p_1^+ p_2^+}} \begin{cases} p_2^+ p_1^L, & \lambda_1 = +, \lambda_2 = + \\ m(p_2^+ - p_1^+), & \lambda_1 = -, \lambda_2 = + \\ 0, & \lambda_1 = +, \lambda_2 = - \\ p_1^+ p_2^L, & \lambda_1 = -, \lambda_2 = - \end{cases}$$

www.manaraa.com

A.3.3 spinor part in the pair creation/annihilation vertex

$$\bar{u}(p_2,\lambda_2)\gamma^+ v(p_1,\lambda_1) = 2\sqrt{p_1^+ p_2^+}\,\delta_{\lambda_2,-\lambda_1}$$

$$\bar{u}(p_2,\lambda_2)\gamma^- v(p_1,\lambda_1) = \frac{2}{\sqrt{p_1^+ p_2^+}}\begin{cases} -m(p_2^L + p_1^L), & \lambda_1 = +, \lambda_2 = + \\ -m^2 + p_1^R p_2^L, & \lambda_1 = -, \lambda_2 = + \\ -m^2 + p_1^L p_2^R, & \lambda_1 = +, \lambda_2 = - \\ m(p_1^R + p_2^R), & \lambda_1 = -, \lambda_2 = - \end{cases}$$

$$\bar{u}(p_2,\lambda_2)\gamma^R v(p_1,\lambda_1) = \frac{2}{\sqrt{p_1^+ p_2^+}}\begin{cases} -m(p_1^+ + p_2^+), & \lambda_1 = +, \lambda_2 = + \\ p_2^+ p_1^R, & \lambda_1 = -, \lambda_2 = + \\ p_1^+ p_2^R, & \lambda_1 = +, \lambda_2 = - \\ 0, & \lambda_1 = -, \lambda_2 = - \end{cases} \tag{A.26}$$

$$\bar{u}(p_2,\lambda_2)\gamma^L v(p_1,\lambda_1) = \frac{2}{\sqrt{p_1^+ p_2^+}}\begin{cases} 0, & \lambda_1 = +, \lambda_2 = + \\ p_1^+ p_2^L, & \lambda_1 = -, \lambda_2 = + \\ p_2^+ p_1^L, & \lambda_1 = +, \lambda_2 = - \\ m(p_2^+ + p_1^+), & \lambda_1 = -, \lambda_2 = - \end{cases}$$

www.manaraa.com

$$\bar{v}(p_2,\lambda_2)\gamma^+u(p_1,\lambda_1) = 2\sqrt{p_1^+p_2^+}\delta_{\lambda_2,-\lambda_1}$$

$$\bar{v}(p_2,\lambda_2)\gamma^-u(p_1,\lambda_1) = \frac{2}{\sqrt{p_1^+p_2^+}}\begin{cases} -m_q(p_2^R+p_1^R), & \lambda_1=+,\lambda_2=+ \\ -m_q^2+p_2^Rp_1^L, & \lambda_1=-,\lambda_2=+ \\ -m_q^2+p_1^Lp_2^R, & \lambda_1=+,\lambda_2=- \\ m_q(p_2^L+p_1^L), & \lambda_1=-,\lambda_2=- \end{cases}$$

$$\bar{v}(p_2,\lambda_2)\gamma^Ru(p_1,\lambda_1) = \frac{2}{\sqrt{p_1^+p_2^+}}\begin{cases} 0, & \lambda_1=+,\lambda_2=+ \\ p_2^Rp_1^+, & \lambda_1=-,\lambda_2=+ \\ p_1^Rp_2^+, & \lambda_1=+,\lambda_2=- \\ m_q(p_2^++p_1^+), & \lambda_1=-,\lambda_2=- \end{cases} \tag{A.27}$$

$$\bar{v}(p_2,\lambda_2)\gamma^Lu(p_1,\lambda_1) = \frac{2}{\sqrt{p_1^+p_2^+}}\begin{cases} -m_q(p_2^++p_1^+), & \lambda_1=+,\lambda_2=+ \\ p_1^Lp_2^+, & \lambda_1=-,\lambda_2=+ \\ p_2^Lp_1^+, & \lambda_1=+,\lambda_2=- \\ 0, & \lambda_1=-,\lambda_2=- \end{cases}$$

A.3.4 spinor part in the instantaneous quark vertex

$$\begin{aligned} &\bar{u}(p_2,\lambda_2)\gamma^x\gamma^+\gamma^xu(p_1,\lambda_1) = \bar{u}(p_2,\lambda_2)\gamma^y\gamma^+\gamma^yu(p_1,\lambda_1) = 2\sqrt{p_1^+p_2^+}\delta_{\lambda_2,\lambda_1} \\ &\bar{u}(p_2,\lambda_2)\gamma^x\gamma^+\gamma^yu(p_1,\lambda_1) = -\bar{u}(p_2,\lambda_2)\gamma^y\gamma^+\gamma^xu(p_1,\lambda_1) = 2i\sqrt{p_1^+p_2^+}\delta_{\lambda_2,\lambda_1}2\lambda_1 \end{aligned} \tag{A.28}$$

www.manaraa.com

A.3.5 spinor part in the electroweak current

$$
\begin{aligned}
\bar{v}(p_2,\lambda_2)\gamma^{+}\gamma^{5}u(p_1,\lambda_1) &= 2\sqrt{p_1^{+}p_2^{+}}\begin{cases} 0, & \lambda_1=+,\lambda_2=+ \\ -1, & \lambda_1=-,\lambda_2=+ \\ 1, & \lambda_1=+,\lambda_2=- \\ 0, & \lambda_1=-,\lambda_2=- \end{cases} \\
\bar{v}(p_2,\lambda_2)\gamma^{-}\gamma^{5}u(p_1,\lambda_1) &= \frac{2}{\sqrt{p_1^{+}p_2^{+}}}\begin{cases} m_q(p_2^R-p_1^R), & \lambda_1=+,\lambda_2=+ \\ -m_q^2-p_2^Rp_1^L, & \lambda_1=-,\lambda_2=+ \\ m_q^2+p_2^Lp_1^R, & \lambda_1=+,\lambda_2=- \\ m_q(p_2^L-p_1^L), & \lambda_1=-,\lambda_2=- \end{cases} \\
\bar{v}(p_2,\lambda_2)\gamma^{R}\gamma^{5}u(p_1,\lambda_1) &= \frac{2}{\sqrt{p_1^{+}p_2^{+}}}\begin{cases} 0, & \lambda_1=+,\lambda_2=+ \\ -p_2^Rp_1^{+}, & \lambda_1=-,\lambda_2=+ \\ p_1^Rp_2^{+}, & \lambda_1=+,\lambda_2=- \\ m_q(p_2^{+}-p_1^{+}), & \lambda_1=-,\lambda_2=- \end{cases} \\
\bar{v}(p_2,\lambda_2)\gamma^{L}\gamma^{5}u(p_1,\lambda_1) &= \frac{2}{\sqrt{p_1^{+}p_2^{+}}}\begin{cases} m_q(p_2^{+}+p_1^{+}), & \lambda_1=+,\lambda_2=+ \\ -p_1^Lp_2^{+}, & \lambda_1=-,\lambda_2=+ \\ p_2^Lp_1^{+}, & \lambda_1=+,\lambda_2=- \\ 0, & \lambda_1=-,\lambda_2=- \end{cases}
\end{aligned}
\tag{A.29}
$$

www.manaraa.com

A.4 Spin vector of massive spin 1 particles

Define the spin vector for the massive spin 1 particles with momentum k^μ and spin projection λ:

$$e(k,\lambda=0)=(\frac{k^+}{m},\frac{\vec{k}_\perp^2-m^2}{mk^+},\frac{\vec{k}_\perp}{m}) \tag{A.30}$$

$$e(k,\lambda=\pm1)=(0,\frac{2\boldsymbol{\epsilon}_\lambda^\perp\cdot\vec{k}_\perp}{k^+},\boldsymbol{\epsilon}_\lambda^\perp) \tag{A.31}$$

where $\boldsymbol{\epsilon}_\pm^\perp=(1,\pm i)/\sqrt{2}$ and m is the mass of the particle.

Spin vector identities

- Proca equation:

$$k_\mu e^\mu(k,\lambda)=0\ .$$

- Orthogonality:

$$e^\mu(k,\lambda)e_\mu^*(k,\lambda')=-\delta_{\lambda,\lambda'};\ .$$

- Crossing symmetry:

$$e_\mu^*(k,\lambda)=e_\mu(k,-\lambda),\qquad e^\mu(-k,\lambda)=(-1)^{\lambda+1}e^\mu(k,\lambda)$$

A.5 Polarizations of massless vector bosons

Define the polarization vector for a massless vector boson with momentum k^μ and spin projection $\lambda=\pm1$:

$$\epsilon_\lambda^\mu(k)=(\epsilon_\lambda^+,\epsilon_\lambda^-,\epsilon_\lambda^\perp)=(0,2\frac{\boldsymbol{\epsilon}_\lambda^\perp\cdot\vec{k}_\perp}{k^+},\boldsymbol{\epsilon}_\lambda^\perp)\ , \tag{A.32}$$

where $\boldsymbol{\epsilon}_\pm^\perp=(1,\pm i)/\sqrt{2}$.

A.6 Discrete symmetries

Consider a particle state with momentum p^μ and parity P,

$$\mathbb{P}\,|\phi(p^\mu,\mathrm{P})\rangle=\mathrm{P}\,|\phi(\mathcal{P}^\mu_\nu p^\nu,\mathrm{P})\rangle\ . \tag{A.33}$$

www.manaraa.com

The parity operator is

$$\mathcal{P}^{\mu}_{\nu} = (\mathcal{P}^{-1})^{\mu}_{\nu} = \begin{pmatrix} +1 & & & \\ & -1 & & \\ & & -1 & \\ & & & -1 \end{pmatrix} . \tag{A.34}$$

The current operator under the parity transformation is

$$\mathbb{P}^{-1} J^{\mu} \mathbb{P} = \mathcal{P}^{\mu}_{\nu} J^{\nu} . \tag{A.35}$$

For spin vector,

$$e^{\mu}(\mathcal{P} \cdot k, \lambda) = -\mathcal{P}^{\mu}_{\nu} e^{\nu}(k, \lambda) . \tag{A.36}$$

Consider a particle state with charge conjugation C (if there is one),

$$\mathbb{C} \, |\phi(p^{\mu}, \mathrm{C})\rangle = \mathrm{C} \, |\phi(p^{\mu}, \mathrm{C})\rangle \ . \tag{A.37}$$

The current operator under the charge conjugation is

$$\mathbb{C}^{-1} J^{\mu} \mathbb{C} = -J^{\mu} . \tag{A.38}$$

A.7 QCD color space

The specification of the quark state in the color space is by a three-element column vector c,

$$c = \begin{pmatrix} 1 \\ 0 \\ 0 \end{pmatrix} \text{ for red, } \quad \begin{pmatrix} 0 \\ 1 \\ 0 \end{pmatrix} \text{ for blue, } \quad \begin{pmatrix} 0 \\ 0 \\ 1 \end{pmatrix} \text{ for green.} \tag{A.39}$$

www.manaraa.com

We use the standard basis for the fundamental representation of SU(3), i.e. the Gell-Mann matrices,

$$
\begin{aligned}
T^1 &= \frac{1}{2}\begin{pmatrix} 0 & 1 & 0 \\ 1 & 0 & 0 \\ 0 & 0 & 0 \end{pmatrix}, \quad T^2 = \frac{1}{2}\begin{pmatrix} 0 & -i & 0 \\ i & 0 & 0 \\ 0 & 0 & 0 \end{pmatrix}, \quad T^3 = \frac{1}{2}\begin{pmatrix} 1 & 0 & 0 \\ 0 & -1 & 0 \\ 0 & 0 & 0 \end{pmatrix}, \\
T^4 &= \frac{1}{2}\begin{pmatrix} 0 & 0 & 1 \\ 0 & 0 & 0 \\ 1 & 0 & 0 \end{pmatrix}, \quad T^5 = \frac{1}{2}\begin{pmatrix} 0 & 0 & -i \\ 0 & 0 & 0 \\ i & 0 & 0 \end{pmatrix}, \quad T^6 = \frac{1}{2}\begin{pmatrix} 0 & 0 & 0 \\ 0 & 0 & 1 \\ 0 & 1 & 0 \end{pmatrix}, \\
T^7 &= \frac{1}{2}\begin{pmatrix} 0 & 0 & 0 \\ 0 & 0 & -i \\ 0 & i & 0 \end{pmatrix}, \quad T^8 = \frac{1}{2\sqrt{3}}\begin{pmatrix} 1 & 0 & 0 \\ 0 & 1 & 0 \\ 0 & 0 & -2 \end{pmatrix}.
\end{aligned}
\tag{A.40}
$$

In the matrix notation, $\boldsymbol{A}^\mu = T^a A^\mu_a$ with the gluon index $a = 1, \ldots, 8$. The color matrix element $A^\mu_{cc'} = T^a_{cc'} A^\mu_a$

$$
\boldsymbol{A}^\mu = \frac{1}{2}\begin{pmatrix} \frac{1}{\sqrt{3}}A^\mu_8 + A^\mu_3 & A^\mu_1 - iA^\mu_2 & A^\mu_4 - iA^\mu_5 \\ A^\mu_1 + iA^\mu_2 & \frac{1}{\sqrt{3}}A^\mu_8 - A^\mu_3 & A^\mu_6 - iA^\mu_7 \\ A^\mu_4 + iA^\mu_5 & A^\mu_6 + iA^\mu_7 & -\frac{2}{\sqrt{3}}A^\mu_8 \end{pmatrix}. \tag{A.41}
$$

www.manaraa.com

APPENDIX B. THE LIGHT-FRONT QCD HAMILTONIAN

In this Appendix, we first derive the canonical QCD Hamiltonian according to Ref. [33] with details, which compensate the discussion in Section 1.3. We then turn to the derivation with the participation of an additional background gluon field.

B.1 The light-front QCD Hamiltonian

The strong interaction between quarks and gluons is described by the non-Abelian gauge theory with symmetry group SU(3), known as quantum chromodynamics (QCD). The QCD Lagrangian reads

$$\mathcal{L} = -\frac{1}{4}F^{\mu\nu}{}_a F^a_{\mu\nu} + \overline{\Psi}(i\gamma^\mu \boldsymbol{D}_\mu - \boldsymbol{m})\Psi \,. \tag{B.1}$$

A^ν_a is color vector potential, with the gluon index $a = 1, 2, \ldots, 8$. The quark field $\Psi_{\alpha,c}$, carries the Dirac index $\alpha = 1, 2, \ldots, 4$ and the color index $c = 1, 2, 3$, which are usually suppressed in expressions like $\overline{\Psi}\gamma^\mu \boldsymbol{D}_\mu \Psi = \overline{\Psi}_c \gamma^\mu (\boldsymbol{D}_\mu)_{cc'} \Psi_{c'}$. $\boldsymbol{m} = m\boldsymbol{I}_3 = m\delta_{cc'}$ is diagonal in color space. The vector potential can be parameterized as $(\boldsymbol{A}_\mu)_{cc'} = T^a_{cc'} A^\mu_a$ by the color matrices $T^a_{cc'}$, and its matrix form can be found in Appendix A.7. $F^{\mu\nu}_a \equiv \partial^\mu A^\nu_a - \partial^\nu A^\mu_a - g f^{abc} A^\mu_b A^\nu_c$ is the field tensor, and $\boldsymbol{D}^\mu \equiv \partial_\mu \boldsymbol{I}_3 + ig\boldsymbol{A}^\mu$ is the covariant derivative. The structure constants f^{abc} are complete anti-symmetric, $f^{abc} = f^{cab} = -f^{acb}$. In the following derivations, We will drop the identity operator in the color space, $\boldsymbol{I}_3$, for simplicity.

The QCD Lagrangian is a functional of the twelve components $\boldsymbol{A}^\mu$, Ψ_α, $\overline{\Psi}_\alpha$ and their space-time derivatives. We can denote them collectively as $\mathcal{L} = \mathcal{L}[\phi_r, \partial_\mu \phi_r]$. The equations of motion are

$$\partial_\kappa \Pi^\kappa_r - \delta\mathcal{L}/\delta\phi_r = 0 \,, \tag{B.2}$$

where the generalized momentum fields are $\Pi^\kappa_r \equiv \delta\mathcal{L}/\delta(\partial_\kappa \phi_r)$. The variational derivatives are

$$\frac{\delta\mathcal{L}}{\delta A^s_\kappa} = -\frac{1}{4}F^{\kappa\mu}_a(-gf^{asc}A^c_\mu) \times 4 + \overline{\Psi}(i\gamma^\kappa(igT^s))\Psi = -gf^{sac}F^{\kappa\mu}_a A^c_\mu - g\overline{\Psi}\gamma^\kappa T^s \Psi, \qquad \Pi^\lambda_{A^s_\kappa} = -F^{\lambda\kappa}_s \,, \tag{B.3}$$

$$\frac{\delta\mathcal{L}}{\delta\Psi} = -g\overline{\Psi}\gamma^\mu C_\mu - m\overline{\Psi} - \frac{i}{2}\overline{\Psi}\gamma^\mu \overleftarrow{\partial}_\mu, \quad \Pi^\lambda_\Psi = \frac{i}{2}\overline{\Psi}\gamma^\lambda, \quad \Pi^\lambda_{\overline{\Psi}} = \frac{i}{2}\gamma^\lambda \Psi \,. \tag{B.4}$$

www.manaraa.com

The first four equations of motion give the color-Maxwell equations,

$$\partial_\lambda F_s^{\lambda\kappa} = g J_s^\kappa \,, \tag{B.5}$$

with the current density $J_s^\kappa \equiv f^{sac} F_a^{\kappa\mu} A_\mu^c + \overline{\Psi}\gamma^\kappa T^s \Psi$. In the light-cone gauge of $A_a^+ = 0$, the $\kappa = +$ component of Eq. (B.5) does not contain time derivatives, and can be written as

$$g J_a^+ = \partial_\lambda F_a^{\lambda +} = -\partial^+ \partial_- A_a^- - \partial^+ \partial_i A_a^i \,. \tag{B.6}$$

By disregarding the zero modes [151], one inverts the equation to

$$\frac{1}{2} A_a^- = -g \frac{1}{(\partial^+)^2} J_a^+ - \frac{1}{\partial^+} \partial_i A_a^i \,. \tag{B.7}$$

We define the free solution $\tilde{A}_a^\mu$ such that $\lim_{g\to 0} A_a^\mu = \tilde{A}_a^\mu$. According to Eq. (B.7), the free field reads,

$$\tilde{A}_a^\mu = (0, \tilde{A}_a^-, A_a^i), \quad \text{with } \frac{1}{2}\tilde{A}_a^- \equiv \frac{1}{2} A_a^- + g \frac{1}{(\partial^+)^2} J_a^+ = -\frac{1}{\partial^+} \partial_i A_a^i \,. \tag{B.8}$$

$\tilde{A}_a^\mu$ is thereby purely transverse.

The second group of equation of motions give the adjoint color-Dirac equation,

$$\overline{\Psi}[i\gamma^\mu (\overleftarrow{\partial}_\mu - ig \boldsymbol{A}_\mu) + m] = 0 \,. \tag{B.9}$$

Take Hermitian conjugate on the equation and use the relation $\overline{\Psi} = \Psi^\dagger \gamma^0$, we have

$$[-i\gamma^{\mu\dagger} (\partial_\mu + ig \boldsymbol{A}_\mu) + m]\gamma^0 \Psi = 0 \,. \tag{B.10}$$

By moving γ^0 to the left, we arrive at the color-Dirac equation,

$$[i\gamma^\mu (\partial_\mu + ig \boldsymbol{A}_\mu) - m]\Psi = 0 \,. \tag{B.11}$$

Similar to the gluon field, we also want to separate the dynamical components of the fermion field. Define the projected spinors $\Psi_\pm = \Lambda^\pm \Psi$, with $\Lambda^\pm = \frac{1}{2}\gamma^0\gamma^\pm$, see more definitions of $\Lambda^\pm$ in Appendix A.2. First multiply Eq. (B.42) by γ^0 on the left,

$$\begin{gathered} [i(\gamma^0\gamma^+ \boldsymbol{D}_+ + \gamma^0\gamma^- \boldsymbol{D}_- + \alpha^i \boldsymbol{D}_i) - m\beta]\Psi = 0 \,, \\ \text{which is, } [i(2\Lambda^+ \boldsymbol{D}_+ + 2\Lambda^- \boldsymbol{D}_- + \alpha^i \boldsymbol{D}_i) - m\beta]\Psi = 0 \,. \end{gathered} \tag{B.12}$$

www.manaraa.com

Then multiply the equation by $\Lambda^+(\Lambda^-)$ on the left, and bring it to the right,

$$[i(2\boldsymbol{D}_\pm\Lambda^\pm + \alpha^i \boldsymbol{D}_i\Lambda^\mp) - m\beta\Lambda^\mp]\Psi = 0\ . \tag{B.13}$$

One thereby obtains a coupled set of spinor equations,

$$2i\partial_+\Psi_+ = (-i\alpha^i \boldsymbol{D}_i + m\beta)\Psi_- + 2g\boldsymbol{A}_+\Psi_+\ , \tag{B.14}$$

$$2i\partial_-\Psi_- = (-i\alpha^i \boldsymbol{D}_i + m\beta)\Psi_+ + 2g\boldsymbol{A}_-\Psi_-\ . \tag{B.15}$$

Eq. (B.46) does not contain time derivatives, and can be written as a constraint relation,

$$\Psi_- = \frac{1}{2i\partial_-}(m\beta - i\alpha^i \boldsymbol{D}_i)\Psi_+\ . \tag{B.16}$$

By substituting Eq. (B.47) into Eq. (B.45), we get

$$2iD_+\Psi_+ = (m\beta - i\alpha^i \boldsymbol{D}_i)\frac{1}{2i\partial_-}(m\beta - i\alpha^i \boldsymbol{D}_i)\Psi_+\ . \tag{B.17}$$

In analogy to the free solution $\tilde{A}$, we define the free spinor $\tilde{\Psi} = \tilde{\Psi}_+ + \tilde{\Psi}_-$ with

$$\tilde{\Psi}_+ = \Psi_+, \quad \tilde{\Psi}_- = \frac{1}{2i\partial_-}(m\beta - i\alpha^i\partial_i)\Psi_+\ . \tag{B.18}$$

It is also easy to see that $\tilde{\Psi}_\pm = \Lambda^\pm\tilde{\Psi}$.

We now turn to the construction of the canonical Hamiltonian density through a Legendre transformation,

$$\begin{aligned}\mathcal{P}_+ =&(\partial_+A^s_\kappa)\Pi^+_{A^s_\kappa} + (\partial_+\Psi)\Pi^+_\Psi + (\partial_+\overline{\Psi})\Pi^+_{\overline{\Psi}} - \mathcal{L}\\ =&-F^{+\kappa}_s\partial_+A^s_\kappa + \frac{i}{2}[\overline{\Psi}\gamma^+\partial_+\Psi + h.c.] + \frac{1}{4}F^{\mu\nu}{}_aF^a_{\mu\nu} - \frac{1}{2}[\overline{\Psi}(i\gamma^\mu\boldsymbol{D}_\mu - \boldsymbol{m})\Psi + \overline{\Psi}(-i\gamma^\mu\overleftarrow{\boldsymbol{D}}_\mu - \boldsymbol{m})\Psi]\\ =&-F^{+\kappa}_s\partial_+A^s_\kappa + \frac{i}{2}[\overline{\Psi}\gamma^+\partial_+\Psi + h.c.] + \frac{1}{4}F^{\mu\nu}{}_aF^a_{\mu\nu}\ ,\end{aligned} \tag{B.19}$$

where we have used the color-Dirac equations as in Eqs. (B.40) and (B.42) in the last line. It is convenient to add a total derivative $-\partial_\kappa(F^{\kappa+}_sA^s_+)$ to the Hamiltonian $P^- = 2P_+$,

$$\begin{aligned}P^- =&2\int \mathrm{d}x_+\,\mathrm{d}^2x_\perp\,\mathcal{P}_+\\ =&\int \mathrm{d}x^-\,\mathrm{d}^2x_\perp\ -F^{+\kappa}_s\partial_+A^s_\kappa + \frac{i}{2}[\overline{\Psi}\gamma^+\partial_+\Psi + h.c.] + \frac{1}{4}F^{\mu\nu}{}_aF^a_{\mu\nu} - \partial_\kappa(F^{\kappa+}_sA^s_+)\ .\end{aligned} \tag{B.20}$$

www.manaraa.com

We can rewrite the first and the last term into

$$\begin{aligned}
F_s^{\kappa+}\partial_+ A_\kappa^s - \partial_\kappa(F_s^{\kappa+}A_+^s) =& F_s^{\kappa+}\partial_+ A_\kappa^s - (\partial_\kappa F_s^{\kappa+})A_+^s - F_s^{\kappa+}\partial_\kappa A_+^s \\
=& F_s^{\kappa+}(\partial_+ A_\kappa^s - \partial_\kappa A_+^s) - (\partial_\kappa F_s^{\kappa+})A_+^s \\
=& -F_s^{\kappa+}(F_{\kappa+}^s + g f^{sbc}A_\kappa^b A_+^c) - g J_s^+ A_+^s \\
=& -F_s^{\kappa+}F_{\kappa+}^s - g F_s^{\kappa+} f^{sbc}A_\kappa^b A_+^c - g J_s^+ A_+^s \\
=& -F_s^{\kappa+}F_{\kappa+}^s - g F_s^{\kappa+} f^{sbc}A_\kappa^b A_+^c - g(f^{sac}F_a^{+\mu}A_\mu^c + \overline{\Psi}\gamma^+ T^s \Psi)A_+^s \\
=& -F_s^{\kappa+}F_{\kappa+}^s - g\overline{\Psi}\gamma^+ T^s A_+^s \Psi \,.
\end{aligned} \tag{B.21}$$

The Hamiltonian becomes

$$\begin{aligned}
P^- =& \int \mathrm{d}x^-\, \mathrm{d}^2x_\perp \, \frac{1}{4}F^{\mu\nu}{}_a F^a_{\mu\nu} - F_s^{\kappa+}F_{\kappa+}^s - g\overline{\Psi}\gamma^+ T^s A_+^s \Psi + \frac{i}{2}[\overline{\Psi}\gamma^+\partial_+\Psi + h.c.] \\
=& \int \mathrm{d}x^-\, \mathrm{d}^2x_\perp \, \frac{1}{4}F^{\mu\nu}{}_a F^a_{\mu\nu} - F_s^{\kappa+}F_{\kappa+}^s + \frac{i}{2}[\overline{\Psi}\gamma^+ \boldsymbol{D}_+\Psi + h.c.] \,.
\end{aligned} \tag{B.22}$$

Let us also rewrite the color-electro-magnetic energy density and separate the longitudinal and the transversal contributions,

$$\begin{aligned}
\frac{1}{4}F_a^{\mu\nu}F^a_{\mu\nu} - F_a^{\mu+}F^a_{\mu+} =& \frac{1}{4}(F_a^{ij}F^a_{ij} + F_a^{\mu+}F^a_{\mu+} + F_a^{+\nu}F^a_{+\nu} + F_a^{\mu-}F^a_{\mu-} + F_a^{-\nu}F^a_{-\nu} \\
& - F_a^{+-}F_{+-} - F_a^{-+}F_{-+}) - F_a^{\mu+}F_{\mu+} \\
=& \frac{1}{4}F_a^{ij}F^a_{ij} + \frac{1}{2}(F_a^{\mu+}F^a_{\mu+} + F_a^{\mu-}F^a_{\mu-} - F_a^{+-}F^a_{+-}) - F_a^{\mu+}F^a_{\mu+} \\
=& \frac{1}{4}F_a^{ij}F^a_{ij} - \frac{1}{2}F_a^{+-}F^a_{+-} \,.
\end{aligned} \tag{B.23}$$

Note that $F_a^{\mu+}F^a_{\mu+} = F_a^{\mu-}F^a_{\mu-}$ by $F_a^{\mu-} = F^a_{\nu+}g^{\mu\nu}g^{+-}$. Substituting A_a^- by Eq. (B.7), the color-electric part becomes,

$$\begin{aligned}
F_a^{+-}F^a_{+-} =& -\partial^+ A_a^- \partial_- A_+^a \\
=& -\frac{1}{4}\partial^+ A_a^- \partial^+ A_a^- \\
=& -(-g\frac{1}{\partial^+}J_a^+ - \partial_i A_a^i)^2 \\
=& -g^2\frac{1}{\partial^+}J_a^+\frac{1}{\partial^+}J_a^+ - (\partial_i A_a^i)^2 - 2g\frac{1}{\partial^+}J_a^+\partial_i A_a^i \\
=& g^2 J_a^+\frac{1}{(\partial^+)^2}J_a^+ - (\partial_i A_a^i)^2 - g J_a^+ \tilde{A}_a^- \,.
\end{aligned} \tag{B.24}$$

www.manaraa.com

In deriving the last line, we introduced an extra term $-g^2\frac{1}{\partial^+}(J_a^+\frac{1}{\partial^+}J_a^+)$, and it should vanish under the integral of $\int \mathrm{d}x^-$ in the Hamiltonian. The color-magnetic part can be written as

$$\begin{aligned}
F_a^{ij}F_{ij}^a =& 2\partial^i A_a^j \partial_i A_j^a - 2\partial^i A_a^j \partial_j A_i^a - 4gf^{abc}\partial^i A_a^j A_i^b A_j^c + g^2 f^{abc}A_b^i A_c^j f^{aef} A_i^e A_j^f \\
=& -2A_a^j \partial^i \partial_i A_j^a + 2A_a^j \partial^i \partial_j A_i^a - 4gf^{abc}\partial^i A_a^j A_i^b A_j^c + g^2 f^{abc}A_b^i A_c^j f^{aef} A_i^e A_j^f \\
=& 2A_a^j \nabla_\perp^2 A_j^a - 2(\partial_j A_a^j \partial^i A_i^a) - 4gf^{abc}\partial^i A_a^j A_i^b A_j^c + g^2 f^{abc}A_b^i A_c^j f^{aef} A_i^e A_j^f \ .
\end{aligned} \tag{B.25}$$

For the spinor terms,

$$i\overline{\Psi}\gamma^+ \boldsymbol{D}_+ \Psi = i\Psi^\dagger \gamma^0 \gamma^+ \boldsymbol{D}_+ \Psi = 2i\Psi^\dagger \Lambda^+ \boldsymbol{D}_+ \Psi = 2i\Psi^\dagger \Lambda^+ \boldsymbol{D}_+ \Lambda^+ \Psi = 2i\Psi_+^\dagger \boldsymbol{D}_+ \Psi_+ \ . \tag{B.26}$$

Substitution of the time derivative in Eq. (B.48) and the free spinors defined in Eq. (B.49) leads to

$$\begin{aligned}
& 2i\Psi_+^\dagger \boldsymbol{D}_+ \Psi_+ \\
=& \Psi_+^\dagger (m\beta - i\alpha^i \boldsymbol{D}_i)\frac{1}{2i\partial_-}(m\beta - i\alpha^i \boldsymbol{D}_i)\Psi_+ \\
=& \Psi_+^\dagger (m\beta - i\alpha^i \partial_i)\frac{1}{2i\partial_-}(m\beta - i\alpha^i \partial_i)\Psi_+ + g^2 \Psi_+^\dagger \alpha^i \boldsymbol{A}_i \frac{1}{2i\partial_-}\alpha^i \boldsymbol{A}_i \Psi_+ \\
& + g\Psi_+^\dagger \alpha^i \boldsymbol{A}_i \frac{1}{2i\partial_-}(m\beta - i\alpha^i \partial_i)\Psi_+ + g\Psi_+^\dagger (m\beta - i\alpha^i \partial_i)\frac{1}{2i\partial_-}\alpha^i \boldsymbol{A}_i \Psi_+ \\
=& \Psi_+^\dagger (m\beta - i\alpha^i \partial_i)\frac{1}{2i\partial_-}(m\beta - i\alpha^i \partial_i)\Psi_+ + g^2 \Psi_+^\dagger \alpha^i \boldsymbol{A}_i \frac{1}{2i\partial_-}\alpha^i \boldsymbol{A}_i \Psi_+ + g\Psi_+^\dagger \alpha^i \boldsymbol{A}_i \tilde{\Psi}_- + g\tilde{\Psi}_-^\dagger \alpha^i \boldsymbol{A}_i \Psi_+ \\
=& \tilde{\Psi}_+^\dagger (m\beta - i\alpha^i \partial_i)\frac{1}{2i\partial_-}(m\beta - i\alpha^i \partial_i)\tilde{\Psi}_+ + g^2 \tilde{\Psi}_+^\dagger \alpha^i \boldsymbol{A}_i \frac{1}{2i\partial_-}\alpha^i \boldsymbol{A}_i \tilde{\Psi}_+ + g\tilde{\Psi}_+^\dagger \alpha^i \boldsymbol{A}_i \tilde{\Psi}_- + g\tilde{\Psi}_-^\dagger \alpha^i \boldsymbol{A}_i \tilde{\Psi}_+ \ .
\end{aligned} \tag{B.27}$$

The first term reads,

$$\begin{aligned}
\tilde{\Psi}_+^\dagger (m\beta - i\alpha^i \partial_i)\frac{1}{2i\partial_-}(m\beta - i\alpha^j \partial_j)\tilde{\Psi}_+ =& \tilde{\Psi}^\dagger \Lambda_+ (m\beta - i\alpha^i \partial_i)\frac{1}{2i\partial_-}(m\beta - i\alpha^j \partial_j)\Lambda_+ \tilde{\Psi} \\
=& \tilde{\Psi}^\dagger \Lambda_+ (m\beta - i\alpha^i \partial_i)\frac{1}{2i\partial_-}\Lambda_- (m\beta - i\alpha^j \partial_j)\tilde{\Psi} \\
=& \tilde{\Psi}^\dagger \Lambda_+ \Lambda_+ (m\beta - i\alpha^i \partial_i)\frac{1}{2i\partial_-}(m\beta - i\alpha^j \partial_j)\tilde{\Psi} \\
=& \tilde{\Psi}^\dagger \frac{1}{2}\gamma^0\gamma^+ (m\beta - i\alpha^i \partial_i)\frac{1}{2i\partial_-}(m\beta - i\alpha^j \partial_j)\tilde{\Psi} \\
=& \frac{1}{2}\bar{\tilde{\Psi}}\gamma^+ (m\beta - i\alpha^i \partial_i)\frac{1}{2i\partial_-}(m\beta - i\alpha^j \partial_j)\tilde{\Psi} \\
=& \frac{1}{2}\bar{\tilde{\Psi}}\gamma^+ (m + i\gamma^i \partial_i)\frac{(\gamma^0)^2}{2i\partial_-}(m - i\gamma^j \partial_j)\tilde{\Psi} \\
=& \frac{1}{2}\bar{\tilde{\Psi}}\gamma^+ \frac{m^2 - \nabla_\perp^2}{2i\partial_-}\tilde{\Psi} \ .
\end{aligned} \tag{B.28}$$

www.manaraa.com

The second term reads,

$$g^2\tilde{\Psi}_+^\dagger\alpha^i\boldsymbol{A}_i\frac{1}{2i\partial_-}\alpha^j\boldsymbol{A}_j\tilde{\Psi}_+ = \frac{g^2}{2}\bar{\tilde{\Psi}}\gamma^+\gamma^0\gamma^i\boldsymbol{A}_i\frac{1}{2i\partial_-}\gamma^0\gamma^j\boldsymbol{A}_j\tilde{\Psi} = \frac{g^2}{2}\bar{\tilde{\Psi}}\gamma^i\boldsymbol{A}_i\frac{\gamma^+}{2i\partial_-}\gamma^j\boldsymbol{A}_j\tilde{\Psi}\ . \tag{B.29}$$

The last two terms combine into

$$g\tilde{\Psi}_+^\dagger\alpha^i\boldsymbol{A}_i\tilde{\Psi}_- + g\tilde{\Psi}_-^\dagger\alpha^i\boldsymbol{A}_i\tilde{\Psi}_+ = g(\tilde{\Psi}_+^\dagger+\tilde{\Psi}_-)\alpha^i\boldsymbol{A}_i(\tilde{\Psi}_+^\dagger+\tilde{\Psi}_-) = g\tilde{\Psi}^\dagger\alpha^i\boldsymbol{A}_i\tilde{\Psi} = g\bar{\tilde{\Psi}}\gamma^i\boldsymbol{A}_i\tilde{\Psi}\ . \tag{B.30}$$

We can also define the current density of free fields solution $\tilde{J}_a^\mu$ in analogy to J_a^μ, and notice that their "+" components are the same,

$$\begin{aligned} J_s^+ =& f^{sac}F_a^{+\mu}A_\mu^c + \overline{\Psi}\gamma^+T^s\Psi = f^{sac}\partial^+A_a^\mu A_\mu^c + \overline{\Psi}\gamma^+T^s\Psi \\ =& f^{sac}\partial^+A_a^iA_i^c + \overline{\Psi}\gamma^+T^s\Psi = f^{sac}\partial^+\tilde{A}_a^i\tilde{A}_i^c + \bar{\tilde{\Psi}}\gamma^+T^s\tilde{\Psi} = \tilde{J}_s^+\ . \end{aligned} \tag{B.31}$$

Let us also introduce the fermion current $\tilde{j}_a^\mu \equiv \bar{\tilde{\Psi}}\gamma^\mu T^a\tilde{\Psi}$ as part of the total current $\tilde{J}_a^\mu$. By substituting Eqs. (B.23) to (B.31) into Eq. (B.22), and with $\tilde{A}^i = A^i$, we finally get the front form Hamiltonian,

$$\begin{aligned} P_{QCD}^- = \int \mathrm{d}x^-\,\mathrm{d}^2x_\perp\ & -\frac{1}{2}\tilde{A}_a^j(i\nabla_\perp)^2\tilde{A}_j^a + \frac{1}{2}\bar{\tilde{\Psi}}\gamma^+\frac{m^2-\nabla_\perp^2}{i\partial^+}\tilde{\Psi} \\ & - gf^{abc}\partial^i\tilde{A}_a^j\tilde{A}_i^b\tilde{A}_j^c + g\tilde{J}_a^+\tilde{A}_+^a + g\bar{\tilde{\Psi}}\gamma^i\tilde{\boldsymbol{A}}_i\tilde{\Psi} \\ & - \frac{1}{2}g^2\tilde{J}_a^+\frac{1}{(\partial^+)^2}\tilde{J}_a^+ + \frac{g^2}{4}f^{abc}\tilde{A}_b^i\tilde{A}_c^jf^{aef}\tilde{A}_i^e\tilde{A}_j^f \\ & + \frac{g^2}{2}\bar{\tilde{\Psi}}\gamma^i\tilde{\boldsymbol{A}}_i\frac{\gamma^+}{i\partial^+}\gamma^j\tilde{\boldsymbol{A}}_j\tilde{\Psi}\ . \end{aligned} \tag{B.32}$$

The two terms in the first line are the kinetic energy for the gauge field and the fermion respectively. The three terms in the second line can be written collectively as $g\tilde{J}_a^\mu\tilde{A}_\mu^a$, which include the three-gluon-interaction, the gluon emission and quark-antiquark-pair-production processes. The two terms in the third line are the instantaneous-gluon-interaction and the four-gluon-interaction respectively. The last line contains the instantaneous-fermion-interaction. Note that in Eq. (1.9) of Section 1.3, we dropped the tilde on all variables to have a cleaner notation.

B.2 The light-front QCD Hamiltonian with a background field

In the presence of the background field $\mathcal{A}^\mu$, one should replace the gauge field $\boldsymbol{A}^\mu$ by $\boldsymbol{A}^\mu + \mathcal{A}^\mu$ in the Lagrangian. By doing so, we take into account the kinetic term for the background and its interaction with

www.manaraa.com

the gluon field. The Lagrangian density for QCD with the background field $\mathcal{A}^\mu$ can be written explicitly as below,

$$\mathcal{L} = -\frac{1}{4}F^{\mu\nu}{}_a F^a_{\mu\nu} + \frac{1}{2}[\overline{\Psi}(i\gamma^\mu(\partial_\mu + ig\boldsymbol{C}_\mu) - m)\Psi + \overline{\Psi}(-i\gamma^\mu(\overleftarrow{\partial}_\mu - ig\boldsymbol{C}_\mu) - m)\Psi] \,, \tag{B.33}$$

where $F^{\mu\nu}_a \equiv \partial^\mu C^\nu_a - \partial^\nu C^\mu_a - g f^{abc} C^\mu_b C^\nu_c$ and $\boldsymbol{C}^\mu = \boldsymbol{A}^\mu + \mathcal{A}^\mu$. The variational derivatives are now

$$\frac{\delta\mathcal{L}}{\delta A^s_\kappa} = -\frac{1}{4}F^{\kappa\mu}_a(-gf^{asc}C^c_\mu)\times 4 + \overline{\Psi}(i\gamma^\kappa(igT^s))\Psi = -gf^{sac}F^{\kappa\mu}_a C^c_\mu - g\overline{\Psi}\gamma^\kappa T^s\Psi \,, \qquad \Pi^\lambda_{A^s_\kappa} = -F^{\lambda\kappa}_s \,, \tag{B.34}$$

$$\frac{\delta\mathcal{L}}{\delta\Psi} = -g\overline{\Psi}\gamma^\mu C_\mu - m\overline{\Psi} - \frac{i}{2}\overline{\Psi}\gamma^\mu\overleftarrow{\partial}_\mu, \quad \Pi^\lambda_\Psi = \frac{i}{2}\overline{\Psi}\gamma^\lambda, \quad \Pi^\lambda_{\overline{\Psi}} = \frac{i}{2}\gamma^\lambda\Psi \,. \tag{B.35}$$

The first four equations of motion give the color-Maxwell equations,

$$\partial_\lambda F^{\lambda\kappa}_s = gJ^\kappa_s \,, \tag{B.36}$$

with the current density $J^\kappa_s \equiv f^{sac}F^{\kappa\mu}_a C^c_\mu + \overline{\Psi}\gamma^\kappa T^s\Psi$. In the light-cone gauge of $A^+_a = \mathcal{A}^+_a = 0$, the $\kappa = +$ component of Eq. (B.36) does not contain time derivatives, and can be written as

$$gJ^+_a = \partial_\lambda F^{\lambda+}_a = -\partial^+\partial_- C^-_a - \partial^+\partial_i C^i_a \,. \tag{B.37}$$

By disregarding the zero modes [151], one inverts the equation to

$$\frac{1}{2}A^-_a = -g\frac{1}{(\partial^+)^2}J^+_a - \frac{1}{\partial^+}\partial_i C^i_a - \frac{1}{2}\mathcal{A}^-_a \,. \tag{B.38}$$

We define the free solution $\tilde{A}^\mu_a$ such that $\lim_{g\to 0} A^\mu_a = \tilde{A}^\mu_a$. According to Eq. (B.38), the free field reads,

$$\tilde{A}^\mu_a = (0, \tilde{A}^-_a, A^i_a), \quad \text{with } \frac{1}{2}\tilde{A}^-_a \equiv \frac{1}{2}A^-_a + g\frac{1}{(\partial^+)^2}J^+_a = -\frac{1}{\partial^+}\partial_i C^i_a - \frac{1}{2}\mathcal{A}^-_a \,. \tag{B.39}$$

$\tilde{A}^\mu_a$ is thereby purely transverse.

The second group of equation of motions give the adjoint color-Dirac equation,

$$\overline{\Psi}[i\gamma^\mu(\overleftarrow{\partial}_\mu - ig\boldsymbol{C}_\mu) + m] = 0 \,. \tag{B.40}$$

Take Hermitian conjugate on the equation and use the relation $\overline{\Psi} = \Psi^\dagger\gamma^0$, we have

$$[-i\gamma^{\mu\dagger}(\partial_\mu + ig\boldsymbol{C}_\mu) + m]\gamma^0\Psi = 0 \,. \tag{B.41}$$

www.manaraa.com

By moving γ^0 to the left, we arrive at the color-Dirac equation,

$$[i\gamma^\mu(\partial_\mu + ig\boldsymbol{C}_\mu) - m]\Psi = 0 \,. \tag{B.42}$$

We now separate the dynamical component of the fermion field. First multiply Eq. (B.42) by γ^0 on the left,

$$\begin{gathered}[i(\gamma^0\gamma^+\boldsymbol{D}_+ + \gamma^0\gamma^-\boldsymbol{D}_- + \alpha^i\boldsymbol{D}_i) - m\beta]\Psi = 0 \,, \\ \text{which is,}\ \ [i(2\Lambda^+\boldsymbol{D}_+ + 2\Lambda^-\boldsymbol{D}_- + \alpha^i\boldsymbol{D}_i) - m\beta]\Psi = 0 \,.\end{gathered} \tag{B.43}$$

Then multiply the equation by $\Lambda^+(\Lambda^-)$ on the left, and bring it to the right,

$$[i(2\boldsymbol{D}_\pm\Lambda^\pm + \alpha^i\boldsymbol{D}_i\Lambda^\mp) - m\beta\Lambda^\mp]\Psi = 0 \,. \tag{B.44}$$

One thereby obtains a coupled set of spinor equations,

$$2i\partial_+\Psi_+ = (-i\alpha^i\boldsymbol{D}_i + m\beta)\Psi_- + 2g\boldsymbol{C}_+\Psi_+ \,, \tag{B.45}$$

$$2i\partial_-\Psi_- = (-i\alpha^i\boldsymbol{D}_i + m\beta)\Psi_+ + 2g\boldsymbol{C}_-\Psi_- \,. \tag{B.46}$$

Eq. (B.46) does not contain time derivatives, and can be written as a constraint relation,

$$\Psi_- = \frac{1}{2i\partial_-}(m\beta - i\alpha^i\boldsymbol{D}_i)\Psi_+ \,. \tag{B.47}$$

Note that we already have the background field in light-cone gauge, i.e. $\mathcal{A}_a^+ = 0$. By substituting Eq. (B.47) into Eq. (B.45), we get

$$2iD_+\Psi_+ = (m\beta - i\alpha^i\boldsymbol{D}_i)\frac{1}{2i\partial_-}(m\beta - i\alpha^i\boldsymbol{D}_i)\Psi_+ \,. \tag{B.48}$$

In analogy to the free solution $\tilde{A}$, we define the free spinor $\tilde{\Psi} = \tilde{\Psi}_+ + \tilde{\Psi}_-$ with

$$\tilde{\Psi}_+ = \Psi_+, \quad \tilde{\Psi}_- = \frac{1}{2i\partial_-}(m\beta - i\alpha^i\partial_i)\Psi_+ \,. \tag{B.49}$$

It is also easy to see that $\tilde{\Psi}_\pm = \Lambda^\pm\tilde{\Psi}$.

One can then construct the Hamiltonian density through a Legendre transformation, as in Eq. (B.19).

$$\mathcal{P}_+ = -F_s^{+\kappa}\partial_+A_\kappa^s + \frac{i}{2}[\overline{\Psi}\gamma^+\partial_+\Psi + h.c.] + \frac{1}{4}F^{\mu\nu}{}_aF^a_{\mu\nu} \,. \tag{B.50}$$

www.manaraa.com

The difference is that the field tensor, $F^{\mu\nu}$, now also contains the background field. It is then convenient to add a total derivative $-\partial_\kappa(F_s^{\kappa+}C_+^s)$ to the Hamiltonian,

$$\begin{aligned} P^- =& 2\int \mathrm{d}x_+\,\mathrm{d}^2x_\perp\,\mathcal{P}_+ \\ =& \int \mathrm{d}x^-\,\mathrm{d}^2x_\perp\; -F_s^{+\kappa}\partial_+A_\kappa^s + \frac{i}{2}[\overline{\Psi}\gamma^+\partial_+\Psi + h.c.] + \frac{1}{4}F^{\mu\nu}{}_aF^a_{\mu\nu} - \partial_\kappa(F_s^{\kappa+}C_+^s)\,. \end{aligned} \tag{B.51}$$

We can rewrite the first and the last term into

$$\begin{aligned} & F_s^{\kappa+}\partial_+A_\kappa^s - \partial_\kappa(F_s^{\kappa+}C_+^s) \\ =& F_s^{\kappa+}\partial_+A_\kappa^s - (\partial_\kappa F_s^{\kappa+})C_+^s - F_s^{\kappa+}\partial_\kappa C_+^s \\ =& F_s^{\kappa+}(\partial_+A_\kappa^s - \partial_\kappa C_+^s) - (\partial_\kappa F_s^{\kappa+})C_+^s \\ =& -F_s^{\kappa+}(F_{\kappa+}^s + gf^{sbc}C_\kappa^bC_+^c + \partial_+\mathcal{A}_\kappa^s) - gJ_s^+C_+^s \\ =& -F_s^{\kappa+}F_{\kappa+}^s - gF_s^{\kappa+}f^{sbc}C_\kappa^bC_+^c - F_s^{\kappa+}\partial_+\mathcal{A}_\kappa^s - gJ_s^+C_+^s \\ =& -F_s^{\kappa+}F_{\kappa+}^s - gF_s^{\kappa+}f^{sbc}C_\kappa^bC_+^c - F_s^{\kappa+}\partial_+\mathcal{A}_\kappa^s - g(f^{sac}F_a^{+\mu}C_\mu^c + \overline{\Psi}\gamma^+T^s\Psi)C_+^s \\ =& -F_s^{\kappa+}F_{\kappa+}^s - g\overline{\Psi}\gamma^+T^sC_+^s\Psi - F_s^{\kappa+}\partial_+\mathcal{A}_\kappa^s\,. \end{aligned} \tag{B.52}$$

The last term $-F_s^{\kappa+}\partial_+\mathcal{A}_\kappa^s = \partial^+C_s^i\partial_+\mathcal{A}_i^s$ should cancel under the integral $\int \mathrm{d}x^-$ if both fields A_s^i and $\mathcal{A}_s^i$ vanish on the boundaries of $x^- \to \pm\infty$. The Hamiltonian then becomes

$$\begin{aligned} P^- =& \int \mathrm{d}x^-\,\mathrm{d}^2x_\perp\,\frac{1}{4}F^{\mu\nu}{}_aF^a_{\mu\nu} - F_s^{\kappa+}F_{\kappa+}^s - g\overline{\Psi}\gamma^+T^sC_+^s\Psi + \frac{i}{2}[\overline{\Psi}\gamma^+\partial_+\Psi + h.c.] \\ =& \int \mathrm{d}x^-\,\mathrm{d}^2x_\perp\,\frac{1}{4}F^{\mu\nu}{}_aF^a_{\mu\nu} - F_s^{\kappa+}F_{\kappa+}^s + \frac{i}{2}[\overline{\Psi}\gamma^+\boldsymbol{D}_+\Psi + h.c.]\,. \end{aligned} \tag{B.53}$$

The color-electro-magnetic energy density could be written as $\frac{1}{4}F_a^{\mu\nu}F^a_{\mu\nu} - F_a^{\mu+}F^a_{\mu+} = \frac{1}{4}F_a^{ij}F^a_{ij} - \frac{1}{2}F_a^{+-}F^a_{+-}$ according to Eq. (B.23). Substituting A_a^- by Eq. (B.38), the color-electric part becomes,

$$\begin{aligned} F_a^{+-}F^a_{+-} =& -\partial^+C_a^-\partial_-C_+^a \\ =& -\frac{1}{4}\partial^+C_a^-\partial^+C_a^- \\ =& -(-g\frac{1}{\partial^+}J_a^+ - \partial_iC_a^i)^2 \\ =& -g^2\frac{1}{\partial^+}J_a^+\frac{1}{\partial^+}J_a^+ - (\partial_iC_a^i)^2 - 2g\frac{1}{\partial^+}J_a^+\partial_iC_a^i \\ =& g^2J_a^+\frac{1}{(\partial^+)^2}J_a^+ - (\partial_iC_a^i)^2 - gJ_a^+\tilde{A}_a^- - gJ_a^+\mathcal{A}_a^-\,. \end{aligned} \tag{B.54}$$

www.manaraa.com

Note that in deriving the last line, we introduced an extra term $-g^2\frac{1}{\partial^+}(J_a^+\frac{1}{\partial^+}J_a^+)$, and it should vanish under the integral of $\int \mathrm{d}x^-$ in the Hamiltonian. Similar to Eq. (B.25), the color-magnetic part can be written as

$$F_a^{ij}F_{ij}^a = 2C_a^j\nabla_\perp^2 C_j^a - 2(\partial_j C_a^j \partial^i C_i^a) - 4gf^{abc}\partial^i C_a^j C_i^b C_j^c + g^2 f^{abc}C_b^i C_c^j f^{aef} C_i^e C_j^f \ . \tag{B.55}$$

For the spinor terms, we have

$$g\overline{\Psi}\gamma^+ T^s \mathcal{A}_+^s \Psi = 2g\Psi_+^\dagger T^s \mathcal{A}_+^s \Psi_+ = 2g\tilde{\Psi}_+^\dagger \boldsymbol{\mathcal{A}}_+ \tilde{\Psi}_+ = g\bar{\tilde{\Psi}}\gamma^+ \boldsymbol{\mathcal{A}}_+ \tilde{\Psi} \ , \tag{B.56}$$

and

$$i\overline{\Psi}\gamma^+ \boldsymbol{D}_+ \Psi = i\Psi^\dagger\gamma^0\gamma^+ \boldsymbol{D}_+ \Psi = 2i\Psi^\dagger\Lambda^+ \boldsymbol{D}_+ \Psi = 2i\Psi^\dagger\Lambda^+ \boldsymbol{D}_+ \Lambda^+\Psi = 2i\Psi_+^\dagger \boldsymbol{D}_+ \Psi_+ \ . \tag{B.57}$$

Substitution of the time derivative in Eq. (B.48) and the free spinors defined in Eq. (B.49) leads to

$$\begin{aligned}
&2i\Psi_+^\dagger \boldsymbol{D}_+ \Psi_+ \\
=&\Psi_+^\dagger (m\beta - i\alpha^i \boldsymbol{D}_i)\frac{1}{2i\partial_-}(m\beta - i\alpha^i \boldsymbol{D}_i)\Psi_+ \\
=&\Psi_+^\dagger (m\beta - i\alpha^i \partial_i)\frac{1}{2i\partial_-}(m\beta - i\alpha^i \partial_i)\Psi_+ + g^2\Psi_+^\dagger \alpha^i \boldsymbol{C}_i \frac{1}{2i\partial_-}\alpha^i \boldsymbol{C}_i \Psi_+ \\
&+ g\Psi_+^\dagger \alpha^i \boldsymbol{C}_i \frac{1}{2i\partial_-}(m\beta - i\alpha^i \partial_i)\Psi_+ + g\Psi_+^\dagger (m\beta - i\alpha^i \partial_i)\frac{1}{2i\partial_-}\alpha^i \boldsymbol{C}_i \Psi_+ \\
=&\Psi_+^\dagger (m\beta - i\alpha^i \partial_i)\frac{1}{2i\partial_-}(m\beta - i\alpha^i \partial_i)\Psi_+ + g^2\Psi_+^\dagger \alpha^i \boldsymbol{C}_i \frac{1}{2i\partial_-}\alpha^i \boldsymbol{C}_i \Psi_+ + g\Psi_+^\dagger \alpha^i \boldsymbol{C}_i \tilde{\Psi}_- + g\tilde{\Psi}_-^\dagger \alpha^i \boldsymbol{C}_i \Psi_+ \\
=&\tilde{\Psi}_+^\dagger (m\beta - i\alpha^i \partial_i)\frac{1}{2i\partial_-}(m\beta - i\alpha^i \partial_i)\tilde{\Psi}_+ + g^2\tilde{\Psi}_+^\dagger \alpha^i \boldsymbol{C}_i \frac{1}{2i\partial_-}\alpha^i \boldsymbol{C}_i \tilde{\Psi}_+ + g\tilde{\Psi}_+^\dagger \alpha^i \boldsymbol{C}_i \tilde{\Psi}_- + g\tilde{\Psi}_-^\dagger \alpha^i \boldsymbol{C}_i \tilde{\Psi}_+ \ .
\end{aligned} \tag{B.58}$$

The first term reads,

$$\begin{aligned}
\tilde{\Psi}_+^\dagger (m\beta - i\alpha^i \partial_i)\frac{1}{2i\partial_-}(m\beta - i\alpha^j \partial_j)\tilde{\Psi}_+ =&\tilde{\Psi}^\dagger \Lambda_+ (m\beta - i\alpha^i \partial_i)\frac{1}{2i\partial_-}(m\beta - i\alpha^j \partial_j)\Lambda_+ \tilde{\Psi} \\
=&\tilde{\Psi}^\dagger \Lambda_+ (m\beta - i\alpha^i \partial_i)\frac{1}{2i\partial_-}\Lambda_- (m\beta - i\alpha^j \partial_j)\tilde{\Psi} \\
=&\tilde{\Psi}^\dagger \Lambda_+ \Lambda_+ (m\beta - i\alpha^i \partial_i)\frac{1}{2i\partial_-}(m\beta - i\alpha^j \partial_j)\tilde{\Psi} \\
=&\tilde{\Psi}^\dagger \frac{1}{2}\gamma^0\gamma^+ (m\beta - i\alpha^i \partial_i)\frac{1}{2i\partial_-}(m\beta - i\alpha^j \partial_j)\tilde{\Psi} \\
=&\frac{1}{2}\bar{\tilde{\Psi}}\gamma^+ (m\beta - i\alpha^i \partial_i)\frac{1}{2i\partial_-}(m\beta - i\alpha^j \partial_j)\tilde{\Psi} \\
=&\frac{1}{2}\bar{\tilde{\Psi}}\gamma^+ (m + i\gamma^i \partial_i)\frac{(\gamma^0)^2}{2i\partial_-}(m - i\gamma^j \partial_j)\tilde{\Psi} \\
=&\frac{1}{2}\bar{\tilde{\Psi}}\gamma^+ \frac{m^2 - \nabla_\perp^2}{2i\partial_-}\tilde{\Psi} \ .
\end{aligned} \tag{B.59}$$

www.manaraa.com

The second term reads,

$$g^2\tilde{\Psi}_+^\dagger\alpha^i\boldsymbol{C}_i\frac{1}{2i\partial_-}\alpha^j\boldsymbol{C}_j\tilde{\Psi}_+ = \frac{g^2}{2}\bar{\tilde{\Psi}}\gamma^+\gamma^0\gamma^i\boldsymbol{C}_i\frac{1}{2i\partial_-}\gamma^0\gamma^j\boldsymbol{C}_j\tilde{\Psi} = \frac{g^2}{2}\bar{\tilde{\Psi}}\gamma^i\boldsymbol{C}_i\frac{\gamma^+}{2i\partial_-}\gamma^j\boldsymbol{C}_j\tilde{\Psi}\ . \tag{B.60}$$

The last two terms combine into

$$g\tilde{\Psi}_+^\dagger\alpha^i\boldsymbol{C}_i\tilde{\Psi}_- + g\tilde{\Psi}_-^\dagger\alpha^i\boldsymbol{C}_i\tilde{\Psi}_+ = g(\tilde{\Psi}_+^\dagger + \tilde{\Psi}_-)\alpha^i\boldsymbol{C}_i(\tilde{\Psi}_+^\dagger + \tilde{\Psi}_-) = g\tilde{\Psi}^\dagger\alpha^i\boldsymbol{C}_i\tilde{\Psi} = g\bar{\tilde{\Psi}}\gamma^i\boldsymbol{C}_i\tilde{\Psi}\ . \tag{B.61}$$

Define the current density of free fields solution $\tilde{J}_a^\mu$ in analogy to J_a^μ, and notice that their "+" components are the same,

$$\begin{aligned} J_s^+ =& f^{sac}F_a^{+\mu}A_\mu^c + \overline{\Psi}\gamma^+T^s\Psi = f^{sac}\partial^+A_a^\mu A_\mu^c + \overline{\Psi}\gamma^+T^s\Psi \\ =& f^{sac}\partial^+A_a^iA_i^c + \overline{\Psi}\gamma^+T^s\Psi = f^{sac}\partial^+\tilde{A}_a^i\tilde{A}_i^c + \bar{\tilde{\Psi}}\gamma^+T^s\tilde{\Psi} = \tilde{J}_s^+\ . \end{aligned} \tag{B.62}$$

Define the current density of free fields solution $\tilde{J}_a^\mu$ in analogy to J_a^μ, and notice that their "+" components are the same,

$$J_s^+ = f^{sac}F_a^{+\mu}C_\mu^c + \overline{\Psi}\gamma^+T^s\Psi = f^{sac}\partial^+C_a^iC_i^c + \bar{\tilde{\Psi}}\gamma^+T^s\tilde{\Psi} = \tilde{J}_s^+\ . \tag{B.63}$$

By substituting the above equations into Eq. (B.53), we finally get the front form Hamiltonian with the background field,

$$\begin{aligned} P^- = \int \mathrm{d}x^-\,\mathrm{d}^2x_\perp\ & -\frac{1}{2}C_a^j(i\nabla)_\perp^2C_j^a + \frac{1}{2}\bar{\tilde{\Psi}}\gamma^+\frac{m^2-\nabla_\perp^2}{2i\partial_-}\tilde{\Psi} \\ & - gf^{abc}\partial^iC_a^jC_i^bC_j^c + g\tilde{J}_a^+\tilde{A}_+^a + g\tilde{J}_a^+\mathcal{A}_+^a + g\bar{\tilde{\Psi}}\gamma^i\boldsymbol{C}_i\tilde{\Psi} \\ & - \frac{1}{2}g^2\tilde{J}_a^+\frac{1}{(\partial^+)^2}\tilde{J}_a^+ + \frac{g^2}{4}f^{abc}C_b^iC_c^jf^{aef}C_i^eC_j^f \\ & + \frac{g^2}{2}\bar{\tilde{\Psi}}\gamma^i\boldsymbol{C}_i\frac{\gamma^+}{2i\partial_-}\gamma^j\boldsymbol{C}_j\tilde{\Psi}\ . \end{aligned} \tag{B.64}$$

The two terms in the first line are the kinetic energy for the gauge field, the background field and the fermion. The four terms in the second line can be written collectively as $g\tilde{J}_a^\mu C_\mu^a$, which include the three-gluon-interaction, the gluon emission and quark-antiquark-pair-production processes. The two terms in the third line are the instantaneous-gluon-interaction and the four-gluon-interaction respectively. The last line contains the instantaneous-fermion-interaction. For each interaction involving the gluon field, it also involves the background field. In studying the evolution of a QCD system interacting with a background field,

www.manaraa.com

one usually neglect the kinetic energy of the background field. It is often convenient to do the calculation in the interaction picture, where we split the Hamiltonian into two parts, the full light-front QCD Hamiltonian P^-_{QCD} as in Eq. (B.32) and the interaction terms introduced by the background field $V_{int} = P^- - P^-_{QCD}$.

www.manaraa.com

APPENDIX C. THE BASIS FUNCTION REPRESENTATION

In Chapter 2, we adopt the light-front wavefunctions of the heavy quarkonia obtained in the BLFQ approach by Ref. [3] to calculate various observables. The wavefunctions are solved in a basis representation as in Eq. (C.1).

$$\psi^{(m_j)}_{\sigma_1,\sigma_2/h}(\vec{k}_\perp, x) = \sum_{n,m,l} \psi_h(n,m,l,\sigma_1,\sigma_2,m_j)\phi_{nm}(\vec{k}_\perp/\sqrt{x(1-x)})\chi_l(x)\ . \tag{C.1}$$

The transverse 2D harmonic oscillator (HO) function ϕ_{nm} is defined as

$$\phi_{nm}(\vec{k}_\perp;\kappa) = \kappa^{-1}\sqrt{\frac{4\pi n!}{(n+|m|)!}}\left(\frac{k^\perp}{\kappa}\right)^{|m|}\exp(-(k^\perp)^2/(2\kappa^2))L_n^{|m|}((k^\perp)^2/\kappa^2)\exp(im\theta)\ , \tag{C.2}$$

where $k^\perp = |\vec{k}_\perp|$ and $\theta = \arg k^\perp$. κ is the harmonic oscillator basis parameter in mass dimension. The orthonormality relation is

$$\int \frac{\mathrm{d}^2\vec{k}_\perp}{(2\pi)^2}\phi^*_{n'm'}(\vec{k}_\perp)\phi_{nm}(\vec{k}_\perp) = \delta_{nn'}\delta_{mm'}\ . \tag{C.3}$$

$k^R = k^x + ik^y$ ($k^L = k^x - ik^y$) is the complex representation of $\vec{k}_\perp(\vec{k}^*_\perp)$. The recurrence relations are

$$k^R\phi_{n,m}(\vec{k}_\perp) = \kappa\begin{cases}\sqrt{n+|m|+1}\phi_{n,m+1}(\vec{k}_\perp) - \theta(n-1)\sqrt{n}\phi_{n-1,m+1}(\vec{k}_\perp) & \text{if } m\geq 0\\ \sqrt{n+|m|}\phi_{n,m+1}(\vec{k}_\perp) - \sqrt{n+1}\phi_{n+1,m+1}(\vec{k}_\perp) & \text{if } m<0\end{cases} \tag{C.4}$$

$$k^L\phi_{n,m}(\vec{k}_\perp) = \kappa\begin{cases}\sqrt{n+|m|}\phi_{n,m-1}(\vec{k}_\perp) - \sqrt{n+1}\phi_{n+1,m-1}(\vec{k}_\perp) & \text{if } m>0\\ \sqrt{n+|m|+1}\phi_{n,m-1}(\vec{k}_\perp) - \theta(n-1)\sqrt{n}\phi_{n-1,m-1}(\vec{k}_\perp) & \text{if } m\leq 0\end{cases} \tag{C.5}$$

The Talmi-Moshinsky (TM) transformation [152] reads:

$$\phi_{n_1m_1}(\vec{p}_1;b_1)\phi_{n_2m_2}(\vec{p}_2;b_2) = \sum_{NMnm}\mathcal{M}^{NMnm}_{n_1m_1n_2-m_2}(b_2/b_1)\phi_{NM}(\vec{P};B)\phi_{nm}(\vec{p};b)\ , \tag{C.6}$$

where

$$\vec{P} = \vec{p}_1 + \vec{p}_2, \qquad \vec{p} = \frac{b_2^2}{b_1^2+b_2^2}\vec{p}_1 - \frac{b_1^2}{b_1^2+b_2^2}\vec{p}_2\ ,$$

www.manaraa.com

and

$$B = \sqrt{b_1^2 + b_2^2}, \qquad b = \frac{b_1 b_2}{\sqrt{b_1^2 + b_2^2}} .$$

The longitudinal basis function is

$$\chi_l(x) = \sqrt{4\pi(2l+\alpha+\beta+1)} \sqrt{\frac{\Gamma(l+1)\Gamma(l+\alpha+\beta+1)}{\Gamma(l+\alpha+1)\Gamma(l+\beta+1)}} x^{\beta/2}(1-x)^{\alpha/2} P_l^{(\alpha,\beta)}(2x-1) , \tag{C.7}$$

where $P_l^{(\alpha,\beta)}$ is the Jacobi polynomial. Its orthonormality relation is

$$\frac{1}{4\pi}\int_0^1 \mathrm{d}x \chi_l(x)\chi_{l'}(x) = \delta_{ll'} . \tag{C.8}$$

The hadron matrix element requires the evaluation of the convolution of two meson wavefunctions. The integrand of two meson wavefunctions reads as the following in the basis representation:

$$\begin{aligned}\psi^{(m_j)}_{s\bar{s}/h}(\vec{k}_\perp, x)\psi^{(m'_j)*}_{s'\bar{s}'/h'}(\vec{k}'_\perp, x') = &\sum_{n_1,m_1,l_1} \psi_h(n_1, m_1, l_1, s, \bar{s}, m_j)\phi_{n_1 m_1}(\vec{k}_\perp/\sqrt{x(1-x)})\chi_{l_1}(x) \\ &\times \sum_{n_2,m_2,l_2} \psi^*_{h'}(n_2, m_2, l_2, s', \bar{s}', m'_j)\phi_{n_2 m_2}(-\vec{k}'_\perp/\sqrt{x'(1-x')})\chi_{l_2}(x') .\end{aligned} \tag{C.9}$$

The integration in the transverse and longitudinal dimensions makes up the convolution. It is usually advantageous to carry out the transverse integral first since it can be performed analytically by applying the Talmi-Moshinsky transformation in Eq. (C.6). The remaining longitudinal integral could be performed numerically through Gaussian quadrature.

C.1 The transverse integral

For convenience, we define a generalized form of the transverse integral as $\Pi(t, x, z, \vec{\Delta}_\perp)$. Note that in general, some order (notated as t) of k^R (or k^L) could appear in the integrand. To simplify the expression, we also define $x_1 \equiv x'(1-x'), x_2 \equiv x(1-x)$ and $\vec{k}'_\perp = \vec{k}_\perp + \vec{l}_\perp$ ($\vec{l}_\perp \equiv (1-x)\vec{\Delta}_\perp$). The integral can be carried out by separating the overlapping momentum $\vec{k}_\perp$ and the transferred momentum $\vec{l}_\perp$. One can achieve such separation through a Talmi-Moshinsky transformation, and before that, one should operate a change of

www.manaraa.com

variables.

$$
\begin{aligned}
\Pi(t,x,z,\vec{\Delta}_\perp) \equiv & \int \frac{\mathrm{d}^2\vec{k}_\perp}{(2\pi)^2}(k^R)^t\phi_{n_1m_1}(\vec{k}_\perp/\sqrt{x_2})\phi_{n_2m_2}(-(\vec{k}_\perp+\vec{l}_\perp)/\sqrt{x_1}) \\
=&\left(\sqrt{\frac{x_1x_2}{x_1+x_2}}\right)^{t+2}\int\frac{\mathrm{d}^2\vec{k}_\perp}{(2\pi)^2}(k^R)^t\phi_{n_1m_1}(\sqrt{\frac{x_1}{x_1+x_2}}\vec{k}_\perp)\phi_{n_2m_2}(-\sqrt{\frac{x_2}{x_1+x_2}}\vec{k}_\perp-\frac{1}{\sqrt{x_1}}\vec{l}_\perp) \\
=&\left(\sqrt{\frac{x_1x_2}{x_1+x_2}}\right)^{t+2}\int\frac{\mathrm{d}^2\vec{k}_\perp}{(2\pi)^2}(k^R-\sqrt{\frac{x_2}{x_1(x_1+x_2)}}l^R)^t \\
&\times\phi_{n_1m_1}(\sqrt{\frac{x_1}{x_1+x_2}}\vec{k}_\perp-\frac{\sqrt{x_2}}{x_1+x_2}\vec{l}_\perp)\phi_{n_2m_2}(-\sqrt{\frac{x_2}{x_1+x_2}}\vec{k}_\perp-\frac{\sqrt{x_1}}{x_1+x_2}\vec{l}_\perp) \\
=&\left(\sqrt{\frac{x_1x_2}{x_1+x_2}}\right)^{t+2}\int\frac{\mathrm{d}^2\vec{k}_\perp}{(2\pi)^2}\sum_{s=0}^{t}\binom{t}{s}(k^R)^s(-\sqrt{\frac{x_2}{x_1(x_1+x_2)}}l^R)^{t-s} \\
&\times\phi_{n_1m_1}(\underbrace{\sqrt{\frac{x_1}{x_1+x_2}}\vec{k}_\perp-\frac{\sqrt{x_2}}{x_1+x_2}\vec{l}_\perp}_{\equiv\vec{p}_1})\phi_{n_2m_2}(\underbrace{-\sqrt{\frac{x_2}{x_1+x_2}}\vec{k}_\perp-\frac{\sqrt{x_1}}{x_1+x_2}\vec{l}_\perp}_{\equiv\vec{p}_2}) .
\end{aligned}
\tag{C.10}
$$

Note that I did not write out the scale parameter κ explicitly in the harmonic oscillators. In the electromagnetic process, the initial and final hadrons have the same κ. However, in the electroweak decay, the initial and final hadrons could have different κ's. In the derivation below, let us first take the latter case, which is more general, and then reduce the result to the former.

$$
\phi_{n_1m_1}(\vec{p}_1;\kappa_1)\phi_{n_2m_2}(\vec{p}_2;\kappa_2) = \sqrt{x_1x_2}\phi_{n_1m_1}(\sqrt{x_2}\vec{p}_1;\sqrt{x_2}\kappa_1)\phi_{n_2m_2}(\sqrt{x_1}\vec{p}_2;\sqrt{x_1}\kappa_2) \tag{C.11}
$$

Applying the TM transformation,

$$
\phi_{n_1m_1}(\sqrt{x_2}\vec{p}_1;\sqrt{x_2}\kappa_1)\phi_{n_2m_2}(\sqrt{x_1}\vec{p}_2;\sqrt{x_1}\kappa_2) = \sum_{NMnm}\mathcal{M}^{NMnm}_{n_1m_1n_2m_2}(\sqrt{x_1}\kappa_2/\sqrt{x_2}\kappa_1)\phi_{NM}(\vec{P};B)\phi_{nm}(\vec{p};b) , \tag{C.12}
$$

where

$$
\vec{P} = \sqrt{x_2}\vec{p}_1+\sqrt{x_1}\vec{p}_2 = -\vec{l}_\perp, \qquad B = \sqrt{x_2\kappa_1^2+x_1\kappa_2^2} ,
$$

and

$$
\vec{p} = \frac{x_1\kappa_2^2}{x_2\kappa_1^2+x_1\kappa_2^2}\sqrt{x_2}\vec{p}_1-\frac{x_2\kappa_1^2}{x_2\kappa_1^2+x_1\kappa_2^2}\sqrt{x_1}\vec{p}_2 = \sqrt{\frac{x_1x_2}{x_1+x_2}}\vec{k}_\perp+\frac{x_1x_2(\kappa_1^2-\kappa_2^2)}{(x_1+x_2)(x_2\kappa_1^2+x_1\kappa_2^2)}\vec{l}_\perp, \qquad b = \frac{\sqrt{x_1x_2}\kappa_1\kappa_2}{\sqrt{x_2\kappa_1^2+x_1\kappa_2^2}} .
$$

www.manaraa.com

In the case where $\kappa_1 = \kappa_2 = \kappa$, one can consider rewriting the two harmonic oscillators after the transformation on the same mass scale. This would be beneficial to the calculations in practice, where one only needs to define the harmonic oscillator functions with one value of κ.

$$\begin{aligned}\phi_{NM}(\vec{P};B)\phi_{nm}(\vec{p};b) =&\phi_{NM}(-\vec{l}_\perp;\ \sqrt{x_2+x_1}\kappa)\phi_{nm}(\sqrt{\frac{x_1x_2}{x_1+x_2}}\vec{k}_\perp;\ \sqrt{\frac{x_1x_2}{x_1+x_2}}\kappa)\\ =&\phi_{NM}(-\frac{\vec{l}_\perp}{\sqrt{x_2+x_1}};\kappa)\frac{1}{\sqrt{x_2+x_1}}\phi_{nm}(\vec{k}_\perp;\kappa)\sqrt{\frac{x_1+x_2}{x_1x_2}}\end{aligned} \tag{C.13}$$

Back to Eqs. (C.11) and (C.12), we have

$$\phi_{n_1m_1}(\vec{p}_1;\kappa)\phi_{n_2m_2}(\vec{p}_2;\kappa) = \sum_{NMnm}\mathcal{M}^{NMnm}_{n_1m_1n_2m_2}(\sqrt{x_1}/\sqrt{x_2})\phi_{NM}(-\frac{\vec{l}_\perp}{\sqrt{x_2+x_1}};\kappa)\phi_{nm}(\vec{k}_\perp;\kappa)\ . \tag{C.14}$$

Now we have successfully separated the overlapping momentum $\vec{k}_\perp$ and the transferred momentum $\vec{l}_\perp$,

$$\begin{aligned}\Pi(t,x,z,\vec{\Delta}_\perp) =&\left(\sqrt{\frac{x_1x_2}{x_1+x_2}}\right)^{t+2}\int\frac{\mathrm{d}^2\vec{k}_\perp}{(2\pi)^2}\sum_{s=0}^{t}\binom{t}{s}(k^R)^s(-\sqrt{\frac{x_2}{x_1(x_1+x_2)}}l^R)^{t-s}\sum_{NMnm}\mathcal{M}^{NMnm}_{n_1m_1n_2m_2}(\sqrt{x_1}/\sqrt{x_2})\\ &\times\phi_{NM}(-\frac{\vec{l}_\perp}{\sqrt{x_2+x_1}})\phi_{nm}(\vec{k}_\perp)\ .\end{aligned} \tag{C.15}$$

The integral over one 2D-HO function could be carried out directly,

$$\int\frac{\mathrm{d}^2\vec{k}_\perp}{(2\pi)^2}(k^R)^s\phi_{nm}(\vec{k}_\perp) = (-1)^n2^s\kappa^{s+1}\sqrt{\frac{(n+s)!}{\pi n!}}\delta_{m+s,0}\ . \tag{C.16}$$

$$\begin{aligned}\Pi(t,x,z,\vec{\Delta}_\perp) =&\left(\sqrt{\frac{x_1x_2}{x_1+x_2}}\right)^{t+2}\sum_{s=0}^{t}\binom{t}{s}(-\sqrt{\frac{x_2}{x_1(x_1+x_2)}}l^R)^{t-s}\sum_{Nnm}\mathcal{M}^{NMn-s}_{n_1m_1n_2m_2}(\sqrt{x_1}/\sqrt{x_2})\\ &\times\phi_{NM}(-\frac{1}{\sqrt{x_1+x_2}}\vec{l}_\perp)(-1)^n2^s\kappa^{s+1}\sqrt{\frac{(n+s)!}{\pi n!}}\ .\end{aligned} \tag{C.17}$$

In most cases of the hadron matrix elements, $t = 0, 1$,

$$\Pi(0,x,z,\vec{\Delta}_\perp) =\frac{x_1x_2}{x_1+x_2}\sum_{Nnm}\mathcal{M}^{NMn0}_{n_1m_1n_2m_2}(x_1,x_2)\phi_{NM}(-\frac{1}{\sqrt{x_1+x_2}}\vec{l}_\perp)(-1)^n\frac{\kappa}{\sqrt{\pi}}\ . \tag{C.18}$$

$$\begin{aligned}\Pi(1,x,z,\vec{\Delta}_\perp) =&-\frac{x_2}{x_1+x_2}l^R\Pi(0,x,z,\vec{l}_\perp)\\ &+\left(\sqrt{\frac{x_1x_2}{x_1+x_2}}\right)^3\sum_{Nnm}\mathcal{M}^{NMn-1}_{n_1m_1n_2m_2}(x_1,x_2)\phi_{NM}(-\frac{1}{\sqrt{x_1+x_2}}\vec{l}_\perp)(-1)^n\kappa^2\sqrt{\frac{(n+1)}{\pi}}\ .\end{aligned} \tag{C.19}$$

www.manaraa.com

Alternatively, one could perform the TM transformation by letting $\vec{p}_\perp$ carrying the transferred momentum. Starting from Eq. (C.10),

$$\begin{aligned}\Pi(t,x,z,\vec{\Delta}_\perp) \equiv& \int \frac{\mathrm{d}^2\vec{k}_\perp}{(2\pi)^2}(k^R)^t\phi_{n_1m_1}(\vec{k}_\perp/\sqrt{x_2})\phi_{n_2-m_2}((\vec{k}_\perp+\vec{l}_\perp)/\sqrt{x_1}) \\ =&\left(\sqrt{\frac{x_1x_2}{x_1+x_2}}\right)^{t+2}\int\frac{\mathrm{d}^2\vec{k}_\perp}{(2\pi)^2}\sum_{s=0}^{t}\binom{t}{s}(k^R)^s(-\sqrt{\frac{x_2}{x_1(x_1+x_2)}}l^R)^{t-s} \\ &\times\phi_{n_1m_1}(\underbrace{\sqrt{\frac{x_1}{x_1+x_2}}\vec{k}_\perp-\frac{\sqrt{x_2}}{x_1+x_2}\vec{l}_\perp}_{\equiv\vec{p}_1})\phi_{n_2-m_2}(\underbrace{\sqrt{\frac{x_2}{x_1+x_2}}\vec{k}_\perp+\frac{\sqrt{x_1}}{x_1+x_2}\vec{l}_\perp}_{\equiv\vec{p}_2}).\end{aligned} \tag{C.20}$$

As in the previous derivation, I restore the κ's in the 2D-HOs for generality.

$$\phi_{n_1m_1}(\vec{p}_1;\kappa_1)\phi_{n_2-m_2}(\vec{p}_2;\kappa_2) = \sqrt{x_1x_2}\phi_{n_1m_1}(\frac{\kappa_2}{\kappa_1}\sqrt{x_1}\vec{p}_1;\ \sqrt{x_1}\kappa_2)\phi_{n_2-m_2}(\frac{\kappa_1}{\kappa_2}\sqrt{x_2}\vec{p}_2;\ \sqrt{x_2}\kappa_1) \tag{C.21}$$

Applying the TM transformation,

$$\phi_{n_1m_1}(\frac{\kappa_2}{\kappa_1}\sqrt{x_1}\vec{p}_1;\ \sqrt{x_1}\kappa_2)\phi_{n_2-m_2}(\frac{\kappa_1}{\kappa_2}\sqrt{x_2}\vec{p}_2;\ \sqrt{x_2}\kappa_1) = \sum_{NMnm}\mathcal{M}^{NMnm}_{n_1m_1n_2-m_2}(\sqrt{x_2}\kappa_1/\sqrt{x_1}\kappa_2)\ \phi_{NM}(\vec{P};B)\phi_{nm}(\vec{p};b)\ , \tag{C.22}$$

where

$$\vec{P} = \frac{\kappa_2}{\kappa_1}\sqrt{x_1}\vec{p}_1+\frac{\kappa_1}{\kappa_2}\sqrt{x_2}\vec{p}_2 = \frac{\kappa_2^2x_1+\kappa_1^2x_2}{\kappa_1\kappa_2\sqrt{x_1+x_2}}\vec{k}_\perp+\frac{(\kappa_2^2-\kappa_1^2)\sqrt{x_1x_2}}{\kappa_1\kappa_2(x_1+x_2)}\vec{l}_\perp, \qquad B = \sqrt{x_1\kappa_2^2+x_2\kappa_1^2}\ ,$$

and

$$\vec{p} = \frac{x_2\kappa_1^2}{x_1\kappa_2^2+x_2\kappa_1^2}\frac{\kappa_2}{\kappa_1}\sqrt{x_1}\vec{p}_1-\frac{x_1\kappa_2^2}{x_1\kappa_2^2+x_2\kappa_1^2}\frac{\kappa_1}{\kappa_2}\sqrt{x_2}\vec{p}_2 = -\frac{\kappa_1\kappa_2\sqrt{x_1x_2}}{x_1\kappa_2^2+x_2\kappa_1^2}\vec{l}_\perp, \qquad b = \frac{\sqrt{x_1x_2}\kappa_1\kappa_2}{\sqrt{x_1\kappa_2^2+x_2\kappa_1^2}}\ .$$

In the case where $\kappa_1=\kappa_2=\kappa$, let us rewrite the two harmonic oscillators after the transformation on the same mass scale.

$$\begin{aligned}\phi_{NM}(\vec{P};B)\phi_{nm}(\vec{p};b) =&\phi_{NM}(\sqrt{x_1+x_2}\vec{k}_\perp;\ \sqrt{x_1+x_2}\kappa)\phi_{nm}(-\frac{\sqrt{x_1x_2}}{x_1+x_2}\vec{l}_\perp;\ \sqrt{\frac{x_1x_2}{x_1+x_2}}\kappa) \\ =&\phi_{NM}(\vec{k}_\perp;\kappa)\frac{1}{\sqrt{x_1+x_2}}\phi_{nm}(-\frac{1}{\sqrt{x_1+x_2}}\vec{l}_\perp;\kappa)\sqrt{\frac{x_1+x_2}{x_1x_2}}\end{aligned} \tag{C.23}$$

Back to Eqs. (C.21) and (C.22),

$$\phi_{n_1m_1}(\vec{p}_1;\kappa)\phi_{n_2-m_2}(\vec{p}_2;\kappa) = \sum_{NMnm}\mathcal{M}^{NMnm}_{n_1m_1n_2-m_2}(\sqrt{x_2}/\sqrt{x_1})\phi_{NM}(\vec{k}_\perp;\kappa)\phi_{nm}(-\frac{1}{\sqrt{x_1+x_2}}\vec{l}_\perp;\kappa)\ . \tag{C.24}$$

www.manaraa.com

Again, we have successfully separated the overlapping momentum $\vec{k}_\perp$ and the transferred momentum $\vec{l}_\perp$,

$$\Pi(t,x,z,\vec{\Delta}_\perp) = \left(\sqrt{\frac{x_1x_2}{x_1+x_2}}\right)^{t+2} \int \frac{\mathrm{d}^2\vec{k}_\perp}{(2\pi)^2} \sum_{s=0}^{t} \binom{t}{s} (\vec{k}_\perp)^s (-\sqrt{\frac{x_2}{x_1(x_1+x_2)}}\vec{l}_\perp)^{t-s} \sum_{NMnm} \mathcal{M}^{NMnm}_{n_1m_1n_2-m_2}(\sqrt{x_2}/\sqrt{x_1}) \times \phi_{NM}(\vec{k}_\perp)\phi_{nm}(-\frac{1}{\sqrt{x_1+x_2}}\vec{l}_\perp) \,. \tag{C.25}$$

The integral over one 2D-HO function could be carried out directly,

$$\int \frac{\mathrm{d}^2\vec{k}_\perp}{(2\pi)^2} (k^R)^s \phi_{NM}(\vec{k}_\perp) = (-1)^N 2^s \kappa^{s+1} \sqrt{\frac{(N+s)!}{\pi N!}} \delta_{M+s,0} \,. \tag{C.26}$$

$$\Pi(t,x,z,\vec{\Delta}_\perp) = \left(\sqrt{\frac{x_1x_2}{x_1+x_2}}\right)^{t+2} \sum_{s=0}^{t} \binom{t}{s} (-\sqrt{\frac{x_2}{x_1(x_1+x_2)}} l^R)^{t-s} \sum_{Nnm} \mathcal{M}^{N-snm}_{n_1m_1n_2-m_2}(\sqrt{x_2}/\sqrt{x_1}) \times \phi_{nm}(-\frac{1}{\sqrt{x_1+x_2}}\vec{l}_\perp)(-1)^N 2^s \kappa^{s+1} \sqrt{\frac{(N+s)!}{\pi N!}} \,. \tag{C.27}$$

We thereby arrive at an alternative expression to Eq. (C.17).

C.2 The longitudinal integral

The longitudinal integral is also in the form of basis function convolution,

$$\int_0^1 \mathrm{d}x f(x)\chi_l(x)\chi_{l'}(x) \,. \tag{C.28}$$

Considering that the basis function $\chi_l(x)$ is a modified polynomial function, the n-point Gaussian quadrature rule is a suitable choice to carry out the integral. This method yields an exact result for polynomials of degree $2n-1$ or less by a choice of nodes x_i and weights w_i for $i = 1,\ldots,n$.

$$\int_a^b \mathrm{d}x f(x) = \sum_i^n w_i f(x_i) \,.$$

www.manaraa.com

APPENDIX D. LORENTZ STRUCTURE DECOMPOSITION

According to spacetime translational invariance, the matrix element of the EM current operator satisfies

$$\langle \psi'_h(P', j', m'_j)| J^\mu(x) |\psi_h(P, j, m_j)\rangle = \langle \psi'_h(P', j', m'_j)| J^\mu(0) |\psi_h(P, j, m_j)\rangle e^{i(P-P')x} . \tag{D.1}$$

The current conservation condition $\partial_\mu J^\mu = 0$ leads to

$$(P' - P)_\mu \langle \psi'_h(P', j', m'_j)| J^\mu(0) |\psi_h(P, j, m_j)\rangle = 0 . \tag{D.2}$$

The charge operator on the light front is defined as

$$Q \equiv \int \mathrm{d}x_+ \, \mathrm{d}^2\boldsymbol{x}_\perp J^+(x) . \tag{D.3}$$

The eigenvalue of Q on for a particle state is interpreted as the charge of that particle,

$$Q |\psi_h(P, j, m_j)\rangle = e_q |\psi_h(P, j, m_j)\rangle \ . \tag{D.4}$$

The evaluation of the charge operator on a particle state leads to a normalization relation at zero momentum transfer.

$$\langle \psi_h(P', j, m_j)| Q |\psi_h(P, j, m_j)\rangle = \int \mathrm{d}x_+ \, \mathrm{d}^2\boldsymbol{x}_\perp \langle \psi_h(P', j, m_j)| J^+(x) |\psi_h(P, j, m_j)\rangle \ . \tag{D.5}$$

$$\langle \psi_h(P', j, m_j)| J^+(0) |\psi_h(P, j, m_j)\rangle = 2e_q P^+ \delta^3(P - P') . \tag{D.6}$$

The form factors of particle transitions are those coefficients F_i of vectors V_i obtained by decomposing the hadron matrix element,

$$\langle \psi'_h(P', j', m'_j)| J^\mu(0) |\psi_h(P, j, m_j)\rangle = \sum_i^n F_i V_i^\mu . \tag{D.7}$$

www.manaraa.com

D.1 Spin 0 mesons

In the quark model, a spin-0 ($J = 0$) meson could be either a scalar 0^+ or a pseudo-scalar 0^-. And C = 1 for quarkonium. The matrix element of the current reads

$$\langle h'_{q\bar{q}}(P', j' = m'_i = 0)|\, J^\mu(0)\, |h_{q\bar{q}}(P, j = m_i = 0)\rangle = e_q \mathscr{J}^\mu \,, \tag{D.8}$$

where $\mathscr{J}^\mu$ is a four-vector function of P'^μ and P^μ. Relevant scalars are $|P'|$, $|P|$ and $P' \cdot P$. The first two are fixed by the on shell conditions,

$$P'^\mu P'_\mu = m^2_{h'}, \qquad P^\mu P_\mu = m^2_h \,. \tag{D.9}$$

Therefore the coefficients of vectors should only depend on $P' \cdot P$. Define

$$q^\mu \equiv P'^\mu - P^\mu, \qquad \bar{p}^\mu \equiv P'^\mu + P^\mu \,, \tag{D.10}$$

and decompose $\mathscr{J}^\mu$ into the form of

$$\mathscr{J}^\mu = q^\mu H(q^2) + \bar{p}^\mu F(q^2) \,, \tag{D.11}$$

The condition of current conservation in Equation (D.2) requires,

$$q_\mu \cdot q^\mu H(q^2) + q_\mu \cdot \bar{p}^\mu F(q^2) = 0 \,. \tag{D.12}$$

This means there is only one independent form factor,

$$H(q^2) = -\frac{q_\mu \cdot \bar{p}^\mu}{q_\mu \cdot q^\mu} F(q^2) = -\frac{m^2_{h'} - m^2_h}{q^2} F(q^2) \,. \tag{D.13}$$

It follows that

$$\langle h'_{q\bar{q}}(P')|\, J^\mu(0)\, |h_{q\bar{q}}(P)\rangle = e_q[\bar{p}^\mu - \frac{m^2_{h'} - m^2_h}{q^2} q^\mu] F(q^2) \,, \tag{D.14}$$

and $F(q^2)$ is the electromagnetic form factor. To satisfy hermiticity,

$$\langle h'_{q\bar{q}}(P')|\, J^\mu(0)\, |h_{q\bar{q}}(P)\rangle = \langle h_{q\bar{q}}(P)|\, J^\mu(0)\, |h'_{q\bar{q}}(P')\rangle^* \,, \tag{D.15}$$

$F(q^2)$ must be real.

www.manaraa.com

For the elastic scattering, $h' = h$, thus $m_{h'} = m_h$,

$$\langle h_{q\bar{q}}(P')|\, J^{\mu}(0)\, |h_{q\bar{q}}(P)\rangle = e_q \bar{p}^{\mu} F(q^2)\ . \tag{D.16}$$

Compare with the normalization relation in Eq. (D.6), we get $F(0) = 1$.

Let us now analyze the symmetries of parity and charge conjugation (see Appendix A.6), and find out what kind of transitions are allowed. We first insert two complete sets of the parity operator to the matrix element,

$$\begin{aligned}
\langle h'_{q\bar{q}}(P', \mathrm{P}_2)|\, J^{\mu}(0)\, |h_{q\bar{q}}(P, \mathrm{P}_1)\rangle =& \langle h'_{q\bar{q}}(P', \mathrm{P}_2)|\, \mathbb{P}\mathbb{P}^{-1} J^{\mu}(0) \mathbb{P}\mathbb{P}^{-1}\, |h_{q\bar{q}}(P, \mathrm{P}_1)\rangle \\
=& \mathrm{P}_2\mathrm{P}_1 \mathcal{P}^{\mu}_{\nu} \langle h'_{q\bar{q}}(\mathcal{P}\cdot P', \mathrm{P}_2)|\, J^{\nu}(0)\, |h_{q\bar{q}}(\mathcal{P}\cdot P, \mathrm{P}_1)\rangle \\
=& e_q \mathrm{P}_2\mathrm{P}_1 \mathcal{P}^{\mu}_{\nu}\mathcal{P}^{\nu}_{\rho}[\bar{p}^{\rho} - \frac{m^2_{h'} - m^2_h}{q^2} q^{\rho}] F(q^2) \\
=& e_q \mathrm{P}_2\mathrm{P}_1 [\bar{p}^{\mu} - \frac{m^2_{h'} - m^2_h}{q^2} q^{\mu}] F(q^2)\ .
\end{aligned} \tag{D.17}$$

Compare with Eq (D.14), we arrive at

$$\mathrm{P}_2\mathrm{P}_1 = +1\ . \tag{D.18}$$

This means the electromagnetic transitions of spin 0 particles preserves the parity. The allowed transition modes are $0^+ \to 0^+$ (scalar-to-scalar) and $0^- \to 0^-$ (pseudoscalar-to-pseudoscalar).

We then consider the charge conjugation of quarkonium.

$$\begin{aligned}
\langle h'_{q\bar{q}}(P', \mathrm{C}_2)|\, J^{\mu}(0)\, |h_{q\bar{q}}(P, \mathrm{C}_1)\rangle =& \langle h'_{q\bar{q}}(P', \mathrm{C}_2)|\, \mathbb{C}\mathbb{C}^{-1} J^{\mu}(0) \mathbb{C}\mathbb{C}^{-1}\, |h_{q\bar{q}}(P, \mathrm{C}_1)\rangle \\
=& -\mathrm{C}_2\mathrm{C}_1 \langle h'_{q\bar{q}}(P', \mathrm{C}_2)|\, J^{\mu}(0)\, |h_{q\bar{q}}(P, \mathrm{C}_1)\rangle\ .
\end{aligned} \tag{D.19}$$

Compare with Eq (D.14), we arrive at

$$\mathrm{C}_2\mathrm{C}_1 = -1\ . \tag{D.20}$$

This means the electromagnetic transitions of quarkonium must change the charge conjugation. However, all the spin 0 quarkonium have the same parity conjugation $\mathrm{C} = +1$. Therefore the form factors for spin-0 quarkonium are zero.

www.manaraa.com

D.2 Spin-1 mesons

In the quark model, a spin 1 ($J = 1$) meson could be either a vector 1^- or an axial-vector 1^+. And C $= -1$ for vector quarkonium, C $= \pm 1$ for axial-vector quarkonium . The matrix element of the current reads

$$\langle h'_{q\bar{q}}(P', j' = 1, m'_j = 0, \pm 1)|\, J^\mu(0)\, |h_{q\bar{q}}(P, j = 1, m_j = 0, \pm 1)\rangle = e_q e^{\alpha *}(P', m'_j)\Gamma^\mu_{\alpha\beta} e^\beta(P, m_j)\ , \tag{D.21}$$

where e, e^* are spin vectors defined in Appendix A.4 and $\Gamma^\mu_{\alpha\beta}$ is a 3rd-order tensor function of P^μ, P'^μ, $g^{\mu\nu}$ and $\epsilon^{\mu\nu\rho\sigma}$. All possible non-vanishing combinations of $\Gamma^\mu_{\alpha\beta}$ are

$$\begin{aligned}
P^\mu, P'^\mu :& P^\mu P_\alpha P_\beta, P^\mu P_\alpha P'_\beta, P^\mu P'_\alpha P_\beta, P^\mu P'_\alpha P'_\beta, P'^\mu P'_\alpha P'_\beta, P'^\mu P'_\alpha P_\beta, P'^\mu P_\alpha P'_\beta, P'^\mu P_\alpha P_\beta\ , \\
g_{\alpha\beta} :& P^\mu g_{\alpha\beta}, P'^\mu g_{\alpha\beta}, g^\mu_\alpha P_\beta, g^\mu_\beta P_\alpha, g^\mu_\alpha P'_\beta, g^\mu_\beta P'_\alpha\ , \\
\epsilon^{\mu\nu\rho\sigma} :& \epsilon^\mu_{\alpha\beta\rho} P^\rho, \epsilon^\mu_{\alpha\beta\rho} P'^\rho, \epsilon^\mu_{\alpha\rho\sigma} P^\rho P'^\sigma P_\beta, \epsilon^\mu_{\beta\rho\sigma} P^\rho P'^\sigma P_\alpha, \epsilon^\mu_{\alpha\rho\sigma} P^\rho P'^\sigma P'_\beta, \epsilon^\mu_{\beta\rho\sigma} P^\rho P'^\sigma P'_\alpha, \\
& P'^\mu \epsilon_{\alpha\beta\rho\sigma} P^\rho P'^\sigma, P^\mu \epsilon_{\alpha\beta\rho\sigma} P^\rho P'^\sigma\ .
\end{aligned} \tag{D.22}$$

Contracting with the spin vectors in Eq. (D.21), and with the Proca equation in Appendix A.4,

$$P_\beta e^\beta(P, m_j) = 0\ , \qquad P'_\alpha e^{\alpha *}(P', m'_j) = 0\ , \tag{D.23}$$

we get all possible non-vanishing vectors of $e^{\alpha *}(P', m'_j)\Gamma^\mu_{\alpha\beta} e^\beta(P, m_j)$.

$$\begin{aligned}
& P^\mu (e^*(P', m'_j)\cdot P)(e(P, m_j)\cdot P'), P'^\mu (e^*(P', m'_j)\cdot P)(e(P, m_j)\cdot P')\ , \\
& P^\mu (e^*(P', m'_j)\cdot e(P, m_j)), P'^\mu (e^*(P', m'_j)\cdot e(P, m_j)), \\
& e^\mu(P, m_j)(e^*(P', m'_j)\cdot P), e^{\mu *}(P', m'_j)(e(P, m_j)\cdot P')\ , \\
& \epsilon^\mu_{\alpha\beta\rho} P^\rho e^{\alpha *}(P', m'_j) e^\beta(P, m_j), \epsilon^\mu_{\alpha\beta\rho} P'^\rho e^{\alpha *}(P', m'_j) e^\beta(P, m_j), \\
& \epsilon^\mu_{\beta\rho\sigma} P^\rho P'^\sigma (e^*(P', m'_j)\cdot P) e^\beta(P, m_j), \epsilon^\mu_{\alpha\rho\sigma} P^\rho P'^\sigma (e(P, m_j)\cdot P') e^{\alpha *}(P', m'_j), \\
& P'^\mu \epsilon_{\alpha\beta\rho\sigma} P^\rho P'^\sigma e^{\alpha *}(P', m'_j) e^\beta(P, m_j), P^\mu \epsilon_{\alpha\beta\rho\sigma} P^\rho P'^\sigma e^{\alpha *}(P', m'_j) e^\beta(P, m_j)\ .
\end{aligned} \tag{D.24}$$

Their coefficients are functions of $|P'|$, $|P|$ and $P'\cdot P$. The first two are fixed by on shell conditions,

$$P'^\mu P'_\mu = m^2_{h'}, \qquad P^\mu P_\mu = m^2_h\ . \tag{D.25}$$

www.manaraa.com

Therefore those coefficients should only depend on $P' \cdot P$, or q^2 if we define,

$$q^\mu \equiv P'^\mu - P^\mu, \qquad \bar{p}^\mu \equiv P'^\mu + P^\mu \ . \tag{D.26}$$

That leads to

$$q_\mu q^\mu = q^2 \ , \qquad q_\mu \bar{p}^\mu = m_{h'}^2 - m_h^2 \equiv \Delta_m \ . \tag{D.27}$$

We now have twelve candidates of form factors, $F_{1,\ldots,12}$,

$$\begin{aligned}
& e^{\alpha *}(P', m_j')\Gamma^\mu_{\alpha\beta} e^\beta(P, m_j) \\
&\quad = \bar{p}^\mu (e^*(P', m_j') \cdot P)(e(P, m_j) \cdot P') F_1 + q^\mu (e^*(P', m_j') \cdot P)(e(P, m_j) \cdot P') F_2 \\
&\quad + \bar{p}^\mu (e^*(P', m_j') \cdot e(P, m_j)) F_3 + q^\mu (e^*(P', m_j') \cdot e(P, m_j)) F_4 \\
&\quad + e^\mu(P, m_j)(e^*(P', m_j') \cdot P) F_5 + e^{\mu *}(P', m_j')(e(P, m_j) \cdot P') F_6 \\
&\quad + \epsilon^\mu_{\alpha\beta\rho} \bar{p}^\rho e^{\alpha *}(P', m_j') e^\beta(P, m_j) F_7 + \epsilon^\mu_{\alpha\beta\rho} q^\rho e^{\alpha *}(P', m_j') e^\beta(P, m_j) F_8 \\
&\quad + \epsilon^\mu_{\beta\rho\sigma} \bar{p}^\rho q^\sigma (e^*(P', m_j') \cdot P) e^\beta(P, m_j) F_9 + \epsilon^\mu_{\alpha\rho\sigma} \bar{p}^\rho q^\sigma (e(P, m_j) \cdot P') e^{\alpha *}(P', m_j') F_{10} \\
&\quad + q^\mu \epsilon_{\alpha\beta\rho\sigma} \bar{p}^\rho q^\sigma e^{\alpha *}(P', m_j') e^\beta(P, m_j) F_{11} + \bar{p}^\mu \epsilon_{\alpha\beta\rho\sigma} \bar{p}^\rho q^\sigma e^{\alpha *}(P', m_j') e^\beta(P, m_j) F_{12} \ .
\end{aligned} \tag{D.28}$$

The condition of current conservation in Eq. (D.2) requires,

$$q_\mu e^{\alpha *}(P', m_j') \Gamma^\mu_{\alpha\beta} e^\beta(P, m_j) = 0 \ . \tag{D.29}$$

That is,

$$\begin{aligned}
0 =& (e^*(P', m_j') \cdot P)(e(P, m_j) \cdot P')[\Delta_m F_1 + q^2 F_2] \\
&+ (e^*(P', m_j') \cdot e(P, m_j))[\Delta_m F_3 + q^2 F_4] \\
&+ (e(P, m_j) \cdot P')(e^*(P', m_j') \cdot P)[F_5 - F_6] \\
&+ q_\mu \epsilon^\mu_{\alpha\beta\rho} \bar{p}^\rho e^{\alpha *}(P', m_j') e^\beta(P, m_j)[F_7 - q^2 F_{11} - \Delta_m F_{12}] \\
&+ q_\mu \epsilon^\mu_{\alpha\beta\rho} q^\rho e^{\alpha *}(P', m_j') e^\beta(P, m_j) F_8 \\
&+ q_\mu \epsilon^\mu_{\beta\rho\sigma} \bar{p}^\rho q^\sigma (e^*(P', m_j') \cdot P) e^\beta(P, m_j) F_9 \\
&+ q_\mu \epsilon^\mu_{\alpha\rho\sigma} \bar{p}^\rho q^\sigma (e(P, m_j) \cdot P') e^{\alpha *}(P', m_j') F_{10} \ .
\end{aligned} \tag{D.30}$$

www.manaraa.com

F_8, F_9 and F_{10} could survive since their associated components vanish,

$$q_\mu \epsilon^\mu_{\beta\rho\sigma} \bar{p}^\rho q^\sigma = q_\sigma \epsilon^\sigma_{\beta\rho\mu} \bar{p}^\rho q^\mu = -q_\sigma \epsilon^\mu_{\beta\rho\sigma} \bar{p}^\rho q^\mu \to q_\mu \epsilon^\mu_{\beta\rho\sigma} \bar{p}^\rho q^\sigma = 0 \,. \tag{D.31}$$

The other terms should satisfy

$$\begin{aligned} &\Delta_m F_1 + q^2 F_2 = 0 \,, \\ &\Delta_m F_3 + q^2 F_4 = 0 \,, \\ &F_5 - F_6 = 0 \,, \\ &F_7 - q^2 F_{11} - \Delta_m F_{12} = 0 \,. \end{aligned} \tag{D.32}$$

Taking these relations into account, we rewrite the vector decomposition with new coefficients,

$$\begin{aligned} & e^{\alpha *}(P', m'_j) \Gamma^\mu_{\alpha\beta} e^\beta(P, m_j) \\ &= (e^*(P', m'_j) \cdot P)(e(P, m_j) \cdot P')[\bar{p}^\mu - q^\mu \frac{\Delta_m}{q^2}] G_1 \\ &\quad + (e^*(P', m'_j) \cdot e(P, m_j))[\bar{p}^\mu - q^\mu \frac{\Delta_m}{q^2}] G_2 \\ &\quad + [e^\mu(P, m_j)(e^*(P', m'_j) \cdot P) + e^{\mu *}(P', m'_j)(e(P, m_j) \cdot P')] G_3 \\ &\quad + [\epsilon^\mu_{\alpha\beta\rho} \bar{p}^\rho + q^\mu \epsilon_{\alpha\beta\rho\sigma} \bar{p}^\rho q^\sigma \frac{1}{q^2}] e^{\alpha *}(P', m'_j) e^\beta(P, m_j) F_7 \\ &\quad + \epsilon^\mu_{\alpha\beta\rho} q^\rho e^{\alpha *}(P', m'_j) e^\beta(P, m_j) G_4 \\ &\quad + \epsilon^\mu_{\beta\rho\sigma} \bar{p}^\rho q^\sigma (e^*(P', m'_j) \cdot P) e^\beta(P, m_j) G_5 + \epsilon^\mu_{\alpha\rho\sigma} \bar{p}^\rho q^\sigma (e(P, m_j) \cdot P') e^{\alpha *}(P', m'_j) G_6 \\ &\quad + \epsilon_{\alpha\beta\rho\sigma} \bar{p}^\rho q^\sigma e^{\alpha *}(P', m'_j) e^\beta(P, m_j) [\bar{p}^\mu - \frac{\Delta_m}{q^2} q^\mu] F_{12} \,. \end{aligned} \tag{D.33}$$

Inserting two complete sets of parity operators,

$$\begin{aligned} & \langle h'_{q\bar{q}}(P', m'_j, \mathrm{P}_2) | \, J^\mu(0) \, | h_{q\bar{q}}(P, m_j, \mathrm{P}_1) \rangle \\ &\quad = \langle h'_{q\bar{q}}(P', m'_j, \mathrm{P}_2) | \, \mathbb{P}\mathbb{P}^{-1} J^\mu(0) \mathbb{P}\mathbb{P}^{-1} \, | h_{q\bar{q}}(P, m_j, \mathrm{P}_1) \rangle \\ &\quad = \mathrm{P}_2 \mathrm{P}_1 \mathcal{P}^\mu_\nu \langle h'_{q\bar{q}}(\mathcal{P} \cdot P', m'_j, \mathrm{P}_2) | \, J^\nu(0) \, | h_{q\bar{q}}(\mathcal{P} \cdot P, m_j, \mathrm{P}_1) \rangle \,. \end{aligned} \tag{D.34}$$

www.manaraa.com

With Eqs. (D.21) and (D.33), we get

$$
\begin{aligned}
&\langle h'_{q\bar{q}}(\mathcal{P}\cdot P', m'_j, \mathrm{P}_2)|J^\nu(0)\,|h_{q\bar{q}}(\mathcal{P}\cdot P, m_j, \mathrm{P}_1)\rangle\,/e_q \\
&\quad=(e^*(\mathcal{P}\cdot P', m'_j)\cdot(\mathcal{P}\cdot P))(e(\mathcal{P}\cdot P, m_j)\cdot(\mathcal{P}\cdot P'))\mathcal{P}^\nu_\kappa[\bar{p}^\kappa - q^\kappa\frac{\Delta_m}{q^2}]G_1 \\
&\qquad+(e^*(\mathcal{P}\cdot P', m'_j)\cdot e(\mathcal{P}\cdot P, m_j))\mathcal{P}^\nu_\kappa[\bar{p}^\kappa - q^\kappa\frac{\Delta_m}{q^2}]G_2 \\
&\qquad+[e^\nu(\mathcal{P}\cdot P, m_j)(e^*(\mathcal{P}\cdot P', m'_j)\cdot(\mathcal{P}\cdot P)) \\
&\qquad+e^{\nu *}(\mathcal{P}\cdot P', m'_j)(e(\mathcal{P}\cdot P, m_j)\cdot(\mathcal{P}\cdot P'))]G_3 \\
&\qquad+\epsilon^\nu_{\alpha\beta\rho}\mathcal{P}^\rho_\kappa q^\kappa e^{\alpha *}(\mathcal{P}\cdot P', m'_j)e^\beta(\mathcal{P}\cdot P, m_j)G_4 \\
&\qquad+\epsilon^\nu_{\beta\rho\sigma}\mathcal{P}^\rho_{\kappa_1}\mathcal{P}^\sigma_{\kappa_2}\bar{p}^{\kappa_1}q^{\kappa_2}(e^*(\mathcal{P}\cdot P', m'_j)\cdot(\mathcal{P}\cdot P))e^\beta(\mathcal{P}\cdot P, m_j)G_5 \\
&\qquad+\epsilon^\nu_{\alpha\rho\sigma}\mathcal{P}^\rho_{\kappa_1}\mathcal{P}^\sigma_{\kappa_2}\bar{p}^{\kappa_1}q^{\kappa_2}(e(\mathcal{P}\cdot P, m_j)\cdot(\mathcal{P}\cdot P'))e^{\alpha *}(\mathcal{P}\cdot P', m'_j)G_6 \\
&\qquad+\epsilon_{\alpha\beta\rho\sigma}\mathcal{P}^\rho_{\kappa_1}\mathcal{P}^\sigma_{\kappa_2}\bar{p}^{\kappa_1}q^{\kappa_2}e^{\alpha *}(\mathcal{P}\cdot P', m'_j)e^\beta(\mathcal{P}\cdot P, m_j)\mathcal{P}^\nu_\kappa[\bar{p}^\kappa - q^\kappa\frac{\Delta_m}{q^2}]G_7\ .
\end{aligned}
\tag{D.35}
$$

The effect of parity transformation on spin vector are

$$
e^\mu(\mathcal{P}\cdot P, m_j) = -\mathcal{P}^\mu_\nu e^\nu(P, m_j)\ , \tag{D.36}
$$

$$
e^*(\mathcal{P}\cdot P', m'_j)\cdot(\mathcal{P}\cdot P) = -\mathcal{P}^\nu_\kappa e^{\kappa *}(P', m'_j)\mathcal{P}^\chi_\nu P_\chi = -e^*(P', m'_j)\cdot P\ , \tag{D.37}
$$

$$
e^*(\mathcal{P}\cdot P', m'_j)\cdot e(\mathcal{P}\cdot P, m_j) = \mathcal{P}^\nu_\kappa e^{\kappa *}(P', m'_j)\mathcal{P}^\chi_\nu e^{\chi *}(P', m'_j) = e^*(P', m'_j)\cdot e(P, m_j)\ . \tag{D.38}
$$

The definition of Levi-Civita tensor leads to

$$
\mathcal{P}^\rho_{\kappa_1}\mathcal{P}^\sigma_{\kappa_2}\mathcal{P}^\alpha_{\kappa_3}\mathcal{P}^\beta_{\kappa_4}\epsilon_{\rho\sigma\alpha\beta} = \epsilon_{\kappa_1\kappa_2\kappa_3\kappa_4}(\det\mathcal{P}) = -\epsilon_{\kappa_1\kappa_2\kappa_3\kappa_4}\ . \tag{D.39}
$$

It follows that

$$
\mathcal{P}^\rho_{\kappa_1}\mathcal{P}^\sigma_{\kappa_2}\mathcal{P}^\alpha_{\kappa_3}\mathcal{P}^\beta_{\kappa_4}\mathcal{P}^{\kappa_4}_\mu\epsilon_{\rho\sigma\alpha\beta} = \mathcal{P}^\rho_{\kappa_1}\mathcal{P}^\sigma_{\kappa_2}\mathcal{P}^\alpha_{\kappa_3}\epsilon_{\rho\sigma\alpha\mu} = -\epsilon_{\kappa_1\kappa_2\kappa_3\kappa_4}\mathcal{P}^{\kappa_4}_\mu\ . \tag{D.40}
$$

www.manaraa.com

The matrix element under the parity transformation becomes

$$\begin{aligned}
&\langle h'_{q\bar{q}}(\mathcal{P}\cdot P', m'_j, \mathrm{P}_2)|J^\nu(0)\,|h_{q\bar{q}}(\mathcal{P}\cdot P, m_j, \mathrm{P}_1)\rangle\,/e_q \\
&\quad=(e^*(P', m'_j)\cdot P)(e(P, m_j)\cdot P')\mathcal{P}^\nu_\kappa[\bar{p}^\kappa - q^\kappa\frac{\Delta_m}{q^2}]G_1 \\
&\quad\quad+(e^*(P', m'_j)\cdot e(P, m_j))\mathcal{P}^\nu_\kappa[\bar{p}^\kappa - q^\kappa\frac{\Delta_m}{q^2}]G_2 \\
&\quad\quad+\mathcal{P}^\nu_\kappa[e^\kappa(P, m_j)(e^*(P', m'_j)\cdot P) + e^{\kappa *}(P', m'_j)(e(P, m_j)\cdot P')]G_3 \\
&\quad\quad-\mathcal{P}^\nu_\kappa\epsilon^\kappa_{\kappa_1\kappa_2\kappa_3}q^{\kappa_3}e^{\kappa_1 *}(P', m'_j)e^{\kappa_2}(P, m_j)G_4 \\
&\quad\quad-\mathcal{P}^\nu_\kappa\epsilon^\kappa_{\kappa_3\kappa_1\kappa_2}\bar{p}^{\kappa_1}q^{\kappa_2}(e^*(P', m'_j)\cdot P)e^{\kappa_3}(P, m_j)G_5 \\
&\quad\quad-\mathcal{P}^\nu_\kappa\epsilon^\kappa_{\kappa_3\kappa_1\kappa_2}\bar{p}^{\kappa_1}q^{\kappa_2}(e(P, m_j)\cdot P')e^{\kappa_3 *}(P', m'_j)G_6 \\
&\quad\quad-\epsilon_{\kappa_3\kappa_4\kappa_1\kappa_2}\bar{p}^{\kappa_1}q^{\kappa_2}e^{\kappa_3 *}(P', m'_j)e^{\kappa_4}(P, m_j)\mathcal{P}^\nu_\kappa[\bar{p}^\kappa - q^\kappa\frac{\Delta_m}{q^2}]G_7\ .
\end{aligned} \tag{D.41}$$

Insert Eq. (D.41) into Eq. (D.34), we find that

$$\mathrm{P}_2\mathrm{P}_1 = \begin{cases} +1 & \to G_4, G_5, G_6, G_7 = 0 \\ -1 & \to G_1, G_2, G_3 = 0 \end{cases}\ . \tag{D.42}$$

This implies that G_1, G_2, G_3 are the form factors of parity conserved transitions, and G_4, G_5, G_6, G_7 are the form factors of parity flipped transitions. We will discuss them separately in the following.

Vector-to-vector (axial-vector-to-axial-vector) Form Factor

Following our previous discussion, the vector-to-vector (axial-vector-to-axial-vector) transition does not change partiy, and their form factors are defined as

$$\begin{aligned}
&\langle h'_{q\bar{q}}(P', j' = 1, m'_j = 0, \pm 1, \mathrm{P}_2 = \mathrm{P}_1)|\,J^\mu(0)\,|h_{q\bar{q}}(P, j = 1, m_j = 0, \pm 1, \mathrm{P}_1 = \pm 1)\rangle \\
&=e_q\Big[(e^*(P', m'_j)\cdot P)(e(P, m_j)\cdot P')[\bar{p}^\mu - q^\mu\frac{\Delta_m}{q^2}]G_1(q^2) \\
&\quad+(e^*(P', m'_j)\cdot e(P, m_j))[\bar{p}^\mu - q^\mu\frac{\Delta_m}{q^2}]G_2(q^2) \\
&\quad+[e^\mu(P, m_j)(e^*(P', m'_j)\cdot P) + e^{\mu *}(P', m'_j)(e(P, m_j)\cdot P')]G_3(q^2)\Big]\ .
\end{aligned} \tag{D.43}$$

www.manaraa.com

For the elastic scattering, $h' = h$, thus $m_{h'} = m_h$ and $\Delta_m = 0$,

$$\begin{aligned}
&\langle h_{q\bar{q}}(P', j' = 1, m'_j, \mathrm{P}_2 = \mathrm{P}_1)|\, J^\mu(0)\, |h_{q\bar{q}}(P, j = 1, m_j, \mathrm{P}_1 = \pm 1)\rangle \\
=&e_q\Big[(e^*(P', m'_j)\cdot P)(e(P, m_j)\cdot P')\bar{p}^\mu G_1(q^2) + (e^*(P', m'_j)\cdot e(P, m_j))\bar{p}^\mu G_2(q^2) \\
&+ [e^\mu(P, m_j)(e^*(P', m'_j)\cdot P) + e^{\mu *}(P', m'_j)(e(P, m_j)\cdot P')]G_3(q^2)\Big] .
\end{aligned} \tag{D.44}$$

Now $G_i(q^2)$ are the elastic form factors. Setting $P' = P$ and $\mu = +$, we have

$$\langle h_{q\bar{q}}(P, j' = 1, m'_j, \mathrm{P}_2 = \mathrm{P}_1)|\, J^+(0)\, |h_{q\bar{q}}(P, j = 1, m_j, \mathrm{P}_1 = \pm 1)\rangle = -2e_q P^+ G_2(0) . \tag{D.45}$$

Eq. (D.6) implies that $G_2(0) = -1$.

As we have seen in Eq. (D.19), the electromagnetic transition must flip the charge conjugation of the particle, so the vector 1^{--} to vector 1^{--} or axial-vector $1^{+-}(1^{++})$ to axial-vector $1^{+-}(1^{++})$ transitions are forbidden. The only allowed transition is

$$1^{+-}(\text{axial-vector}) \to 1^{++}(\text{axial-vector}) ,$$

A widely used convention is formulated with the J^+ current in the Drell-Yan frame,

$$\begin{aligned}
&\langle h_{q\bar{q}}(P', j' = 1, m'_j, \mathrm{P}_2 = \mathrm{P}_1)|\, J^+(0)\, |h_{q\bar{q}}(P, j = 1, m_j, \mathrm{P}_1 = \pm 1)\rangle \\
=&e_q\Big[2P^+[(e^*(P', m'_j)\cdot P)(e(P, m_j)\cdot P')G_1(q^2) + (e^*(P', m'_j)\cdot e(P, m_j))G_2(q^2)] \\
&+ [e^+(P, m_j)(e^*(P', m'_j)\cdot P) + e^{+*}(P', m'_j)(e(P, m_j)\cdot P')]G_3(q^2)\Big] .
\end{aligned} \tag{D.46}$$

Vector Axial-vector Transition Form Factor

The vector axial-vector transitions flip the parity, and their form factors are defined as

$$\begin{aligned}
&\langle f'(P', j' = 1, m'_j = 0, \pm 1, \mathrm{P}_2 = -\mathrm{P}_1)|\, J^\mu(0)\, |f(P, j = 1, m_j = 0, \pm 1, \mathrm{P}_1 = \pm 1)\rangle \\
=&e_q\Big[\epsilon^\mu_{\alpha\beta\rho} q^\rho e^{\alpha *}(P', m'_j) e^\beta(P, m_j) H_1(q^2) + \epsilon^\mu_{\beta\rho\sigma}\bar{p}^\rho q^\sigma (e^*(P', m'_j)\cdot P) e^\beta(P, m_j) H_2(q^2) \\
&+ \epsilon^\mu_{\alpha\rho\sigma}\bar{p}^\rho q^\sigma (e(P, m_j)\cdot P') e^{\alpha *}(P', m'_j) H_3(q^2) \\
&+ \epsilon_{\alpha\beta\rho\sigma}\bar{p}^\rho q^\sigma e^{\alpha *}(P', m'_j) e^\beta(P, m_j)[\bar{p}^\mu - q^\mu \frac{\Delta_m}{q^2}] H_4(q^2)\Big] .
\end{aligned} \tag{D.47}$$

www.manaraa.com

D.3 Spin-0 ↔ spin-1 mesons

The matrix element of the transition between a spin-0 and a spin-1 meson reads

$$\langle h'_{q\bar{q}}(P', j' = 1, m'_j = 0, \pm 1)|\, J^\mu(0)\, |h_{q\bar{q}}(P, j = 0, m_j = 0)\rangle = e^{\alpha *}(P', m'_j)\Gamma^\mu_\alpha \,, \tag{D.48}$$

where e^* is the spin vector defined in Appendix A.4 and Γ^μ_α is a 2nd-order tensor function of P^μ, P'^μ, $g^{\mu\nu}$ and $\epsilon^{\mu\nu\rho\sigma}$. Note that we did not write out the charge here for simplicity. All possible non-vanishing combinations are

$$\begin{aligned} P^\mu, P'^\mu :& P^\mu P_\alpha, P^\mu P'_\alpha, P'^\mu P'_\alpha, P'^\mu P_\alpha \,, \\ g_{\alpha\beta} :& g^\mu_\alpha \,, \\ \epsilon^{\mu\nu\rho\sigma} :& \epsilon^\mu_{\alpha\rho\sigma} P^\rho P'^\sigma \,. \end{aligned} \tag{D.49}$$

Contracting with the spin vectors in Eq. (D.21), and according to the Proca equation in A.4,

$$P_\beta e^\beta(P, m_j) = 0 \,, \qquad P'_\alpha e^{\alpha *}(P', m'_j) = 0 \,, \tag{D.50}$$

we get all possible non-vanishing vectors of $e^{\alpha *}(P', m'_j)\Gamma^\mu_\alpha$.

$$\begin{aligned} & P^\mu(e^*(P', m'_j)\cdot P), P'^\mu(e^*(P', m'_j)\cdot P) \,, \\ & e^{\mu *}(P', m'_j) \,, \\ & \epsilon^\mu_{\alpha\rho\sigma} P^\rho P'^\sigma e^{\alpha *}(P', m'_j) \,. \end{aligned} \tag{D.51}$$

Their coefficients are functions of $|P'|$, $|P|$ and $P' \cdot P$. The first two are fixed by on shell conditions,

$$P'^\mu P'_\mu = m^2_{h'}, \qquad P^\mu P_\mu = m^2_h \,. \tag{D.52}$$

Therefore those coefficients should only depend on $P' \cdot P$. For convenience, we define

$$q^\mu \equiv P'^\mu - P^\mu, \qquad \bar{p}^\mu \equiv P'^\mu + P^\mu \,. \tag{D.53}$$

The on shell condition now reads

$$q_\mu q^\mu = q^2 \,, \qquad q_\mu \bar{p}^\mu = m^2_{h'} - m^2_h \equiv \Delta_m \,. \tag{D.54}$$

www.manaraa.com

We thereby write $e^{\alpha *}(P', m'_j)\Gamma^\mu_\alpha$ as a linear combination of the vectors we found,

$$\begin{aligned} e^{\alpha *}(P', m'_j)\Gamma^\mu_\alpha =& \bar{p}^\mu (e^*(P', m'_j)\cdot P)F_1 + q^\mu (e^*(P', m'_j)\cdot P)F_2 + e^{\mu *}(P', m'_j)F_3 \\ &+ \epsilon^\mu_{\alpha\rho\sigma}\bar{p}^\rho q^\sigma e^{\alpha *}(P', m'_j)F_4 \ . \end{aligned} \tag{D.55}$$

The condition of current conservation in Eq. (D.2) requires,

$$q_\mu e^{\alpha *}(P', m'_j)\Gamma^\mu_\alpha = 0 \ . \tag{D.56}$$

That is,

$$0 = (e^*(P', m'_j)\cdot P)[\Delta_m F_1 + q^2 F_2 - F_3] + \epsilon^\mu_{\alpha\rho\sigma}\bar{p}^\rho q^\sigma q_\mu e^{\alpha *}(P', m'_j)F_4 \ . \tag{D.57}$$

F_4 survives since

$$\epsilon^\mu_{\alpha\rho\sigma}\bar{p}^\rho q^\sigma q_\mu = 0 \tag{D.58}$$

The other terms satisfy,

$$\Delta_m F_1 + q^2 F_2 - F_3 = 0 \tag{D.59}$$

We therefore rewrite the vector decomposition with new coefficients,

$$\begin{aligned} e^{\alpha *}(P', m'_j)\Gamma^\mu_\alpha =& [\bar{p}^\mu (e^*(P', m'_j)\cdot P) - q^\mu (e^*(P', m'_j)\cdot P)\Delta_m/q^2]H_1 \\ &+ [e^{\mu *}(P', m'_j) + q^\mu (e^*(P', m'_j)\cdot P)/q^2]H_2 + \epsilon^\mu_{\alpha\rho\sigma}\bar{p}^\rho q^\sigma e^{\alpha *}(P', m'_j)H_3 \ . \end{aligned} \tag{D.60}$$

Parity invariance requires that

$$\begin{aligned} &\langle h'_{q\bar{q}}(P', j' = 1, m'_j, \mathrm{P}_2)|J^\mu(0)\,|h_{q\bar{q}}(P, j = 0, m_j, \mathrm{P}_1)\rangle \\ &\quad = \langle h'_{q\bar{q}}(P', j' = 1, m'_j, \mathrm{P}_2)|\,\mathbb{P}\mathbb{P}^{-1}J^\mu(0)\mathbb{P}\mathbb{P}^{-1}\,|h_{q\bar{q}}(P, j = 0, m_j, \mathrm{P}_1)\rangle \\ &\quad = \mathrm{P}_2\mathrm{P}_1\mathcal{P}^\mu_\nu\,\langle h'_{q\bar{q}}(\mathcal{P}\cdot P', j' = 1, m'_j, \mathrm{P}_2)|\,J^\nu(0)\,|h_{q\bar{q}}(\mathcal{P}\cdot P, j = 0, m_j, \mathrm{P}_1)\rangle \ . \end{aligned} \tag{D.61}$$

The matrix element under the parity transformation reads

$$\begin{aligned} &\langle h'_{q\bar{q}}(\mathcal{P}\cdot P', j' = 1, m'_j, \mathrm{P}_2)|J^\nu(0)\,|h_{q\bar{q}}(\mathcal{P}\cdot P, j = 0, m_j, \mathrm{P}_1)\rangle \\ &\quad = \mathcal{P}^\nu_\kappa[\bar{p}^\kappa (e^*(\mathcal{P}\cdot P', m'_j)\cdot(\mathcal{P}\cdot P)) - q^\kappa (e^*(\mathcal{P}\cdot P', m'_j)\cdot(\mathcal{P}\cdot P))\Delta_m/q^2]H_1 \\ &\quad\quad - \mathcal{P}^\nu_\kappa[e^{\kappa *}(\mathcal{P}\cdot P', m'_j) + \mathcal{P}^\nu_\kappa q^\kappa (e^*(\mathcal{P}\cdot P', m'_j)\cdot(\mathcal{P}\cdot P))/q^2]H_2 \\ &\quad\quad - \mathcal{P}^\rho_{\kappa_1}\mathcal{P}^\sigma_{\kappa_2}\mathcal{P}^\alpha_{\kappa_3}\epsilon^\nu_{\alpha\rho\sigma}\bar{p}^{\kappa_1}q^{\kappa_2}e^{\kappa_3 *}(P', m'_j)H_3 \ . \end{aligned} \tag{D.62}$$

www.manaraa.com

By using Eqs. (D.36) to (D.40), we get

$$\begin{aligned}
&\langle h'_{q\bar{q}}(\mathcal{P}\cdot P', j'=1, m'_j, \mathrm{P}_2)|\bar{\Psi}\gamma^\nu\Psi|h_{q\bar{q}}(\mathcal{P}\cdot P, j=0, m_j, \mathrm{P}_1)\rangle \\
&\quad = -\mathcal{P}^\nu_\kappa[\bar{p}^\kappa(e^*(P', m'_j)\cdot P) - q^\kappa(e^*(P', m'_j)\cdot P)\Delta_m/q^2]H_1 \\
&\quad\quad -\mathcal{P}^\nu_\kappa[e^{\kappa *}(P', m'_j) + \mathcal{P}^\nu_\kappa q^\kappa(e^*(P', m'_j)\cdot P)/q^2]H_2 \\
&\quad\quad +\mathcal{P}^\nu_\kappa\epsilon^\kappa_{\kappa_3\kappa_1\kappa_2}\bar{p}^{\kappa 1}q^{\kappa 2}e^{\kappa 3 *}(P', m'_j)H_3\ .
\end{aligned} \tag{D.63}$$

Plug it back into Eq. (D.61), we find

$$\mathrm{P}_2\mathrm{P}_1 = \begin{cases} +1 & \to H_1, H_2 = 0 \\ -1 & \to H_3 = 0 \end{cases}. \tag{D.64}$$

H_1, H_2 are form factors of parity flipped transition, and H_3 are form factors of parity conserved transition. We will discuss them separately in the following.

Scalar-to-vector (pseudoscalar-to-axial-vector) Transition Form Factor

The scalar-to-vector (pseudoscalar-to-axial-vector) form factors are defined as

$$\begin{aligned}
&\langle h'_{q\bar{q}}(P', j'=1, m'_j=0,\pm 1, \mathrm{P}_2=-\mathrm{P}_1)|\, J^\mu(0)\,|h_{q\bar{q}}(P, j=0, m_j=0, \mathrm{P}_1=\pm 1)\rangle \\
=&[\bar{p}^\mu(e^*(P', m'_j)\cdot P) - q^\mu(e^*(P', m'_j)\cdot P)\Delta_m/q^2]H_1(q^2) \\
&+[e^{\mu *}(P', m'_j) + q^\mu(e^*(P', m'_j)\cdot P)/q^2]H_2(q^2)\ .
\end{aligned} \tag{D.65}$$

As we have seen in Eq. (D.19), the electromagnetic transition must flip the charge conjugation of the particle, so the allowed transitions are

$$0^{++}(\text{scalar}) \to 1^{--}(\text{vector})\ ,$$

$$0^{-+}(\text{ pseudoscalar }) \to 1^{+-}(\text{axial-vector }).$$

The transition between pseudoscalar 0^{-+} and axial-vector 1^{++} is forbidden.

www.manaraa.com

Scalar-to-axial-vector (pseudoscalar-to-vector) Transition Form Factor

The scalar-to-axial-vector (pseudoscalar-to-vector) form factors are defined as

$$\begin{aligned}&\langle h'_{q\bar{q}}(P', j' = 1, m'_j = 0, \pm 1, \mathrm{P}_2 = \mathrm{P}_1)|\, J^\mu(0)\, |h_{q\bar{q}}(P, j = 0, m_j = 0, \mathrm{P}_1 = \pm 1)\rangle \\ =&\epsilon^\mu_{\alpha\rho\sigma} \bar{p}^\rho q^\sigma e^{\alpha *}(P', m'_j) H_3(q^2)\ .\end{aligned} \tag{D.66}$$

As we have seen in Eq. (D.19), the electromagnetic transition must flip the charge conjugation of the particle, so the allowed transitions are

$$0^{++}(\text{scalar}) \to 1^{+-}(\text{axial-vector})\ ,$$

$$0^{-+}(\text{ pseudoscalar }) \to 1^{--}(\text{vector }).$$

The transition between scalar 0^{++} and axial-vector 1^{++} is forbidden.

www.manaraa.com